University of Strathclyde

Strathclyde Institute of Pharmacy and Biomedical Sciences

Metabolic Reprogramming of Dendritic Cells by Intracellular Protozoan Parasites

By

Kerrie Elizabeth Hargrave

A thesis submitted in the fulfilment of the requirements for the degree of Doctor of Philosophy

2018

This thesis is the result of the author's original research. It has been composed by the author and has not been previously submitted for examination, which has led to the award of a degree.

Signed:

Date:

Acknowledgements

Foremost, I would like to thank my supervisor Professor Craig W Roberts, whose encouragement, support and calming words has been a source of inspiration and motivation throughout the past four years.

I also wish to thank Dr Owain Millington, Dr Jenny Crowe, Dr Susan Chalmers, Dr Gareth Westrop and the Roberts Lab group for their expertise, guidance, help and patience over the trials and tribulations of the last few years. Specifically, I would like to thank Dr Stuart Woods and his no-nonsense approach. He was always there when I needed him and I honestly believe I would never have gotten this far without him.

I also could not have submitted this thesis without the support and friendship of Chelsey Wilson, Shehla Hridi and Aimee Franssen. From the very start, Chelsey has been my partner in crime and has always known the best way to cheer me up on a bad science day…a muffin!

I must also acknowledge Ross Brisco, Lyndsey McGill, Sarah Mitchell, Amy Ferguson and Connor Craig. We have grown up together and I know they will always be there for me.

Finally, words cannot describe the incredible gratitude I feel towards my mum and dad (Anne and Tom Hargrave), without whom I am certain I would never have reached this point. They have always actively supported and encouraged me to pursue this dream. It is to you both that I dedicate this thesis.

Abstract

Upon activation, immune cells such as macrophages and dendritic cells alter their metabolism to support phagocytosis, antigen processing, cytokine production and T cell activation. Even in an oxygenated environment, immune cells change their metabolism from oxidative phosphorylation (OXPHOS) to aerobic glycolysis. This is referred to as the 'Warburg effect'. Aerobic glycolysis benefits the immune response by rapidly generating ATP whilst disruption of OXPHOS results in accumulation of intermediate metabolites which are used for other immunological purposes. The situation is further complicated by intracellular pathogens that compete for host resources or even manipulate metabolic pathways for their own gain. To combat this, hosts have evolved mechanisms to restrict the availability of certain metabolites to suppress pathogen growth. The following studies were undertaken to determine the interplay between DCs and *Leishmania* and *Toxoplasma*. A polyomics approach comprising of transcriptomic and metabolic analyses validated with functional assays was employed to investigate the effect of *L. mexicana* or *T. gondii* on the BMDC phenotype. The data observes transcript and metabolic changes including aerobic glycolysis and reduced oxidative phosphorylation demonstrating the Warburg effect. Consistent with this, LDH activity was upregulated and mitochondrial membrane potential reduced in *L. mexicana* and *T. gondii* infected BMDC cultures. In addition, certain changes to BMDC metabolism would appear to be parasite evolved to promote their growth and survival. In *L. mexicana* infected BMDCs, accumulation of itaconate (a TCA intermediate) could be associated with the reduction of pro-inflammatory cytokine production. Furthermore, changes in arginine metabolism including

upregulation of arginase, ornithine and proline production were observed in *T. gondii* infected BMDCs and are likely to reflect the coevolution of parasite and host. These results highlight the complex interplay of host and parasite metabolism with the developing immune response in BMDCs.

Contents

Title page…… I

Copyright……..….II

Acknowledgements…..…….III

Abstract……....IV-V

Contents……..……VI-X

List of Figures……..…….X-XII

List of Tables……..XII-XIII

Abbreviations……XIV-XVI

Chapter 1. 1

Introduction..... 1

1.1 Metabolic reprogramming of innate immune cells..... 2

1.1.1 Energy metabolism within innate immune cells..... 2

1.1.2. History of the Warburg effect 4

1.2. Macrophage metabolic reprogramming during an immune response..... 7

1.2.1. General Overview of Macrophage activation 7

1.2.2. Metabolic reprogramming of macrophages 8

1.3. Dendritic cell metabolic reprogramming during an immune response..... 11

1.3.1. Overview of dendritic cell activation 12

1.3.2. Evidence of metabolic reprogramming in DCs. 14

1.3.2.1 Differentiation 14

1.3.2.2. Resting 15

1.3.2.3. Activation..... 15

1.4. Changes in the immune cell metabolome can influence effector function..... 17

1.5. Metabolic Reprogramming of Dendritic cells during infections 18

1.6 Overview of intracellular parasitism..... 19

1.7 Toxoplasma gondii 21

1.7.1 The discovery of *Toxoplasma gondii* 21

1.7.2 Epidemiology..... 21

1.7.3 Transmission..... 22

1.7.4 Life cycle **22**
1.7.5 Outcome of disease **25**
1.7.6. General overview of the innate host response to *T. gondii.* **28**
1.7.6.1. Host cell infection 28
1.7.6.2. Innate immunity 28
1.7.6.3. *Toxoplasma* subverts the innate immune response 32

1.8. *Leishmania* **34**
1.8.1 Discovery of *Leishmania* **34**
1.8.2 Epidemiology **34**
1.8.3 Transmission **35**
1.8.4 Life cycle **35**
1.8.5 Disease outcome **36**
1.8.6 General overview of the innate host response to *Leishmania* **38**
1.8.7 The immune response to Leishmania is dependent on parasite strain and host genetic background **42**

1.9. Metabolic reprogramming in response to *Leishmania* and *Toxoplasma* **45**

1.10. PI3K – Akt – mTOR pathway regulation during host cell metabolism **46**
1.10.1. Pathway overview **46**
1.10.2. Evidence of *L. mexicana* or *T. gondii* modulating PI3K-AKT-mTOR pathway **51**

1.11. Experimental techniques for investigating cellular metabolism **52**
1.11.1. Liquid chromatography mass spectroscopy **52**
1.11.2. RNA-sequencing **55**
1.11.3. The multi-omics approach: combining transcriptomics with metabolomics **56**

1.12. Aims and Objectives **58**

Chapter 2 ..... **60**

Materials and Methods **60**
2.1. Animals **61**
2.2 *Leishmania* Culture **61**
2.3. Maintenance of *Toxoplasma gondii in vitro* **62**
2.4. Soluble *Leishmania* antigen (SLA) and Tachyzoite lysate antigen (TLA) preparation. **62**
2.5. CFSE labelling of *L. mexicana* or *T. gondii* parasites **63**
2.6. BMDC Culture **63**
2.7. Stimulation of BMDCs **64**
2.8. Co-culturing of BMDCs with parasites **65**
2.9. Extraction for Liquid chromatography mass spectroscopy **65**
2.10 LCMS (University of Strathclyde) **65**
2.11. LCMS (Glasgow polyomics) **67**
2.12. Data processing **68**

2.13. Metabolite identification 68
2.14. Data analysis 69
2.15. Transcriptomics 69
2.16. Flow Cytometry 70
2.17. ELISA 72
2.18. Assaying cell supernatant nitric oxide 73
2.19. Arginase assay 73
2.20. 2-NBDG uptake assay 74
2.21. Lactate dehydrogenase assay 74
2.22. Mitochondrial Staining 75
2.23. Cytokine bead array (CBA) 76

Chapter 3 78

Dendritic cells have a spectrum of activation states with distinct overlapping metabolic profiles 78

3.1 Introduction 79

3.2. Results 82
3.2.1 Dendritic cell morphology, CD40 and IL-12 levels vary according to activation stimuli 82
3.2.2 Dendritic cells undergo holistic changes in metabolism according to activation stimuli 84
3.2.3 Metabolic pathways of interest 92
3.2.3.1 Glycolysis 93
3.2.3.2. TCA cycle 97
3.2.3.3. Pentose phosphate pathway 100
3.2.3.4. Arginine metabolism 103
3.2.4. Activation stimuli alters glucose uptake in BMDCs. 106
3.2.5. BMDC iNOS expression and NO production is influenced by activation stimuli 111

3.3 Summary Table and Discussion 113

Chapter 4 119

***Leishmania mexicana* and *Toxoplasma gondii* metabolic reprogramming of dendritic cells** 119

4.1 Introduction 120

4.2 Results 122
4.2.1 Dendritic cells effectively internalise *L. mexicana* and *T. gondii* parasite during infection. 122
4.2.2 Dendritic cell activation markers are influenced by *L. mexicana* and *T. gondii* infection 124
4.2.3. IL-12 production is not altered in BMDCs infected with *L. mexicana* or *T. gondii* 126

4.2.4. Dendritic cells undergo distinct but overlapping global metabolic changes when activated with LPS or co-cultured with either *L. mexicana* or *T. gondii*.....128
4.2.5. Metabolic pathways of interest 137
4.2.5.1 Glycolysis 137
4.2.5.2 TCA cycle..... 140
4.2.5.3 Pentose phosphate pathway 143
4.2.6. *T. gondii* but not *L. mexicana* increased glucose uptake (via 2-NBDG) in dendritic cells.....146
4.2.7. *L. mexicana* and *T. gondii* up- regulate LDH activity in BMDCs 148
4.2.8. Mitochondrial morphology and mitochondrial membrane potential changes during BMDC activation and parasite infection. 150
4.2.8.1 Mitochondrial morphology..... 150
4.2.8.2. Mitochondrial membrane potential 153
4.2.9. *L. mexicana* and *T. gondii* direct BMDC arginine metabolism toward different metabolic 'end goals' to LPS stimulation 157
4.2.9.1 Intracellular iNOS expression is not altered in BMDCs cultures infected with *T. gondii* or *L. mexicana.*..... 157
4.2.9.2. BMDCs upregulate arginase-1 activity in response to *T. gondii* but not *L. mexicana*. 159
4.2.9.3. Both *L. mexicana* and *T. gondii* alter the relative intensity of arginine metabolism intermediates but not NO production. 161
4.3. Summary Table and Discussion.....164

Chapter 5 172
***Leishmania mexicana* and *Toxoplasma gondii* alter the transcriptome of dendritic cells 172**
5.1 Introduction 173
5.2. Results.....174
5.2.1. High quality transcriptomic data was obtained for dendritic cells activated with LPS or co-cultured with either *L. mexicana* or *T. gondii* 174
5.2.2. Dendritic cells undergo distinct but overlapping holistic transcript changes when activated with LPS or co-cultured with either *L. mexicana* or *T. gondii*.....176
5.2.3. Using the cytokine profile of DCs stimulated with LPS or co-cultured with *L. mexicana* and *T. gondii* to further validate the reliability of the transcriptomic data.....190
5.2.4. The activation profile of LPS activated BMDCs is different to that of *L. mexicana* or *T. gondii* infected BMDC cultures.....193
5.2.5. Metabolic pathways of interest 196
5.2.5.1 Glycolysis 196
5.2.5.2 TCA cycle..... 199
5.2.5.3 Oxidative phosphorylation 202
5.2.5.4 Pentose phosphate pathway 208
5.2.5.5. Arginine metabolism 211

5.2.6. Transcriptomic analysis of signalling pathways in LPS activated and parasite infected BMDC cultures.....214
5.2.6.1. PI3K-AKT-mTOR signalling pathway..... 214
5.2.6.2. Nuclear receptor Nur77 (nr4a1 transcript) as a key transcriptional regulator during BMDC metabolic reprogramming with intracellular protozoan parasites. 217
5.3. Summary Table and Discussion.....220

6. General discussion.....229

7. References.....242

8.Appendix.....271

List of Figures

Figure 1.1. Cellular metabolism.....4
Figure 1.2. Metabolic reprogramming of classical or alternatively activated macrophages.....11
Figure 1.3. A schematic depicting the *Toxoplasma* gondii life cycle. 25
Figure 1.4. The immune response to *T. gondii*.....32
Figure 1.5. A schematic depicting the *Leishmania* spp life cycle 36
Figure 1.6. The immune response to *Leishmania* spp 43
Figure 1.7. PI3K-AKT-mTOR signalling 50

Figure 3.1. CD40 expression, IL-12 production and morphology changes in BMDCs stimulated with different activation stimuli.....83
Figure 3.2 Orthogonal Projections to Latent Structures Discriminant Analysis of BMDCs with different activation stimuli. 86
Figure 3.3. Global metabolic activity of BMDCs treated with LPS, IFN-γ or IL-4 92
Figure 3.4. Glycolysis differences in LPS, IFN-γ or IL-4 stimulated BMDCs .96
Figure 3.5. TCA cycle changes in LPS +/- IFN-γ and IL-4 activated BMDCs 99
Figure 3.6. Pentose phosphate pathway (PPP) differences in BMDCs treated with different activation stimuli.....102
Figure 3.7. Arginine metabolism changes BMDCs stimulated with LPS, IFN-γ or IL-4. 105
Figure 3.8. Optimising the concentration and length of time 2-NBDG can be exposed to BMDCs 108
Figure 3.9. Glucose uptake is altered in LPS (+/- IFN-γ) and IL-4 treated BMDCs. 110
Figure 3.11. iNOS expression is up-regulated and NO production is increased during BMDC activation. 112

Figure 4.1. BMDCs effectively internalise *L. mexicana* or *T. gondii* parasites 123
Figure 4.2. *L. mexicana* or *T. gondii* alters the cellular activation of BMDCs 125
Figure 4.3. *L. mexicana* or *T. gondii* do not modulate the IL-12 production of BMDCs. 127
Figure 4.4. Orthogonal Projections to Latent Structures Discriminant Analysis of BMDCs co-cultured with *L. mexicana* or *T. gondii* 130
Figure 4.5. Global metabolic activity of BMDCs activated with LPS or co-cultured with *L. mexicana* or *T. gondii*. 135
Figure 4.6. Glycolysis differences in *L. mexicana* or *T. gondii* co-cultured BMDCs 139
Figure 4.7. TCA cycle changes in BMDCs infected with parasites 142
Figure 4.8. Pentose phosphate pathway (PPP) differences in BMDCs infected with *L. mexicana* or *T. gondii*. 145
Figure 4.9. Determining glucose uptake in BMDCs exposed to *L. mexicana* or *T. gondii* using glucose analog, 2-NBDG 147
Figure 4.10. *L. mexicana* and *T. gondii* modulate Lactate dehydrogenase activity (LDH) in BMDCs 149
Figure 4.11. LPS activation but not parasite infection alters mitochondria morphology within BMDCs 152
Figure 4.12. LPS activation and parasite infection decreases mitochondria membrane potential within BMDCs 156
Figure 4.13. Intracellular iNOS expression is not altered in BMDCs infected with *L. mexicana* or *T. gondii* 158
Figure 4.14. BMDCs up-regulate Arginase-1 expression in response to *T. gondii* but not *L. mexicana* 160
Figure 4.15. Arginine metabolism and Nitric oxide changes in parasite treated dendritic cells 163

Figure 5.1. Orthogonal Projections to Latent Structures Discriminant Analysis of transcript changes in BMDCs activated with LPS or co-cultured with *L. mexicana* or *T. gondii*. 177
Figure 5.2. mRNA and protein levels of cytokines expressed by BMDCs when stimulated with LPS or co-cultured with *L. mexicana* or *T. gondii* 192
Figure 5.3. Changes in expression in the mRNA levels of co-stimulatory molecules when stimulated with LPS or co-cultured with *L. mexicana* or *T. gondii* 195
Figure 5.4. LPS activation or infection with *L. mexicana* or *T. gondii* changes the expression of genes encoding enzymes of the glycolysis pathway 198
Figure 5.5. mRNA changes to enzymes regulating TCA cycle in LPS activated and parasite co-cultured BMDCs. 201
Figure 5.6. mRNA changes to enzymes regulating ETC in LPS activated and parasite co-cultured BMDCs 205
Figure 5.8. LPS activation or infection with *L. mexicana* or *T. gondii* changes the expression of mRNA levels encoding enzymes of the PPP 210

Figure 5.9. Changes in arginine metabolism mRNA transcripts in LPS activated or parasite treated BMDCs 213
Figure 5.10. Transcriptomic analysis of PI3K-AKT-mTOR pathway in LPS activated and parasite infected BMDC cultures 216
Figure 5.11. Transcriptomic analysis of Nur77 as a key transcriptional regulator during BMDC metabolic reprogramming with parasites. 219

Figure 6.1. BMDC metabolic reprogramming upon LPS stimulation. 232
Figure 6.2. BMDC metabolic reprogramming during *L. mexicana* infection. 239
Figure 6.3. BMDC metabolic reprogramming during *T. gondii* infection. 240
Figure 6.4. Proposed anti-inflammatory effects of parasites……..234

Figure 8.1 Orthogonal Projections to Latent Structures Discriminant Analysis of BMDCs stimulated with LPS, IFN-γ or IL-4. (Biological run 2).....272
Figure 8.2. Orthogonal Projections to Latent Structures Discriminant Analysis of DCs co-cultured with *L. mexicana* or *T. gondii* (Biological run 2 and run 3). 286
Figure 8.3. Global metabolic activity of DCs treated with TLA, SLA or co-cultured with PFA fixed *L. mexicana* or *T. gondii*. 302

List of Tables

Table 1.1. *Leishmania* species used in Research.....37

Table 2.1. Flow Cytometry Antibodies.....71
Table 2.2. ELISA Antibodies 72

Table 3.1. VIP score of BMDCs treated with LPS, IFN-γ , LPS + IFN-γ or IL-4 87
Table 3.2 Summary of Findings 113

Table 4.1. VIP scores of BMDC cultures activated with LPS or infected with *L. mexicana* or *T. gondii* 131
Table 4.2 Summary of Findings 164

Table 5.1. High quality transcriptomic data was obtained for BMDC activated with LPS or co-cultured with either *L. mexicana* or *T. gondii* [1] 175
Table 5.2. VIP Score of transcript expression changes in LPS activated BMDC cultures or infected with *L. mexicana* or *T. gondii*.....178
Table 5.3. Summary of Findings 220

Table 8.1. VIP scores, formula, m/z ratios and retention times of BMDCs activated with LPS, IFN-γ or IL-4. 273
Table 8.2. Pairwise analysis between LPS activated and naïve BMDCs...277
Table 8.3 Pairwise analysis between IFN-γ treated and naïve BMDCs 278

Table 8.4. Pairwise analysis between LPS + IFN-γ stimulated and naïve BMDCs 279
Table 8.5. Pairwise analysis between IL-4 treated and naïve BMDCs.....281
Table 8.6. VIP score of BMDCs treated with LPS, IFN-γ, LPS+IFN-γ or IL-4 (Biological run 2) 283
Table 8.7. VIP scores, formula, m/z ratios and retention times of DCs activated with LPS or infected with *L. mexicana* or *T. gondii* (Biological run 1). 287
Table 8.8. Pairwise analysis between LPS stimulated and naïve BMDCs..290
Table 8.9. Pairwise analysis between *T. gondii* infected and naïve BMDC cultures 291
Table 8.10. Pairwise analysis between *L. mexicana* infected and naïve BMDC cultures 292
Table 8.11. VIP scores of DCs activated with LPS or infected with *L. mexicana* or *T. gondii* (Biological run 2). 294
Table 8.12. VIP scores of DCs activated with LPS or infected with *L. mexicana* or *T. gondii* (Biological run 3) 295
Table 8.13. Pairwise analysis of transcripts between LPS stimulated and naïve BMDCs 303
Table 8.14. Pairwise analysis of transcripts between *T. gondii* infected and naïve BMDC cultures. 315
Table 8.15. Pairwise analysis of transcripts between *L. mexicana* infected and naïve BMDC cultures. 325

Abbreviations

ΔΨ	Mitochondrial membrane potential
2-DG	2-deoxyglucose
5-LO	5-lipoxygenase
AASS	Aspartate-arginosuccinate shunt
ADP	Adenosine diphosphate
AKT	Protein kinase B
AMPK	5'-adenosinemonophosphage activated protein kinase
APC	Antigen presenting cells
Arg1	Arginase-1
ANOVA	Analysis of variance
ATP	Adenosine triphosphate
BMDC	Bone marrow-derived dendritic cell
BSA	Bovine serum albumin
°C	degree celsius
CARKL	Carbohydrate kinase-like protein
CD	Cluster of differentiation
cDNA	Complementary DNA
CFSE	5,6-carboxyfluorescein diacetate succinimidyl ester
CIC	Mitochondrial citrate carrier
CO2	Carbon dioxide
COX	Cyclooxygenase
cRPMI	Complete RPMI
DC	Dendritic cell
DMEM	Dulbecco's Modified Eagle's Medium
DMSO	Dimethyl sulfoxide
DNA	Deoxyribonucleic acid
EDTA	Ethylenediaminetetraacetic acid
ELISA	Enzyme-linked immunosorbent assay
ETC	Electron transport chain
FACS	Fluorescence-aided cell sorting
FADH2	Flavin adenine dinucleotide
FBS	Foetal bovine serum
FLUC	Strain of Type II *Toxoplasma gondii*
G6P	Glucose-6-phosphate
GFP	Green Fluorscent protein
GLUT	Glucose transporter
GM-CSF	Granulocyte-monocyte colony stimulating factor
Gp63	Glycoprotein 63
H2SO4	Sulfuric acid
HIF-1α	Hypoxia-inducible Factor alpha
HK1	Hexokinase 1
HRE	Hypoxia Response Element
HRP	Horseradish peroxidase
IDH	Isocitrate Dehydrogenase
IFN	Interferon
Ig	Immunoglobulin

IKK	Inhibitor of NFκB kinase
IL	Interleukin
iNOS	Inducible nitric oxide synthase
IRAK	IL-1R associated kinase
Irg1	Immune responsive gene 1
JNK	Jun N-terminal kinase
kDa	Kilodalton
Kg	Kilogram
KO	Knock-out
L. mexicana	*Leishmania mexicana*
LDH	Lactate dehydrogenase
LPS	Lipopolysaccharide
LT	Leukotriene
LXA	Lipoxin
MAPK	Mitogen-activated protein kinase
mg	Milligram
MHC	Major histocompatibility complex
MIP	Macrophage inflammatory protein
ml	Millilitre
mM	millimolar
MMP	Matrix metalloproteinase
MOI	Multiplicity of infection
mRNA	Messenger RNA
mROS	Mitochondrial ROS
mTOR	Mechanistic target of rapamycin
mTORC1	mTOR complex 1
MyD88	Myeloid differentiation primary response gene 88
NAD	Nicotinamide adenine dinucleotide
NADP	Nicotinamide adenine dinucleotide phosphate
NFκB	Nuclear factor κ-light chain enhancer of activated B cells
ng	Nanogram
NK	Natural killer
NO	Nitric oxide
NADPH oxidase	Nicotinamide adenine dinucleotide phosphate oxidase
OXPHOS	Oxidative phosphorylation
PAMP	Pathogen-associated molecular pattern
PBMC	Peripheral blood mononuclear cell
PBS	Phosphate buffered saline
PCR	Polymerase chain reaction
PDK3	Pyruvate dehydrogenase kinase 3
PFA	Paraformaldehyde
PFK2	Phosphofructokinase-2
PG	Prostaglandin
PGE2	Prostaglandin E2
PHD2	Prolyl hydroxylase 2
PI	Propidium iodide
PI3K	Phosphoinositide 3-kinase
PKM2	Pyruvate kinase M2

PL	Proton leak
PPAR	Peroxisome proliferator-activated receptor
PPP	Pentose phosphate pathway
PRR	Pattern recognition receptor
RET	Reverse electron transport
RNA	Ribonucleic acid
RNS	Reactive nitrogen species
ROS	Reactive oxygen species
RPMI-1640	Roswell Park Memorial Institute-1640 medium
rRNA	Ribosomal RNA
RT-qPCR	Quantitative reverse transcription PCR
SDH	Succinate dehydrogenase
S.E.M	Standard error of the mean
SNP	Single nucleotide polymorphism
SLA	Soluble *Leishmania* antigen
SRC	Spare respiratory capacity
STAT	Signal transducer and activator of transcription
T. gondii	*Toxoplasma gondii*
TCA	Tricarboxylic acid
TGF-β	Transforming growth factor-β
Th	T helper
TLA	*Toxoplasma* lysate antigen
TLR	Toll-like receptor
TMRM	Tetramethylrhodamine, methyl ester perchlorate
TNF-α	Tumour necrosis factor-α
TNFR1	TNF-α receptor 1
TRAF6	TNF receptor associated factor 6
WT	Wild type
μg	Microgram
μl	Microlitre
μm	Micrometre

Chapter 1.

Introduction

1.1 Metabolic reprogramming of innate immune cells

1.1.1 Energy metabolism within innate immune cells

Cellular energy metabolism is responsible for the production of ATP which is used in all energy dependent processes within cells (Erecinska *et al*., 1982; Rolfe *et al*., 1997). In the most simplistic form, this can be produced through glycolysis in the cytosol and yields 2 ATP molecules. Pyruvate is made as a by-product of this process and in anaerobic conditions it is fermented to lactate (Berg *et al*., 2002). In aerobic conditions, pyruvate can be fed into the TCA cycle located within the mitochondria to produce 36 ATP molecules. This is dependent on a functioning electron transport chain and this entire process is termed, oxidative phosphorylation (Reviewed in Buck *et al*., 2017).

Glycolysis and therefore ultimately oxidative phosphorylation, are dependent on the uptake of extracellular glucose via 14 glucose transporters (GLUT 1-14) (Figure 1.1). Glucose is irreversibly converted into glucose-6-phosphate by hexokinase (HK) (Berg *et al*., 2002) and through an additional ten enzymatic steps to the end-product pyruvate in the cytosol. This process requires Nicotinamide adenine dinucleotide (NAD^+) to proceed and yields 2 molecules of ATP. From here, pyruvate enters into the mitochondria where it is decarboxylated to acetyl coA. Acetyl coA can then be fed into the TCA cycle where reducing equivalents NADH and Flavin adenine dinucleotide ($FADH_2$) (Berg *et al*., 2002) are generated from a series of enzyme catalysed reactions. NADH and $FADH_2$ are essential during energy generation as they act as electron donors for complex I and complex II of the ETC, which is located on

the inner mitochondrial membrane (Cooper, 2000). Using redox reactions, electrons are transported from complex to complex until complex IV where the electrons are transferred to a molecule of oxygen, generating water. The transport of electrons down the ETC, creates energy necessary to pump protons (H^+) into the mitochondrial inter-membrane space. This creates a 'mitochondrial membrane potential' which complex V (also termed, ATP synthase) can use to drive the ATP production. At this point, H^+ are also returned back across the membrane (Berg *et al*., 2002) (Reviwed by Buck *et al*., 2017).

Cells under low oxygen (hypoxic) conditions cannot utilise OXPHOS and use anaerobic glycolysis instead. This pathway is signficantly less efficient (Pearce & Pearce, 2013). Instead of entering the TCA cycle as acetyl-coA, pyruvate is converted into lactate by lactate dehydrogenase (LDH). Excess lactate is then exported from the cell via monocarboxylate transporters. This conversion from pyruvate to lactate is necessary to allow NAD+ to be replenished from NADH. This is essential for further anaerobic glycolysis (Figure 1.1) (O'Neill *et al*., 2016).

Not surprisingly, approximately 95% of a naïve immune cell's energy is generated via oxidative phosphorylation under normoxic conditions. However, it has now been shown that under certain conditions, immune cells favour ATP production by glycolysis, even in an oxygenated environment. This is known as aerobic glycolysis or 'the Warburg effect'. This change to fundamental energy metabolism has important functional benefits for the immune cell (Everts *et al*., 2012; Everts *et al*., 2014; Krawcyzk *et al*., 2010).

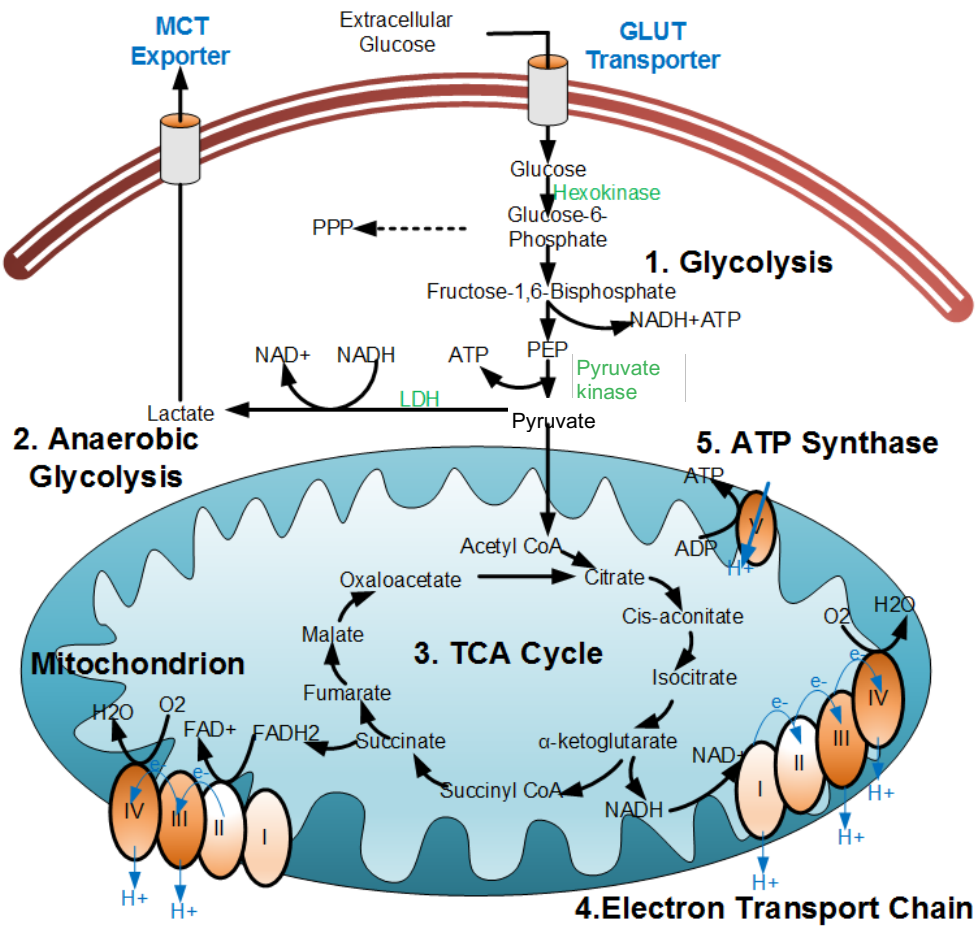

Figure 1.1. Cellular metabolism (1) Glucose is taken up via glucose transporters (GLUT) and metabolised to pyruvate via the glycolysis pathway. This generates a small amount of energy. (2) In hypoxic conditions, anaerobic glycolysis occurs where pyruvate is metabolised to lactate. (3) In oxygenated environments, pyruvate enters the mitochondria and is catabolised to acetyl-coA, which is then fed into the TCA cycle. The TCA generates NADH and FADH2 which transfer electrons to the electron transport chain (ETC) (Complexes I and II) (4) Transfer of electrons through the ETC will generate energy to pump hydrogen ions across the inner mitochondrial membrane creating a mitochondrial membrane potential. (5) The mitochondrial membrane potential is used by ATP synthase to generate large amounts of ATP.

1.1.2. History of the Warburg effect

The Warburg effect was a concept first introduced by Otto Warburg in 1924 when characterising the metabolic profile of cancerous tumours under normoxic conditions (Warburg *et al*., 1925; Warburg *et al*., 1927). He found that within these tumours, glycolysis dominates even though sufficient oxygen is still available for oxidative phosphorylation to continue. Warburg devoted most of his life to understanding why a tumour cell, that could consume adequate oxygen would use the less efficient glycolysis pathway. However, after many years of research, Otto Warburg believed that this was a unique characteristic of tumour cells and dismissed reports from other researchers who described aerobic glycolysis in white blood cells. Warburg deemed these descriptions as just artefacts of the immune cell preparation method, not realising that white blood cells were becoming unintentionally activated in these studies, subsequently changing their metabolic profile. (Warburg *et al*., 1958; Reviewed Koppenol *et al*., 2011).

The concept of the Warburg effect re-surfaced briefly in the 1950s with the discovery that glucose consumption was high, but oxygen intake was poor in LPS activated neutrophils (Sbarra *et al*., 1959). Although, this was the first time the Warburg phenomenon had been published in another cell type, this research went largely unnoticed. It was not until almost 20 years later, when Hard and Newsholme individually investigated the metabolism of the macrophage (Hard *et al*., 1970; Newsholme *et al*, 1986; Newsholme *et al*., 1987) and showed very similar findings to

those of the tumour cells and the neutrophils, that the Warburg effect was fully accepted that upon activation, oxidative phosphorylation switched to aerobic glycolysis (Gurthrie *et al*., 1984; Borregaard *et al*., 1987).

Recently researchers have re-discovered this area of immunology and termed the field 'Immunometabolism' (O'Neill *et al*., 2011 and Pearce *et al*., 2013). This emerging field describes the bi-directional interplay between immunity and metabolism and links the impact the immune response has on metabolic diseases with how changes in metabolism (and diseases) influence immune effector function. New technology such as liquid chromatography mass spectroscopy (LCMS), gas chromatography mass spectroscopy (GCMS) and Nuclear Magnetic Resonance (NMR) in tandem with increased computing power can detect, identify and measure metabolites with high specificity (Reviewed in Kaddurah-Daouk *et al*., 2008; Kaddurah-Daouk *et al*, 2009). Furthermore, this has allowed the mechanism behind these metabolic changes to be investigated and their impact on the immune response studied. Pioneering work by the Pearce laboratory and O'Neill *et al* demonstrates the mounting evidence for immune-metabolic interplay at the molecular, cellular, organ and organism levels (Everts *et al*., 2012; Everts *et al*., 2014; O'Neill *et al*., 2016). In line with the work presented in this thesis, the following literature review focuses on how changes in metabolic profile can impact the function of two important immune cells, macrophages and dendritic cells both proximally and distally.

1.2. Macrophage metabolic reprogramming during an immune response

1.2.1. General Overview of Macrophage activation

Studies have demonstrated a spectrum of activation exists in macrophages that is dependent on the stimuli they encounter in their environment (Gordon, 2003; Mosser and Edwards, 2008). Nomenclature of these phenotypes is complex and often contradictory. The vast majority of the literature divides macrophages broadly into M1 (classical activation) and M2 (alternative activation). Stimulation with LPS (sometimes termed innate activation) or LPS in combination with IFN-γ (termed classical activation) is generally associated with nitric oxide synthase (iNOS) activity and the production of reactive oxygen species (ROS) (Rattigan *et al*., 2018). However, LPS stimulation in the absence of IFN-γ is also known to induce arginase expression and cause arginine depletion and polyamine production. Whereas the addition of IFN-γ inhibits arginase (Menzies *et al*.,2009). Cellular activation by LPS + IFN-γ induces antimicrobial immunity and inflammatory responses (Gordon, 2003).

In comparison, IL-4 and IL-13, both IL-4Rα ligands, stimulate what is termed as 'alternative' or M2 activation of macrophages. These cells produce anti-inflammatory cytokines (IL-10 and TGF-β), can suppress ROS production and express arginase at high levels. This competes with iNOS for L-arginine which is their common substrate and thus reduces nitric oxide production. IL-4 and IL-13 stimulated macrophages are associated with wound healing, disease resolution and sometimes humoral immunity (Gordon, 2003; Odegaard *et al*., 2008; Rodriguez-Prados *et al* 2010., Stout & Suttles, 2004).

The above phenotypic differences in the metabolism of macrophages have been well studied largely due to the immunological importance of these processes, but more recent studies have concentrated on additional metabolic pathways (Stout & Suttles, 2004; Mosser & Edwards, 2008; Stein *et al*., 1992).

1.2.2. Metabolic reprogramming of macrophages

Metabolic reprogramming in macrophages has mostly been studied following LPS stimulation. LPS stimulation is primarily associated with a switch from OXPHOS to aerobic glycolysis even in an oxygenated environment (often referred as the Warburg effect) (Reviewed in Van den Bossche *et al*., 2017). Studies demonstrate that this enhanced glycolytic flux is correlated with a change to their functions (Lachmandas *et al*., 2016; Blagih *et al*., 2012). Upon TLR activation, this switch in the metabolic profile of macrophages supports phagocytosis, antigen processing and cytokine production (Aderem *et al*., 2000). This has consequences for distal immune responses including T cell activation. This benefits the immune response by rapidly generating ATP and utilising TCA intermediates for other immune mediator purposes (Jha *et al*., 2015; Vats *et al*., 2006; El Kasmi *et al*., 2015).

Evidence shows that upon metabolic reprogramming to aerobic glycolysis in LPS stimulated macrophages there is an increase in the transcription of many glycolytic and glucose transport enzymes (Figure 1.2) (Papandreou *et al*., 2006; Kim *et al*., 2006; Semenza *et al*., 1996; Duvel *et al*., 2010). TLR-activated macrophages express highly active isoforms of phosphofructokinase (u-PFK2) and pyruvate kinase (PKM2),

promoting glycolytic flux. Activated macrophages express two isoforms of PKM. PKM1 is constitutively expressed and metabolises phosphoenolpyruvate to pyruvate during glycolysis. PKM2, however, functions to re-direct intermediates of the glycolysis pathway to other biosynthesis pathways not the TCA cycle, reducing the conversion of pyruvate into the 'waste-product' lactate (Rodriquez-Prados *et al*., 2010; Galvan-Pena & O'Neill, 2014).

With less pyruvate being converted to acetyl-coA the TCA cycle activity in the mitochondria are reduced, Jha *et al* observed through a multi-omics approach (RNA-seq-based profiling and mass spectroscopy-based analysis) that two functional breaks happen in TCA cycle of macrophages stimulated with LPS for 24 hours (Jha *et al*., 2015). These break-points included the isocitrate to α -ketoglutarate conversion step (catalysed by isocitrate dehydrogenase) and succinate to malate conversion step (catalysed by succinate dehydrogenase). These breaks led to the accumulation of the TCA intermediates succinate, citrate and isocitrate with possible consequences to the functional phenotype of the cell (Tannahill *et al*., 2013; Jha *et al*., 2015; Infantino *et al*., 2011).

In order to compensate for these TCA cycle 'breaks', glutaminolysis, β-oxidation (Tannahill *et al*., 2013), the aspartate-arginosuccinate shunt (AASS) and the pentose phosphate pathway (PPP) were increased (Jha *et al*., 2015). It has been proposed that up-regulation of these latter pathways can help replenish the intermediates of the TCA cycle at these specific 'break' points or provide an alternative metabolite that can be used instead. For example, ribose-5-phosphate and erythrose-4-phosphate can be used

in the synthesis of nucleotides or amino acids. Additionally, the PPP is seen as a much-needed source of reducing equivalents in the form of NADPH (Haschemi *et al*., 2012).

Finally, down-regulation of oxidative phosphorylation from the electron transport chain is observed in LPS-stimulated macrophages (Brown, 1999; Reviewed in Rambold *et al*., 2017). Studies theorise that excess nitric oxide produced from the conversion of arginine to citrulline via inducible nitric oxide synthase (iNOS) might possibly lead to NO-mediated nitrosylation of electron transport chain components, decreasing mitochondrial membrane potential and activity (Brown, 1999; Reviewed in Everts *et al*., 2012).

This is substantially different to the metabolic reprogramming that occurs in IL-4 and IL-13 treated macrophages (Figure 1.2). In these cells, the switch from oxidative phosphorylation to aerobic glycolysis is not observed. Studies demonstrate that macrophages stimulated with these cytokines express less enzymatically-active forms of many glycolytic enzymes e.g. PFKB1 (Rodriquez *et al*., 2010; Galvan-Pena & O'Neill, 2014). The PPP is also down-regulated due to increased expression in the PPP inhibitor CARKL (Haschemi *et al*., 2012).

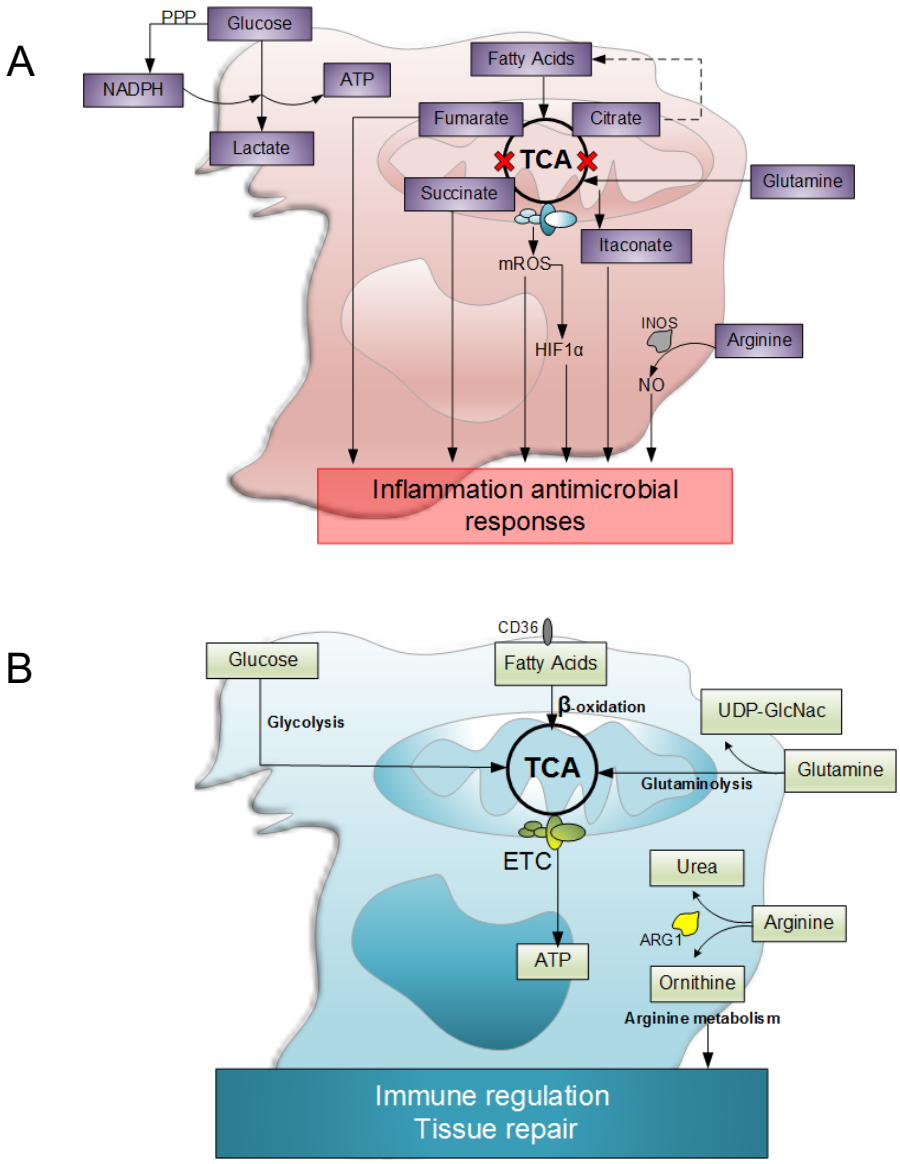

Figure 1.2. Metabolic reprogramming of classical or alternatively activated macrophages. (A) Classically activated macrophages induce aerobic glycolysis which results in lactate production and increased levels of TCA intermediates. Upon activation, the HIF-1α transcription factor can drive pro-inflammatory cytokine production. In addition, arginine is diverted to citrulline and NO in this inflammatory phenotype (B) Alternatively activated macrophages utilise oxidative phosphorylation and fatty acid β-oxidation. Arg1 drives the production of arginine to ornithine and polyamines.

1.3. Dendritic cell metabolic reprogramming during an immune response

1.3.1. Overview of dendritic cell activation

Dendritic cells are the main antigen presenting cell within the immune system capable of providing a bridge between the innate and adaptive immune response. Prior to maturing, naïve DCs migrate throughout host tissues acting as sentinel cells. However, once a DC has encountered a pathogen, it migrates through the lymphatic vessels to present the antigen to specific T cells within the spleen or the lymph node. During this process the DC undergoes maturation, characterised by up regulation of co-stimulatory molecules (including CD40, CD80, CD86) and activates the T cell. Furthermore, DCs are pivotal in the differentiation and polarisation of T cells into different sub-types (Reviewed in Steinman *et al*., 2006).

There are a number of distinct DC sub-types each with a unique ability to process, traffic, or present antigens to T cells. Dendritic cells can be derived from both myeloid and lymphoid lineage progenitors expanding the heterogeneity of this cell type. 'Classical DCs' are found in secondary lymphoid organs and can be characterised depending on which surface markers they express upon activation (Saas *et al*., 2017). $CD11c^+$ DCs specialise in cytokine and $CD4^+$ T cell activation whilst $CD8^+$ DCs are necessary for cross presentation of exogenous antigens and are potent activators of $CD8^+$ T cells. Upon stimulation, other classical DC subsets also exist including tolerogenic DCs, $CD1a^+$ DCs and thymic DCs.

In contrast, non-classical DC subsets are present in non-lymphoid organs and blood and are required to survey the peripheral immune system and respond to infection. Two distinct subsets include circulating and tissue resident plasmacytoid DCs which produce type I interferons and monocyte derived inflammatory DCs or iDCs (Reviewed in Steinman *et al*., 2006). One notable difference between monocyte derived iDCs (either *in vitro* or *in vivo*) in comparison to classical DC subsets is their ability to express iNOS and are potent producers of NO, mandatory for controlling infections. This difference in NO production is yet just another example of how heterogeneity and metabolism are linked in immune cells.

In comparison to macrophages which are well documented within the literature, there is less information concerning dendritic cells with regards to metabolic reprogramming. *In vitro,* differentiation of DCs from bone marrow results in a relatively pure population of cells that genetically and functionally closely resemble *in vivo* iDCs. As iDCs are thought to be in reserve, rapidly recruited to the site of infection during an immune response, understanding how their metabolism alters from surveying the periphery to responding to infection is essential. However, similar to the macrophage literature there is contradictory nomenclature regarding DC activation with some literature referring to DCs as M1-like or M2-like (Kadowaki *et al*., 2012; Martinez *et al*., 2014). Further studies are clearly needed to unambiguously phenotype DC activation under different conditions.

1.3.2. Evidence of metabolic reprogramming in DCs.

Whilst much is known about the metabolic reprogramming of macrophages following different activation stimuli, the metabolism of DCs have been scarcely studied. This section will highlight what is already known in the literature regarding DC metabolism and what questions remain unanswered.

1.3.2.1 Differentiation

The differentiation of bone-marrow progenitor stem cells into DCs by granulocyte monocyte – colony stimulating factor (GM-CSF) is a highly energy-demanding stage for DCs. Cell differentiation increases the expression of the peroxisome proliferation-activated receptor-γ (PPAR-γ) and its associated molecule, PPARγ co-activator 1α (PGC1α). These molecules are essential in regulating the metabolism of lipids which is necessary for the formation of new mitochondria (Pearce and Everts, 2015). Studies also show the intermediates of the TCA cycle, citrate, isocitrate and α-ketoglutarate all positively correlate with DC differentiation (Pearce and Everts, 2015). Citrate is extremely important in this differentiation process as it can be converted into acetyl-coA, a molecule necessary for the synthesis of fatty acids. Fatty acids can then be used for the formation of membranes, organelles and lysosomes.

1.3.2.2. Resting

Under non-inflammatory conditions, most DCs are found surveying the peripheral tissues in a resting immature state. Resting GM-CSF-induced bone-marrow-derived DCs have (1) few anabolic/catabolic demands, (2) are moderately immobile, (3) do not express many mediators and (4) do not readily interact with T cells (Pearce *et al*., 2013). If necessary, resting DCs can metabolise proteins and triacylglycerols into amino acids and fatty acids which can then fuel oxidative phosphorylation and ATP generation (Pearce and Everts, 2015). Unstimulated DCs also consume glucose, albeit at a much lower level relative to differentiating or activated DCs (McGettrick *et al*., 2013).

1.3.2.3. Activation

Activation of DCs during inflammation is initially demonstrated by elevated glucose uptake and increased production of lactate (McGettrick *et al*., 2013). As mentioned previously, this is consistent with the Warburg effect which solely uses aerobic glycolysis to re-cycle NAD+ and produce ATP (Vander Heiden *et al*., 2010; Krawczyk *et al*., 2010). This altered metabolome is essential during activation where priming T cells, cytokine secretion and migration to the lymph node all require substantial energy (Pearce *et al*., 2013; Cortese *et al*., 2014). Initial studies by Everts *et al* suggest that DCs stimulated with LPS undergo metabolic reprogramming from OXPHOS to sustained aerobic glycolysis over a 12-hour period (Everts *et al*., 2012). Additionally,

research indicates that oxidative phosphorylation is suppressed in an NO-mediated manner in DCs activated with LPS from 6 hours. Nitric oxide inhibits the mitochondrial electron transport chain by nitrosylation of iron-sulphur containing proteins. Briefly, suppression of the ETC (complexes I, II and IV) results in the reversal of ATP synthase (complex V) where protons are delivered out of the intermembrane space in order to maintain membrane potential within the mitochondrion (Pearce *et al*., 2013). This process consumes ATP and is facilitated by glycolysis. This is termed the reverse electron transport where glycolytic-ATP is necessary for cell survival as well as the production of mitochondrial ROS for pathogen destruction.

As during differentiation, fatty acid synthesis and lipid digestion from droplets is also deemed necessary during DC activation. Everts *et al* suggest that fatty acid biosynthesis during cell activation is required for elongation of both the endoplasmic reticulum and the Golgi apparatus. Elongation of the endoplasmic reticulum (ER) is essential in maintaining elevated protein levels necessary for the production of cytokines and other host defence molecules needed to resolve an infection. (Everts *et al*., 2014).

1.4. Changes in the immune cell metabolome can influence effector function

The major metabolomic feature associated with the phenotype of an inflammatory macrophage is the shift from oxidative phosphorylation to aerobic glycolysis. Notably, activation also leads to functional breaks in the TCA cycle (Jha *et al*., 2015). The resultant accumulation of certain metabolites can have a direct impact on the immune response.

The accumulation of succinate has been shown to lead to HIF-1α activation (via inhibition of prolyl hydroxylases). HIF-1α then induces IL-1β directly because the gene promoter for IL-1β contains a HIF-1α binding site (Tannahill *et al*., 2013; reviewed in O'Neill and Pearce, 2016).

The functional TCA break can also result in the build-up of citrate and isocitrate. Accumulated citrate seems to be especially relevant for the production of 3 pro-inflammatory mediators, prostaglandins, NO and ROS. Upon TLR-stimulation, the mitochondrial citrate carrier is up-regulated allowing excess citrate access to the cytosol where it is cleaved by citrate lysase to form acetyl coA and oxaloacetate (Infantino *et al*., 2011). Acetyl coA is an essential precursor of fatty acid and prostaglandin biosynthesis (via arachidonic acid) (Everts *et al*., 2014; Dennis & Norris, 2015). In addition, citrate can generate NADPH via malic acid and pyruvate and this NADPH can either be used by iNOS to generate NO or NADPH oxidase to produce ROS (Segal *et al*., 2012; O'Neill, 2011).

Recently, studies have demonstrated that itaconate is derived from citrate (via cis-aconitate) (Michelucci *et al*., 2012; Strelko *et al*., 2011; Lampropoulou *et al*., 2016). This metabolite has been shown to accumulate and limit pro-inflammatory changes within a macrophage. By inhibiting succinate dehydrogenase and activating Nrf2, itaconate can limit pro-inflammatory mediators (e.g. IL-1β and ROS) and induce type I interferons. In addition, itaconate has been shown to directly block isocitrate lysase (an enzyme used in glycoxylate shunt of bacteria). Inhibiting this shunt has been shown to supress the growth of certain pathogens including the bacteria *Mycobacterium tuberculosis* and the helminth, *Ascaris suum* (Michelucci *et al*., 2012; McFadden *et al*., 1977; Patel & McFadden, 1978). These data provide compelling evidence for itaconate to potentially interfere with other pathogens including parasites within host innate immune cells.

1.5. Metabolic Reprogramming of Dendritic cells during infections

The vast majority of the work described thus far in the literature has used LPS as a surrogate immune activator rather than an actual pathogen. Limited research has been conducted on establishing how the host cell metabolome is altered in any cell type during live infection. Investigating how host cells reprogram their metabolism in response to intracellular pathogens is complex, especially as these pathogens can also alter host cell metabolism for their own survival (Reviewed by Naderer *et al*., 2008). Although, the studies performed with LPS have been extremely informative, the intricacy of establishing the extent to which intracellular pathogens e.g. *L. mexicana* or *T. gondii* reprogram host cell metabolism has not been extensively studied.

1.6 Overview of intracellular parasitism

Parasitism has evolved independently on many occasions over millions of years and in a variety of diverse clades. Even focusing on unicellular organisms, obligate parasites are found in diverse genres including the alveolates (e.g. Plasmodium, *Toxoplasma* and Cryptosporidium), the Discristates (e.g. *Leishmania* and Trypanosoma), the excavates (e.g. Trichomonas and Giardia), the Opisthokonts (e.g. encephalitozoon) and Amoebazoa (e.g. Entamoeba) (Sibley *et al*., 2012). While some of these parasites are extracellular, others inhabit intracellular niches within their host and it has been suggested that the relative few in this group attest to the challenges of making this adaptation (Sibley *et al*., 2011). Obvious challenges include evolving the ability to gain access to the host cell and creating an environment that will sustain life, allow growth, multiplication and eventual transmission. Survival in this environment is dependent on evading the host immune response and on the ability to scavenge nutrients from host cells (Sibley *et al*., 2012; Alexander *et al*., 1999). To facilitate this, parasites have evolved transporters that can increase the availability of critical nutrients in their intracellular niches and can also alter host cell immune responses and metabolism through interfering with signalling cascades and thus subverting cellular processes (Curruthers *et al*., 1997; Butcher *et al*., 2011; Alexander, 1985; Xu *et al*., 2010).

The mammalian hosts have responded to this parasitic infection by evolving appropriate immune responses that limit parasite multiplication and reduce the adverse consequences of infection. It is now recognised that as part of an immune response

there are changes to host cell metabolism. The study of metabolic changes associated with the immune response has recently received a lot of attention and this field is often referred to as 'immunometabolism'. Some of the metabolic changes occurring during an immune response can be considered physiological and serve to provide additional energy or precursors for synthesis of proteins, fatty acids or lipids (Krawcyzk *et al*., 2010; Kelly *et al*., 2015). In some cases, changing levels of metabolites in the local environment can influence or even regulate the developing immune response (Infantino *et al*., 2011; Mills *et al*., 2016; Michelucci *et al*., 2013). Other metabolic changes can be considered as anti-parasitic as they can directly target intracellular parasites by producing effector molecules including RNI and ROI (Wei *et al,* 1995; Calegari-Silva *et al*., 2015). Lastly, metabolic changes can act to prevent parasite multiplication through depleting certain metabolites such as arginine or tryptophan so that they are not available to the parasite (Fox *et al*., 2004; Muleme *et al*., 2009; Silva *et al*., 2002).

Two intracellular protozoan parasites that have evolved independently are the apicomplexan parasite, *T. gondii* and the kinetoplastid parasite, *Leishmania* (Sibley *et al*., 2011; Alexander *et al*., 1999). Both parasites have evolved different invasion mechanisms, biochemical needs and survival strategies, with the host evolving distinct immune responses to these infections. These two parasites are important human pathogens and worthy of study for this alone. However, for the above reasons they provide valuable case studies to investigate how intracellular parasites have evolved mechanisms to alter host metabolism and evade the immune response and of course how hosts have responded.

1.7 *Toxoplasma gondii*

1.7.1 The discovery of *Toxoplasma gondii*

Toxoplasma gondii is an obligate intracellular protozoan parasite from the Apicomplexan subphyla. *T. gondii* was first isolated in 1908 by two individual research groups. Nicolle & Manceaux isolated the parasite from the spleen of a small African rodent known as the *Ctenodactylus gundi* whilst Splendore discovered *T. gondii* in rabbit tissues (Nicolle & Manceaux, 1908; Splendore, 1908). *T. gondii* can infect nearly all warm-blooded animals as it is capable of surviving inside most nucleated cells. However, the parasite can only reproduce in one definitive host, the Felidae family (e.g. domestic cat). From the definite host, *T. gondii* can be transmitted to many various intermediate hosts including humans. Human infection is extremely common and currently affects over 25% of the global population (WHO, 2015).

1.7.2 Epidemiology

The population structure of *T. gondii* is remarkably clonal. The three predominant clonal lineages of *T. gondii* are defined as Type I, II and III. Type I was originally described by Sibley and Cesbron-Delauw (Howe & Sibley *et al*., 1995). Since then, two further clonal lineages designated IV and V have been described (Saeij *et al*., 2005) and further recombinant strains are now recognised. Type 1, exemplified by the RH strain can cause severe disease and death in mice, is generally unable to form cysts and is associated with severe disease in humans (Sibley & Boothroyd, 1992). Type II strains are less virulent in mice and form cysts in their tissues. This clonal lineage is most commonly found in human infections in the Europe and Northern America

(Howe & Sibley, 1995). Type II strains have been widely used in the laboratory and although, type II strains are generally responsible for less severe disease in mice disease progression is ultimately dependent on their genetic background (Brown & Mcleod, 1990). Specifically, MHC 1 haplotype determines whether mice develop toxoplasmic encephalitis, but susceptibility to acute infection can also be affected by route of infection (Mcleod *et al*., 1989).

1.7.3 Transmission

T. gondii can be transmitted to the host via various routes and at different stages of its lifecycle. The most common routes of transmission in humans include eating raw/undercooked meat containing tissue cysts or from food and water that are contaminated with oocysts from the cat's faeces (Su *et al*., 2003). In addition, congenital transmission can typically occur when a women experiences infection for the first time when pregnant. In this scenario, the fast dividing tachyzoites cross the placental barrier (Remington, 1990). In rare cases, congenital toxoplasmosis can occur in previously infected women when the parasite is reactivated during pregnancy. If tachyzoites re-activate and cross the placental barrier during pregnancy, the foetus can develop congenital toxoplasmosis (Andrade *et al*., 2010).

1.7.4 Life cycle

The life cycle of *T. gondii* is extremely complex and can be divided up into the asexual (extra-intestinal) and the sexual (enteroepithelial) stages (Figure 1.3). Both stages normally begin with the ingestion of tissue cysts or oocysts. The extra-intestinal stage of the life-cycle is asexual and can occur in many and potentially any mammalian host. After oral ingestion, the oocysts or tissue cysts release sporozoites or bradyzoites

respectively which invade and infect the gut epithelial cells. Once inside the parasitophorous vacuole of epithelial cells, these infective stages give rise to fast dividing tachyzoites (Dubey, 1998). Within 24-48 hours, these tachyzoites can lyse the epithelial cells freeing them up to spread throughout the body and infect other cells including macrophages, neutrophils, dendritic cells and other epithelial cells within the host. This stage of infection is characterised by the presence of tachyzoites and flu-like illness. known as the acute phase. The chronic phase begins when tachyzoites transform back into bradyzoites which form intracellular cysts in various tissues including muscle (skeletal and cardiac) and neuronal (Dubley & Frenkel, 1976). This transformation from tachyzoites to bradyzoites is associated with the development of a protective host immune response. This process can be triggered by changes in pH, heat shock or inhibition of mitochondrial function. (Lyons *et al*., 2002; Dubey *et al*., 1997). Nutrient starvation would also appear to play a role as arginine deprivation is known to trigger bradyzoite differentiation. It is well-known that tissue cysts containing bradyzoites can persist for life without causing any serious health issues. However, in situations where the host becomes immunocompromised disease reactivation can occur. This is likely due to the occasional rupture of cysts which release bradyzoites that transform to tachyzoites which are then able to multiply in the absence of an intact immune system (Hunter & Reichmann, 2001).

The enteroepithelial stage only occurs in the intestine of felines and consist of asexual and sexual multiplication. Similar to the extra-intestinal stages, tissue cysts that are consumed release bradyzoites which infect epithelial cells after digestion (Dubey *et al*., 1997). However, at this stage, the parasite divide through multiple rounds of

schizogony to produce merozoites. Merozoites can then infect new cells where they undergo gametogenesis to develop into macrogametes and microgametes. The microgamete then fertilises the macrogamete forming a zygote. Eventually these zygotes develop into oocysts. As this process occurs in the gut ileum of a cat, these oocysts can then be released into the environment through excretion into cat's feces over the course of many weeks. Initially these oocysts are non-infective and require sporulation to develop infective sporozoites. Oocysts are resistant to desiccation and can survive outside a cat for a long period of time latently waiting to infect another host (Frenkel *et al*., 1975).

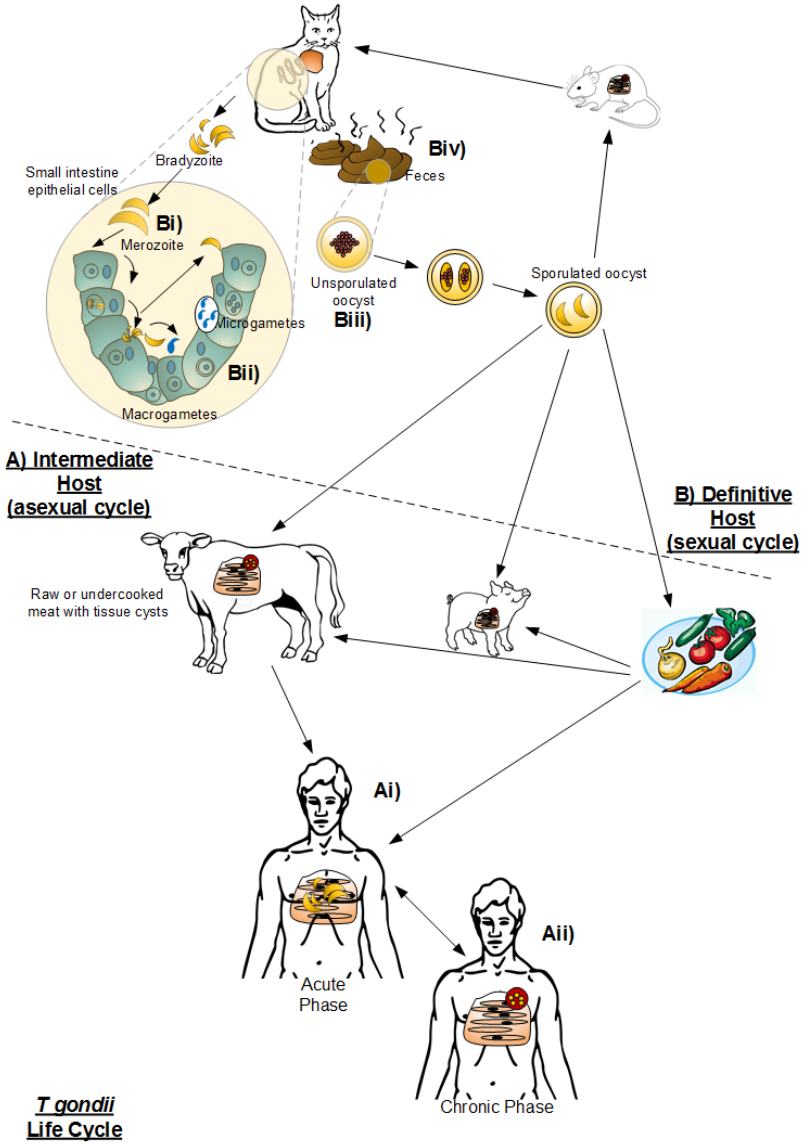

Figure 1.3. A schematic depicting the *Toxoplasma gondii* life cycle. (A) The extra intestinal stage of *T. gondii* can occur in any warm-blooded mammal following the ingestion of tissue cysts or oocyst. (Ai) Exposed bradyzoites or sporozoites will convert into fast dividing tachyzoites infecting any nucleated cell. (Aii) The tachyzoites form tissue cysts by converting back into slow dividing bradyzoites allowing the parasite to exist indefinitely within the host. (B) The intraepithelial lifecycle can occur only in cats following the ingestion of tissue cysts or oocysts. (Bi) Bradyzoites or sporozoites released from these cysts undergo schizony, forming merozoites. (Bii) Merozoites can differentiate into a macrogamete or a microgamete. (Biii) A oocyst forms when a macrogamete is fertilised by the microgamete. Biv) The oocysts are release into the environment by cat faeces.

1.7.5 Outcome of disease

The outcome of human disease is dependent on the health of the individual in question and most descriptions in the literature are based on the infections in Europe and North America with type I, II and III clonal lineages. In immunocompetent individuals, *T. gondii* infection is normally mild to asymptomatic and can enter the latent chronic phase without the individual ever knowing (Montoya & Liesenfeld *et al*., 2004). However, there is increasing evidence that people with chronic *T. gondii* infection have increased incidences of various psychoneuroloigcal diseases including schizophrenia and depression. Some studies have found correlations between *T. gondii* infection and how people score in certain personality attributes or even the likelihood of being involved in a road traffic accident (Flegr *et al*. 2002). The ability of *T. gondii* infection to affect behaviour is supported by rodent studies that demonstrate infection changes to the behaviour of mice in the open field test or the plus maze. In general mice infected with *T. gondii* are less neophobic, less anxious and are thus more likely to be successfully captured by a cat. This has been hypothesised to be an evolutionary adaptation that favours the perpetuation of the life cycle (reviewed by Henriquez *et al*., 2009). Other studies have demonstrated that *T. gondii* infection specifically alters rodent perception of cat urine odour which again is believed to favour the completion of the life cycle (Ingram *et al*., 2013).

T. gondii infection is problematic in people who are immune compromised including those with AIDS, malignancies or undergoing immunosuppressive therapy post organ transplantation. It is believed that toxoplasmosis in these immunocompromised patients occurs with an underperforming immune system leads to an inability to deal

with tissue cyst rupture (Montoya & Liesenfeld, 2004). This allows disease reactivation often causing neurological disease and sometimes dissemination and systemic disease with multiple organ involvement.

In the case of congenital toxoplasmosis, The severity of disease is determined by the stage of pregnancy in which the pregnant women contracted the disease. Infection in the first trimester results in the most severe illness in the foetus, whereas infection in the second and third trimester results in progressively less severe foetal disease. Spontaneous abortion is also a possibility but has reduced likelihood as pregnancy develops. Conversely, the probability of foetal infection increases as the pregnancy advances (Allain *et al*., 1998). Severe congenital infection can include life threatening neurological disease including hydrocephalus, mental impairment and blindness, but many children are born apparently asymptomatic. However, essentially all people born with congenital toxoplasmosis will ultimately develop recurring ocular disease later in life.

There is an increasing understanding that certain clonal lineages and recombinant strains that are more prevalent in South America can cause different and more severe disease patterns. Studies have shown that Type IV and V (South American strains) may cause more severe ocular disease than its counterparts due to poor host adaptation and the inhibition of protective host immune responses (e.g. IFN-γ) (de-la-Torre *et al*., 2013)

1.7.6. General overview of the innate host response to *T. gondii.*

1.7.6.1. Host cell infection

Once *T. gondii* tachyzoites egress from gut epithelial cells they must recognise and infect a new host cell in order to survive. *Toxoplasma* tachyzoites actively enter immune cells. By recognition (via GPI-anchored surface antigens known as SAGs) and attachment (via Ca2+ dependent secretion of microneme proteins) the parasite can invade the host cell and form their own membrane bound parasitophorous vacuole (Mineo & Kasper., 1994; Carruthers *et al*., 1999). By preventing this vacuole from being fused with other lytic endosomes, *Toxoplasma* can isolate itself and prolong its survival. To replicate within these cells, *T. gondii* must engineer pores to salvage host nutrients.

1.7.6.2. Innate immunity

The host response to *T. gondii* is extremely complex and involves both innate and adaptive branches of the immune system (Figure 1.4) (Reviewed in Filisetti *et al*., 2004). The initial cells recruited to the site of infection are neutrophils where their rapid recruitment is paramount for successful control of *T. gondii* infection (Bliss *et al*., 2000). Neutrophils phagocytose the tachyzoites and kill them by the release of RNI, ROS and NETs (neutrophil extracellular traps, containing chromatin and antimicrobial components) (Brinkman *et al*., 2004; Abi Abdallah *et al*., 2011; Abi Abdallah *et al*., 2012). Neutrophils are an important early source of pro-inflammatory cytokines including IL-12, TNF- α, CCL3 and CCL4 (also known as macrophage inflammatory protein, MIP-1α and MIP-1β) (Bliss *et al*., 2000). These cytokines serve

to attract macrophages, immature dendritic cells (iDC) and T cells to the site of infection (Denkers *et al*., 2004).

Once recruited, macrophages are arguably the most important cell necessary to limit a *T. gondii* infection. As well as being key producers of IL-12, their functions include phagocytosis, phagolysosome degradation, antigen presentation and the production of ROS and RNI (e.g. nitric oxide) (Stafford *et al*., 2002). They can also limit the availability of key metabolites such as iron, arginine and tryptophan, in which the parasite has been shown to be auxotrophic for these nutrients (Fox *et al*., 2004; Butcher *et al*., 2011). Ultimately, *T. gondii* infected murine macrophages clear infection through autophagy. By releasing GTP-ases, the PV encompassing the tachyzoites will be degraded re-trapping the parasites in an auto phagosome (Zhao *et al*., 2007).

Dendritic cells are demonstrated to be the main source of IL-12 during *T. gondii* infection. Studies by Liu *et al*., showed that depletion of DCs reduced IL-12 and increased the susceptibility of the host to acute infection (Liu *et al*., 2006). In addition, DCs provide a bridge between the innate and adaptive immune response. DC acquire antigen by phagocytosis and through antigen processing and MHC class II up-regulation, the DC will become mature (Kobayashi *et al*., 2013). A mature DC will then migrate to T cell rich regions of the spleen and lymph node and activate specific T cells. However, in some circumstances studies have observed that *Toxoplasma* uptake by migratory dendritic cells can actually help facilitate parasite dissemination to other areas of the body including the liver, spleen and central nervous system (CNS) (Sanecka *et al*., 2012; Lambert *et al*, 2009).

As part of the innate immune system, natural killer cells are an essential source of IFN-γ before specific CD4+ and CD8+ T cells are activated. Subsequently, they can also aid polarisation of the CD4+ T cell response as they promote classical activation and pro-inflammatory cytokine secretion from macrophages, DCs and neutrophils. Notably, NK cells can also directly kill infected cells by recognising that *T. gondii* has altered the MHC Class I complex (e.g. downregulated) on the surface of these infected cells (Zamai *et al*., 1998). This leads to binding of the Fas ligand and the release of cytotoxic proteins which will result in apoptosis.

Ultimately, the actions of the innate cells will culminate in the development of an adaptive T cell response. Interaction of T cells with professional antigen presenting cells (e.g. DCs and macrophages) will result in the proliferation, differentiation and development of specific CD4+ and CD8+ T cells (via co-stimulatory molecule expression and IL-12 secretion) (Kobayashi *et al*., 2003; Zhao *et al*., 2007). IL-12 production polarises a CD4+ T cell towards a Th1 cells and this results in IFN-γ and TNF- α secretion further maturing macrophages and dendritic cells (Reis e Sousa *et al*., 1999). Th1 cells also produce IL-2 that further proliferates CD4+ and CD8+ T cells. It has been observed that CD8+ T cells are necessary to control *T. gondii* infection (Parker *et al*., 1991). Like NK cells, they secrete IFN-γ and TNF- α and are cytotoxic to infected cells. Moreover, an effective immune response will not only control an active infection but generate a robust CD8+ T cell memory response necessary upon cyst re-activation (Joshi *et al*., 2007; Zhao *et al*., 2008). However,

virulence of *T. gondii* is associated with reduced numbers of activated CD8+ T cells (Tait *et al*., 2010).

Furthermore, humoral immunity may be crucial in limiting parasite dissemination throughout the body (Kaneko *et al*., 2004). IgM, IgG and IgA (Kaneko *et al*., 2004; Nimiri *et al*, 2004; Igarashi *et al*., 2008) have all been shown to be protective in *T. gondii* infection. During early infection, IgM acts to opsonise the parasites, enhance innate immune cell function, activate the complement pathway and prevent *T. gondii* invasion into host cells whilst IgG is necessary to cross the placenta and provide protection to the foetus during congenital toxoplasmosis.

In order to protect a host from generating an over-reactive immune response, immune regulatory mechanisms are required. IL-10, IL-27 and TGF-β are all key immune regulatory mediators required to suppress a Th1 driven immune response (Hunter *et al*., 2001; Hunter *et al*., 2004). These cytokines have been observed to suppress DC and macrophage maturation and function by down-regulating IL-12 and co-stimulatory molecules whilst promoting Treg generation.

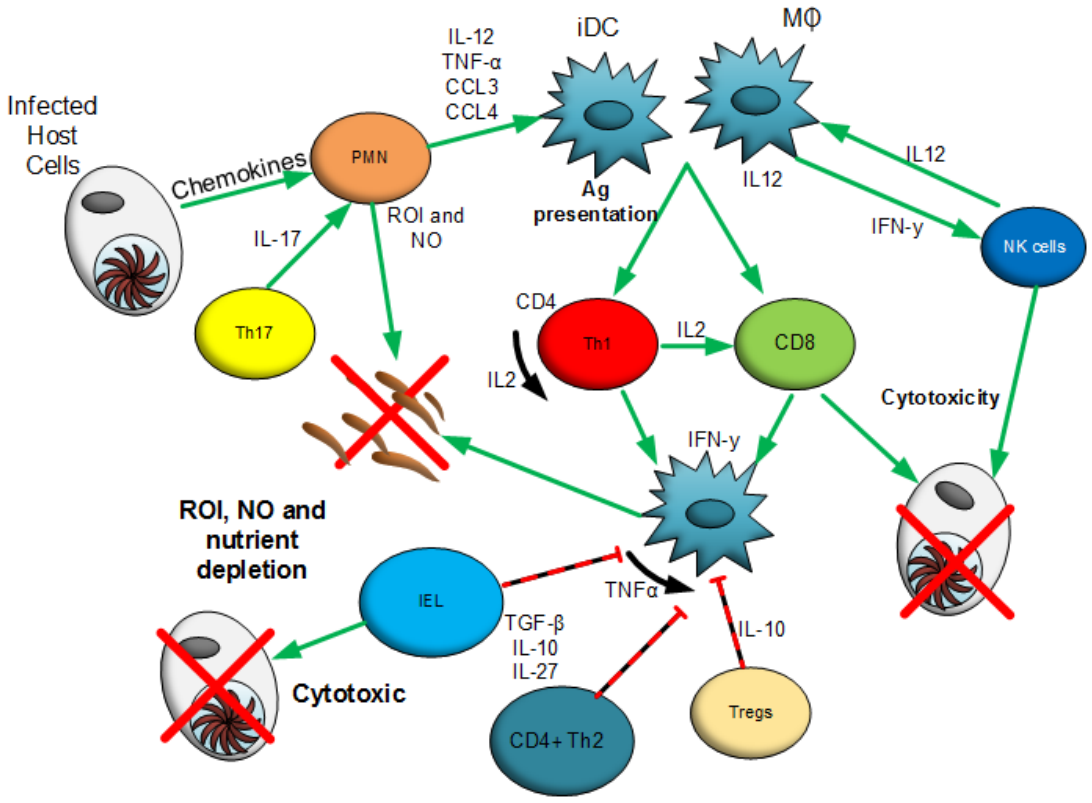

Figure 1.4. The immune response to *T. gondii* Both the innate and adaptive branches of the immune response are involved in controlling *T. gondii* infection. Upon active invasion, Infected cells secrete chemokines that attract neutrophils to the site of infection. These neutrophils further secrete chemokines and cytokines that attract immature DC and macrophages. Both cell types secrete IL-12 which will activate NK cells to produce IFN-γ and exert their cytotoxic properties. IFN- γ can act to further activate macrophages. Specific $CD4^+$ and $CD8^+$ T cell responses are activated upon DCs migrating to the LN, presenting antigen and secreting IL-12. This will promote a Th1 response. Inside the host cell, parasite death is mediated by IFN- γ and TNF- α dependent ROS and NO production. Regulation of this immune response is mediated by TGF-β, IL-10, IL-27, Th2 type $CD4^+$ T cells, T regulatory cells.

1.7.6.3. Toxoplasma subverts the innate immune response

T. gondii has at least 3 secretory organelles, the micronemes, the rhoptries and the dense granules. Proteins secreted from these have mostly been named MIC, ROP and GRA with a number usually in the order they were cloned (Reviewed by Dlugonska., 2008). Microneme proteins are involved largely in attachment and invasion of the host cells, rhoptry proteins are released during invasion alongside dense granule proteins which help modify the parasitophorous vacuole (Carruthers *et al*., 1999). Many of the rhoptry and dense granule proteins are known to have immunomodulatory effects including suppressing a wide range of host signalling pathways essential for generating an efficient immune response (Carruthers *et al*., 1997). Examples include GRA15 in type II strains which promotes the release of IL-12 via NF-kB signalling, this can drive classically activated macrophages (Rosowski *et al*., 2011) and ROP16 which can target STAT3 and STAT6 (Butcher *et al*., 2011). Present in all *T. gondii* type strains is the dense granule protein TgIST which suppresses an IFN response by blocking the repressor complex to STAT1 binding sites (Gay *et al*., 2016).

1.8. *Leishmania*

1.8.1 Discovery of *Leishmania*

Leishmania is a kinetoplastid protozoan parasite which causes the vector-borne disease, leishmaniasis. It was officially discovered in the 20th century by the Scottish pathologist William Boog Leishman and the Irish doctor Charles Donovan. Both men worked independently on this research but published papers within weeks of each other describing 'ovoid bodies' in either spleen samples taken in life and *post-mortem* from British soldiers in India (Leishman) or native Indians (Donovan). Initially, the ovoid bodies were thought to be degenerated forms of trypanosomes and mislabelled as trypanosomiasis or 'Dum-dum fever'. However, after 4 years of debate, both scientists agreed that the 'bodies' belonged to the newly discovered genus termed *Leishmania donovani.* Since then, many different *Leishmania* species have been discovered both in the new and old world (Reviewed by Cox *et al*., 2017).

1.8.2 Epidemiology

Leishmaniasis is widespread and encompasses diseases caused by many different *Leishmania* species. It has been identified in 98 countries in tropical and subtropical areas including Europe, Africa, Asia and America. However, approximately 90% of diagnosed cases are observed in Afghanistan, Algeria, Bangladesh, Bolivia, Columbia, Ethiopia, India, Iran, Peru, Sudan and Syria. Meta data shows that between 0.9 to 1.7 million individuals are infected and 20,000 – 30,000 people die from leishmaniasis each year (WHO, 2015). Three distinct clinical forms of the disease exist and are known as cutaneous, mucocutaneous and visceral leishmaniasis (Reviewed in Desjeux *et al*, 2004; Steverding *et al*., 2017).

1.8.3 Transmission

Leishmania parasites are transmitted by the bite of a female sand-fly of which two genera exist, *Phlebotomus papatasi* and *Lutzomyia longipalpis* (Killick-Kendrick *et al*., 1989; Reviewed in Fernanda *et al*., 2016). It is well-accepted that the *Phlebotomus* genus is usually responsible for Old World leishmaniasis whilst *Lutzomyia* is accountable for most New World diseases. It is only the female sand-fly who carries leishmaniasis, this is because the blood taken during a bite is required only for egg development. The transmission pattern of *Leishmania* can be varied (inter-species or intra-species) as a female sand-fly will feed from almost all mammalian species.

1.8.4 Life cycle

Leishmania parasites can form two distinct stages during their life cycle depending on whether they live extracellularly in the sand-fly alimentary tract or intracellularly in the phagolysosome of an immune cell (Figure 1.5; adapted from Killick-Kendrick *et al*., 1989). During a blood meal with a mammalian host, the female sand-fly injects infectious, flagellated promastigotes from its proboscis into the recipient's skin. In cutaneous leishmaniasis, these parasites then infect resident macrophages. Inside the phagolysosome of the immune cell, the promastigotes transform into amastigotes and proliferate. Once the host cell cannot facilitate any additional parasites, the cell bursts, releasing the amastigotes which will then infect neighbouring macrophages as well as any migratory immune cells including neutrophils and dendritic cells. In visceral leishmaniasis, amastigotes can also spread via the blood circulation and infect cells of the liver, spleen, bone marrow, lymph node and intestine.

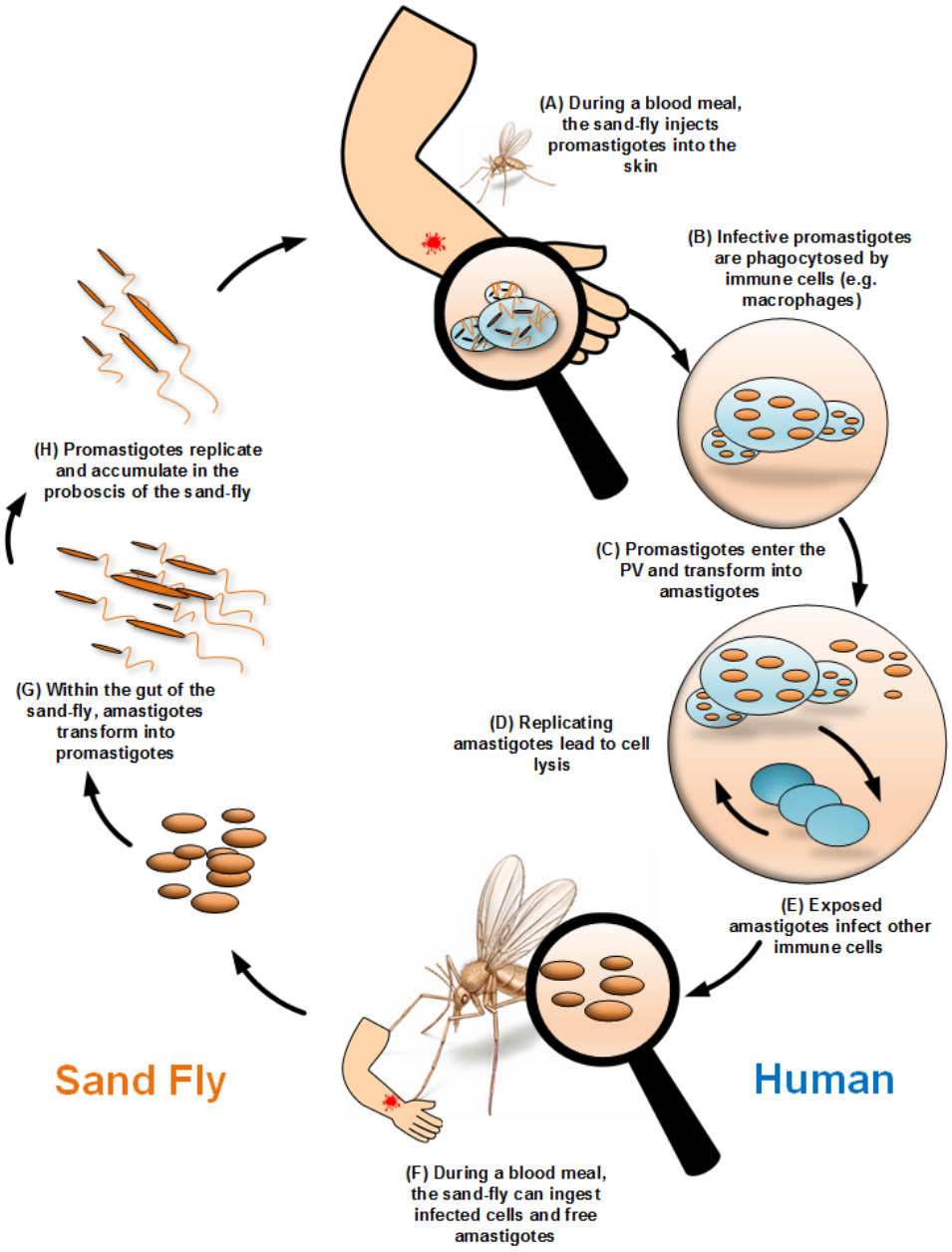

Figure 1.5. The life cycle of *Leishmania*. Schematic depicting the lifecycle of *Leishmania*. Steps are labelled A – H and highlight the lifecycle in both Humans and Sand-fly.

1.8.5 Disease outcome

Many different clinical manifestations of leishmaniasis exist and depend largely on which *Leishmania* species the host becomes infected with. The major symptom of cutaneous leishmaniasis is large lesions of the skin. These lesions are not related to mortality but can either be healing or non-healing, depending on the *Leishmania* species and the immunogenetics of the host (Shaw *et al*., 1995). In comparison, visceral leishmaniasis is almost always fatal and this is primarily due to parasite dissemination and lesion formation in major organs. Current anti-leishmaniasis drugs include pentavalent antimony, amphotericin B or miltefosine but are either relatively ineffective, extremely toxic or incredibly expensive (Craft *et al*., 2014).

Currently there are 18 different species of *Leishmania* that are pathogenic to humans but the most common for research purposes include *Leishmania major, Leishmania mexicana* and *Leishmania donovani* (Table 1.1).

Table 2.1. *Leishmania* species used in Research

Species	Old/ New World	Clinical disease	Distribution
L. major	Old world	Cutaneous	North and Central Africa, Middle East, Central Asia
L. mexicana (L. pifanoi)	New world	Diffuse and localised Cutaneous	USA, Ecuador, Venezuela, Peru
L. donovani	Old world	Post-kala-azar dermal and visceral	Central Africa, South Asia, Middle East, India, China.

1.8.6 General overview of the innate host response to *Leishmania*

Initiation of the immune response to *Leishmania* begins when the sand-fly takes a blood meal (Figure 1.6). The disruption of the microvasculature of the skin and the saliva of the sand-fly triggers the production of inflammatory mediators providing cues for the recruitment of innate immune cells (Titus and Ribeiro *et al*., 1988; von Stebut *et al*., 2007; Tacchini-Cottier *et al*., 2000; Peters *et al*., 2008). Within hours of infection, neutrophils are recruited into the infected skin by epidermal cell expression of CXCL1 and the production of alarmin from tissue damage. Neutrophils are key for the production of chemokines such as CCL3 initiating the recruitment of macrophages and DCs necessary for the generation of adaptive immunity. As early as 24 hours post infection, macrophages and DCs have been identified in infected tissue (van Zandbergen *et al*., 2004). Aside from directing the recruitment of other innate immune cell subsets, neutrophils can also act as 'trojan horses'; quietly allowing the parasites access to macrophages by allowing *Leishmania* to evade FcR-mediated uptake and intracellular killing (Laskay *et al*., 2008). However, this Trojan horse concept is controversial as Peters *et al*., (2008) demonstrated that neutrophils can act as primary host cells in their own right as they phagocytose a large proportion of promastigotes.

Aside from CCL3 from neutrophils, *Leishmania* infection also directly induces CCL2 (also known as monocyte chemoattractant protein-1B (MCP-1B)) from endothelial and smooth muscle cells located at the site of infection. This chemokine can also help with cell recruitment attracting DCs, monocytes, NK cells and T cells (Daly and Rollins, 2003). Interestingly, the exact mechanisms of how *Leishmania* parasites enter

DCs are unclear with some studies indicating that dDCs are capable of phagocytosing *L. major* first-hand (Ng *et al*., 2008) whilst others show that neutrophil entrapment is a necessary step (Ribeiro *et al*., 2012).

The subsequent initiation of adaptive immunity occurs when DCs migrate (via CCR7/ CCL19 and CCL21 axis) and present parasite-derived material in the draining lymph node, activating naïve T cells via MHC Class II – TCR interactions and additional co-stimulatory molecules (Itano *et al*., 2003; Von Stebut *et al*., 1998). However, the mechanism by which DCs present *Leishmania*-derived material to T cells is poorly defined and seems to depend on the DC subset involved. Studies show that DCs that reside in the skin (including Langerhans cells (LCs) and dermal DCs (dDCs)) in addition to monocyte derived DCs (moDCs) which are rapidly recruited to the site of inflammation are all DC subsets received by the draining lymph node initiating adaptive immunity during *Leishmania* infection (Itano *et al*., 2003, Serbina *et al*., 2013, Sen *et al*., 2010).

The developing adaptive immune response and thus disease outcome is normally dependent on cytokine production (expressed by innate cells). In 1986, it was demonstrated that production of cytokines can skew an immune response toward pathology or resolution (Mossman *et al*., 1986). In terms of *L. major*, the development of a Th1 or Th2 response directly correlate to whether the disease will be healing or non-healing (Heinzel *et al*., 1989). Many studies have demonstrated that IFN-y and IL-12 (Th1 cytokines) are necessary for resistance to *L. major* whilst IL-4 (Th2 cytokine) enhances a Th2 non-healing phenotype (Heinzel *et al*., 1989; Launois *et al*.,

1995; Reiner *et al*., 1995). In addition, IL-17/IL-23/Th17 cells and IL-10/ Treg cells are also associated with parasite survival and disease progression (Belkaid *et al*., 2001).

In relation to *L. mexicana* infection, disease progression has been correlated with the failure to mount an effect Th1-type response with a lack of IL-12 production and a defective T cell response (Rodriguez-Sosa *et al*., 2001). However, numerous studies have accepted that IL-4 and IL-13 are important contributors to disease progression and lesion development and that deficiency of IL-4 may aid resolution (Satoskar *et al*., 1995; Alexander *et al*., 2002)

Discussed above is the difference in immune phenotype in mice infected with *L. major* or *L. mexicana*. Studies have shown that both species have divergent virulence mechanism for manipulation of the host cell function thus affecting disease outcome (Bogdan and Rollinghof, 1998). Cysteine proteinases are key factors associated with *L. mexicana* that have been identified as being responsible for the increased virulence of *L. mexicana* over *L. major* in mice (Mottram et al., 2004; Alexander *et al*., 1998). It has been demonstrated that *L. mexicana* can modulate expression of surface molecules and production of cytokines. This was observed by Contreras *et al* (2014) that IL-12 (IL-12p70) was inhibited following exposure to *L. mexicana* promastigotes and that MHC Class II and co-stimulatory molecules, CD80 and CD86 were down-regulated. Further to this, pulsed with exogenous antigens, DCs exposed to *L. mexicana* failed to stimulate antigen-specific T cells to produce high levels of the Th1 associated cytokine IFN-y. Interestingly, it has been shown that some *Leishmani*a

species can modulate host cell function from within the cells by utilising parasite derived factors such as Cysteine proteases B (CPBs) of *L. mexicana* (primary expressed by amastigotes). CPBs are shown to modulate intracellular signalling. For example, Cameron *et al* (2004) have observed that CPB can degrade NFkB and IkB in macrophages, respectively down-regulating IL-12 production and impair IFN-y production. In *vivo*, Alexander *et al*., (1998) showed that infection with CPB deficient *L. mexicana*, impaired Th2 cytokines but increased Th1 cytokines altering the development of protective immunity.

Additionally, whilst certain *Leishmania* species promastigotes inhibit phagosome lysosome fusion process prior to transformation to amastigotes (Desjardin and Descoteaux *et al*., 1997; Mosser and Miles, 2000) this does not seem to be the case with *L. mexicana*. However, *L. mexicana* was the first species to show that amastigotes resided in a phagolysosome (Alexander and Vickerman, 1975)

Amastigotes have evolved to thrive and replicate in the harsh conditions of these highly acidic vesicles as they contain an abundance of nutrients that the parasite can utilise for proliferation and survival. For example, while host cells restrict the availability *L. major* has to iron by pumping into the cytosol via the NRAMP1 protein (Hergaux *et al*., 1999), *L. amazononensis* amastigotes have found a way to salvage iron via LIT1, an iron transporter situated in or near the phagolysosome which converts Fe^{3+} to Fe^{2+} (Huynh *et al*., 2007). However, this is just one-way amastigotes utilise host-mediated nutrients to survival intracellularly. How the metabolic state of host

cells effects intracellular parasites is described in further detail in subsequent sections (*Metabolic reprogramming in response to L. mexicana and T. gondii*).

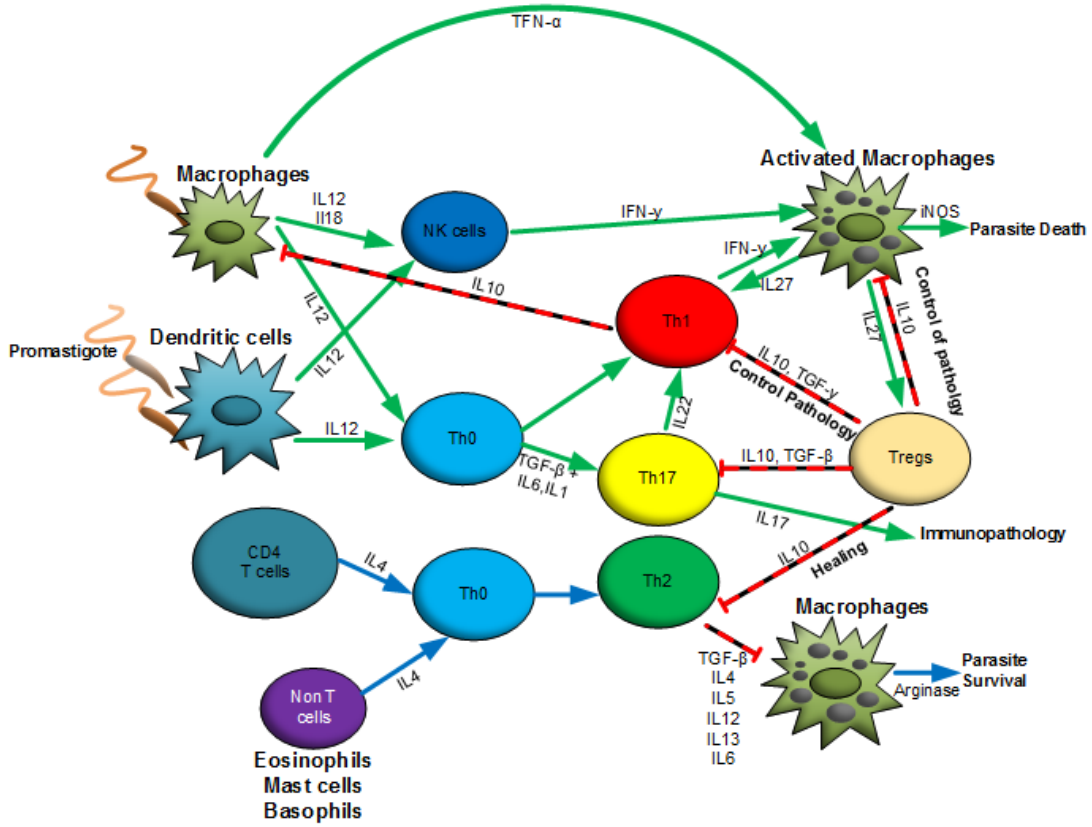

Figure 1.6. The immune response to *Leishmania major* Following phagocytosis macrophages and dendritic cells are activated to produce pro-inflammatory cytokines such as IL-12. Upon migration to the LN and presentation of antigen, a specific CD4+ Th1 driven immune response is generated. T cells will produce IFN-γ leading to the induction of parasite killing by NO production. Overproduction of inflammatory cytokines results in severe immunopathology and non-healing infection. In contrast, anti-inflammatory cytokines promote differentiation of Th0 toward Th2 that inhibit macrophage and DC function and lead to *Leishmania spp* survival. TGF-β and IL-27 cytokines secreted by macrophages or DCs stimulate Treg cells to produce IL-10 that form a negative feedback loop on the macrophages and DCs suppressing the release of inflammatory mediators

1.8.7. The immune response to *Leishmania* is dependent on parasite strain and host genetic background

The development of leishmaniasis is largely dependent on parasite strain and host genetic background (Shaw *et al,* 1995) (Handman *et al,* 2005). In murine models, the most notable comparison can be observed between BALB/c mice and C57BL/6 mice which, following infection with *Leishmania major* (*L. major*) generate very different immunological responses and disease outcomes. BALB/c mice develop non-healing lesions and progressive leishmaniasis, whereas C57BL/6 mice form small lesions that heal quickly (Alexander *et al,* 1985, reviewed Sacks and Noben-Trauth, 2002). As mentioned previously, resistance is driven by a Th1 response reliant on IL-12, IFN-γ and NO production whilst susceptibility is determined by a Th2 immune response (IL-4, IL-13, IL-10 and TGF-β) – that suppresses parasite killing promoting a non-healing phenotype (Wilhelm *et al,* 2001; Wei *et al,* 1995; Bogdan *et al,* 1990; Erb *et al,* 1996 and Groux *et al,* 1999). In the case of *L. mexicana*, susceptibility depends on the strain of mouse or site of infection and is not necessarily associated with a Th2 type response, but rather the lack of a robust Th1 response (Rodriguez-Sosa *et al*., 2001; Rosas *et al*., 2005)

Whilst, *L. major* is the most widely studied infection model for cutaneous infection, as noted previously cutaneous infection with *L. amazonensis* or *L. mexicana,* or visceral infection with *L. donovani,* will often have very different and contradictory responses to those observed in *L. major* infection (McMahon-Pratt and Alexander, 2004). Examples were described in the previous section in terms of immunological

response, metabolic alterations of the parasite itself and influence the strain of parasite has on the metabolome of host cells. The remainder of this thesis will focus solely on *L. mexicana*. Infection with this strain normally leads to persistent infection in most mouse strains, even in C57BL/6 mice that are resistant to *L. major* (Torrentera *et al*., 2002). In recent years, how this parasite can evade host clearance and manipulate the host immune response to become chronically persist has been extensively questioned but how *L. mexicana* can impact the metabolome of host cells (especially innate immune cells) has gone unanswered.

1.9. Metabolic reprogramming in response to *Leishmania* and *Toxoplasma*

Many parasites proliferate in vacuoles that have the ability to fuse with late endocytic vesicles, phagosomes and autophagosomes within macrophages. The fusion of these compartments likely allows the continuous flow of carbon sources and essential nutrients between the parasite and the host cell. *Leishmania* and *Toxoplasma* are auxotrophic for many amino acids and must scavenge from their niche (McConville *et al*., 2007; Blume *et al*., 2009; Fox *et al*., 2004). Nutrients taken up by the parasites are used for proteins, polyamine synthesis and also as a carbon source. However, there is increasing evidence that the metabolic state of macrophages has a profound effect on intracellular *L. mexicana* or *T. gondii* growth. Macrophage activation increases the glycolytic flux necessary for the production of ROS and other reactive nitrogen species via NADPH oxidase. In addition, by directing arginine to citrulline via nitric oxide synthase (iNOS), NO production is also increased. Increasing iNOS activity in these

cells, suppresses the enzymes able to convert arginine to ornithine and proline (Wei *et al,* 1995; Colegani-Silva *et al*., 2015). Depletion of host arginine/ ornithine levels are detrimental to parasite survival as low cellular ornithine or polyamines inhibit growth and increase vulnerability to oxidative stress (Gordon, 2003; Roberts *et al*., 2004). Furthermore, in response to IFN-γ cells can upregulate indoleamine 2,3 – dioxygenase which depletes tryptophan for which *T. gondii* and *L. mexicana* is an auxotroph (Fox *et al*., 2004; Murray *et al*., 1989; Schaible and Kaufmann, 2005).

In comparison, parasites are likely to thrive in macrophages stimulated with IL-4 or IL-13. These cells depend on oxidative phosphorylation to survive and preferentially divert arginine towards ornithine and urea via arginase-1, a competitive inhibitor of NOS2 (Naderer *et al*., 2008). Ornithine is a major precursor for polyamine biosynthesis and this is essential to parasite growth and survival (Gordon, 2003; Kropf *et al*., 2005). A study by Woods *et al*. 2003, demonstrated a protective role for arginase-1 in controlling Type II *Toxoplasma* multiplication via a STAT6 independent mechanism that can compensate for NO deficiency during infection (Woods *et al*., 2013).

1.10. PI3K – Akt – mTOR pathway regulation during host cell metabolism

1.10.1. Pathway overview

One pathway of considerable interest to modulate cellular metabolism in immune cells is the phosphoinositide 3-kinase (PI3K) signal transduction pathway. PI3K was first discovered as an oncogene and since then this pathway has been extensively studied

in cancer models where the enzyme directly regulates cell quiescence, proliferation and longevity upon activation with epidermal growth factors. In many cancers, this pathway is overactive, suppressing apoptosis and promoting proliferation (Ohtani *et al*., 2008).

Recent studies have demonstrated that signalling via a subgroup of the PI3K family may be responsible for regulating metabolic changes and thus effector function within immune cells during activation (Xie *et al*., 2014). Briefly, by phosphorylating phosphatidylinositol (4,5)-bisphosphate (PIP2) on the inositol ring 3'-OH position, the second messenger phosphatidylinositol (3,4,5)-trisphosphate (PIP3) is generated. Subsequently, PIP3 activates protein kinase B (PKB/ AKT) by recruiting it to the plasma membrane. AKT can then have a number of downstream effects including activating cAMP response element-binding protein (CREB), inhibiting cyclin-dependent kinase inhibitor 1B ($p27^{Kip1}$), localising FOXO proteins to the cytoplasm and activating mammalian target of rapamycin (mTOR). The PI3K pathway is antagonised by phosphatase and tensin homologue deleted on chromosome 10 (PTEN) or glycogen synthase kinase 3 beta (GSK3B) (Reviewed in Convarrubias *et al*., 2018)(Figure 1.7).

mTOR is a conserved serine threonine kinase and the literature accepts it as a key regulator of metabolism in many cell types. In mammals, mTOR is spilt into two distinct complexes, mTORC1 and mTORC2 (Reviewed in Convarrubias *et al*., 2018). Other subunits are unique to and help define the two complexes including Raptor and Rictor. The function of mTORC1 depends on the cell type. In proliferating cells,

mTORC1 regulates anabolic processes including the synthesis of macromolecules whilst in the liver, mTORC1 inhibits catabolic metabolism to facilitate nutrient storage. mTORC2 (re)activates AKT. Therefore, there is a bi-directional interplay between mTOR and AKT. AKT is necessary to activate mTORC1 but by negative feedback, mTORC1 can suppress mTORC2 and AKT activation.

Studies have demonstrated that how the PI3K signalling transduction pathway initially proceeds in macrophages depends on the polarising signals that are encountered. During LPS activation, TLR-4 interacts with PI3K adapter protein BCAP which initiates AKT and mTORC1 activation through the inactivation of the TSC complex (Troutman *et al*., 2012). This results in the activation of the GTPase Rheb which will stimulate mTORC1. The MEK/ERK and Ικκβ pathways have also been implicated (Vergadi *et al*., 2017). In the case of IL-4, cytokine binding to the receptor will activate Jak1 and Jak3, phosphorylate and activate Stat6 to recruit IRS2. IRS2 can then engage with PI3K in the manner described above to activate AKT and mTOR (Byles *et al*., 2013; Van Dyken *et al*., 2013).

Research into role of mTOR and AKT in dendritic cells is still in its infancy. Preliminary studies demonstrate that during the development of monocytes into efficient BMDCs mTORC1, promotes the expression of MYC (Pearce and Everts, 2015). This transcription like factor induces the genes that encode the proteins involved in the glycolysis pathway, mitochondrial biogenesis, glutaminolysis and the electron transport chain. In resting and activated DC, mTOR is crucial in controlling anabolic processes as well as detecting and controlling growth factors, nutrient levels

and energy status (Convarrubias *et al*., 2018). Recently, HIF-1α, a target of mTOR and AKT has been implicated during the activation of DCs (Weichhart *et al*., 2008; Weichhart *et al*., 2009; Amiel *et al*., 2012). Studies show that this molecule can promote the expression of many glycolysis pathway enzymes during LPS stimulation (Pearce and Everts, 2015). However, a recent study has suggested that aerobic glycolysis in DCs can also be mediated by AKT independently of mTOR during the acute phase of LPS activation. This AKT activation is also independent of PI3K and regulated by TBK and Ικκε. The possible role for this is unclear.

The enzyme AMP – activated kinase (AMPK) is also essential during DC activation as it opposes the mTOR signalling. When there is a reduction in the energy required for the cell to function, a build-up of AMP activates AMPK (Moreira *et al*., 2016). The primary function of the AMPK signalling pathway is to suppress biosynthetic pathways and induce the catabolic processes of many metabolites to gain nutrients and ATP. This is achieved by inhibiting the formation of the elF4F complex, essential for the translation of proteins to be synthesised (Jaramillo *et al*., 2011; Muraille *et al*., 2014). Examples include increasing glucose uptake and fatty acid oxidation. In addition, AMPK can produce metabolites from autophagy, by breaking down macromolecular compounds within the host cell (Muraille *et al*., 2014). Furthermore, some studies also indicate a role for AMPK in inflammation, where a decrease in AMPK activity in macrophages correlates with a classically activated immune cell (Pearce and Everts, 2015).

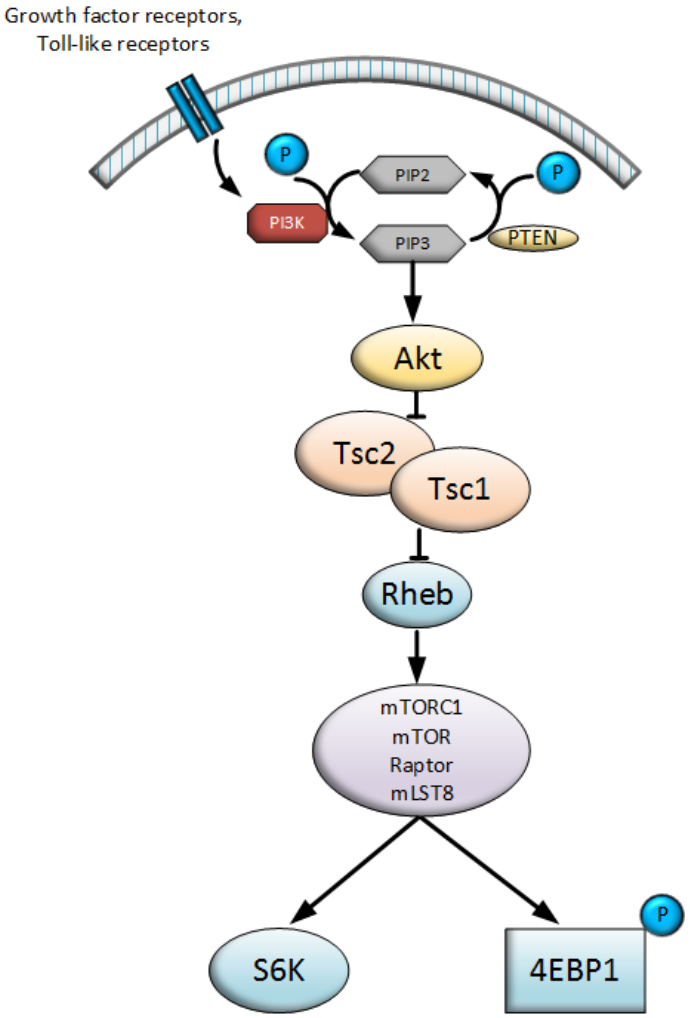

Figure 1.7. PI3K-AKT-mTOR signalling. Upon receptor recognition (via growth factors and TLRs), PI3K is activated which leads to the formation of PIP3 that phosphorylates Akt. PTEN inhibits this pathway. Akt activates downstream molecules mTOR and S6K that regulates mRNA translation and protein synthesis. AMPK and TSC1/TSC2 complex inhibit this complex whilst 4EBP1 inhibits mRNA translation and protein synthesis.

1.10.2. Evidence of *L. mexicana* or *T. gondii* modulating PI3K-AKT-mTOR pathway

Changing levels of metabolites in the local environment can influence or even regulate the developing immune response and that this can be modulated by pathogens. However, recently it has been demonstrated that pathogens may influence the signalling transduction pathways involved in regulating cellular metabolism and function, including PI3K-AKT-mTOR (Moreira *et al*., 2016). Studies have demonstrated that *L. mexican*a infection was suppressed in p110y-/- mice. The authors show that this is the catalytic subunit of class Ib PI3K and that loss of this molecule impairs phagocytic uptake of *Leishmani*a parasites by macrophages, neutrophils and DCs (Cummings *et al*., 2012).

In addition, AKT has been shown to activate NF-ϰb which controls transcription of the iNOS gene. In this study, upon activation with LPS, the activation of PKB/Akt by *L. amazonensis* infection resulted in the suppression of NO by macrophages (via the translocation of p50 inhibitory subunits to the nucleus) (Calegari – Silva *et al*., 2015). Moreover, activation of AKT by *Leishmania* infection can alter cytokine production and even promote cell survival in immune cells (Vazquez-Lopez *et al*., 2015; Muhkerjee *et al*., 2013). Furthermore, Singh *et al* observed that activation of HIF-1α in *L. donovani* infected macrophages promotes parasite survival whilst Jaramillo *et al* observed that *L. major* inhibit host cell protein synthesis by directly cleaving mTORC1 by the parasite-specific molecule GP63. This can inactivate S6k (protein S6 kinase), eIF4E (eukaryotic initiation factor 4E) and 4EBP1 (eukaryotic initiation binding

protein) which all serve to promote protein synthesis and cell survival (Singh *et al*., 2012; Jaramillo *et al*., 2011).

The influence *T. gondii* has on the PI3K-AKT-mTOR pathway in immune cells is less well established. Generally, studies have shown that whilst PI3K inhibitors can suppress *T. gondii* replication, *T. gondii* itself can regulate the PI3K-AKT signalling pathway to suppress ROS (via NADPH oxidase 4) (Zhou *et al*., 2013). In addition, HIF-1α is required for *T. gondii* growth in an oxygenated environment whilst *T. gondii* stimulated mTOR dependent host cell growth despite impaired signalling to S6K1 and 4E-BP1 (Wiley *et al*., 2010; Wang *et al*., 2009). However, further studies are necessary to determine to what extent *Toxoplasma* influences PI3K-AKT-mTOR signalling transduction pathway or if this highly successful parasite alters other pathways that regulate metabolism.

1.11. Experimental techniques for investigating cellular metabolism

1.11.1. Liquid chromatography mass spectroscopy

The field of immunometabolism has progressed rapidly in recent years due to the application of mass spectroscopy (MS) for analysing biological samples. Briefly, gas or liquid chromatography (GC/LC) separates the complex mixture before MS is used to identify the masses of molecules and fragments in the sample by forcing a neutral species to gain or lose a charge. This is known as the mass-to-charge ratio (m/z). Linking both methods together (e.g. LCMS) can minimise signal suppression and allows for greater sensitivity (shown via a retention time). This highlights the

importance of tandem spectroscopy for accurate metabolite identification (Cambiaghi *et al*., 2017).

Metabolomic data may be analysed using untargeted or targeted approaches. Untargeted metabolomics assesses all the metabolites within an extract leading to the discovery of unexpected metabolite changes on a global scale. In addition, it is also unbiased, and can be used to investigate perturbations of interconnecting pathways. However, as metabolite identification depends on mobile phase, pH, solvent, column chemistry and ionization technique, it remains impossible to use the same LCMS method to recover all metabolite classes. Furthermore, there are a large number of metabolites that cannot be identified as they have yet to be annotated on larger metabolomics databases such as KEGG (Kyoto Encyclopaedia of Gene and Genomes). In contrast, targeted metabolites can allow the user to measure the exact concentration of pre-defined metabolites based on a standard curve. Metabolomics is at its optimal when both techniques are combined together (Cambiaghi *et al*., 2017).

Despite the fore-mentioned technological advances of LCMS over the last decade, current challenges still exist. The major obstacle for many researchers working in the field of immunometabolism is designing a workflow enabling scientists to assign biological meaning to these identified metabolites and how their role differs during pathogenesis. This is extremely time-consuming and labour-intensive owing to the fact that in untargeted metabolomics only a subset of all metabolites identified can be validated by standards with the rest being putatively identified. Further mechanistic

work must always be conducted *in vitro* and *in vivo* to understand the physiological role of the metabolite changes witnessed (t'Kindt *et al*., 2010).

Methods to analyse complex untargeted metabolomics datasets normally include computational tools necessary to process and interpret this seemly meaningless data. In summary, once a raw file is uploaded to mzmatch, mass spectral peaks must be chosen, realigned and annotated compared to a standard. The instrumental and chemical noise should then be removed via a blank to reveal only the biologically relevant data (Creek *et al*., 2012). To check the statistical relevance and understand the data, online tools and statistical programs such as MetaboAnalyst (Chong *et al*., 2018; Xia and Wishart 2010) and SIMCA (Umetrics at Sartorius Stedim Biotech) must be used. Additional checks to identify putative metabolites can be made using the m/z ratios or retention times of the mass spectral ion using Xcalibur. Furthermore, to interpret the data biologically, the data must be pathway-mapped. This allows the user to understand the link a metabolite has to certain pathways and if these pathways are interconnected. This can allow the metabolomics changes to be placed in the context for further mechanistic validation studies (Zhou *et al*., 2015; Zhou *et al*., 2016).

One common recent advancement in the field is stable isotope assisted metabolomics using carbon (C^{13}), nitrogen (^{15}N) or deuterium (^{2}H). This allows the researcher to gain information on how certain metabolites are utilised within a pathway. Ultimately, this should reveal the metabolic fate of a particular nutrient. However, in this study, this technique would still be unhelpful as the stable isotope assisted metabolomic method

cannot distinguish the different metabolic pathways of a pathogen from those of a host cell whilst in that host immune cell (t'Kindt *et al*., 2010).

In order to fully determine the true physiological changes of an immune cell during infection, users must aim for an integrative approach. It is well-known that genes, transcripts, proteins and metabolites are only moderately correlated with each other and that post-translational changes, environmental stimuli and enzyme regulation may modulate any of these processes revealing a slightly different biological output that what was predicted. By integrating at least two of the four 'omics', genomics, transcriptomic, proteomics and metabolomics, researchers can start to determine the relationship between all these distinct stages during disease.

1.11.2. RNA-sequencing

Sequencing methods have been used within immunology since the 1980s. However, with recent rapid development of technologies and a reduction in cost, next generation sequencing (NGS) has become indispensable in characterising multiple aspects of genomics research (Reviewed in Benichou *et al*., 2011). So far, it has been used to re-sequence the genome of previously sequenced organisms, sequence the genomes of organisms with unknown sequences and even determine RNA abundance levels (RNA-seq) (Kircher *et al*., 2010; Kuroda *et al*., 2010; Kassahn *et al*., 2011).

Many technologies exist for next generation sequencing but this thesis will focus on the Illumina system (Shendure *et al*, 2008). Briefly, Illumina uses reversible deoxy-

nucleoside triphosphate (dNTP) terminators. DNA segments are attached to primers and amplified with dideoxy-NTPs (ddNTPs). These ddNTPs are labelled with a fluorescent dye and blocked at the 3'OH side to ensure that only one nucleotide is added at each step. After incorporation, the unused nucleotides are washed off. Scanning will detect the last nucleotide added. To enable the next sequencing cycle to start, the blocking label is removed (Shendure *et al*., 2008; Mardis *et al*., 2008). The advantage of the Illumina over other systems is that this sequencing presents a better yield even if it does not obtain the greatest read length (Mardis *et al*., 2008; Margulies *et al*., 2008). Currently, most research labs do not have the technical expertise to sequence and process their samples 'in house' and outsource to specialised companies e.g. Eurofins. These companies then compute the data into easy to read expression values (FPKM, Fragments per kilobase of transcript per million mapped reads; RPKM, Reads per kilobase per million mapped reads) or $\log_2$ (fold change).

Although, RNA sequencing presents a unique opportunity within the field of immunology, it brings with it major challenges including data storage and data analysis. As with other omics datasets, transcriptomics must be interpreted correctly in order to be biologically relevant. So far, only a few analysis software programs with the complexity of the immune system in mind have been developed (Biocyc) (Caspi *et al*., 2016). Therefore, in order to fully characterise the immune response during infection, an integrative approach must be utilised.

1.11.3. The multi-omics approach: combining transcriptomics with metabolomics as an unconventional way to study immunometabolism

Within the last 5 years, the field of immunometabolism has been revolutionised by the development of a high throughput Seahorse extracellular flux analyser from Agilent Technologies that survey rapid changes in intracellular metabolism. The Seahorse permits the simultaneous assessment of glycolytic and oxidative metabolism through the coupled sensing of oxygen consumption and extracellular acidification (Kang *et al*., 2018). Furthermore, the Seahorse-based method has been developed to assess the activity of components of the electron transport chain through inhibiting specific aspects of cellular metabolism (Kang *et al*., 2018). However, experts in the field are now starting to understand the limitations of the seahorse analyser. One such drawback is that the analyser is limited to only observing the shift from oxidative phosphorylation to aerobic glycolysis under different conditions. Therefore, more complex immunometabolism studies that are desiring a greater insight into all aspects of cellular metabolism have started to adopt a multi-omic approach.

Polyomics or multi-omics are terms used to describe the approach of combining multiple omics dataset such as metabolomics with transcriptomics. The field of immunology is changing, gone are the days where measuring one immune cell effector function is proof of the state of the overall immune response during disease. Advances in technology has allowed not just the analysis of a cellular transcriptome or a metabolome profile in isolation but to merge these complex data together. Using this approach has opened up an infinite amount of immunology related questions to be answered, especially in relation to the interplay between pathogens and the immune

system. Combining metabolomics and transcriptomics in this situation has allowed researchers to take a complete uninterrupted snapshot of the relationship between parasite and immune cell at one particular time point. Understanding this up and down regulation of gene transcripts in conjugation with an increased or decreased presence of metabolites will allow scientists to establish the flux of metabolites through a metabolic pathway and investigate in detail how parasites influence this. In addition, transcriptomics details other immune-related genes that are influenced during infection and in relation to this study might help establish not just how parasites alter the mechanism regulating host metabolism e.g. mTOR/AMPK axis but also how they modulate immune cell effector function e.g. cytokine production.

1.12. Aims and Objectives

The ability of macrophages to undergo metabolic reprogramming is now well characterised and during the studies described herein some progress has been made in investigating similar processes in dendritic cells. Most studies to date have concentrated on using defined molecules or combinations of molecules including LPS, IL-4 and IFN-γ to investigate cellular metabolism, but have stopped short of using live infections. Logically, studies using live infections are important in understanding the host pathogen interplay during infection, but come with their challenges. Firstly, it is not easily possible to determine the source (host or pathogen) of the metabolites present in co-culture experiments. Secondly, the establishment, growth and multiplication of the parasite adds an extra degree of complexity to an already temporally dynamic immune response. The studies described in this thesis aim to investigate the extent to which *Leishmania mexicana* and *Toxoplasma gondii* can

metabolically reprogram dendritic cell metabolism and explore the hypothesis that certain changes will be parasite evolved mechanisms to subvert the host immune response, while others are host evolved to control parasites. Specific aims include:

1. To establish a baseline illustrating the spectrum of dendritic cell metabolism induced by combinations of LPS, IFN-γ, LPS + IFN-γ and IL-4 in concert with key immunological parameters.
2. To determine to what extent, two evolutionary distinct, obligate, intracellular parasites (*Leishmania mexicana* and *Toxoplasma gondii*) occupying unique metabolic, anatomical and immunological niches specifically reprogram the dendritic cell.
3. To use RNA-sequencing and transcriptomic analyses to validate the metabolomic and functional findings in aim 2 and gain further insight into host parasite inter-relationship.

Chapter 2

Materials and Methods

2.1. Animals

Male 8-12-week-old BALB/c mice were obtained from the University of Strathclyde Biological Procedures Unit (Glasgow, UK). Experiments were performed in strict accordance with the UK Home Office Animal Scientific Procedures Act 1986 and were approved by the Home Office and University of Strathclyde Animal welfare ethical review. All experimental designs were reported in accordance to the ARRIVE guidelines.

2.2 *Leishmania* Culture

Wild-type strain M293 *L. mexicana* promastigotes were cultured *in vitro* at 27°C in Home M media (Life technologies, Paisley, UK) supplemented with 10% foetal calf serum gold (PAA Laboratories, UK), 2mM L-glutamine (Sigma, UK) and 100µg/ml streptomycin (Cambrex, UK). Parasites were transferred into new media every 7 days. Parasites were checked for infectivity in mice once during this project.

For co-culturing *in vitro L. mexicana* promastigotes with bone marrow derived dendritic cells, *L. mexicana* parasites were counted on a haemocytometer and diluted to the desired concentration in RPMI (90% Roswell Park Memorial Institute medium, 1% penicillin/streptomycin, 1% L-glutamine and 10% heat inactivated foetal calf serum) (Themo Fisher Scientific, UK; Lonza, slough, UK) for a multiplicity of infection (MOI) of 1:5 BMDC: parasites in 24 well plates.

2.3. Maintenance of *Toxoplasma gondii in vitro*

Toxoplasma gondii tachyzoites were maintained in confluent human foreskin fibroblasts (HFF) cultured in 10ml complete DMEM (Dulbecco's modified Eagle's medium, 2mM L-glutamine, 10% foetal calf serum, 100U/ml penicillin, 100mg/ml streptomycin and 50U/ml amphotericin B at 37°C in 5% CO_2 (Thermo fisher scientific (Gibco), UK). The tachyzoites were then left for several days to allow them to infect the majority of the HFFs. Tachyzoite were harvested by scraping HFFs using a cell scraper and then slowly passaged through a 25G needle at least 10 times. This cell suspension was then diluted 1/10 in complete DMEM and passed into another confluent T75 flask of HFFs. For *in vitro* studies, parasites were counted using a haemocytometer and the appropriate dilution carried out in RPMI. Tachyzoites were added to BMDCs at an MOI of 1:1 in 24 well plates.

2.4. Soluble *Leishmania* antigen (SLA) and Tachyzoite lysate antigen (TLA) preparation.

SLA or TLA was prepared by re-suspending a confluent flask of parasites (either *L. mexicana* or *T. gondii*) in 1ml of Hanks balanced salt solution (HBSS) (Life technologies, Paisley, UK) and flash-freezing the suspension in liquid nitrogen. The suspension was thawed at 60°C, and aspirated 5 times with a needle (25G). This process was repeated 5 times before sterile filtering (0.22μm filter). SLA or TLA concentration was determined using Bradford's protein assay (Bio-Rad).

Coomassie Brilliant Blue G-250 solution (Bio-rad, Watford, UK) was diluted 1:4 with ddH20 before it's addition to either 10µl of SLA or TLA sample or bovine serum albumin standards (BSA, Sigma, UK). This was incubated for 10 minutes at room temperature to allow the reaction to develop. A spectrometer was used to measure absorbance at a wavelength of 570nm. The BSA standards were used to calculate the concentration of SLA or TLA present in the sample.

2.5. CFSE labelling of *L. mexicana* or *T. gondii* parasites

Parasites were fluorescently labelled with 5,6-carboxyfluorescein diacetate succinimidyl ester (CFSE). Parasites were re-suspended at $1x10^7$ in HBSS before the addition of CFSE at the final concentration of 1 µM (Life technologies, Paisley, UK). This was incubated for 10 minutes at 37°C in the dark. Two washing steps were performed by centrifugation (3000rpm) before the parasites were re-suspended in complete RMPI (Lonza, slough, UK) and used immediately for *in vitro* studies by flow cytometry or immunofluorescent staining.

2.6. Bone marrow derived dendritic cell (BMDC) Culture

Bone marrow derived dendritic cells were generated from the femur and tibia bones dissected from the hind legs of scheduled one protocol killed BALB/c mice (8-12 weeks old). After removing the epiphyses from the bones, the bone marrow was flushed out using a 25G needle and syringe filled with complete RPMI (90% RPMI, 1% penicillin/streptomycin, 1% L-glutamine and 10% heat inactivated foetal calf serum) (Lonza, Slough, UK). The cells were then disaggregated to form a single cell suspension before centrifugation for 5 minutes at 1400rpm. Cells were re-suspended

in complete RPMI supplemented with 10% x63 cell (a gift from Professor B Stockinger, MRC labs) conditioned media containing granulocyte – monocyte colony stimulating factor (GM-CSF) to allow for differentiation of cells into BMDC's. The cells were grown at 37^{o}C with 5% CO2.

BMDC's were then fed on day 3 and 5. On day 3, an additional 10ml of complete RPMI containing 10% GM-CSF conditioned media was added to the culture and on day 5, half the volume was replaced with fresh media containing 10% GM-CSF conditioned media.

After 7 days, BMDCs were harvested by removing the medium and rinsing the plates in cold sterile HBSS. Adherent cells were detached using a plunger of a 1ml syringe. The cells were then washed, counted via haemocytometer, resuspended in complete RPMI, without GM-CSF and plated-out to the desired concentration needed depending on the *in vitro* assay. Dendritic cells were left to settle and attach overnight before use. Cell were routinely 70-80% CD11c+ by flow cytometry.

2.7. Stimulation of BMDCs

BMDCs replated at 1x10^{5} (in 100µl complete RPMI) were stimulated with combinations of LPS (*E-coli* 0127, 1µg/ml final concentration), IFN-γ (100u/ml final concentration) or IL-4 (100u/ml final concentration)(Sigma-Aldrich) as indicated for 24 hours.

2.8. Co-culturing of BMDCs with parasites

Most experiments conducted require co-culturing of $1x10^6$ BMDCs/ml with intracellular parasites. In these experiments, *L. mexicana* promastigotes or *T. gondii* tachyzoites were prepared as described previously and then added to BMDCs at a multiplicity of infection (MOI) ratio of either 5:1 (*L. mexicana*) or 1:1 (*T. gondii*).

2.9. Extraction for Liquid chromatography mass spectroscopy

Plates containing cells were placed on ice 10 minutes prior to the extraction process in order to suppress further cellular metabolism changes. Then the supernatant was discarded and the cells were washed twice with ice cold PBS (Thermo fisher, UK). An extraction mixture of cold methanol (VWR Chemicals, Leicestershire, UK), water and chloroform (VWR Chemicals, Leicestershire, UK) in a 60%:20%:20% ratio was then added onto the BMDCs before the well was scraped thoroughly. The extraction mixture with cells were then transferred into appropriately labelled Eppendorf's before being placed on a shaker at 4°C for 1 hour. These samples were then centrifuged at 13 000rpm for 15 minutes at 4°C. The supernatant from these samples was then transferred into LCMS vials (Sigma-Aldrich/ Merck, Germany) and stored at -80^{o}C awaiting LCMS.

2.10 LCMS (University of Strathclyde)

Metabolic profiling was performed on a LC-MS platform consisting of a Accela 600 HPLC system combined with an Exactive (Orbitrap) mass spectrometer from Thermo Fisher Scientific (Bremen, Germany). The column used was the zwitterionic ZIC-pHILLIC column (150mm x 4.6mm; 3.5µm, Merck, Germany). The injection volume

was 10µl and the flow rate was 0.3ml/min. The ZIC-pHILLIC column was eluted using a gradient of mobile phase A, 20mM ammonium carbonate pH9.2, and mobile phase B, acetonitrile (ACN). The concentration of A was used increased from 20% to 80% over 30 minutes and then held at 92% for 5 minutes, before it was equilibrated at 20%.

The two solvent blanks were run first to equilibrate the column, then four standards containing known metabolites and then the experimental samples which were randomly sequenced. The settings are described in detail by Westrop *et al*., (2015). Briefly, the Electospray Ionisation (ESI) interface was operated in a positive/negative polarity switching mode. The spray voltage was 4.5 kV for positive mode and 4.0 kV for negative mode. The temperature of the ion transfer capillary was 275°C and sheath and auxiliary gas flow was 50 and 17 arbitrary units, respectively. The full scan range was 75 to 1200 m/z for both positive and negative modes with settings of AGC target and resolution as Balanced and High (1e6 and 50,000), respectively. The data were recorded using the Xcalibur 2.1.0 software package (Thermo Fisher Scientific). Mass calibration was performed for both ESI polarities before the analysis using the standard Thermo Calmix solution with addition of some additional compounds to cover the low mass range and the signals of 83.0604 m/z (2xACN+H) and 91.0037 m/z (2 x formate-H) were selected as lock masses for positive and negative mode, respectively, during each analytical run.

2.11. LCMS (Glasgow polyomics)

Some metabolomic samples were run at the Glasgow Polyomics facility by Gavin Blackburn and Erin Manson. Metabolic profiling was performed on a hydrophilic interaction liquid chromatography (HILIC) combined to a Dionex Utimate 3000 RSLC system (Thermo Fisher Scientific, UK) using a ZIC-pHILIC column (150 mm x 4.6 mm, 5µm column, Merck Sequant). The column was maintained at 30oC and samples were eluted with a linear gradient (20mM ammonium carbonate in water, A and acetonitrile, B) over 24 min at a flow rate of 0.3ml/ min.

The injection volume was 10µl and samples were maintained at 5°C prior to injection. The MS Thermo Orbitrap QExactive (Thermo Fisher Scientific) operated a polarity switching mode with the settings as follows: Resolution, 70, 000; AGC, 1e6; m/z range, 70-1050; Sheath gas, 40; Auxiliary gas, 5; Sweep gas, 1; Probe temperature, 150°C and capillary temperature, 320°C. For positive mode ionisation: source voltage +3.8 kV, S-Lens RF Level 30.00, S-Lens Voltage -25.00 (V), Skimmer Voltage -15.00 (V), Inject Flatopole Offset -8.00 (V), Bent Flatapole DC -6.00 (V). For negative mode ionisation: source voltage-3.8 kV. The calibration mass range was extended to cover small metabolites by inclusion of low-mass calibrants with the standard Thermo calmix masses (below *m/z* 138), butylamine (C4H11N1) for positive ion electrospray ionisation (PIESI) mode (*m/z* 74.096426) and COF3 for negative ion electospray ionisation (NIESI) mode (*m/z* 84.9906726). To enhance calibration stability, lock-mass correction was also applied to each analytical run shown below.

2.12. Data processing

Raw data files of metabolite standard solutions were processed using ToxID 2.1 (Thermo Fisher Scientific Inc., Hemel Hempstead, UK) with +/- 3ppm (parts per million) mass accuracy of both ESI positive and negative modes. After checking the appearance of the ion chromatograms with respect to peak shape, the standards were used to calibrate IDEOM v19. Raw files of the sample metabolites were processed by converting the data files to mxXML open format using msConvert (ProteoWizard). Chromatograms were extracted using a detection algorithm from XCMS and stored in PeakMLfiles before aligning replicate peaks and combining them using mzMatch.R. A CSV file was generated after noise filtering and gap filling (quality control), which was then imported into IDEOM v19 for metabolite identification. This identification is based on accurate mass (+/- ppm) and predicted retention time. Any lipids and peptides were excluded from the putatively identified metabolites in IDEOM (Creek *et al*., 2012).

2.13. Metabolite identification

The identity of the metabolites was confirmed by accurate mass and matching the sample retention time to that of an authentic standard (+/- 0.3 mins). The confirmed metabolites correspond to the metabolic standards initiative (MSI) level 1 whilst metabolites putatively identified by accurate mass and predicted retention time correspond to MSI level 2.

2.14. Data analysis

Prior to Orthogonal partial least squares discriminant analysis (OPLS-DA), the data were mean-centred and Pareto (Par) scaled. OPLS and VIP (Variable importance in the projection) plot was performed using SIMCA-P13 (Umetrics, Sweden).

For metabolomics data, a non-parametric one-tailed Mann Whitney test was used for all individual putatively identified metabolites. $p < 0.05$ was considered significant. Graph Pad prism 7 was used for plotting the graphs and heat maps. Heat-maps show the fold change in each metabolite compared to the control.

All functional data was performed by a one-way ANOVA with either a Bonferroni or Dunnett post-test unless otherwise stated. Throughout this thesis, * = $p < 0.05$, ** = $p < 0.01$ and *** = $p < 0.001$.

Transcriptomics analysis is described in the Transcriptomics section (See below).

2.15. Transcriptomics

BMDCs activated with LPS or co-cultured with intracellular parasites were harvested and the mRNA was extracted from the cell pellets using the RNeasy mini kit (Qiagen) with QIAshredder column (Qiagen, Manchester, UK). A agilent 2100 bio analyser was used to assess the quality of the RNA extracted (Agilent, Cheshire, UK). RNA samples with a concentration >20ng/μl and RIN >8 was sent to be processed for RNA-seq using the Illuminia sequencing technology at Eurofins GATC Biotech, Konstanz, Germany. As stated in the expression analysis report, the company used Bowtie generating

transcriptome alignments to align the RNA-seq reads to the reference transcriptome (mouse). Potential exon-exon splice junctions of the initial alignment were identified by Tophat. Cufflinks (part of CummeRbund software) was then used to identify and quantify the transcripts from a pre-processed RNA-seq alignment assembly. After this, Cuffmerge merges the pieces of the transcripts into full length transcripts and annotated the transcripts. Finally, merged transcripts from two (or more) samples were compared using Cuffdiff to determine the differential expression at transcript level. This includes giving a measure of significance (Benjamini-Hochberg correction) between the samples using fragment per kilobase per million mapped reads (FPKM) for each transcript. For interpretation purposes, each transcript is shown as Log_2 (fold change) compared to the control and illustrated in a heat map.

2.16. Flow Cytometry

0.5 – $1x10^6$ Cells were prepared for flow cytometry by transferring into FACS tubes, washed twice with PBS and then stained with an appropriate combination of fluorochrome-conjugated antibodies, pre-diluted in FACSFlow (1:400) (Table 2.1) (Biolegend or Ebioscience, UK). Cells were then incubated at 4°C for 30 minutes, washed and resuspend in 200µl for acquisition. (cells were incubated for a further 30 minutes if streptavidin conjugated antibody was required) For intracellular staining, the washed cells were resuspended in Cytofix/Cytoperm (BD Bioscience, Oxford, UK) for 20 minutes to permeabilise the cells before being washed in Perm/Wash (HBSS (Life technologies, Paisley, UK), BSA, TritonX-100, Sodium azide (all Sigma, Dorset, UK) and stained with fluorochrome-conjugated intracellular antibodies

(1/100)(Biosciences, Hatfield, UK) diluted in Perm/Wash. After an incubation of 30 minutes, the cells were then washed a further twice in Perm/Wash then FACS Flow.

The cells were then acquired on a FACS Canto flow cytometer installed with FACSDiva software (BD Biosciences) and analysed using FlowJo software (FlowJo LLC). Prior to cell acquisition, compensation on unstained cells or isotype was required to ensure that the cells are gated on their FSC (forward side scatter) and SSC (side scatter) profiles. This was achieved by adjusting the voltage of the photomultiplier tube and using the correct CompBeads (PE, FITC or APC) (BS Bioscience)

Table 2.1. Flow Cytometry Antibodies

Cell Marker - Surface	**Primary Antibody**	**Clone**	**Isotype control**
Fc Block	Anti-mouse FcBlock CD16/32	93	N/A
CD11c	Anti-mouse CD11c PE Anti-mouse CD11c FITC	N418	Armenian Hamster IgG cocktail- PE or FITC
CD40	Anti-mouse CD40 APC	3/23	Rat IgG2a, kappa
CD80 (B7-1)	Anti-mouse CD80 FITC	16-10A1	Armenian Hamster IgG cocktail - FITC
CD86	Anti-mouse CD86 APC-Cy7	GL1	Rat/ IgG2a kappa
Intracellular			
NOS2	Anti-mouse NOS2 PE	CXNFT	Rat/ IgG2a kappa

2.17. ELISA

Supernatants from the cultured BMDCs were collected and quantified by enzyme-linked immunosorbent assay (ELISA) to determine the concentration of the cytokine, IL-12 (Table 2.2). Briefly, a 96 well ELISA plate was coated with 50µl of the capture antibody (2µg/ml) and incubated overnight at 4°C. The plates were then washed with wash buffer (0.05% Tween 20 in pH7.4 PBS) three times before the addition of the samples (1/50 dilution) and standard (20ng/ml) (30µl per well). The plate was then incubated for 2hrs at 37°C. The washing step was repeated as described above. After this time, a 1/1000 dilution of biotinylated antibody (50µl) was added for a 1 hr before another washing step. Lastly, 50µl Streptavidin-HRP (1/500 dilution) was added for 45 minutes before the addition of TMB to develop the washed plates. The cytokine concentration was calculated from the absorbance read at 450nm on a SpectraMax spectrophotometer and compared to the standard curve generated.

Table 2.2. ELISA Antibodies

Cytokine	Standard Starting Concentration (Recombinant protein)	Capture Antibody	Primary Antibody	Biotinylated Antibody
L-12p40/70 (BD Pharmingen)	rIL-12 (2µg/ml)	Rat anti-mouse IL-12	-	Biotin Rat anti-mouse IL-12

2.18. Assaying cell supernatant nitric oxide

The levels of nitric oxide within cell supernatant was measured by Griess Assay. Standards were prepared using serial dilutions of $NaNO_2$, starting at 100μM in RPMI 1640. 50μl of each supernatant extract and standard were plated in triplicate, in a 96 well ELISA plate. Equal volumes of Griess reagent (1:1 mix of 2% sulphanilamide in 5% H3PO4 and 0.2% Naphthylene diamine HCL in ddH2O) was added and left in the dark for 10 minutes. The plate was read at a wavelength of 540nm in a spectrophotometer (Spectramax 190, Molecular Devices, USA).

2.19. Arginase assay

Urea as an indicator of arginase activity was determined within the cell using an Arginase assay. The supernatant was removed and the cells were scraped thoroughly with PBS using the plunger of a 1ml syringe. The cells in appropriately labelled eppendorfs were then centrifuged for 4 mins at 13000rpm. The pellets were then re-suspended in 50μl of 0.1% Triton-100 containing the proteases inhibitor Pepstatin A (5mg/ml), Aprotinin (1mg/ml) and Antipain (5mg/ml) (Millipore/ Merck, Germany) . The samples were the incubated at 25°C for 30 minutes on the shaker (300rpm). After this time, 50μl of 10mM Managanese Chloride Tetra hydrate (MnCl2) (USB Amersham Int plc) in 50mM TRIS (pH7.5) (Sigma Aldrich) was added before the samples were incubated in a 55°C water bath for 10 mins. To new eppendorfs, 25μl Arginine buffer was added (0.5M Arginine in ddH20, pH9.7)(Sigma-Aldrich). This reaction was allowed to develop on a shaker (300rpm) for 60 mins at 37°C. The

standards are made from a Urea stock solution (0.00192g in 1ml H20). To both the standards and the samples, 400μl of Acid mixture containing H2SO4, H3PO4, H20 (ratio 1:3:7) and 25μl ISPF dissolved in 100% ethanol was added. The eppendorf's were then incubated in a water bath at 95°C for 45 mins. After a cooling down phase, the samples and standards were pipetted onto a 96 well plate and read at 540nm using a spectrophotometer.

2.20. 2-NBDG uptake assay

(2-N-7-Nitrobenz-2-oxa-1,3-diazol-4-yl) Amino)-2-Deoxyglucose is a fluorescent glucose analog that is used to monitor glucose uptake within cells (Thermo fisher; Catalog number: N13195). Cells were either activated by LPS or co-cultured with parasites prior to the addition of 2-NBDG. To optimise the use of 2-NBDG within BMDCs, the compound was given at different concentration over a time period of either 30 minutes, 60 minutes or 120 minutes. From these preliminary experiments, it was confirmed that a concentration of 50μM for 2 hours, is necessary for this fluorescent glucose analog to work efficiently in BMDCs. Cells treated with 2-NBDG were then analysed by flow cytometry to show the Mean fluorescent intensity (MFI) or % 2-NBDG uptake within the BMDCs.

2.21. Lactate dehydrogenase assay

Lactate dehydrogenase (LDH) is an enzyme that interconverts pyruvate to lactate. In this thesis, LDH was evaluated using the Lactate Dehydrogenase Activity Assay Kit supplied by Sigma-Aldrich (Catalog number: MAK066). This kit reduces NAD to NADH, which is specifically detected as a colorimetric assay. Briefly, $1x10^6$ BMDCs

were rapidly homogenised on ice in LDH assay buffer. These cells were then pelleted (13 000rpm for 15 minutes at 4ºC) before the supernatant was removed for further analysis. The supernatants were appropriately diluted 1 in 50 in LDH assay buffer before the addition of 50μl Master Reaction mix (LDH Assay buffer (48μl) and LDH Substrate mix (2μl)). 0-12.5 nmole/well of NADH were used as standards. To investigate LDH activity, measurements were taken every 2 minutes at an absorbance of 450nm until the highest sample exceeded the linear range of the standard curve. The LDH activity was then determined using the following equation.

LDH activity = B x Sample dilution factor / (Reaction time) x V

B = Amount (nmole) of NADH generated between $T_{initial}$ and $T_{final.}$

Reaction time = $T_{final} - T_{initial}$ (minutes)

V = sample volume (mL) added to well.

2.22. Mitochondrial Staining

BMDCs were plated at $1x10^5$ in 100µl complete RPMI into a Lab-teck chambered 1.0 borosilicate coverglass system (Catalog no: 155411; Thermo Scientific). The BMDCs were left to settle overnight before live staining. Briefly, the cells were washed with PBS before the addition of Tetramethylrhodamine, Methyl Ester, Perchlorate (TMRM) and Mitotracker Green or Red CMX Ros (Thermo fisher). All dyes were added at a final concentration of 100nM for 45 minutes in complete phenol red free RPMI. Cells were washed with PBS to remove Mitotracker green dye but not those stained with TMRM.

The cells were placed in a heated stage top chamber (OKO labs H301-mini heats) before imaging. BMDCs were imaged on a Nikon Eclipse Ti inverted epifluorescence microscope with a 100x 1.3 NA oil immersion objective lens plus a 1.5x adapter (Nikon) and Flash 4.0 CMOS camera (Hammamatsu) with the help of Dr Susan Chalmers. The samples were imaged with an excitation light of 470nm (Mitotracker green) and 550nm (TMRM) (pE4000LED light source, coolLED). Camera recording and excitation light controlled by Win Fluor v3.9.1 software (John Dempster, University of Strathclyde). Image analysis was performed on Image J.

2.23. Cytokine bead array (CBA)

Concentrations of different cytokines were determined in the supernatant of naïve BMDCs, LPS stimulated BMDCs, *L. mexicana* infected BMDC cultures and BMDCs co-cultured with *T. gondii* using the Legendplex ™ Mouse Inflammation Panel (Cat no; 740150; Biolegend, UK), which can simultaneously measure. IL-1α, IL-1β, IL-12p70, TNF-α, IL-6, MCP-1, IL-10, IFN- β and IL-23 in a single sample. The assay was carried out as per the manufacturer's instructions. Briefly, samples were diluted 1 in 2 with assay buffer and then 25μl of samples and standard mix was added to a 96 well filter plate with 25μl assay buffer and 25μl Legendplex™ capture bed mix. Following a 2-hour incubation at room temperature with shaking, samples and standard were washed with wash buffer using a vacuum chamber to remove the wash. 25μl of biotinylated-specific antibody mix was added to each well and incubated for 1 hour as before. Without washing, 25μl of Streptavidin-phyoerythrin (PE) conjugated secondary antibody was added and incubated as before for a further 30 minutes. Samples and standards were washed twice as above, resuspended in 200μl of wash

buffer and transferred to FACS tubes for analysis on FASC canto flow cytometer using FACS Diva software. PMT voltages were set using RAW beads provided in the kit.

Each cytokine is associated with its own bead population and these populations are identified by a specific allophycoyanin (APC) mean fluorescent intensity (MFI), Legendplex analysis software was used to identify these bead populations and the MFI from the PE signal. Cytokine concentrations were then interpolated in the Legendplex software using the standard curve.

Chapter 3

Dendritic cells have a spectrum of activation states with distinct overlapping metabolic profiles

3.1 Introduction

In the field of immunometabolism, the most characterised innate immune cell within the literature is the macrophage (Reviewed in O'Neill at al., 2016; Galvan-Pena *et al*., 2014). As discussed in detail in the introduction to this thesis, research has shown that different stimuli can alter the activation state including the metabolic profile of macrophages (Stout *et al*., 2004). Innately activated macrophages are those stimulated with bacterial LPS whilst classically activated macrophages (termed M1 macrophages) are those activated by LPS in combination with IFN-γ (Newsholme *et al*., 1986; Newsholme *et al*., 1987 O'Neill and Hardie, 2013). This activation state commonly correlates with infection or inflammation. These cells have reduced oxidative phosphorylation relative to resting macrophages, but enhanced aerobic glycolysis. This switch in energy metabolism is often referred to as the Warburg effect (Warburg *et al*., 1927; Reviewed in Koppenol at al., 2011; Kelly *et al*., 2015). This is accompanied by decoupling of the electron transport chain from the TCA cycle, resulting in (1) the accumulation of TCA cycle intermediates (Tannahill *et al*., 2013; Jha *et al*., 2015; Infantino *et al*., 2011), (2) the build-up of lactic acid via glycolysis and (3) the diversion of additional glucose 6 phosphate through the pentose phosphate pathway (Hashemi *et al*., 2012). It has been suggested that this switch to the Warburg effect in oxygenated environments is necessary to generate high levels of ATP rapidly to cope with increased energy demands required for phagocytosis, migration, cytokine production and secretion (Oren *et al*., 1963; Galvan-Pena *et al*., 2014). In addition, recent research has suggested that as ATP produced from OXPHOS is used in the generation of ROS and NO, ATP generated from aerobic glycolysis becomes essential for the production of energy for cell survival (Van Heiden *et al*., 2010).

In comparison, M2 macrophages activated through IL-4 have been reported to rely primarily on OXPHOS for their energy demands (Odegaard and Chawla, 2011; Pearce and Pearce, 2013; Galvan-Pena and O'Neill, 2014). Why the switch to glycolysis does not occur in these cells is not known but these cells generate higher levels of the anti-inflammatory cytokines, IL-10, IL-4 and IL-13 and less of the pro-inflammatory cytokines and the toxic mediators, ROS and NO. In contrast to low NO or iNOS (inducible nitric oxide synthase) expression, M2 macrophages express arginase which metabolises arginine to urea and ornithine (Munder *et al*., 2009). Ornithine in M2 macrophages is normally converted to polyamines (Spermidine, Spermine and Putrescine) and proline (Yu *et al*., 2003), which is seen as anti-inflammatory and can contribute to wound healing.

As mentioned in the introduction further phenotypes of macrophages have been at least partially characterised (Mosser *et al*., 2008, Reviewed in Rattigan *et al*., 2018). From these recent studies, activation of these diverse macrophage phenotypes appears to be dependent on either (1) the stimuli experienced (2) the length of time the cell is exposed to a stimulus or (3) when during their lifetime do macrophages become activated with a particular stimulus (Nagy *et al*., 2015).

In contrast, the metabolism of dendritic cells during different activation states has been scarcely studied. However, dendritic cells are known to be responsive to many of the same mediators as macrophages and share a number of functions (Cortese *et al*., 2014; O'Neill *et al*., 2016; Everts *et al*., 2012). The role of BMDCs as primary antigen

presenting cells and their provision of a bridge from the innate to adaptive immune response makes their characterisation essential. Therefore, the work described in this chapter aims to determine the spectrum of dendritic cell activation, including key immunological parameters and metabolic changes induced by combinations of LPS, IFN-γ and IL-4.

3.2. Results

3.2.1 Dendritic cell morphology, CD40 and IL-12 levels vary according to activation stimuli

Using flow cytometry, BMDCs were identified by gating on the cell surface marker CD11c. The proportion of $CD40^+$ expressing cells were then quantified by determining the proportion of cells showing staining above that of the unstained or isotype control. Whilst a small percentage of unstimulated BMDCs expressed CD40 (Figure 3.1A), stimulation of BMDCs with the LPS, resulted in a significant increase in the proportion of $CD40^+$ expressing cells ($p=0.0001$). CD40 expression was also increased in BMDCs stimulated with LPS in combination with IFN-γ ($p=<0.0001$), relative to unstimulated cells. However, CD40 was unaffected by stimulation with IFN-γ or IL-4 alone. The production of IL-12 was concomitant with CD40 expression where LPS (+/- IFN-γ) ($p=0.0280$) significantly up-regulated IL-12 production (Figure 3.1B). Furthermore, BMDCs stimulated with LPS alone or in combination with IFN-γ were found to adopt a 'rounded up' morphology relative to unstimulated cells. In contrast, BMDCs treated with IL-4 appeared elongated with distinct dendrites present (Figure 3.1C).

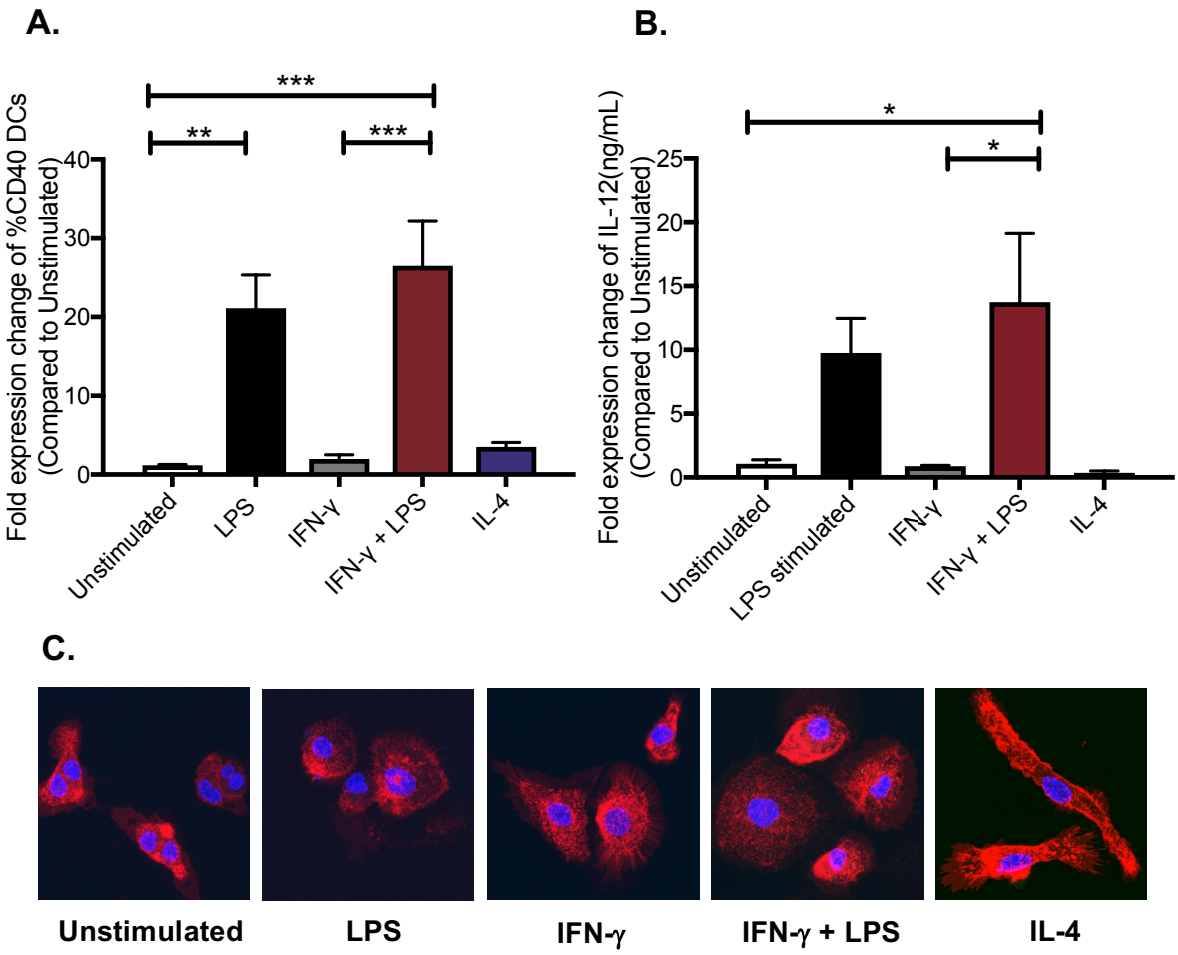

Figure 3.1. CD40 expression, IL-12 production and morphology changes in BMDCs stimulated with different activation stimuli. Bone marrow derived DCs were stimulated with combinations of LPS, IFN-γ, or IL-4 as indicated for 24 hours. After this time, cells were analysed by (A) flow cytometry to determine the proportion of cell expressing the activation marker, CD40, (B) supernatants were collected and used to determine the IL-12 production (ng/ml) or (C) stained with cholera toxin-AF647 (staining membrane – red) and DAPI (DNA staining – blue). Results are an average of the fold expression change of three independent experiments (n=3) compared to naïve cells and show the mean +/- SEM. Statistical analysis performed using 1-way ANOVA with Bonferroni post-test. Significant differences were identified as ***P<0.001, **P<0.01 and *P<0.05

3.2.2 Dendritic cells undergo holistic changes in metabolism according to activation stimuli

Global metabolic analysis using orthogonal partial least squares discriminant analysis (OPLS-DA) consistently found distinct separation between naïve BMDCs and those activated with LPS (+/- IFN-γ) or IL-4 (Figure 3.2). Unless otherwise stated the remainder of this chapter will focus on the data from only one biological run. The holistic changes in metabolism are fully detailed in a VIP score list which orders the most important variables across the model as a whole (based on relative intensities of each metabolite) (Table 3.1). Formula, m/z, ratios and retention times for this data is available in Table 8.1. Separate pairwise comparisons for each individual stimulus compared to the control is shown in Table 8.2 – 8.5. The data includes all putatively identified metabolites (recognised by accurate mass to < 3ppm and by predicted retention time via IDEOM) as well as metabolites confirmed via known standards (retention time match of +/- 0.2min). Data from biological run 2 are available in Figure 8.1 and Table 8.6.

The functional role of each metabolite listed on the VIP table is described within the table (Table 3.1). Notably, multiple metabolites from specific pathways, including glycolysis, TCA cycle, OXPHOS and arginine metabolism are evident in the VIP table and these will be discussed in detail later in this chapter. In addition, metabolites of interest include didemethyl tocotrienol, orthophosphate, mesaconate, aspartate, taurine, phosphonate, O-acetyl-L-serine, glutathione, [SP (16:0)] N-(hexoadecanoyl)-sphing-4-einine, phosphocreatine, and sn-glycero-3-phosphoethanolamine. These metabolites had a VIP score ≥ 2.00 and encompass a wide range of different cellular

functions. [SP (16:0)] N-(hexoadecanoyl)-sphing-4-einine and sn-glycero-3-phosphoethanolamine are components of the cell membrane whilst orthophosphate, phosphonate and phosphocreatine are necessary to synthesise and store phosphates for cellular signalling. O-Acetyl-L-serine and mesaconate are intermediate for cysteine biosynthesis or vitamin B12 synthesis respectively. Notably, 3 of the top 15 metabolites function as antioxidants (Didemethyl tocotrienol, taurine and glutathione).

Furthermore, heat maps classified by amino acids, carbohydrates and nucleotides were constructed in order to illustrate the fold change difference between BMDCs treated with activation stimuli and naïve BMDCs (Figure 3.3). The heat maps clearly demonstrate the similarities and also the differences of all the intracellular metabolites based on LCMS detection between the activated groups. This demonstrates a spectrum of activation in BMDCs.

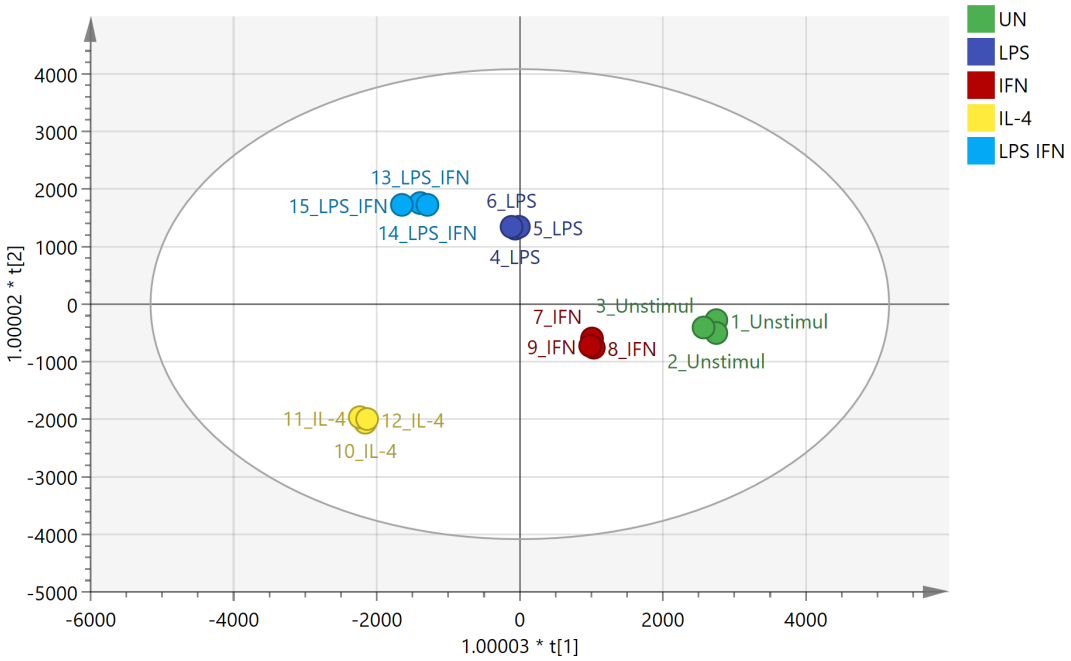

Figure 3.2 Orthogonal Projections to Latent Structures Discriminant Analysis of BMDCs with different activation stimuli. Bone marrow derived BMDCs were stimulated with combinations of LPS, IFN-γ or IL-4 as indicated for 24 hours. After this time, the metabolites of the BMDCs were extracted and measured via Liquid chromatography mass spectroscopy (LCMS). The data was then analysed by SIMCA and Projections to Latent Structures Discriminant Analysis (OPLS-DA) was generated. Key: green, Unstimulated-; dark blue, LPS; red, IFN-γ; yellow, IL-4 and light blue, LPS + IFN-γ. The confidence ellipses are based on Hotelling's T^2 = 95%. N= 2.

Table 3.1. VIP score of BMDCs treated with LPS, IFN-γ , LPS + IFN-γ or IL-4

Metabolite	M1.VIP [4+6+0][1]	2.44693 * M1.VIP [4] cvSE[2]	Role[3]
didesmethyl tocotrienol	10.4661	3.38762	Antioxidant
Orthophosphate	6.25254	6.12936	Oxidative phosphorylation
Citrate	6.12453	3.76885	TCA intermediate
Mesaconate	6.0072	1.81045	Vitamin B12 biosynthesis
(R)-Lactate	4.71875	1.84347	Glycolysis end-product
L-Aspartate	4.16522	0.422868	Non-essential AA
Taurine	4.01094	1.91337	Antioxidant, osmoregulation, membrane stabilisation and calcium signalling.
Phosphonate	3.57691	1.52852	Intake of phosphate into cells
(S)-Malate	3.57235	3.00074	TCA intermediate
O-Acetyl-L-serine	3.47418	1.78496	Intermediate of cysteine biosynthesis
L-1-Pyrroline-3-hydroxy-5-carboxylate	3.32851	1.23207	Intermediate of proline biosynthesis to glutamate
Glutathione	3.08722	1.56513	Antioxidant
[SP (16:0)] N-(hexadecanoyl)-sphing-4-enine	2.65325	0.856109	Component of membrane
Phosphocreatine	2.27599	0.460029	Stores phosphates
Theophylline	2.10964	2.81174	
sn-glycero-3-Phosphoethanolamine	2.09417	1.01854	Component of membrane
Ethanolamine phosphate	2.04952	1.08794	Derivative of phospholipids
L-Glutamine	1.86488	0.797577	Non-essential and conditionally essential AA
N-(L-Arginino) succinate	1.77658	0.652732	Precursor of arginine in urea cycle or citrulline-NO cycle, precursor to TCA metabolite fumarate
myo-Inositol	1.74874	0.696057	Cell signal transduction and osmoregulation
Sulfate	1.66235	0.407945	
Succinate	1.59789	0.308169	TCA intermediate
sn-Glycerol 3-phosphate	1.57173	0.487452	Associated with glycolysis and TCA cycle.

[FA trihydroxy(4:0)] 2_3_4-trihydroxy-butanoic acid	1.54532	0.833252	
ATP	1.47544	0.522892	Energy
D-Glucosamine	1.47071	0.441111	Biosynthesis of glycosylated proteins and lipids
[FA (5:1/13:0)] 13-(2-cyclopentenyl)-tridecanoic acid	1.38737	0.634557	
L-Gulonate	1.37893	0.745524	Pentose and glucoronate interconversions
2-Oxoglutarate	1.2703	0.326084	TCA intermediate
3'-Phosphoadenylyl sulfate	1.26677	0.979296	Associated with nucleotide biosynthesis
Creatine	1.2391	0.529488	Recycling ATP
2-Furoate	1.21503	0.406937	
5-Hydroxyisourate	1.16044	1.49434	Associated with purine
L-Arginine	1.15269	0.794265	Arginine metabolism
D-Sorbitol	1.1308	0.356313	Converted to fructose
[FA hydroxy(6:0)] 6-hydroxy-hexanal	1.11838	0.51621	Fatty acid
L-Serine	1.10113	0.365254	Non-essential AA
UTP	1.08881	0.604077	Nucleotide
L-Dehydroascorbate	1.08629	0.285279	Oxidised form of Vitamin C
2-C-Methyl-D-erythritol 4-phosphate	1.03783	1.57526	Isoprenoid precursor biosynthesis
[PR] Loroxanthin ester/ Loroxanthin dodecenoate	1.00883	0.517075	
UDP-glucose	0.976127	0.319294	Nucleotide sugar
N-Acetyl-L-aspartate	0.953206	0.545355	Derivative of aspartic acid
[SP (16:0)] N-(hexadecanoyl)-sphinganine	0.950639	0.662099	Lipid
L-Citrulline	0.940013	0.258818	Arginine metabolism
[PC (15:0)] 1-pentadecanoyl-sn-glycero-3-phosphocholine	0.932165	0.562698	Membrane component
6-aza-uridine	0.925117	0.443286	
L-Leucine	0.905953	0.737123	Essential AA
[PR] (+)-15-nor-4-thujopsen-3-one	0.904191	0.718263	
L-Ornithine	0.876937	0.1977	
allopurinol	0.871505	0.610457	
N-stearoyl glutamine	0.870186	0.751156	Fatty acid compounds
[PC (15:1)] 1-(1Z-pentadecenyl)-sn-glycero-3-phosphocholine	0.867095	0.533002	Membrane component
[FA (20:3)] 8Z_1Z1_14Z-Eicosatrien-5-ynoic acid	0.845798	0.632257	Fatty acid
(R)-2-Hydroxyglutarate	0.83493	0.325581	Associated with TCA
Diacetyl	0.829856	0.861658	

[SP (24:0)] N-(15Z-tetracosenoyl)-sphing-4-enine	0.803521	0.40176	Component of membrane
[ST] (22R_25R)-spirosol-5-en-3beta-ol	0.796073	0.278574	
L-Alanine	0.794513	0.275643	Non-essential AA
UDP-N-acetyl-D-glucosamine	0.785286	0.363136	Nucleotide sugar and co-enzyme
adrenochrome o-semiquinone	0.781977	0.778221	Associated with anti-oxidants
L-Asparagine	0.776196	0.454245	Non-essential AA
[SP (22:0)] N-(docosanoyl)-sphing-4-enine	0.769309	0.499132	Component of membrane
Pyruvate	0.760384	0.51047	Glycolysis intermediate
N-Acetyl-L-glutamate	0.74924	0.377203	Associated with arginine
[PE (16:1)] 1-(1Z-hexadecenyl)-sn-glycero-3-phosphoethanolamine	0.744485	0.598925	Component of membrane
Ximaosteroid C	0.735728	0.556407	Lipid
[PR] bacteriohopane-31_32_33_34-tetrol-35-cyclitol	0.730611	0.349674	Lipid
1-Phosphatidyl-1D-myo-inositol3-phosphate	0.722662	0.292006	Unknown
2-Hydroxyethanesulfonate	0.712362	0.507633	Unknown
Kigelinone	0.699282	0.180029	Unknown
3-phosphoglucarate	0.697729	0.178821	Associated with glycolysis
[PR] 9_13-di-cis-retinoic acid	0.692376	0.606399	Plasma metabolite
5-Oxoavermectin "2a" aglycone	0.683401	0.570923	
Pantothenate	0.674156	0.377367	Vitamin B5
7E_9E_11-Dodecatrienyl acetate	0.644897	0.426483	Lipid
Allantoin	0.64189	0.234061	Oxidation of uric acid and purines
[Fv] Naringenin	0.640858	0.115156	Flavonoid
2-Dehydro-3-deoxy-L-rhamnonate	0.640359	0.188112	Unknown
6-Methylpretetramide	0.632459	0.536453	Unknown
D-Glucose 6-phosphate	0.632139	0.158251	Associated with glycolysis
[PS (18:0)] 1-octadecanoyl-sn-glycero-3-phosphoserine	0.623219	0.423377	Lipids
Glycerophosphoglycerol	0.622984	0.232312	Associated with glycolysis
L-Tyrosine	0.606042	0.238681	Non-essential AA
Ophiobolin A	0.601909	0.428307	
4-Methylene-L-glutamine	0.59971	0.296795	Unknown
L-Glutamate	0.59164	0.547677	Arginine metabolism
Hydantoin-5-propionate	0.588453	0.423188	Histidine degradation
L-Methionine	0.585776	0.252513	AA
1-deoxynojirimycin	0.577137	0.229225	Glucosidase inhibitor
N-Undecanoylglycine	0.570744	0.595704	Fatty acid metabolite
L-Histidine	0.570655	0.298001	Essential AA

ethyl propionate	0.565569	0.526147	Propionic acid
Cholesterolsulfate	0.554617	0.533973	Regulatory and stabilising function on membrane
1-18:3-2-16:2-monogalactosyldiacylglycerol	0.548609	0.581037	Lipid
4_5-epoxy-17R-HDHA	0.54561	0.184857	Lipid
[PG (16:0)] 1-hexadecanoyl-sn-glycero-3-phospho-(1'-sn-glycerol)	0.545099	0.322113	Lipid
L-Valine	0.542589	0.208265	Essential AA
CTP	0.5416	0.355846	Nucleotide
meso-2_6-Diaminoheptanedioate	0.5356	0.187259	
nonulose 9-phosphate	0.522813	0.455789	Associated with PPP
(3R)-hydroxy-N-acetyl-(L)-arginine	0.520271	0.209255	Associated with Arginine
5-Hydroxypentanoate	0.514897	0.400311	Unknown
Hippurate	0.514027	0.196979	
Phenolsulfonphthalein	0.514	0.364634	Phenol red
[FA hydroxy(26:0)] 2-hydroxy-hexacosanoic acid	0.511841[4]	0.536062	Fatty acid

[1]The data was analysed on SIMCA. The value represents the difference between the distinct groups.

[2] The value highlights variety within each sample groups

[3] Metabolites from each metabolic pathway are highlighted in the VIP table where glycolysis is coloured green, TCA cycle; blue, OXPHOS; yellow and arginine metabolism; orange. Undetermined metabolites are greyed out.

[4] The VIP list was limited to a VIP score of ≥ 0.50

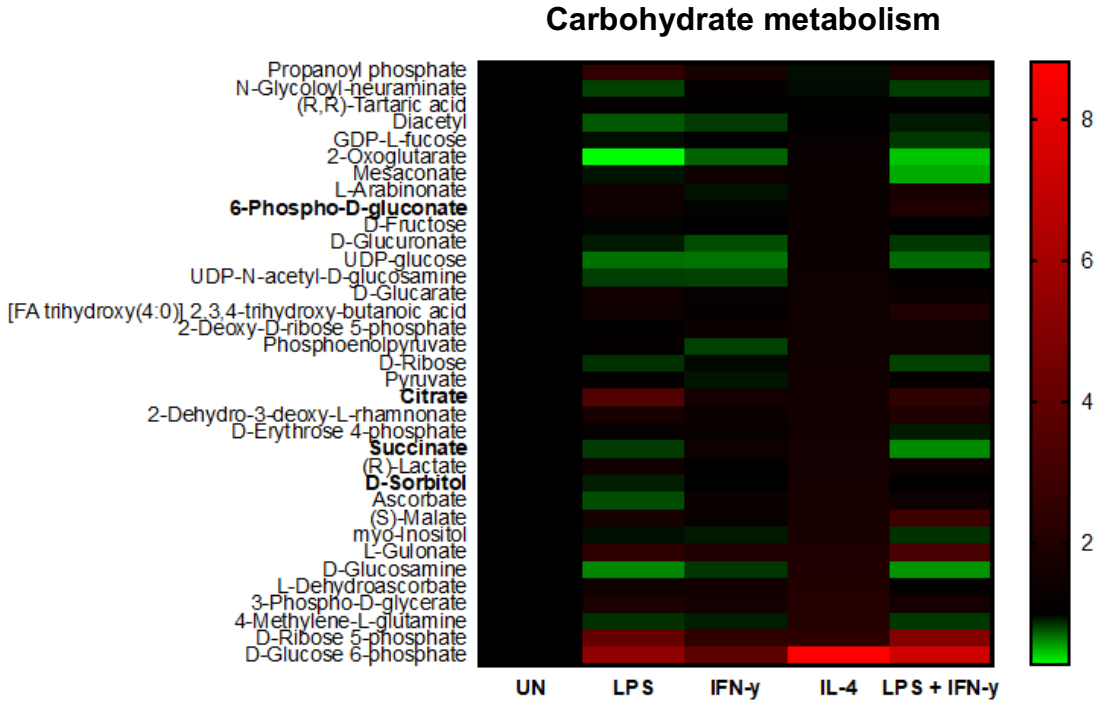
Carbohydrate metabolism
Propanoyl phosphate
N-Glycoloyl-neuraminate
(R,R)-Tartaric acid
Diacetyl
GDP-L-fucose
2-Oxoglutarate
Mesaconate
L-Arabinonate
6-Phospho-D-gluconate
D-Fructose
D-Glucuronate
UDP-glucose
UDP-N-acetyl-D-glucosamine
D-Glucarate
[FA trihydroxy(4:0)] 2,3,4-trihydroxy-butanoic acid
2-Deoxy-D-ribose 5-phosphate
Phosphoenolpyruvate
D-Ribose
Pyruvate
Citrate
2-Dehydro-3-deoxy-L-rhamnonate
D-Erythrose 4-phosphate
Succinate
(R)-Lactate
D-Sorbitol
Ascorbate
(S)-Malate
myo-Inositol
L-Gulonate
D-Glucosamine
L-Dehydroascorbate
3-Phospho-D-glycerate
4-Methylene-L-glutamine
D-Ribose 5-phosphate
D-Glucose 6-phosphate
8
6
4
2
UN
LPS
IFN-y
IL-4
LPS + IFN-y

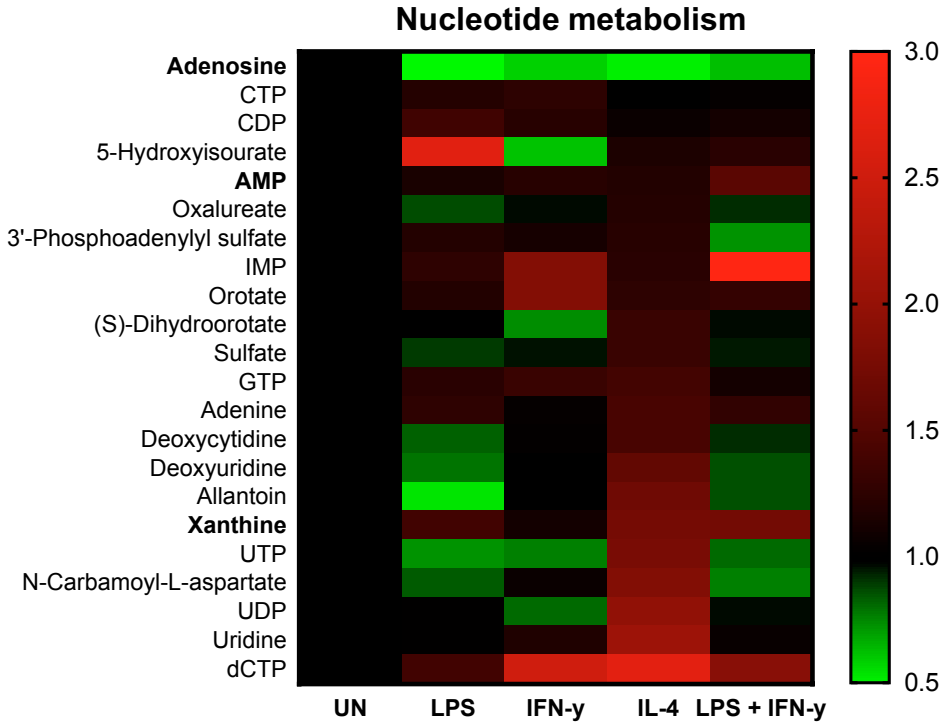
Nucleotide metabolism
Adenosine
CTP
CDP
5-Hydroxyisourate
AMP
Oxalureate
3'-Phosphoadenylyl sulfate
IMP
Orotate
(S)-Dihydroorotate
Sulfate
GTP
Adenine
Deoxycytidine
Deoxyuridine
Allantoin
Xanthine
UTP
N-Carbamoyl-L-aspartate
UDP
Uridine
dCTP
3.0
2.5
2.0
1.5
1.0
0.5
UN
LPS
IFN-y
IL-4
LPS + IFN-y

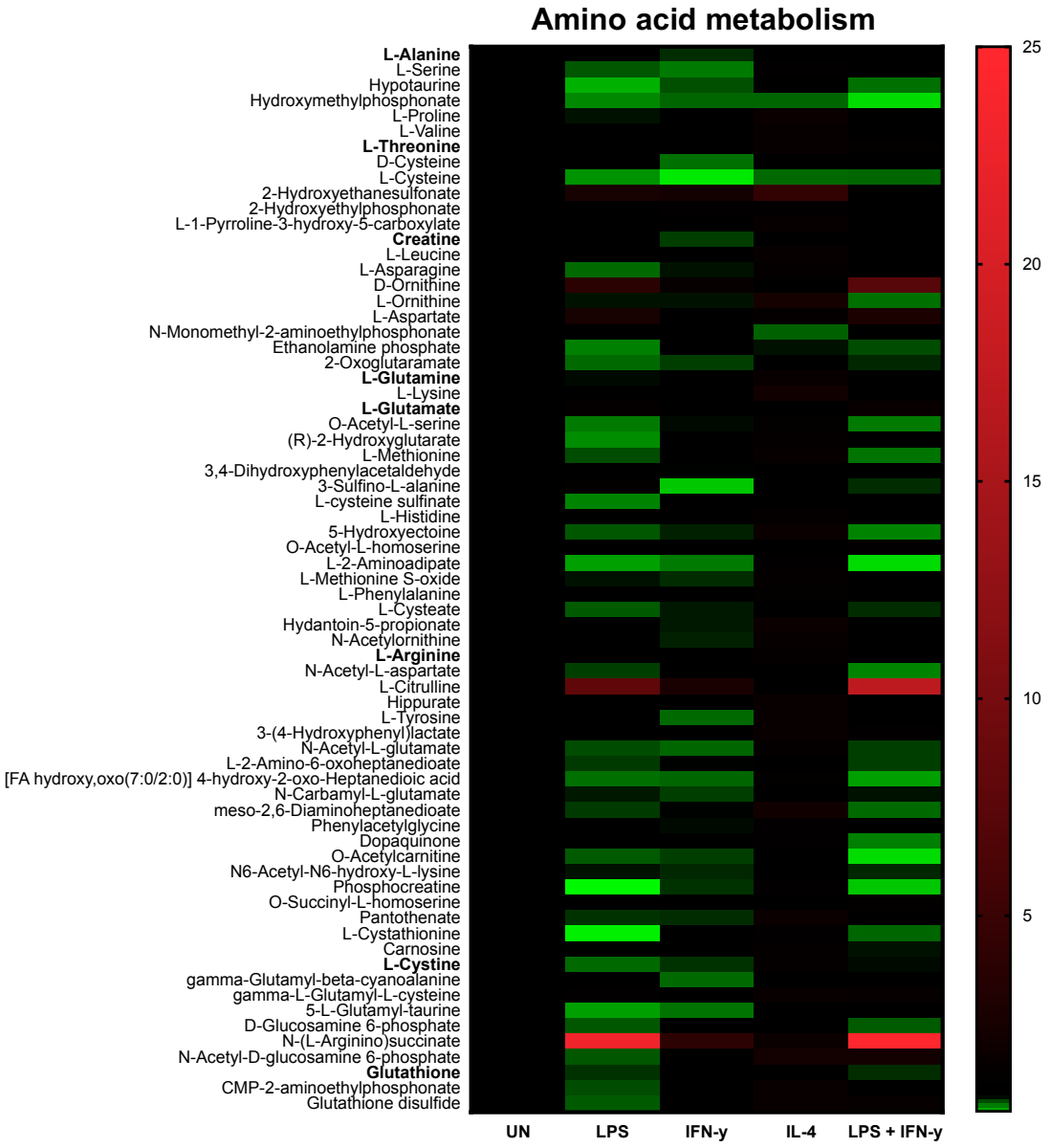

Figure 3.3. Global metabolic activity of BMDCs treated with LPS, IFN-γ or IL-4. Bone marrow derived DCs were stimulated with combinations of LPS, IFN-γ or IL-4 as indicated for 24 hours. After this time, the metabolites of the BMDCs were extracted and measured via Liquid chromatography mass spectroscopy (LCMS). A heat map was constructed from the analysed data on IDEOM and Prism7 and shows the fold change increase (Red) or the decrease (Green) of each metabolite compared to its representative unstimulated control (Black). Standards are highlighted in bold. N=2

3.2.3 Metabolic pathways of interest

As mentioned above, the presence or absence of many metabolite intermediates within pathways can be indicative of the activation status of an immune cell. These include glycolysis, TCA cycle and arginine metabolism (which had many metabolites present with a VIP score of ≥0.50). These particular pathways and PPP (an extension of glycolysis) have been selected for further analysis as they play crucial roles in either energy generation or have been shown to be crucial in altering an immune response to infection.

3.2.3.1 Glycolysis

Glucose-6-phosphate, fructose 1,6-biphosphate, phospho-D-glycerate, phosphoenolpyruvate, pyruvate and lactate are all metabolites of the glycolysis pathway. To reiterate, glycolysis is the first step in the breakdown of glucose to produce the high-energy molecules, ATP and NADH. Within this pathway, glucose is metabolised into pyruvate (under aerobic conditions) or lactate (in an anaerobic environment). In comparison to naïve BMDCs, those treated with LPS, IFN-γ or LPS + IFN-γ had a significant up-regulation of both glucose 6 phosphate (p=0.0015; 0.0353; <0.0001) and fructose 1,6 bisphosphate (p=0.0005; 0.0090; 0.0002) (Figure 3.4). Significant difference was also observed in the levels of phospho-D-glycerate in IFN- γ (p=0.05) and LPS + IFN-γ (p=0.05) stimulated BMDC compared to control cells. Phosphoenolpyruvate (p=0.05), pyruvate (p=0.05) and lactate (p=0.05) was significantly increased between naïve and BMDCs activated with LPS + IFN-γ. Lactate was also significantly elevated in LPS stimulated cells (p=0.05).

Significant up-regulation of glycolysis intermediates was also observed in BMDCs treated with IL-4 including an increase in levels of glucose-6-phosphate ($p=0.0001$), fructose 1, 6 phosphate ($p=0.05$), phospho-D-glycerate ($p=0.0376$), phosphoenolpyruvate ($p=0.0471$), pyruvate ($p=0.0064$) and lactate ($p=0.0150$).

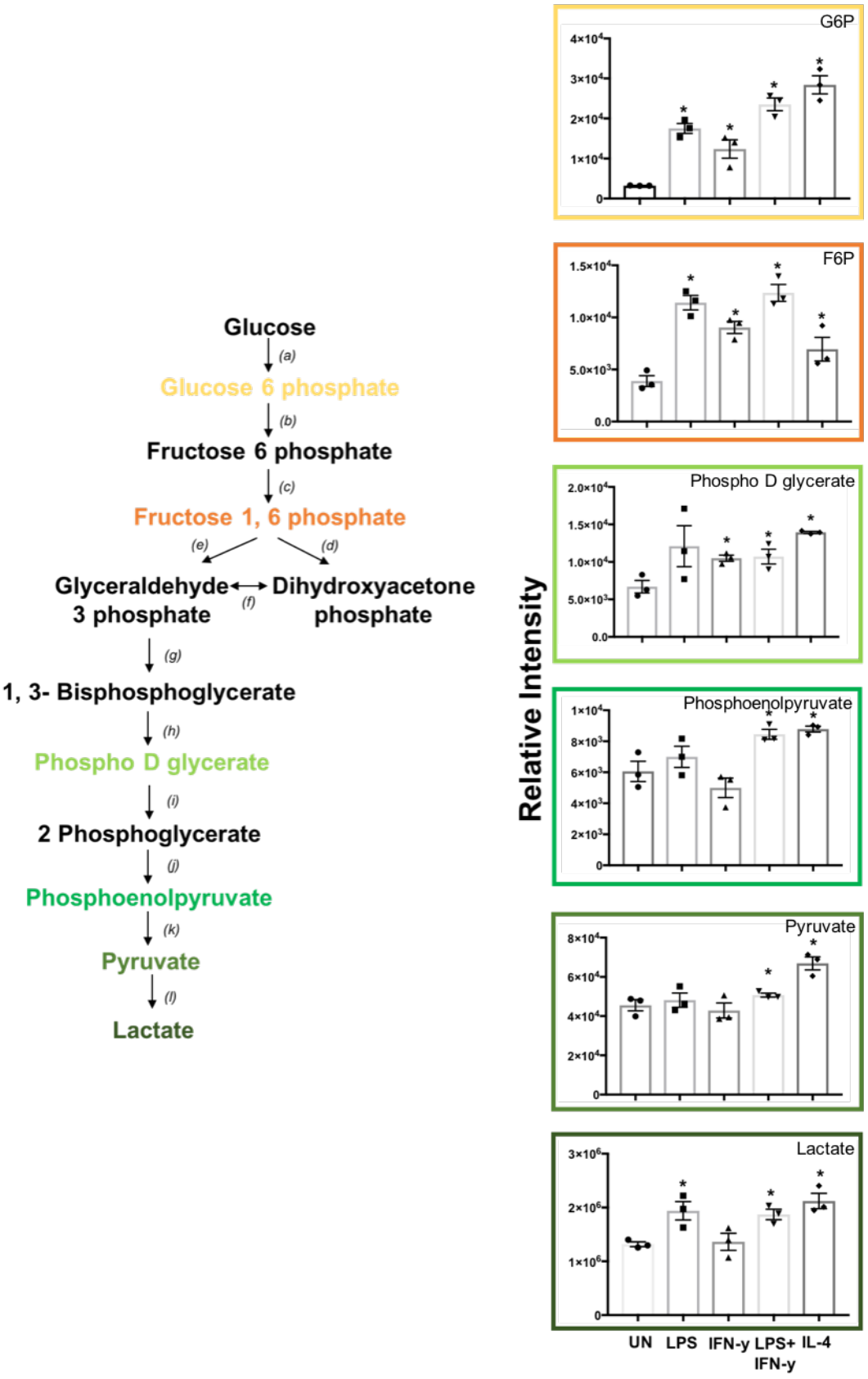
Glucose
(a)
Glucose 6 phosphate
(b)
Fructose 6 phosphate
(c)
Fructose 1, 6 phosphate
(e)
(d)
Glyceraldehyde 3 phosphate
(f)
Dihydroxyacetone phosphate
(g)
1, 3- Bisphosphoglycerate
(h)
Phospho D glycerate
(i)
2 Phosphoglycerate
(j)
Phosphoenolpyruvate
(k)
Pyruvate
(l)
Lactate
G6P
F6P
Phospho D glycerate
Phosphoenolpyruvate
Pyruvate
Lactate
Relative Intensity
UN
LPS
IFN-y
LPS+ IFN-y
IL-4

Figure 3.4. Glycolysis differences in LPS, IFN-γ or IL-4 stimulated BMDCs. Bone marrow derived DCs were stimulated with either LPS +/- IFN-γ, or IL-4 as indicated for 24 hours. After this time, the metabolites of the BMDCs were extracted and analysed by Liquid Chromatography Mass Spectroscopy (LCMS). For clarity, the diagram focuses on relevant metabolites (shown by the graphs) and enzymes (depicted (a) through to (k)) for Glycolysis only. (a) hexokinase; (b) phosphoglucose isomerase; (c) phosphofructokinase; (d) fructose bisphosphate aldose; (e) triose phosphate isomerase; (f) glyceraldehyde 3-phosphate dehydrogenase; (g) phosphoglycerate kinase; (i) phosphoglycerate mutase (j) enolase (k) pyruvate kinase; (l) lactate dehydrogenase. Statistical analysis was performed using non-parametric Mann Whitney test. Significant differences are $p < 0.05$ where * is compared to unstimulated. Results are representative of two independent runs, n = 2.

3.2.3.2. TCA cycle

From the metabolomics data, it was possible to identify 4 of the intermediates associated with the TCA cycle including citrate, α-ketoglutrate, succinate and malate. The TCA cycle is the second step of generating ATP from glucose. Once metabolised from pyruvate, acetyl-coA can enter the TCA cycle (Figure 3.5). The key reactions of the cycle are the reduction of NAD+ into NADH, these can then be introduced into the electron transport chain (e.g. OXPHOS) to generate ATP.

Significant accumulation of citrate (p=0.006; 0.05, 0.0241) could be seen in LPS, IFN-γ and LPS + IFN-γ activated BMDCs in comparison to naïve cells (Figure 3.5) whilst α- ketoglutarate (p=0.05; 0.05; 0.05) was significantly decreased by these activation stimuli. In addition, significant up-regulation of malate (p= 0.05; 0.0005) was seen in LPS and LPS + IFN-γ activated BMDCs whilst an increase in succinate (p=0.0251; 0.0455) was observed in IFN-γ primed BMDCs. LPS stimulated BMDCs and those activated with LPS + IFN-γ had significantly decreased succinate levels (p=0.05; 0.05). IL-4 treated BMDCs, had significantly increased levels of citrate (p=0.05), succinate (p=0.0017) and malate (p=0.05) when compared to naïve BMDCs (Figure 3.6).

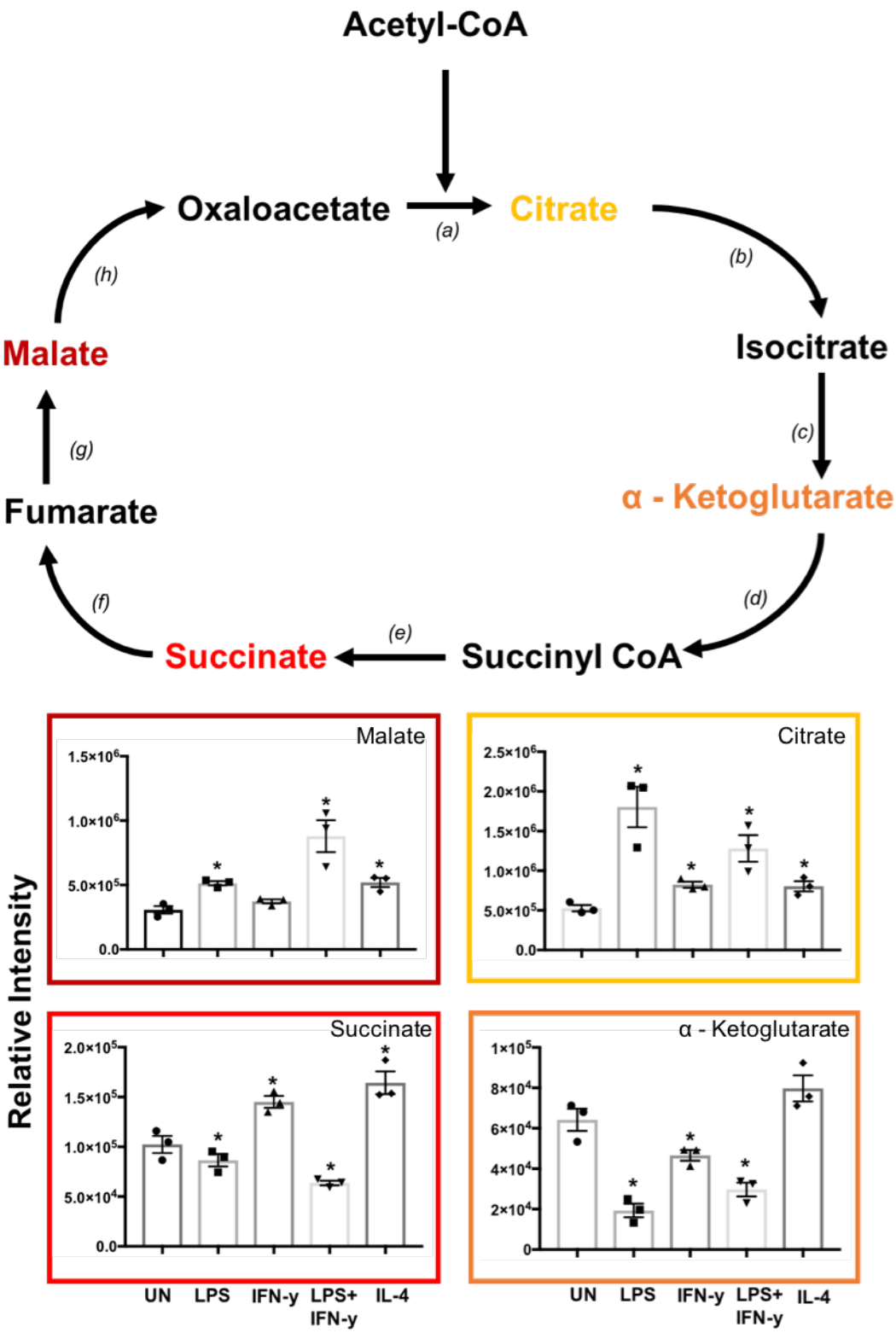
Acetyl-CoA
Oxaloacetate
Citrate
(a)
(b)
Isocitrate
(c)
α - Ketoglutarate
(d)
Succinyl CoA
(e)
Succinate
(f)
Fumarate
(g)
Malate
(h)
Relative Intensity
Malate
Citrate
Succinate
α - Ketoglutarate
UN
LPS
IFN-y
LPS+ IFN-y
IL-4

Figure 3.5. TCA cycle changes in LPS +/- IFN-γ and IL-4 activated BMDCs. Bone marrow derived DCs were stimulated with either LPS +/- IFN-γ, or IL-4 as indicated for 24 hours. After this time, the metabolites of the BMDCs were extracted and analysed by Liquid Chromatography Mass Spectroscopy (LCMS). For clarity, the diagram focuses on relevant metabolites (shown by the graphs) and enzymes (depicted (a) through to (h)) for the Krebs cycle only. (a) citrate synthase; (b) aconitase; (c) isocitrate dehydrogenase; (d) α-ketoglutarate dehydrogenase; (e) succinyl-CoA synthetase; (f) succinate dehydrogenase; (g) fumarase; (h) malate dehydrogenase. Statistical analysis was performed using non-parametric Mann Whitney test. Significant differences are $p < 0.05$ where * is compared to unstimulated. Results are representative of two independent runs, n = 2.

3.2.3.3. Pentose phosphate pathway

The pentose phosphate pathway is frequently described as an extension of glycolysis where the primary role of the PPP is the generation of both NADPH and ribose 5 phosphate, which is the precursor for nucleotide synthesis. PPP metabolites detected by LCMS include glucose 6 phosphate, phosphogluconate, ribose 5 phosphate and erythrose 4 phosphate (Figure 3.6). In comparison to naïve BMDCs, glucose 6 phosphate and ribose 5 phosphate were all significantly increased in IFN-γ primed BMDCs (p=0.0353; 0.0083), LPS stimulated BMDCs, (p=0.0015; <0.0001), LPS + IFN-γ activated BMDCs (p=<0.0001; 0.0001) and those treated with IL-4 (p=<0.0001; 0.0125). Furthermore, phosphogluconate was significantly decreased in IFN-γ stimulated BMDCs (p=0.05) and erythrose 4 phosphate was significantly increased (p=0.0449) in IL-4 treated BMDCs (Figure 3.6).

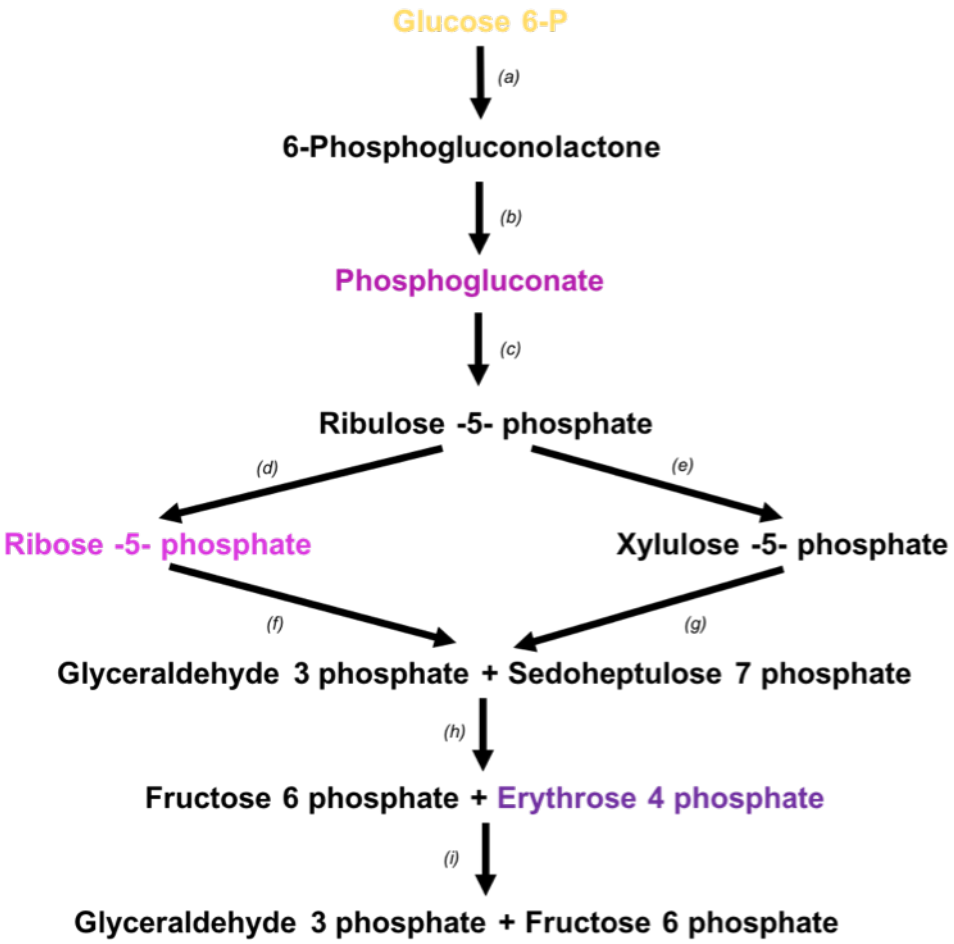
Glucose 6-P
(a)
6-Phosphogluconolactone
(b)
Phosphogluconate
(c)
Ribulose -5- phosphate
(d)
(e)
Ribose -5- phosphate
Xylulose -5- phosphate
(f)
(g)
Glyceraldehyde 3 phosphate + Sedoheptulose 7 phosphate
(h)
Fructose 6 phosphate + Erythrose 4 phosphate
(i)
Glyceraldehyde 3 phosphate + Fructose 6 phosphate

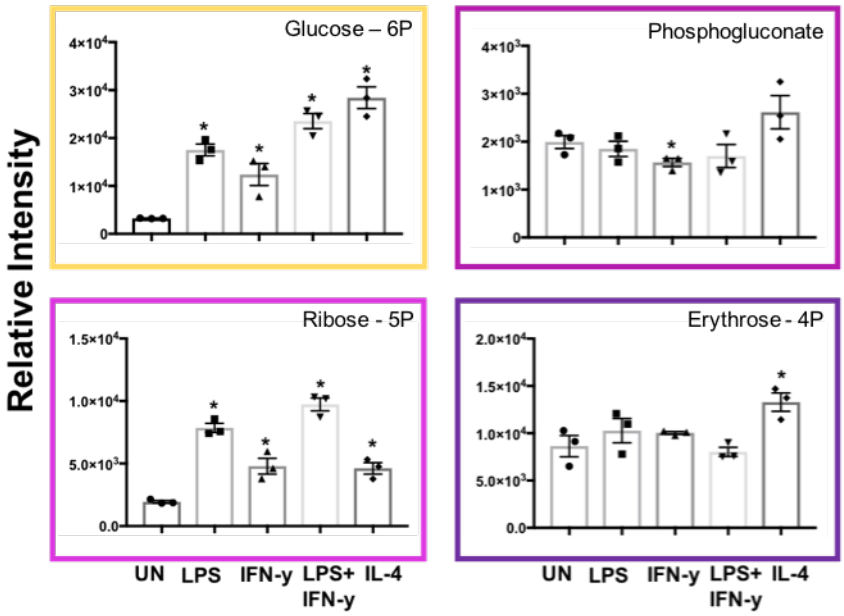
Relative Intensity
Glucose – 6P
Phosphogluconate
Ribose - 5P
Erythrose - 4P
UN
LPS
IFN-y
LPS+ IFN-y
IL-4

Figure 3.6. Pentose phosphate pathway (PPP) differences in BMDCs treated with different activation stimuli. Bone marrow derived DCs were stimulated with either LPS +/- IFN-γ, or IL-4 as indicated for 24 hours. After this time, the metabolites of the BMDCs were extracted and analysed by Liquid Chromatography Mass Spectroscopy (LCMS). For clarity, the diagram focuses on relevant metabolites (shown by the graphs) and enzymes (depicted (a) through to (k)) for PPP only. (a) Glucose 6 phosphate dehydrogenase; (b) Gluconolactonase; (c) 6-phosphogluconate dehydrogenase; (d) ribulose 5 phosphate isomerase; (e) ribulose 5 phosphate 3 epimerase; (f/g/i) transketolase; (h) Transaldolase. Statistical analysis was performed using non-parametric Mann Whitney test. Significant differences are $p < 0.05$ where * is compared to unstimulated. Results are representative of two independent runs, n = 2.

3.2.3.4. Arginine metabolism

Arginine metabolites detected by LCMS include L-Citrulline, L-Ornithine, L-Arginine, L-Proline, Creatine, L-1-pyrroline-3-hydroxy-5-carboxylate and L-Argininosuccinate (Figure 3.7). As described previously within this chapter, there is a distinct metabolic profile between BMDCs primed with IFN-γ, activated with LPS (+/-IFN-γ) or treated with IL-4. In comparison to naïve cells, BMDCs activated with LPS, IFN-γ or LPS + IFN-γ significantly increased citrulline (p=<0.0001; <0.0001) and Argininosuccinate (p=<0.0001). Arginine was also elevated in LPS and IFN-γ treated BMDCs when compared to control cells. (Figure 3.7). Significant down-regulation of ornithine was also observed in LPS + IFN-γ (p=0.05) activated DCs. In addition, BMDCs stimulated with LPS (+/-IFN-γ) significantly increased glutamate (p=0.01; 0.01).

This is in contrast to IL-4 treated cells which had a significantly elevated presence of arginine (p=0.0162), ornithine (p=<0.0001) L-proline (p=0.0043), L-1-pyrroline-3-hydroxy-5-carboxylate (p=0.0012) and creatine (p=0.0244) compared with untreated cells.

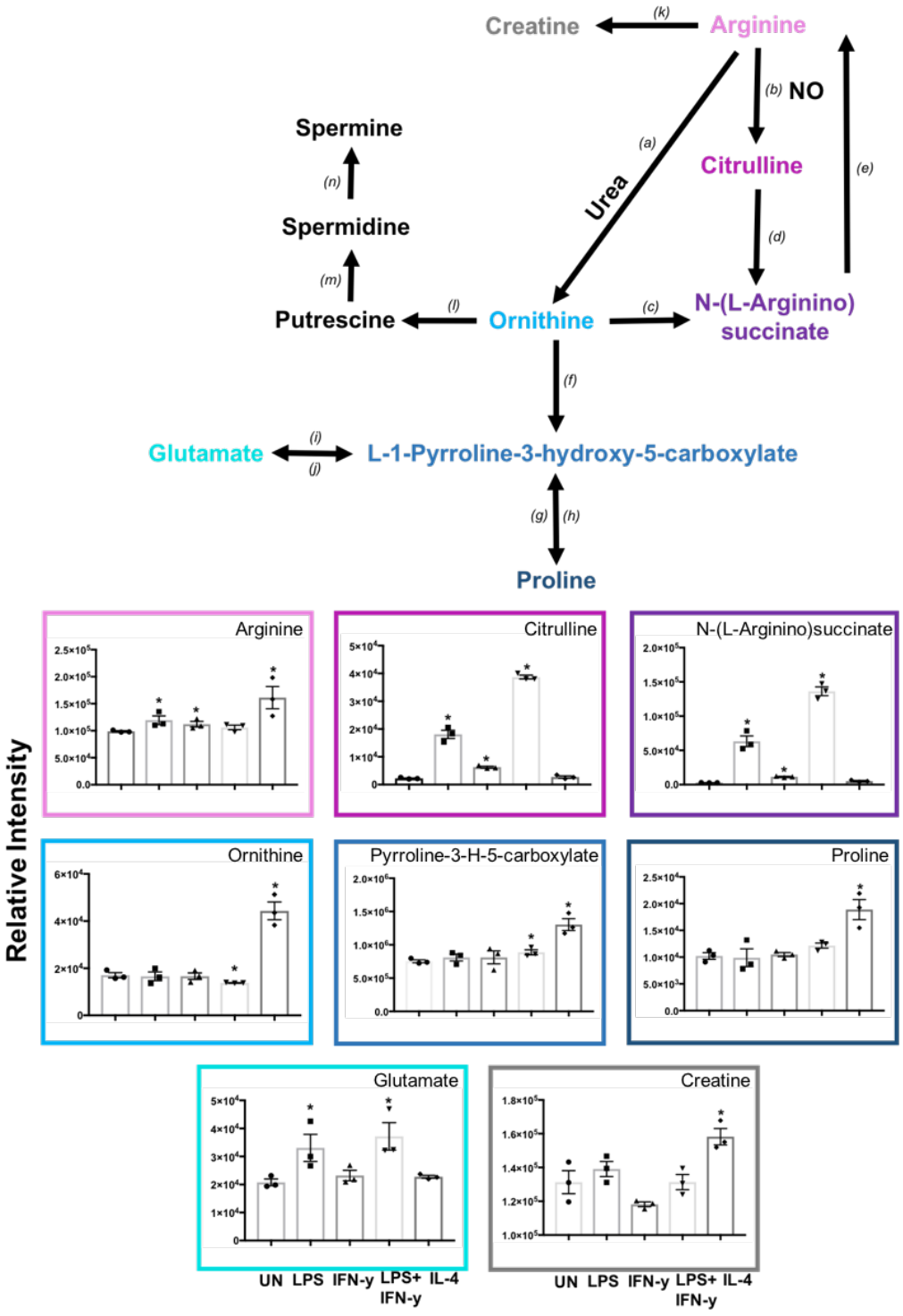
Creatine
(k)
Arginine
(b) NO
Spermine
(a)
Urea
Citrulline
(e)
(n)
Spermidine
(d)
(m)
Putrescine
(l)
Ornithine
(c)
N-(L-Arginino) succinate
(f)
Glutamate
(i)
(j)
L-1-Pyrroline-3-hydroxy-5-carboxylate
(g)
(h)
Proline
Relative Intensity
Arginine
Citrulline
N-(L-Arginino)succinate
Ornithine
Pyrroline-3-H-5-carboxylate
Proline
Glutamate
Creatine
UN
LPS
IFN-y
LPS+ IFN-y
IL-4

Figure 3.7. Arginine metabolism changes BMDCs stimulated with LPS, IFN-γ or IL-4. Bone marrow derived DCs were stimulated with combinations of LPS, IFN-γ, or IL-4 as indicated for 24 hours. After this time, the metabolites of the BMDCs were extracted and analysed by Liquid Chromatography Mass Spectroscopy (LCMS). For clarity, the diagram focuses on relevant metabolites (shown by the graphs) and enzymes (depicted (a) through to (n)) only. (a) arginase; (b) NOS; (c) ornithine transcarbamylase; (d) argininosuccinate synthase; (e) argininosuccinate lyase; (f) ornithine aminotransferase; (g) pyrroline-5-carboxylate reductase; (h) proline dehydrogenase; (i) pyrroline-5-carboxylate synthase; (j) P5C dehydrogenase (k) arginine: glycine amidinotransferase; (l) ornithine decarboxylase; (m) spermidine synthase and (n) spermine synthase. Statistical analysis was performed using non-parametric Mann Whitney test. Significant differences are $p < 0.05$ where * is compared to unstimulated. Results are representative of two independent runs, n = 2.

3.2.4. Activation stimuli alters glucose uptake in BMDCs.

To further investigate the extent activation stimuli influenced the energy metabolism of BMDCs, glucose uptake was measured. 2-NBDG (2-[*N*-(7-nitrobenz-2-oxa-1,3, -diazol-4-yl) is a widely used fluorescent derivative of glucose that is modified with a amino acid at the C2 position. This glucose derivative shows fluorescence at 542 nm when excited at 467 nm (Zou *et al*., 2005). Previous research on this compound has suggested that 2-NBDG is transported into the cell by the same glucose transporter as D-glucose, GLUT and can be used to determine glucose uptake within cells.

Literature has shown that some cells incubated with 2-NBDG may be damaged due to physiological and/ or toxicological effects of the glucose derivative (Zou *et al*., 2005). The FACS plots show no abnormal change in FSC or SSC, indicating that the BMDCs were not physically damaged in the presence of 2-NBDG (Figure 3.8A + B).

In addition, several studies show that 2-NBDG concentration higher than 0.25mM in certain cell lines including HepG2 and L6 might lead to self-quenching (Zou *et al*., 2005). To optimise the 2-NBDG concentration used for glucose uptake measurement in BMDCs, unstimulated BMDCs were incubated with 0, 5, 10, 25, 50, 100, 150, 200 and 250μM of 2-NBDG for either 30, 60 or 120 minutes, respectively. The MFI and rate of 2-NBDG uptake by the cells is both concentration and time dependent (Figure 3.8 C + D). Therefore, based on experimental results and previous literature on this topic, a concentration of 50μM with an incubation time of 120 minutes of 2-NBDG was used for further experiments on LPS stimulated BMDCs.

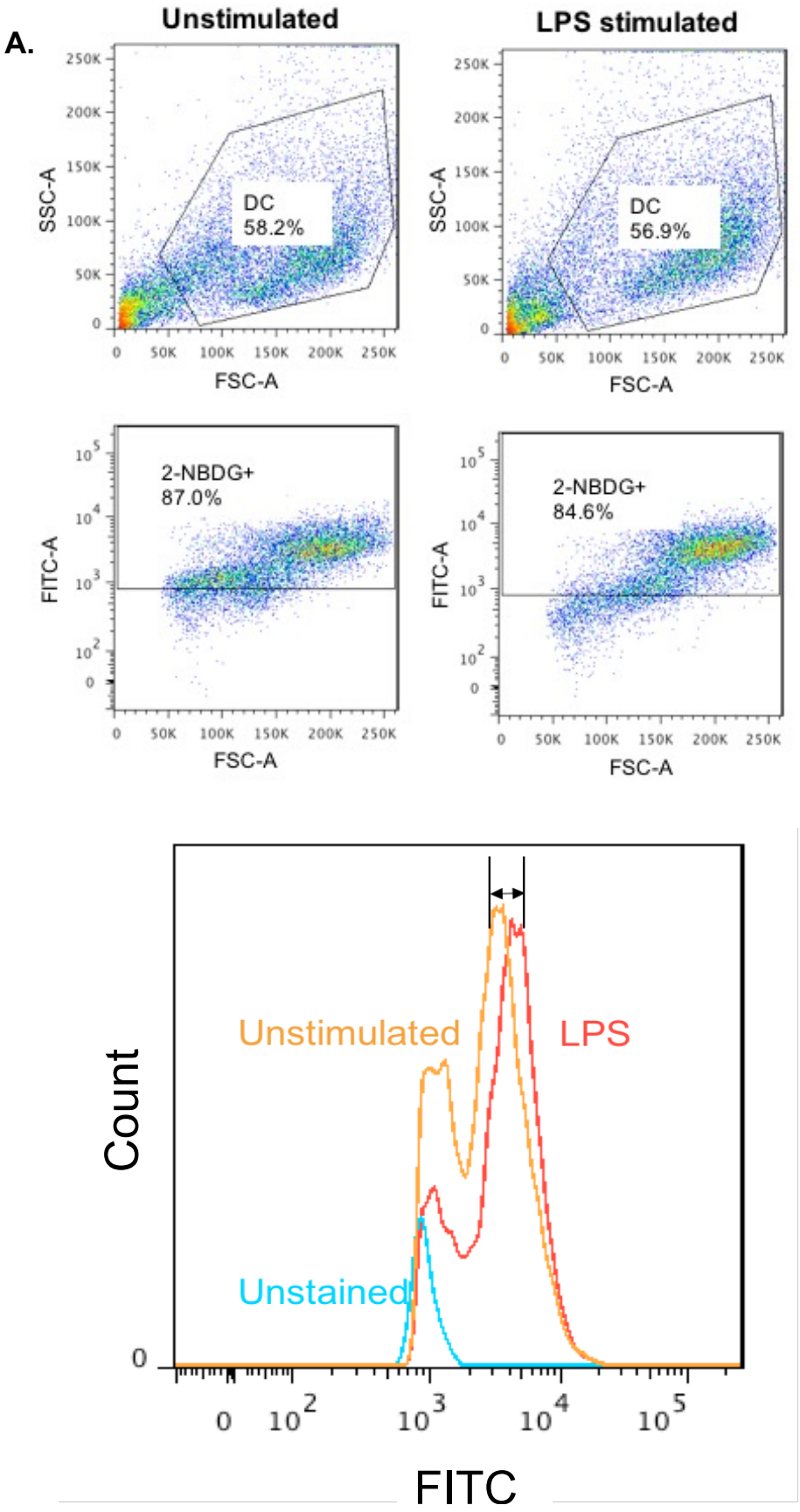
A.
Unstimulated
LPS stimulated
SSC-A
FSC-A
DC
58.2%
DC
56.9%
FITC-A
2-NBDG+
87.0%
2-NBDG+
84.6%
Count
Unstimulated
LPS
Unstained
0
FITC

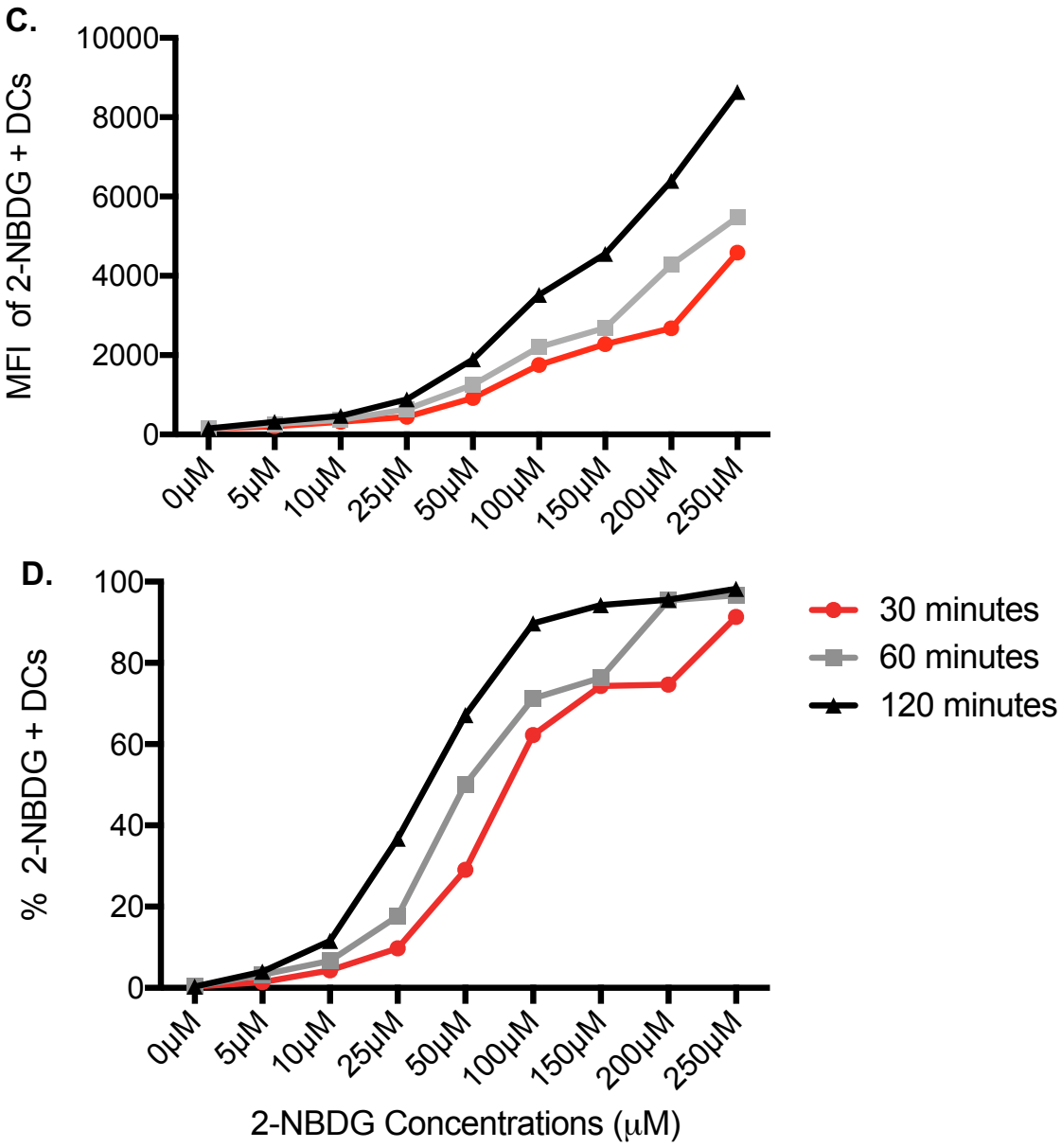

Figure 3.8. Optimising the concentration and length of time 2-NBDG can be exposed to BMDCs. Unstimulated or LPS stimulated bone marrow derived DCs were incubated with 5, 10, 25, 50, 100, 150, 200 or 250μM of 2-NBDG for either 30 minutes (red line), 60 minutes (grey line) or 120 minutes (black line) and then prepared for flow cytometry. (A + B) The gating strategy used to validate cell viability of unstimulated and LPS stimulated BMDCs stained with 2-NBDG. (C) The mean fluorescent intensity (MFI) and (D) the proportion of 2-NBDG uptake by unstimulated BMDCs were then analysed. Results are representative of one preliminary experiment with no mean +/- SEM or significance calculated.

The effects of LPS treatment for either 4, 6, 12 or 24 hours on BMDC 2-NBDG uptake was investigated (Figure 3.9A). Stimulation of BMDCs with LPS for 12 hours or greater was necessary to induce 2-NBDG uptake and 24 hours was used thereafter to determine the effect of stimulants on this process.

To investigate how various stimuli influences glucose uptake of BMDCs, these cells were stimulated with LPS (+/- IFN-γ) or IL-4 for 24 hours before the addition of the glucose analogue, 2-NBDG. BMDCs that have been activated with LPS ($p=0.0101$) or IL-4 (0.0261) take up significantly greater amounts of the glucose analogue, 2-NBDG than unstimulated control cells (Figure 3.9B). No significant difference was seen in 2-NBDG uptake between naïve BMDCs and those stimulated with IFN-γ alone or in combination with LPS.

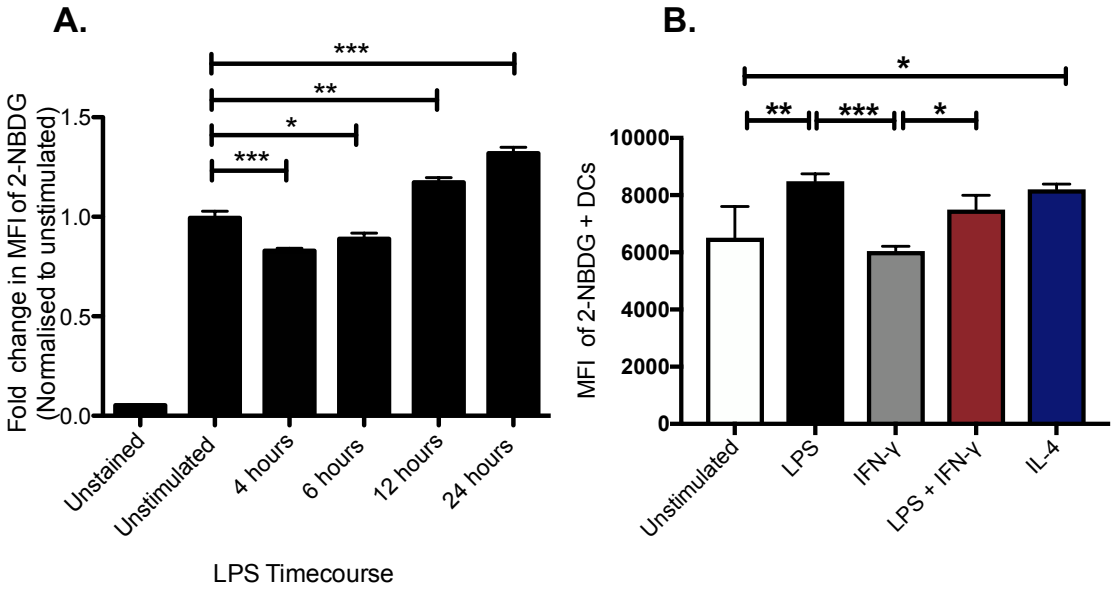

Figure 3.9. Glucose uptake is altered in LPS and IL-4 treated BMDCs. Bone marrow derived DCs were either (A) stimulated with LPS at 4, 6, 12 and 24 hours or (B) treated with LPS (+/- IFN-γ) or IL-4 for 24 hours before the addition of fluorescent 2-NBDG (50μM) for 120 minutes. The mean fluorescent intensity (MFI) of 2-NBDG was then quantified using flow cytometry. (A) shows the fold change in MFI expression as normalised to unstimulated controls whilst (B) are representative of three independent experiments (n = 3) and shows the mean +/- SEM. Statistical analysis performed using 1-way ANOVA using (A) Dunnett or (B) Bonferroni post-test. Significant differences were identified where *P<0.05, **P<0.01 and ***P<0.001.

3.2.5. BMDC iNOS expression and NO production is influenced by activation stimuli

Using flow cytometry, the proportions of iNOS expressing $CD11c^+$ cells were quantified by determining the percentage of cells showing staining above that of the unstained control. Whilst a small percentage of unstimulated BMDCs expressed iNOS, stimulation of BMDCs with LPS, resulted in a significant increase in the proportion of iNOS-expressing cells ($p=0.0171$) (Figure 3.10A). This significant increase in iNOS expression was also shown in BMDCs stimulated with LPS in combination with IFN-γ ($p=<0.0001$). BMDCs did not up-regulate iNOS in the presence of IFN-γ or IL-4 alone.

Consistent with these results the nitrite levels were increased in BMDCs stimulated with LPS alone or combination with IFN-γ ($p=<0.0001$), but not in BMDCs stimulated with IL-4 or IFN-γ alone (Figure 3.10B).

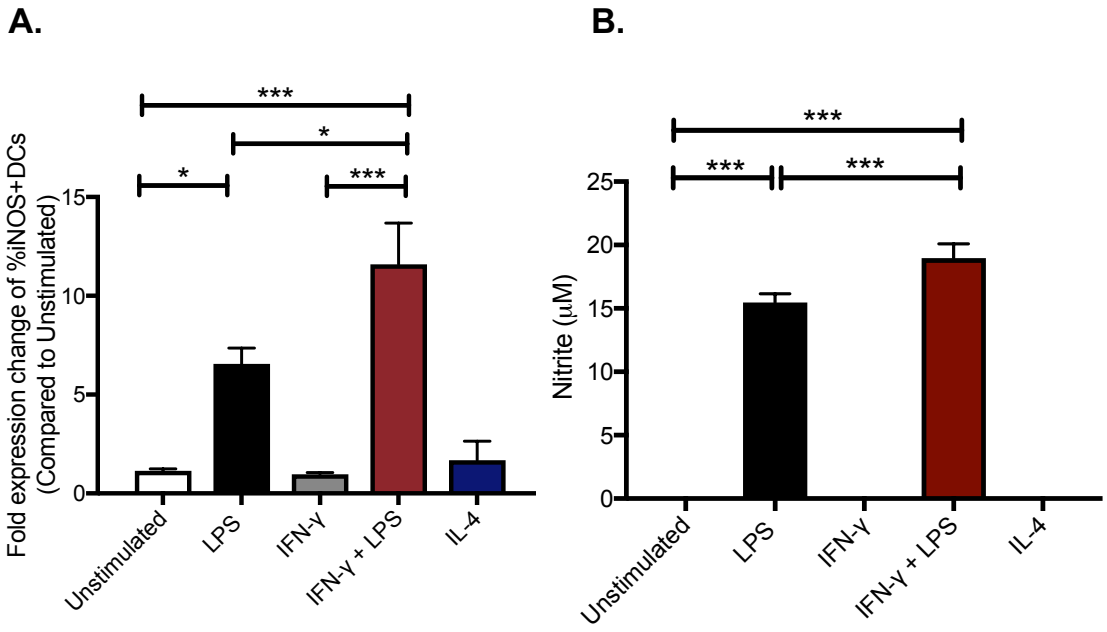

Figure 3.10. iNOS expression is up-regulated and NO production is increased during LPS (+/- IFN-γ) activation in BMDCs. Unstimulated bone marrow derived DCs were stimulated with combinations of LPS, IFN-γ, or IL-4 as indicated for 24 hours. After this time (A) cell were analysed by flow cytometry to determine the proportion of $CD11c^+$ cells expressing iNOS. (B) supernatant was collected and used to determine the nitrite production (μM). Results are either (A) the average of the fold expression change compared to naïve cells of three independent experiment or (B) representative of three independent experiment (n = 3) and show the mean +/- SEM. Statistical analysis performed using one-way ANOVA with Bonferroni post-test. Significant differences were identified as ***P<0.001, **P<0.01 and *P<0.05.

Figure 3.2 Summary of Findings	**LPS**	**IFN-y**	**LPS + IFN-y**	**IL-4**
DC Characteristics				
CD40 expression and IL-12 production	Increased	No Change	Increased	No Change
Global changes				
OPLS-DA separation	Yes	Yes	Yes	Yes
Metabolism changes				
Up-regulated Glycolysis metabolites	G6P, F6P & Lactate	G6P, F6P, Phospho-D-glycerate	G6P, F6P, Phospho-D-glycerate, Phospho-enol-pyruvate, Pyruvate & Lactate	G6P, F6P, Phospho-D-glycerate, Phospho-enol-pyruvate, Pyruvate & Lactate
Glucose uptake	Increased	No change	Slight increase	Increased
TCA intermediates	Up-regulated: Malate & Citrate Down-regulated: Succinate & Ketoglutarate	Up-regulated: Citrate & Succinate Down-regulated: Ketoglutarate	Up-regulated: Malate & Citrate Down-regulated: Succinate & Ketoglutarate	Up-regulated: Malate, Citrate Succinate & Ketoglutarate
Up-regulated metabolites associated with arginine metabolism	Arginine, Citrulline, N- (L-Arginino succinate)	Arginine, Citrulline, N- (L-Arginino succinate)	Citrulline, N- (L-Arginino succinate)	Arginine
iNOS expression and NO production	Increased	No change	Increased	No change

3.3 Discussion

It has been recognised within the literature that when an immune cell becomes activated its metabolism changes in order to meet its bioenergetic and biosynthetic needs (Reviewed in Everts *et al*., 2012; O'Neill *et al*., 2016). These changes in metabolism can influence effector function especially during disease (Kelly *et al*., 2015). Current research in the field of 'immunometabolism' has mainly focused on characterising the basic metabolism changes of activated macrophages during general inflammation (Stout *et al*., 2004). However, this means that other important immune cell types have been scarcely studied including the dendritic cell (Pearce and Everts, 2015). The role of BMDCs as primary antigen presenting cells and their provision of a bridge from the innate to adaptive immune response makes their characterisation essential. Therefore, the work described in this chapter has highlighted the phenotypic and metabolic complexity of BMDCs activated with a variety of stimuli alone or in combination.

To validate the activation stimuli used, their ability to alter key immunological parameters of BMDCs was measured. In keeping with the literature, BMDCs stimulated with LPS significantly up-regulated the activation marker CD40 as well as increasing IL-12 production (Cella *et al*., 1996; Verhasselt *et al*., 1997). CD40 and IL-12 was unaffected in BMDCs exposed to IFN-γ or IL-4. An additive effect occurred when BMDCs were stimulated with LPS in combination with IFN-γ causing a synergistic up-regulation of both CD40 and IL-12. These data validated the experimental approach and demonstrated the spectrum of activation states and

functional phenotypes that occur in BMDCs as a result of stimuli used. This set the foundation to examine how these activation states correlated with uptake of glucose, global changes in metabolism and production of nitric oxide.

Initial results demonstrated increased uptake of glucose in BMDCs stimulated with LPS which was not augmented with the addition of IFN-γ. Notably, IFN-γ also had no effect in the absence of LPS. This is consistent with data from LPS stimulated macrophages which demonstrated that overexpression of the glucose transport receptor, GLUT1 in LPS activated and RAW264.7 macrophages led to increased glucose uptake and shift to a proinflammatory phenotype (Fukuzumi *et al*., 1996; Freemerman *et al*., 2014). A novel finding is the ability of IL-4 stimulation to increase glucose uptake in immune cells, in this case BMDCs. Although, not described in the literature this makes sense as the breakdown of glucose to pyruvate via glycolysis must first commence before pyruvate can be fed into OXPHOS to generate ATP. In addition, studies by Jha *et al*. demonstrated that in IL-4 treated macrophages, glucose was sequestered from the central metabolism and used for the glycosylation of 'alternatively activated' mediators (e.g. mannose receptors) or for the synthesis of urdinine diphosphate N-acetyl glucosamine (UDP-GlcNAc), a nucleotide sugar and a co-enzyme (Jha *et al*., 2015). Consistent with the above results, elevated levels of glycolysis metabolites were detected by LCMS in BMDCs grown in all conditions.

Intermediates of the pentose phosphate pathway were altered in BMDCs irrespective of stimuli. As the PPP can be described as an extension of glycolysis, it was interesting to find that glucose-6-phosphate, phosphogluconate, ribose-5-phosphate were

increased in BMDCs stimulated alone or in combination with LPS and IFN-γ. This is consistent with studies of macrophages where PPP is known to increase following their activation with LPS and IFN- γ. (Freemerman *et al*. 2014; Haschemi *et al*., 2012). A novel finding of the studies described herein, is that IL-4 stimulation led to the elevated ribose 5-phosphate and erythrose-4-phosphate. The functional significance of this subtle difference is unknown, but may indicate the disparity between how erythrose 4-phosphate is further metabolised in LPS (+/- IFN-γ) stimulated BMDCs compared to those treated with IL-4.

LPS (+/- IFN-γ) stimulation led to increased TCA intermediates (malate and citrate) in dendritic cells. Until recently, this was a novel finding but seminal work by Everts *et al* has demonstrated accumulation of certain TCA intermediates in dendritic cells (Everts *et al*., 2012; Krawcyzyk *et al*., 2010). In macrophages, LPS stimulation leads to a decoupling of the electron transport chain from the TCA cycle, leading to an incomplete TCA cycle with 'breaks' and metabolite accumulation (Van den Bossche *et al*., 2016). The intermediates that accumulate have been demonstrated to influence the effector function of dendritic cells and macrophages (Tannahill *et al*., 2013; Jha *et al*., 2015; O'Neill *et al*., 2011). Thus, accumulated citrate is favourably removed from the TCA cycle and used for NADP+ reduction, fatty acid synthesis and production of inflammatory mediators, NO and ROS (Everts *et al*., 2012; O'Neill *et al*., 2011).

Consistent with previous data derived from macrophages, IL-4 was found to increase succinate in BMDCs generation (Everts *et al*., 2014; Jha *et al*., 2015; O'Neill *et al*., 2016). Rather than the Warburg effect, these authors used functional studies (for

example measuring the oxygen consumption rate (OCR) and extracellular acidification rate (ECAR) using the Seahorse Extracellular Flux Analyser) to demonstrate this up-regulation of TCA intermediates in macrophages which is accompanied by increased OXPHOS and ATP generation (Wu *et al*., 2007; Everts *et al*., 2014; Jha *et al*., 2015; O'Neill and Hardie, 2013). Similar studies will be required in dendritic cells to determine if this is also the case.

Another vital function of an immune cell is to generate free radicals used for pathogen defence. One such example is nitric oxide which is metabolised from arginine. Initial results demonstrated that whilst citrulline is elevated within LPS (+/- IFN-γ) stimulated BMDCs, ornithine is increased in IL-4 treated BMDCs. This is consistent with the literature in macrophages and BMDCs where citrulline and NO are present in an inflammatory phenotype and ornithine is elevated during 'alternative activation' or disease resolution (Galvan-Pena *et al*., 2014; Everts *et al*., 2015; O'Neill *et al*., 2011). In addition, the data in this chapter highlights that BMDCs stimulated with LPS (+/- IFN-γ) induce iNOS activity and NO production. These data suggest that BMDCs have a similar dichotomy to macrophages within arginine metabolism.

The results in this chapter confirms that like macrophages (Mosser and Edwards, 2008), dendritic cells adopt a spectrum of activation when stimulated with a variety of stimuli and this can alter the functional phenotype of the cell. Moreover, this data supports studies describing the Warburg effect in LPS (+/- IFN-γ) but not in IFN-γ or IL-4 treated BMDCs. This is exciting foundational data as it suggests that other virulence factors and pathogens not tested in this chapter may differentially activate

BMDCs to control effector function and influence the metabolism of immune cells. Therefore, the rest of this thesis will determine the extent pathogens, especially parasites can target and alter the BMDC metabolism for their own survival. This interplay between BMDCs and parasites will be discussed further in subsequent chapters.

Chapter 4

Leishmania mexicana and *Toxoplasma gondii* metabolic reprogramming of dendritic cells

4.1 Introduction

Intracellular parasites including *L. mexicana* and *T. gondii* persist within host cells by subverting the highly evolved immune response and altering cellular metabolism to derive nutrients (Xu *et al*., 2010). However, host cells have developed methods to limit parasite growth which in addition to killing mechanisms can also include altering the availability of certain essential metabolites (O'Neill *et al*., 2016). For example, *L. mexicana* and *T. gondii* are auxotrophic for tryptophan and arginine and must therefore scavenge these from their host cells (Fox *et al*., 2004; McConville *et al*., 2015; Blume *et al*., 2009), but the host cells, given the appropriate immunological signal can deplete these amino acids. Arginine is effectively reduced through induction of iNOS or Arginase 1 depending on the immunological environment, while tryptophan is depleted through induction of indolamine deoxygenase (IDO) (Munder *et al*., 2009). Immune mediated metabolism changes within the host cell may thus influence parasite growth and survival. The ability of a parasite to subvert immune mediated changes of innate host cells could potentially prevent or delay the development of effective immunity (Pearce *et al*., 2014). Advances in technology especially improvements to LCMS have allowed downstream metabolites to be efficiently detected. A better understanding of this host: pathogen interplay could provide greater insight into the pathogenesis of the diseases caused by these parasites and ultimately inform their treatments (Atamna *et al*.,1997; Gleeson *et al*., 2016; Gobert *et al*.,2001; Olszewski *et al*., 2009). The studies in this chapter aim to answer these fundamental questions in the most simplistic form. Specifically, to determine to what extent, two evolutionary distinct, obligate, intracellular parasites (*Leishmania mexicana* and *Toxoplasma gondii*) occupying unique niches within the cell specifically reprogram the dendritic

cell. LPS stimulation was also used in parallel cultures as a positive control and also to allow comparison of the results obtained using the LCMS employed in chapter 3 (Accela 600 HPLC system combined with an Exactive (Orbitrap)) with the LCMS used in this chapter (Dionex Ultimate 3000 RSLC system with a Thermo Orbitrap QExactive).

4.2 Results

4.2.1 Dendritic cells effectively internalise *L. mexicana* and *T. gondii* parasites during infection.

CFSE labelled *L. mexicana* (MOI 5:1) or *T. gondii* (MOI 1:1) were co-cultured with BMDCs to establish the extent these parasites were effectively taken up by BMDCs. Flow cytometry was used to identify the uptake rate of *L. mexicana* or *T. gondii* in $CD11c^+$ cells. Paraformaldehyde fixed parasites were used as controls to determine whether uptake is parasite specific or immune cell mediated. Compared to control BMDCs, live and PFA fixed *L. mexicana* and *T. gondii* were effectively internalised by BMDCs. *L. mexicana* promastigote internalisation was immune cell mediated with approximately 60% of PFA *L. mexicana* being effectively phagocytosed by BMDCs in comparison to 40% of live promastigotes (Figure 4.1). This is in direct contrast to *T. gondii* infected BMDCs where BMDC uptake was *Toxoplasma* dependent. This was observed by comparing % CFSE labelled live *T. gondii* ingested by $CD11c^+$ cells (80%) with those fixed with PFA (40%) (Figure 4.1).

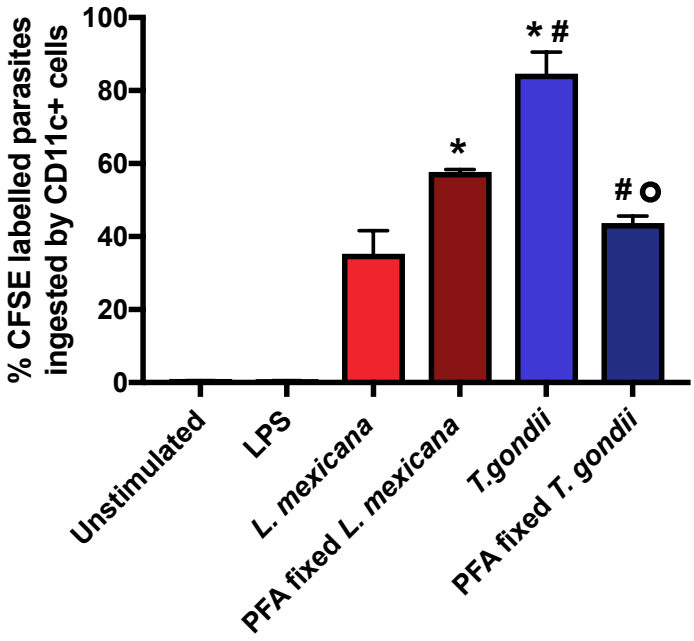

Figure 4.1. BMDCs effectively internalise *L. mexicana* or *T. gondii* parasites Bone marrow derived DCs were co-cultured with either CFSE labelled *L. mexicana* promastigotes (MOI 5:1) or CFSE labelled *T. gondii* tachyzoites (MOI 1:1). After 6 hours, cells were analysed by flow cytometry to determine CFSE parasite uptake. Results are representative of three independent experiments (n = 3) and show mean +/- SEM. A one-way ANOVA was performed with a Bonferroni post-test to determine significance (P< 0.01) where * is significant compared to *L. mexicana*, # is significant compared to PFA fixed *L. mexicana* and ○ is significant compared to *T. gondii*.

4.2.2 Dendritic cell activation markers are influenced by *L. mexicana* and *T. gondii* infection

Using flow cytometry, BMDCs were identified by gating on the cell surface marker CD11c. The proportion of $CD40^+$, $CD80^+$ or $CD86^+$ expressing cells were reported by determining the proportion of cells showing staining above that of the unstained or isotype control. Whilst a small percentage of unstimulated BMDCs expressed CD40, CD80 and CD86 stimulation of BMDCs with LPS resulted in a significant increase in the proportion of CD40 ($p=<0.0001$) and CD80 ($p=0.006$) but not CD86 expressing BMDCs relative to resting cells (Figure 4.2).

BMDC cultures infected with *L. mexicana* alone showed similar CD80 expression levels to non-infected BMDCs. However, CD40 and CD86 expression was up-regulated ($p= 0.006$) in these promastigote infected BMDCs. In addition, there was significantly higher CD40, CD80 and CD86 expression ($p=<0.0001$) in *L. mexicana*-containing BMDCs upon additional LPS activation.

In comparison, BMDC cultures infected with *T. gondii* alone or in combination with LPS elevated CD40 ($p=0.0004$; <0.0001)), CD80 ($p=<0.0001$) and CD86 ($p=<0.0001$) expression in comparison to naïve BMDC cultures. This shows that *T. gondii* augments BMDC activation markers and this can be further increased upon LPS activation. This would suggest that BMDC activation is affected differently by the two parasites under study.

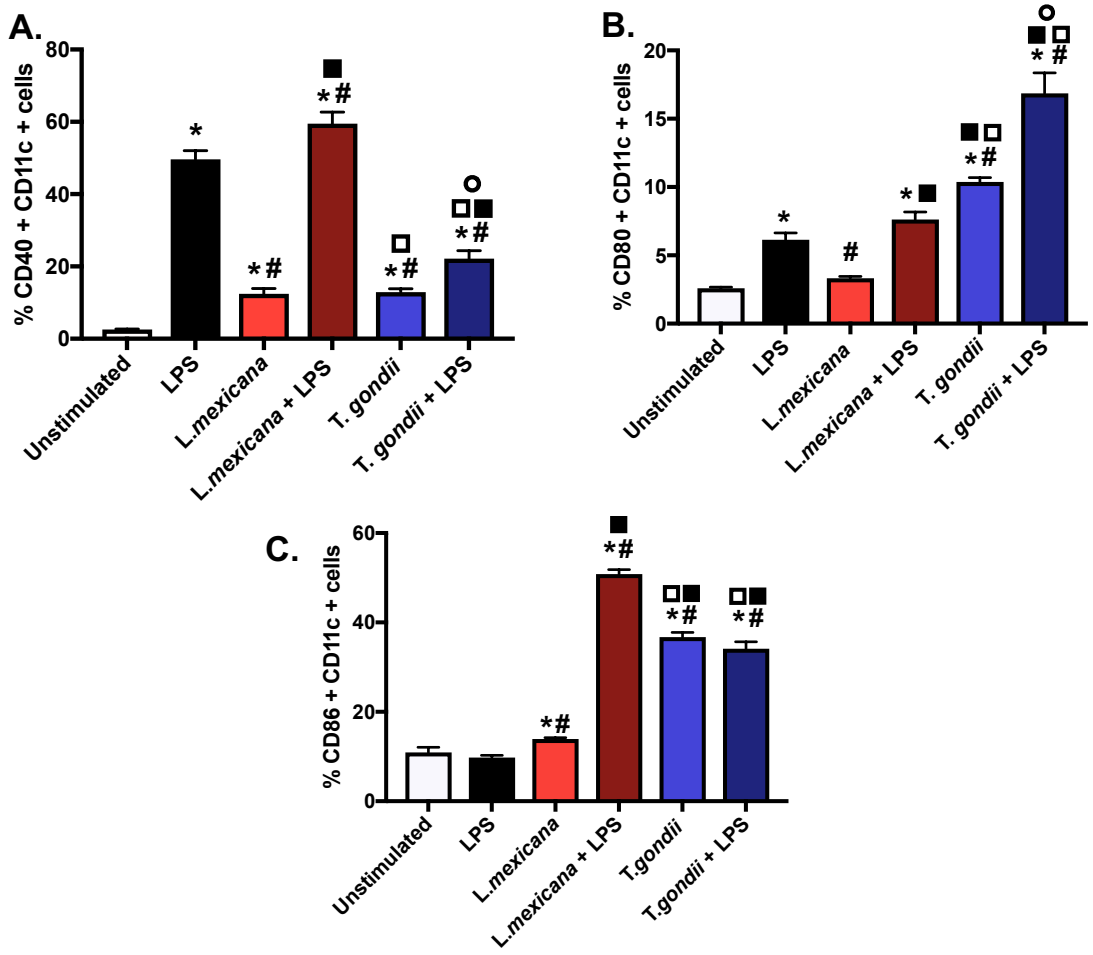

Figure 4.2. *L. mexicana* or *T. gondii* alters the cellular activation of BMDCs. Bone marrow derived DCs were co-cultured with either *L. mexicana* promastigotes (MOI 5:1) or *T. gondii* tachyzoites (MOI 1:1), 4 hours before stimulation with LPS. After 24 hours, cells were analysed by flow cytometry to determine the proportion of $CD11c^{+}$ cells expressing the activation markers (A) CD40, (B) CD80 or (C) CD86. Results are representative of three independent experiments (n = 3) and show mean +/- SEM. A one-way ANOVA with Bonferroni post-test was performed to determine significance ($P< 0.05$) where * is significant compared to unstimulated, # is significant compared to LPS, ■ is significant compared to *L. mexicana*, □ is significant compared to *L. mexicana* + LPS and ○ is significant compared to *T. gondii*.

4.2.3. IL-12 production is not altered in BMDCs infected with *L. mexicana* or *T. gondii*

The level of IL-12 (p40/p70) in the supernatant of BMDCs following parasite co-culture was determined by ELISA. Whilst a small percentage of unstimulated cells generated IL-12, stimulation of BMDCs with LPS resulted in a significant increase in the level of IL-12 within the supernatant ($p=<0.0001$). Supernatant from BMDCs exposed to *L. mexicana* or *T. gondii* alone showed similar expression levels to unstimulated DCs. Additionally, IL-12 expression did not change in parasite-containing BMDCs upon additional LPS activation ($p=<0.0001$) when compared to LPS activated BMDCs. This would suggest that neither *L. mexicana* or *T. gondii* stimulate IL-12 production in infected BMDCs.

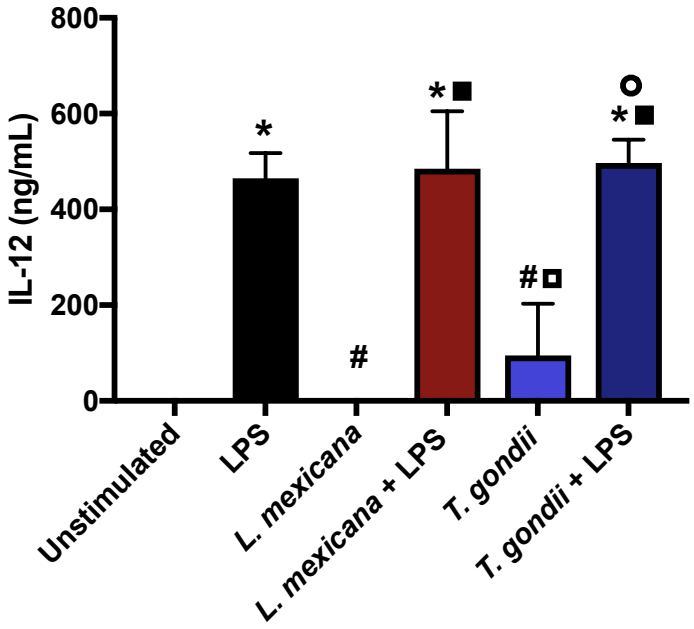

Figure 4.3. *L. mexicana* or *T. gondii* do not modulate the IL-12 production of BMDCs. BMDCs were co-cultured with either *L. mexicana* promastigotes (MOI 5:1) or *T. gondii* tachyzoites (MOI 1:1), 4 hours before stimulation with LPS. After 24 hours, supernatants were analysed by ELISA to determine the amount of IL-12 these cells produced. Results are representative of three independent experiments (n = 3) and show mean +/- SEM. A one-way ANOVA with Bonferroni post-test was performed to determine significance (P< 0.05) where * is significant compared to unstimulated, # is significant compared to LPS, ■ is significant compared to *L. mexicana*, □ is significant compared to *L. mexicana* + LPS and ○ is significant compared to *T. gondii*.

4.2.4. Dendritic cells undergo distinct but overlapping global metabolic changes when activated with LPS or co-cultured with either *L. mexicana* or *T. gondii*

Analysis of holistic changes using orthogonal partial least squares discriminant analysis (OPLS-DA) consistently found distinct separation between naïve BMDC cultures, LPS-stimulated cultures and BMDC cultures infected with *L. mexicana* or *T. gondii* (Figure 4.4). Unless otherwise stated the remainder of this chapter will focus on the data from only one biological run. The holistic changes in metabolism are fully detailed in a VIP score list which orders the most important variables across the model as a whole (based on relative intensities of each metabolite) (Table 4.1). Formula, m/z ratios and retention times for this data is available in Table 8.7. Separate pairwise comparisons of LPS activated, *L. mexicana* infected or *T. gondii* infected BMDC cultures compared to control cells are shown in Table 8.8 – 8.10. The data included 212 putatively identified metabolites (recognised by accurate mass to < 3ppm and by predicted retention time via IDEOM) including 67 metabolites confirmed via known standards (retention time match of +/- 0.2min). Data from biological run 2 and 3 are available in Figure 8.2, Table 8.11 or Table 8.12.

Notably, multiple metabolites from specific pathways, including glycolysis, TCA cycle, OXPHOS and arginine metabolism are evident in the VIP table and these are discussed in detail later in the chapter. In addition, other metabolites of interest include Sn-glycero-3-phosphocholine, choline phosphate, 5-aminopentanoate, L-glutamine and 4-aminobutanoate. These metabolites all have a VIP score ≥ 0.50 (Table 4.1). Sn-glycero-3-phosphocholine serves as a precursor to choline and choline phosphate

biosynthesis. Phosphocholine can become selectively attached to proteins posttranslationally and suppress the immune response. 4-aminobutanoate is a precusor for succinte semialdehyde which can then enter the TCA cycle as succinate whilst 5-aminopenanoate is a degradation product of lysine biosynthesis. Notably, Ovothiol A, a metabolite specific to only *Leishmania spp* was observed in this VIP table, validating *Leishmania* infection in BMDCs (Ariyanayagam *et al*., 2001).

Furthermore, the data obtained is fully detailed as fold change heat maps (Figure 4.5). The heat maps show metabolites confirmed and putatively detected for amino acids, carbohydrates and nucleotides.

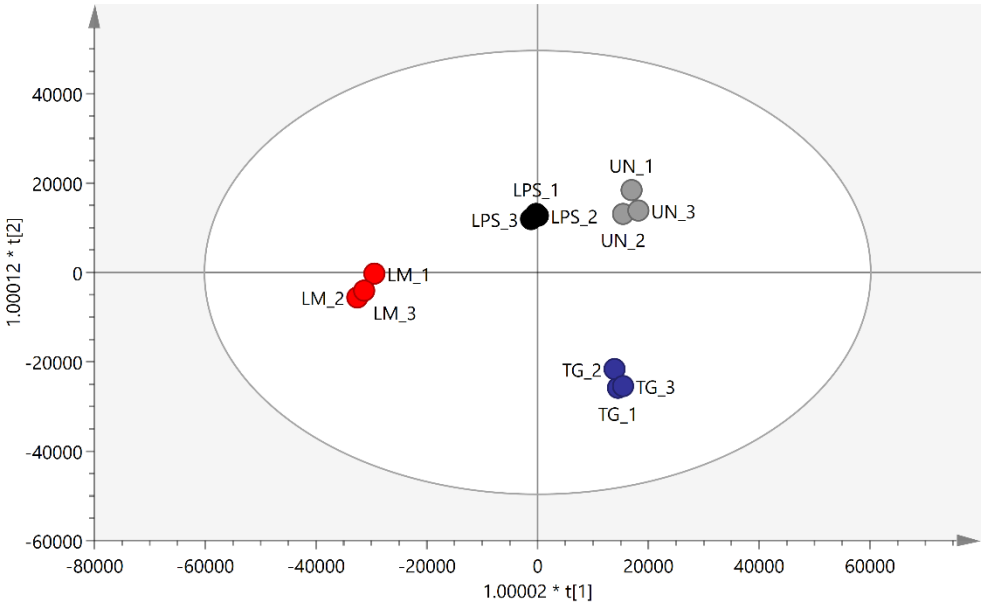

Figure 4.4. Orthogonal Projections to Latent Structures Discriminant Analysis of BMDCs activated with LPS or co-cultured with *L. mexicana* or *T. gondii*. Bone marrow derived DCs were stimulated with LPS or co-cultured *with L. mexicana* or *T. gondii* for 24 hours. After this time, the metabolites of the DCs were extracted and run via Liquid chromatography mass spectroscopy (LCMS). The data was then analysed by SIMCA and a Orthogonal Projections to Latent Structures Discriminant Analysis (OPLS-DA) plot was generated. Key: Grey, unstimulated; Black, LPS; Red, *L. mexicana*; Blue, *T. gondii*. The confidence ellipses are based on Hotelling's T^2 = 95. N = 3.

Table 4.1. VIP scores of BMDC cultures activated with LPS or infected with *L. mexicana* or *T. gondii*

Metabolite Name	M1.VIP [3+2+0][1]	2.44693 * M1.VIP [3] cvSE[2]	Role[3]
Creatine	7.17638	1.91735	Arginine metabolism (Urea cycle)
sn-glycero-3-Phosphocholine	5.37841	1.12957	Phospholipid that serves as precursor of choline
Choline phosphate	5.21489	1.82639	Intermediate in the synthesis of phosphatidylcholine
L-Proline	3.87489	1.71911	Arginine metabolism intermediate
5-Aminopentanoate	3.22087	2.24294	Lysine degradation product
L-Glutamine	2.84404	0.998226	Amino acid
(R)-Lactate	2.30119	0.843689	Glycolysis
4-Aminobutanoate	2.0425	0.564119	Associated with GABA
2-C-Methyl-D-erythritol 4-phosphate	1.8991	1.32314	Isoprenoid pre-cursor biosynthesis
L-Arginine	1.73945	1.24658	Arginine metabolism
L-Leucine	1.71549	0.897266	Amino acid
Hexadecanoic acid	1.58732	1.25919	Saturated fatty acid
Choline	1.55346	0.704989	Associated with acetylcholine
Creatinine	1.52422	0.870155	Urea cycle
L-Carnitine	1.50131	1.55855	Transporter of long chain fatty acids into the mitochondria
L-Glutamate 5-semialdehyde	1.40209	0.626307	Arginine metabolism intermediate
L-1-Pyrroline-3-hydroxy-5-carboxylate	1.39383	0.691196	Arginine metabolism intermediate
(S)-Malate	1.37848	0.97326	TCA intermediate
L-Citrulline	1.37413	0.483455	Arginine metabolism intermediate
Citrate	1.31064	0.762461	TCA intermediate
(R)-2-Hydroxyglutarate	1.29479	0.43532	Converted to α -ketoglutarate
O-Acetylcarnitine	1.26889	0.50991	Transporter of long chain fatty acids into the mitochondria
4-Trimethylammoniobutanoate	1.21407	0.595506	Associated with Carnitine synthesis
L-Ornithine	1.18294	0.501147	Arginine metabolism intermediate
Ovothiol A	1.16876	0.351902	Specific to *L. mexicana*
Orthophosphate	1.15714	0.70353	Associated with Oxidative phosphorylation
L-Glutamate	1.13522	0.618048	Amino acid
Itaconate	1.05636	0.552976	Anti-inflammatory mediator
L-Methionine	0.98744	0.43954	Amino acid
L-Lysine	0.976152	0.294933	Amino acid

4-Imidazolone-5-propanoate	0.968625	0.290111	Metabolism of histidine
L-Phenylalanine	0.925302	0.465894	Amino acid
N6_N6_N6-Trimethyl-L-lysine	0.914794	0.260297	Lysine degradation pathway
Guanidinoacetate	0.859735	1.17965	Associated with Creatine
Dimethisterone	0.856961	0.458559	
Taurine	0.843562	0.753297	Bile acids, anti-oxidant, osmoregulation, calcium signalling
2-Acetolactate	0.806231	0.235882	Precursor of valine and leucine
L-Aspartate	0.804333	0.465368	Amino acid
L-Pipecolate	0.79522	0.290124	Lysine degradation
Glutathione	0.738408	0.336809	Anti-oxidant
[FA trihydroxy(4:0)] 2_3_4-trihydroxy-butanoic acid	0.710498	0.319564	Fatty acid
Triethanolamine	0.679535	0.941787	
Bis(2-ethylhexyl)phthalate	0.673367	0.292212	
Pyridoxine	0.664359	0.437778	Vitamin B6
L-Alanine	0.660627	0.720882	Amino acid
N2-(D-1-Carboxyethyl)-L-arginine	0.656837	0.23401	Associated with arginine and proline metabolism
myo-Inositol	0.64964	0.16835	Mediates cell signal transduction
4-Guanidinobutanoate	0.630218	0.112236	Associated with arginine and urea cycle
N-Acetyl-L-histidine	0.592159	0.328684	Histidine biosynthesis
LL-2_6-Diaminoheptanedioate	0.540204[4]	0.119633	Lysine, threonine, methionine and aspartate

[1]The data was analysed on SIMCA. The value represents the difference between the distinct groups.

[2] The value highlights variety within each sample groups

[3] Metabolites from each metabolic pathway are highlighted in the VIP table where glycolysis is coloured green, TCA cycle; blue, OXPHOS; purple and arginine metabolism; orange. Undetermined metabolites are greyed out.

[4] The VIP list was limited to a VIP score of ≥ 0.50

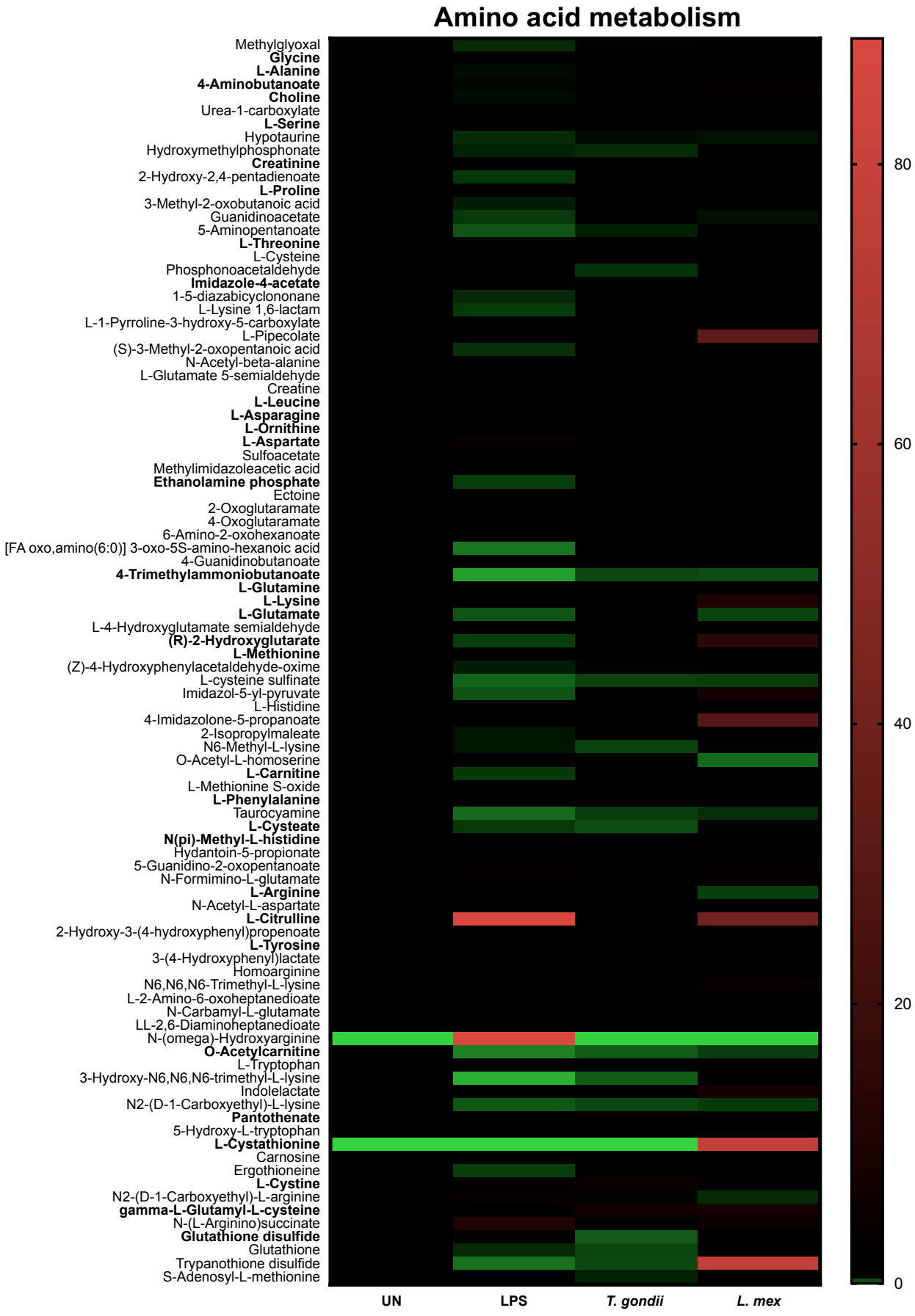
Amino acid metabolism
Methylglyoxal
Glycine
L-Alanine
4-Aminobutanoate
Choline
Urea-1-carboxylate
L-Serine
Hypotaurine
Hydroxymethylphosphonate
Creatinine
2-Hydroxy-2,4-pentadienoate
L-Proline
3-Methyl-2-oxobutanoic acid
Guanidinoacetate
5-Aminopentanoate
L-Threonine
L-Cysteine
Phosphonoacetaldehyde
Imidazole-4-acetate
1-5-diazabicyclononane
L-Lysine 1,6-lactam
L-1-Pyrroline-3-hydroxy-5-carboxylate
L-Pipecolate
(S)-3-Methyl-2-oxopentanoic acid
N-Acetyl-beta-alanine
L-Glutamate 5-semialdehyde
Creatine
L-Leucine
L-Asparagine
L-Ornithine
L-Aspartate
Sulfoacetate
Methylimidazoleacetic acid
Ethanolamine phosphate
Ectoine
2-Oxoglutaramate
4-Oxoglutaramate
6-Amino-2-oxohexanoate
[FA oxo,amino(6:0)] 3-oxo-5S-amino-hexanoic acid
4-Guanidinobutanoate
4-Trimethylammoniobutanoate
L-Glutamine
L-Lysine
L-Glutamate
L-4-Hydroxyglutamate semialdehyde
(R)-2-Hydroxyglutarate
L-Methionine
(Z)-4-Hydroxyphenylacetaldehyde-oxime
L-cysteine sulfinate
Imidazol-5-yl-pyruvate
L-Histidine
4-Imidazolone-5-propanoate
2-Isopropylmaleate
N6-Methyl-L-lysine
O-Acetyl-L-homoserine
L-Carnitine
L-Methionine S-oxide
L-Phenylalanine
Taurocyamine
L-Cysteate
N(pi)-Methyl-L-histidine
Hydantoin-5-propionate
5-Guanidino-2-oxopentanoate
N-Formimino-L-glutamate
L-Arginine
N-Acetyl-L-aspartate
L-Citrulline
2-Hydroxy-3-(4-hydroxyphenyl)propenoate
L-Tyrosine
3-(4-Hydroxyphenyl)lactate
Homoarginine
N6,N6,N6-Trimethyl-L-lysine
L-2-Amino-6-oxoheptanedioate
N-Carbamyl-L-glutamate
LL-2,6-Diaminoheptanedioate
N-(omega)-Hydroxyarginine
O-Acetylcarnitine
L-Tryptophan
3-Hydroxy-N6,N6,N6-trimethyl-L-lysine
Indolelactate
N2-(D-1-Carboxyethyl)-L-lysine
Pantothenate
5-Hydroxy-L-tryptophan
L-Cystathionine
Carnosine
Ergothioneine
L-Cystine
N2-(D-1-Carboxyethyl)-L-arginine
gamma-L-Glutamyl-L-cysteine
N-(L-Arginino)succinate
Glutathione disulfide
Glutathione
Trypanothione disulfide
S-Adenosyl-L-methionine
UN
LPS
T. gondii
L. mex
80
60
40
20
0

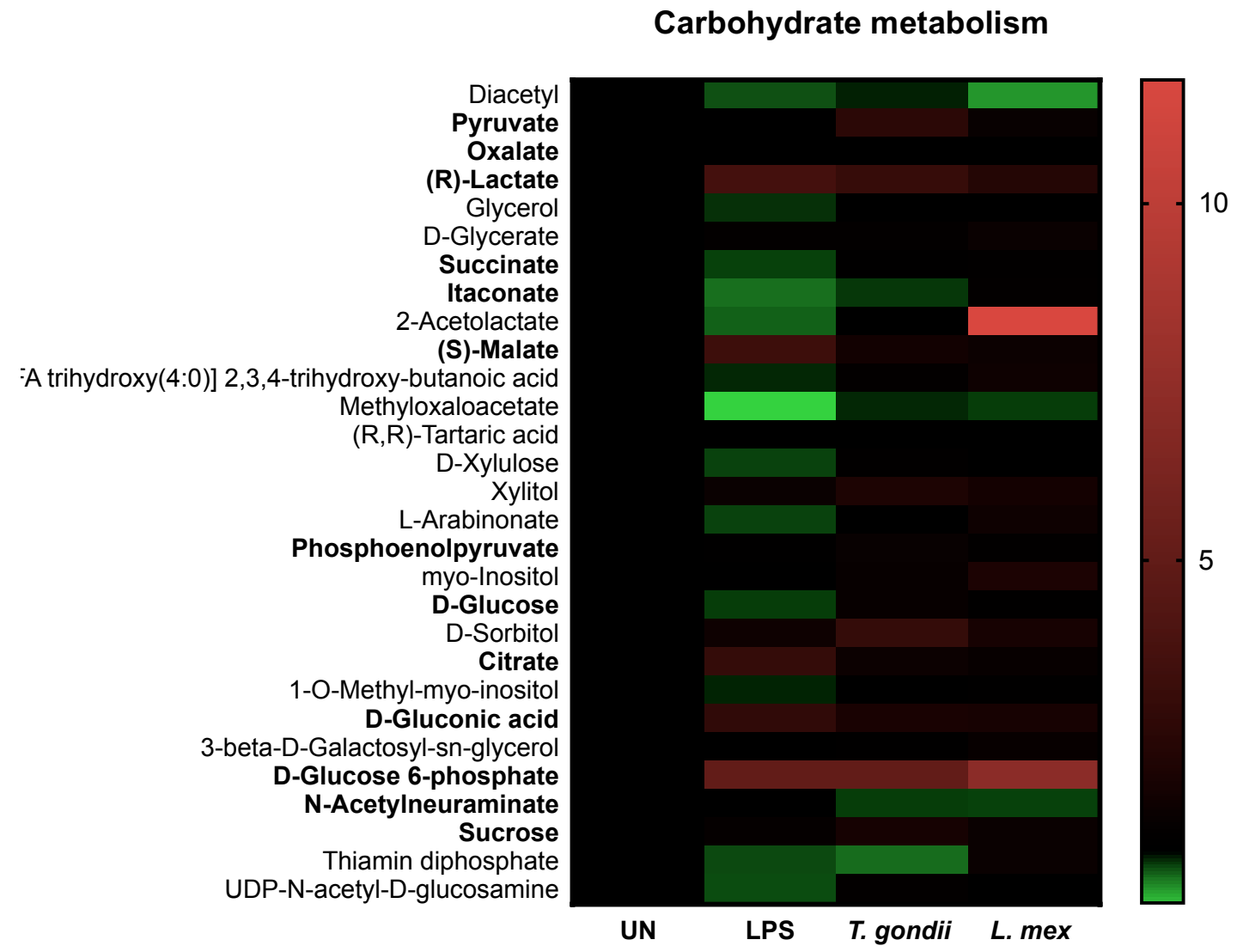
Carbohydrate metabolism
Diacetyl
Pyruvate
Oxalate
(R)-Lactate
Glycerol
D-Glycerate
Succinate
Itaconate
2-Acetolactate
(S)-Malate
FA trihydroxy(4:0)] 2,3,4-trihydroxy-butanoic acid
Methyloxaloacetate
(R,R)-Tartaric acid
D-Xylulose
Xylitol
L-Arabinonate
Phosphoenolpyruvate
myo-Inositol
D-Glucose
D-Sorbitol
Citrate
1-O-Methyl-myo-inositol
D-Gluconic acid
3-beta-D-Galactosyl-sn-glycerol
D-Glucose 6-phosphate
N-Acetylneuraminate
Sucrose
Thiamin diphosphate
UDP-N-acetyl-D-glucosamine
10
5
UN
LPS
T. gondii
L. mex

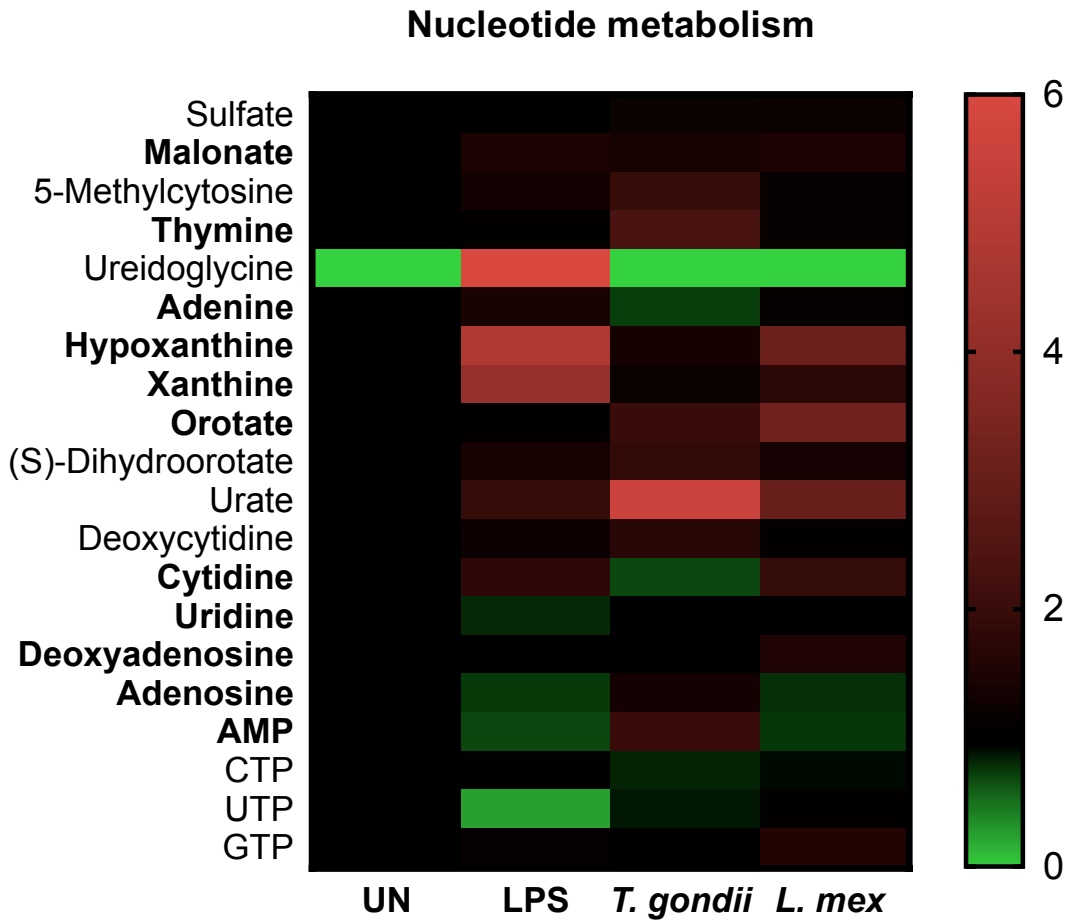

Figure 4.5. Global metabolic activity of BMDCs activated with LPS or co-cultured with *L. mexicana* or *T. gondii*. Bone marrow derived DCs were activated with LPS or exposed to *L. mexicana* or *T. gondii* as indicated for 24 hours. After this time, the metabolites of the BMDCs were extracted and measured via Liquid chromatography mass spectroscopy (LCMS). A heat map was constructed from the analysed data on IDEOM and Prism7 and shows the fold change increase (Red) or the decrease (Green) of each metabolite compared to its representative unstimulated control (Black). Standards are highlighted in bold. N = 3.

Within this thesis, only infection of BMDCs with live *L. mexicana* or *T. gondii* will be discussed in great detail. A limitation of this study when investigating the metabolic profile of BMDCs infected with live parasites is distinguishing whether deviations to the metabolites witnessed is associated with changes in BMDC function or reflects the metabolites of the intracellular parasites. Figure 8.3 show the fold change heat maps of BMDCs co-cultured with either paraformaldehyde (PFA) fixed *L. mexicana*, *T. gondii* or treated with soluble *Leishmania* antigen (SLA) or *Toxoplasma* lysate antigen (TLA). Immobilised PFA parasites were used as a control for live parasites as it was thought that fixed intracellular parasites would not actively influence the host cell metabolism. A marked reduction in the majority of metabolites including intermediates of the glycolysis and pentose phosphate pathway was observed in cultures incubated with PFA-fixed parasites compared to both LPS and unstimulated BMDCs. In contrast, metabolites of the TCA cycle were not reduced in BMDCs exposed to PFA-fixed parasites and metabolites of the arginine pathway were moderately increased.

Different concentrations of soluble *Leishmania* antigen (SLA) and *Toxoplasma* lysate antigen (TLA) were used to elicit changes in the immune cell metabolism in the absence of an active infection. Relatively minor changes in the majority of metabolites including intermediates of the glycolysis and PPP were observed in lysate stimulated cultures in comparison to LPS stimulated and unstimulated BMDCs. This implies that activation of parasite specific TLR receptors alone is insufficient to modify the metabolism of BMDCs and that an active infection is required.

4.2.5. Metabolic pathways of interest

As mentioned above, the presence or absence of many metabolite intermediates within pathways can be indicative of the activation status of an immune cell. These include glycolysis, TCA cycle and arginine metabolism (which had many metabolites present with a VIP score of ≥ 0.50). These particular pathways and PPP (an extension of glycolysis) have been selected for further analysis as they play crucial roles in either energy generation or have been shown to be crucial in altering an immune response to infection.

4.2.5.1 Glycolysis

Glucose, glucose-6-phosphate, fructose-6-phosphate, 2-Phosphoglycerate, phosphoenolpyruvate, pyruvate and lactate are all intermediates of the glycolysis pathway (Figure 4.6). In comparison to naïve BMDCs, those stimulated with LPS had signficantly increased levels of glucose-6-phosphate (p=0.0048), fructose-6-phosphate (p=0.0127), 2-phosphoglycerate (p=0.0025), and lactate (p=0.0140). Signficant accumulation of glucose, glucose-6-phosphate (p=0.0004; 0.0036), fructose-6-phosphate (p=0.0009; 0.0065), 2-phosphoglycerate (p=0.0146; 0.0013), pyruvate (p = <0.05; 0.0008) and lactate (p=<0.05; 0.0445) was also observed in BMDCs co-cultured with either *L. mexicana* or *T. gondii* when compared with unstimulated BMDCs. Phosphoenolpyruvate was signficantly down-regulated in all conditions (LPS, p = 0.0338; *L. mexicana*, 0.05 and *T. gondii*, 0.0006).

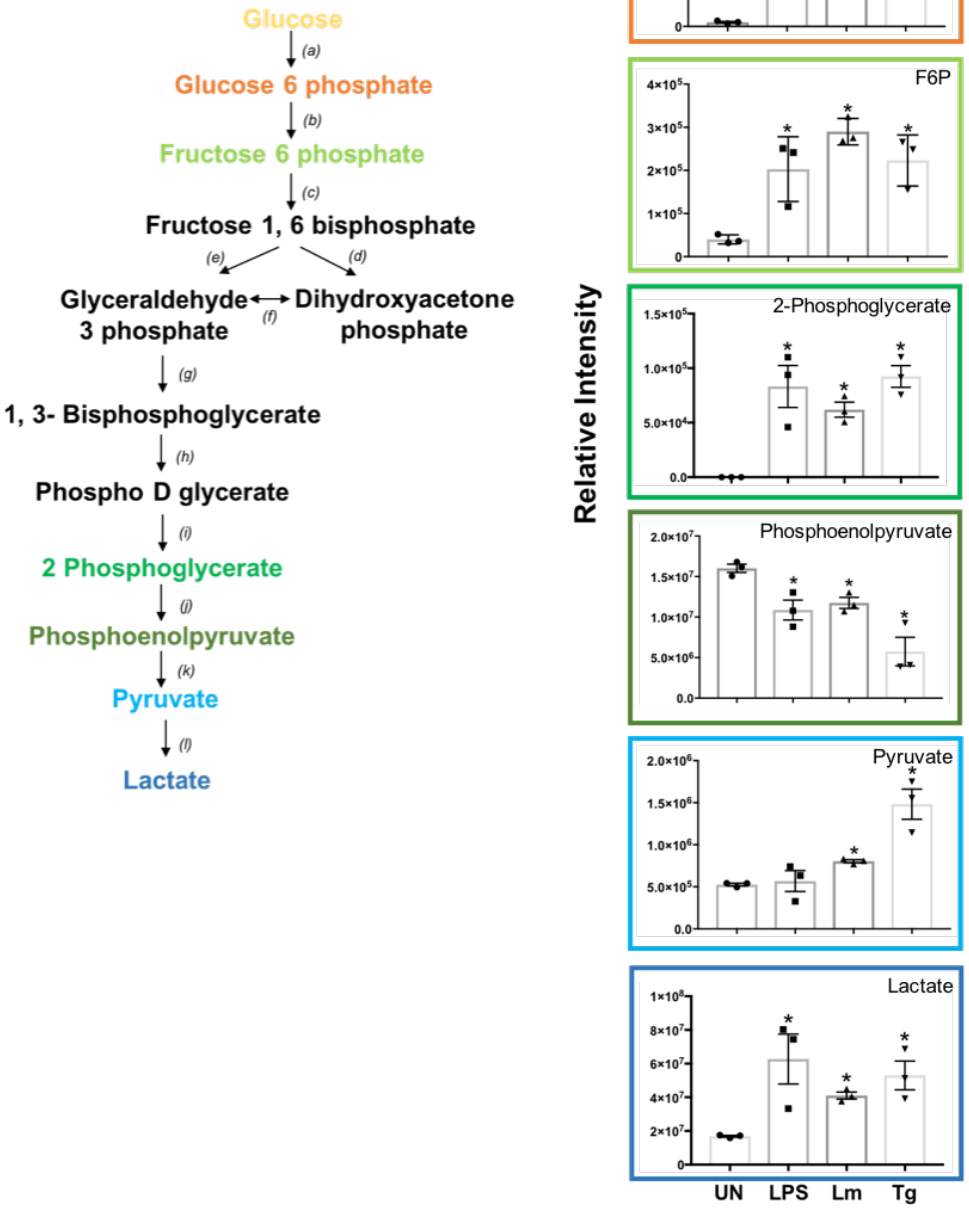
Glucose
(a)
Glucose 6 phosphate
(b)
Fructose 6 phosphate
(c)
Fructose 1, 6 bisphosphate
(e)
(d)
Glyceraldehyde 3 phosphate
(f)
Dihydroxyacetone phosphate
(g)
1, 3- Bisphosphoglycerate
(h)
Phospho D glycerate
(i)
2 Phosphoglycerate
(j)
Phosphoenolpyruvate
(k)
Pyruvate
(l)
Lactate
Relative Intensity
Glucose
G6P
F6P
2-Phosphoglycerate
Phosphoenolpyruvate
Pyruvate
Lactate
UN
LPS
Lm
Tg

Figure 4.6. Glycolysis differences in *L. mexicana* or *T. gondii* co-cultured BMDCs. Bone marrow derived DCs were stimulated with LPS or co-cultured with either *L. mexicana* or *T. gondii* as indicated for 24 hours. After this time, the metabolites of the BMDCs were extracted and analysed by Liquid Chromatography Mass Spectroscopy (LCMS). For clarity, the diagram focuses on relevant metabolites (shown by the graphs) and enzymes (depicted (a) through to (k)) are clearly labelled in this legend. (a) hexokinase; (b) phosphoglucose isomerase; (c) phosphofructokinase; (d) fructose bisphosphate aldose; (e) triose phosphate isomerase; (f) glyceraldehyde 3-phosphate dehydrogenase; (g) phosphoglycerate kinase; (i) phosphoglycerate mutase (j) enolase (k) pyruvate kinase; (l) lactate dehydrogenase. Statistical analysis was performed using a non-parametric Mann-Whitney test. Significant differences are $p < 0.05$ where * is compared to unstimulated. Results are representative of three independent runs (n=3).

4.2.5.2 TCA cycle

From the metabolomics data, it was possible to indentify 6 of the metabolites associated with the TCA cycle including citrate, α-ketoglutarate, succinate, fumarate, malate and itaconate. Significant accumulation of citrate (p=0.0009), α-ketoglutrate (p=<0.0001), fumarate (p=0.05) and malate (0.0199) was seen in LPS activated BMDCs in comparison to unstimulated cells. In LPS stimulated BMDCs, itaconate was observed to be significantly down-regulated compared to naïve cells (p=0.05). Similarly, significant increases in TCA intermediates (including citrate, succinate, malate and itaconate (p=<0.05)) were observed in *L. mexicana* and (citrate and malate (p=<0.05)) *T. gondii* infected BMDCs (Figure 4.7).

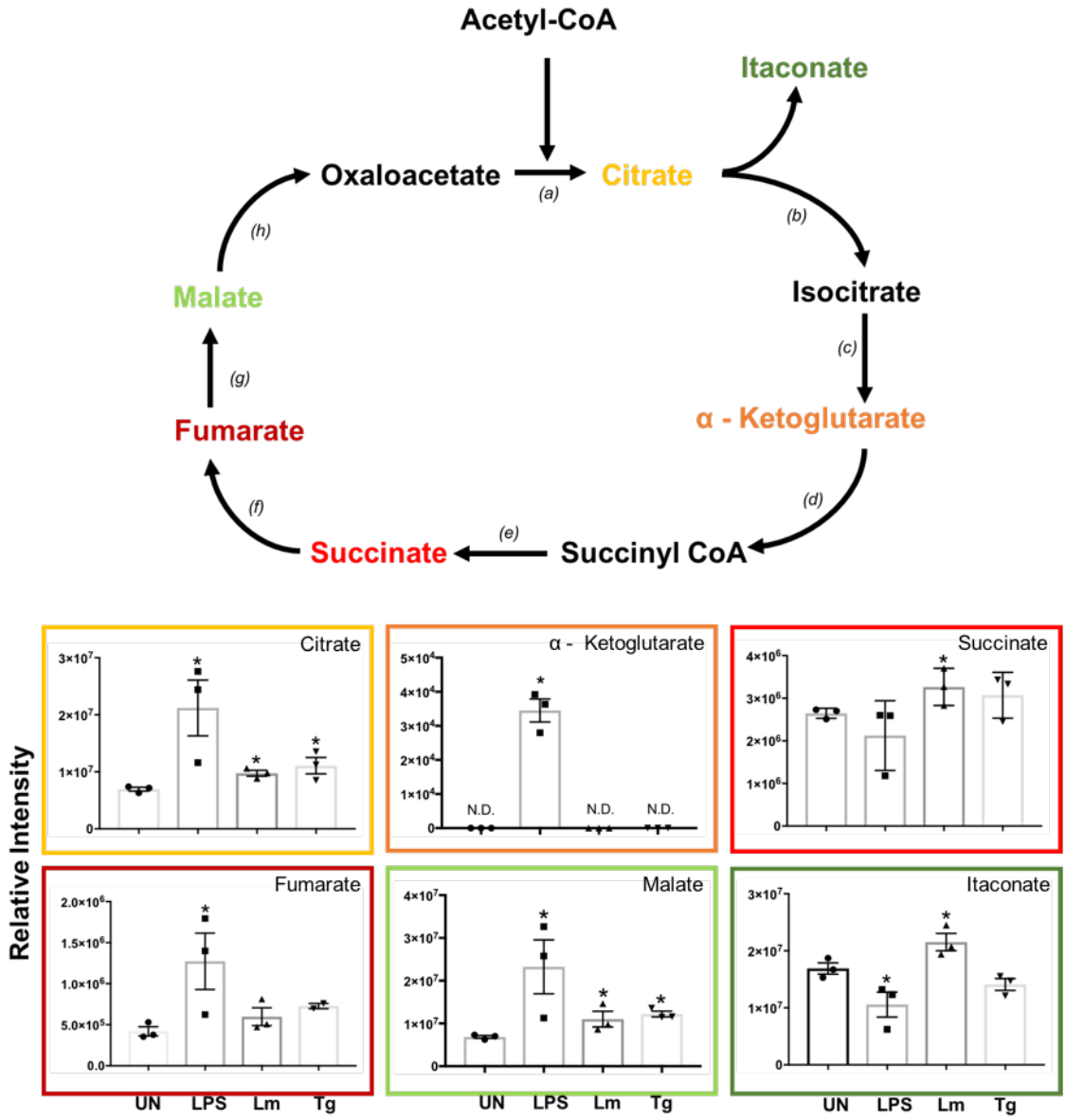
Acetyl-CoA
Itaconate
Oxaloacetate
(a)
Citrate
(b)
(h)
Malate
Isocitrate
(c)
(g)
α - Ketoglutarate
Fumarate
(d)
(f)
(e)
Succinate
Succinyl CoA
Relative Intensity
Citrate
α - Ketoglutarate
Succinate
Fumarate
Malate
Itaconate
N.D.
N.D.
N.D.
UN
LPS
Lm
Tg

Figure 4.7. TCA cycle changes in BMDCs infected with parasites. Bone marrow derived DC cultures were activated with LPS or infected with *L. mexicana* or *T. gondii* for 24 hours. After this time, the metabolites of the BMDCs were extracted and analysed by Liquid Chromatography Mass Spectroscopy (LCMS). For clarity, the diagram focuses on relevant metabolites (shown by the graphs) and enzymes (depicted (a) through to (h)) for the Krebs cycle only. (a) citrate synthase; (b) aconitase; (c) isocitrate dehydrogenase; (d) α-ketoglutarate dehydrogenase; (e) succinyl-CoA synthetase; (f) succinate dehydrogenase; (g) fumarase; (h) malate dehydrogenase. Statistical analysis was performed using a non-parametric Mann-Whitney test. Significant differences are $p < 0.05$ where * is compared to unstimulated. Results are representative of three independent runs (n=3).

4.2.5.3 Pentose phosphate pathway

PPP metabolites detected by LCMS include gluocse-6-phosphate, ribose-5-phosphate and fructose-6-phosphate (Figure 4.8). In comparison to naïve cells, glucose-6-phosphate ($p=0.0048$) and fructose-6-phosphate ($p=0.0127$) were signficantly increased in BMDCs stimulated with LPS or infected with *L. mexicana* or *T. gondii*. Ribose-5-phosphate was seen to be increased in LPS activated, *L. mexicana* or *T. gondii* infected BMDC cultures albeit not signficantly.

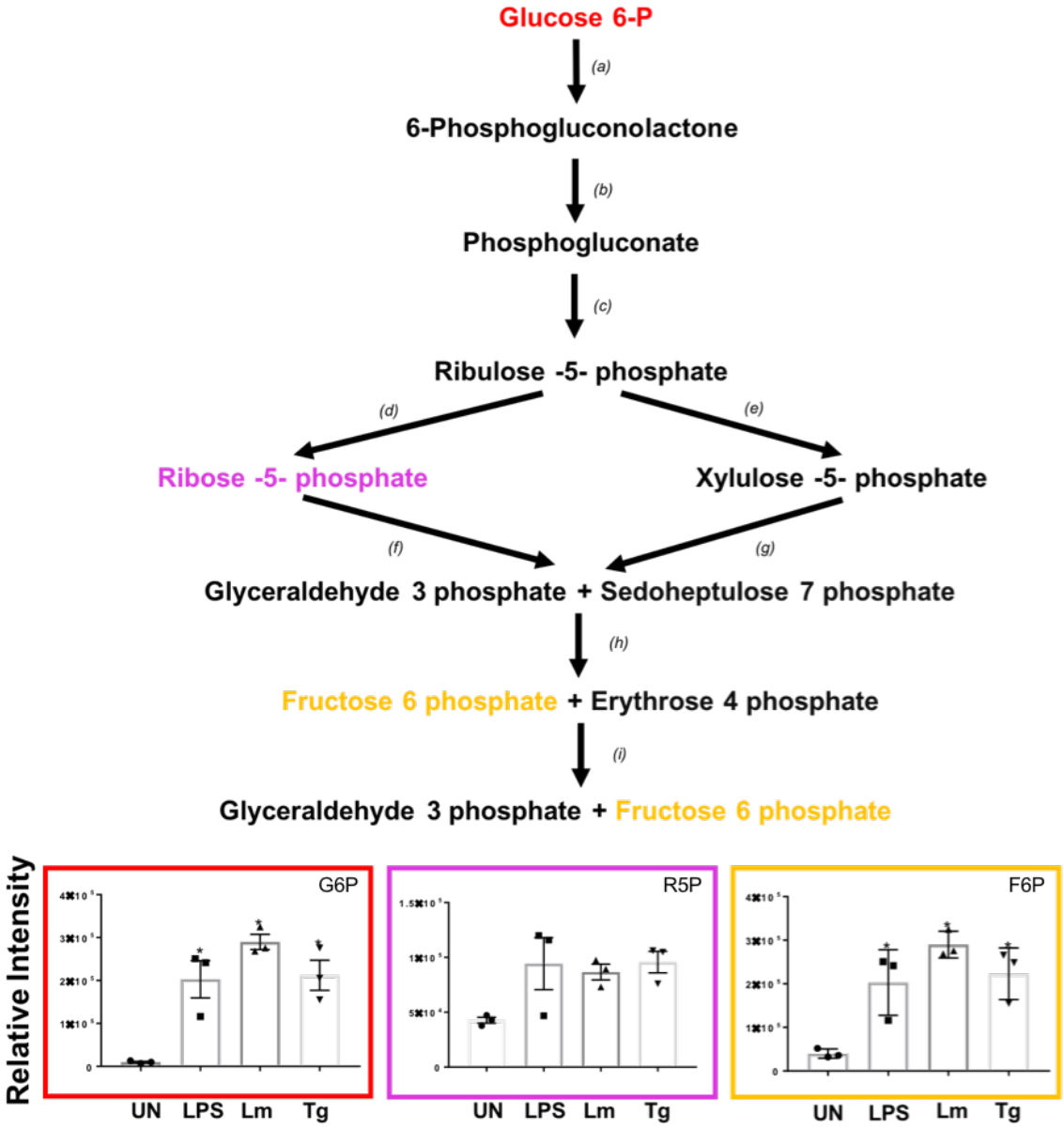
Glucose 6-P
(a)
6-Phosphogluconolactone
(b)
Phosphogluconate
(c)
Ribulose -5- phosphate
(d)
(e)
Ribose -5- phosphate
Xylulose -5- phosphate
(f)
(g)
Glyceraldehyde 3 phosphate + Sedoheptulose 7 phosphate
(h)
Fructose 6 phosphate + Erythrose 4 phosphate
(i)
Glyceraldehyde 3 phosphate + Fructose 6 phosphate
Relative Intensity
G6P
R5P
F6P
UN
LPS
Lm
Tg

Figure 4.8. Pentose phosphate pathway (PPP) differences in BMDCs infected with *L. mexicana* or *T. gondii*. Bone marrow derived DCs were activated with LPS or co-cultured with either *L. mexicana* or *T. gondii* as indicated for 24 hours. After this time, the metabolites of the BMDCs were extracted and analysed by Liquid Chromatography Mass Spectroscopy (LCMS). For clarity, the diagram focuses on relevant metabolites (shown by the graphs) and enzymes (depicted (a) through to (k)) for PPP only. (a) Glucose 6 phosphate dehydrogenase; (b) Gluconolactonase; (c) 6-phosphogluconate dehydrogenase; (d) ribulose 5 phosphate isomerase; (e) ribulose 5 phosphate 3 epimerase; (f/g/i/j) transketolase; (h) transaldolase. Statistical analysis was performed using a non-parametric Mann-Whitney test. Significant differences are $p < 0.05$ where * is compared to unstimulated. Results are representative of three independent runs (n=3).

4.2.6. *T. gondii* but not *L. mexicana* increased glucose uptake (via 2-NBDG) in BMDCs

The ability of cells to uptake 2-NBDG (as a proxy for glucose) was measured as a preliminary indicator of the Warburg effect in LPS-stimulated and *L. mexicana* or *T. gondii* co-cultured BMDCs. The ability of parasites to interfere with LPS induced uptake was also determined by co-culture experiments. As observed in chapter 3, LPS stimulation significantly increased the glucose uptake in BMDCs compared to unstimulated control cells (Figure 4.9) ($p=<0.0001$). In comparison to resting BMDCs, glucose uptake remained unchanged after exposure to *L. mexicana* alone and these cells were refractory to LPS-induced glucose uptake. In contrast, both *T. gondii* infected BMDCs alone and those re-stimulated with LPS ($p=<0.01$) significantly took up glucose in comparison to naïve BMDCs.

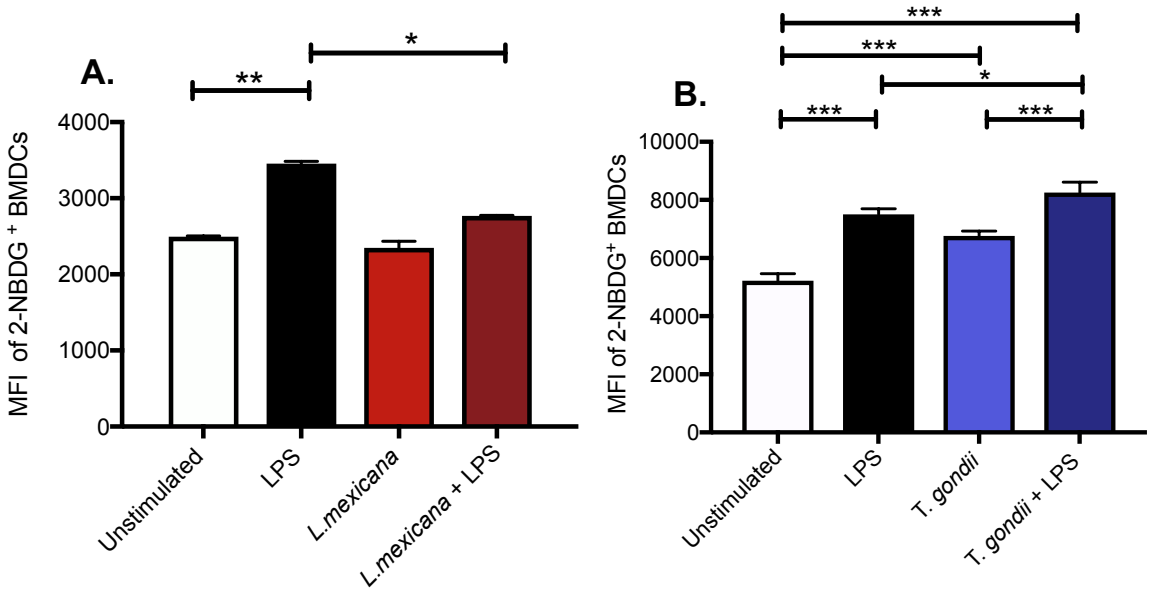

Figure 4.9. Determining glucose uptake in BMDCs exposed to *L. mexicana* or *T. gondii* using glucose analog, 2-NBDG. Bone marrow derived DCs were exposed to *L. mexicana* (5:1 ratio) or *T. gondii* (1:1 ratio), 4 hours prior to LPS stimulation. After 24 hours, fluorescent 2-NBDG (50μM) was added for 120 minutes. The mean fluorescent intensity (MFI) of 2-NBDG uptake in BMDCs was then quantified using flow cytometry. Results are representative of three independent experiments (n = 3) and show the mean +/- SEM. Statistical analysis performed using 1-way ANOVA with Bonferroni post-test. Significant differences were identified where P*<0.05, **P< 0.01 and ***P<0.001.

4.2.7. *L. mexicana* and *T. gondii* up- regulate LDH activity in BMDCs

Lactate dehydrogenase (LDH) activity was measured in BMDCs to further assess the parasites involvement in inducing the Warburg effect. LDH is an oxidoreductase enzyme which converts pyruvate to lactate. As LDH is a fairly stable enzyme with higher activity during anaerobic glycolysis (as noted during the Warburg effect), it has been widely used as an indicator of lactate production. In comparison to naïve BMDCs, LPS stimulated BMDCs had significantly elevated LDH activity (p=0.04; <0.001) (Figure 4.10). This up-regulation in activity was also seen in BMDCs co-cultured with *L. mexicana* alone (p=0.0107) or those also re-stimulated with LPS (p=0.0005). Significantly elevated LDH activity was also clearly evident in *T. gondii* (p=0.0033; 0.0001) co-cultured BMDCs.

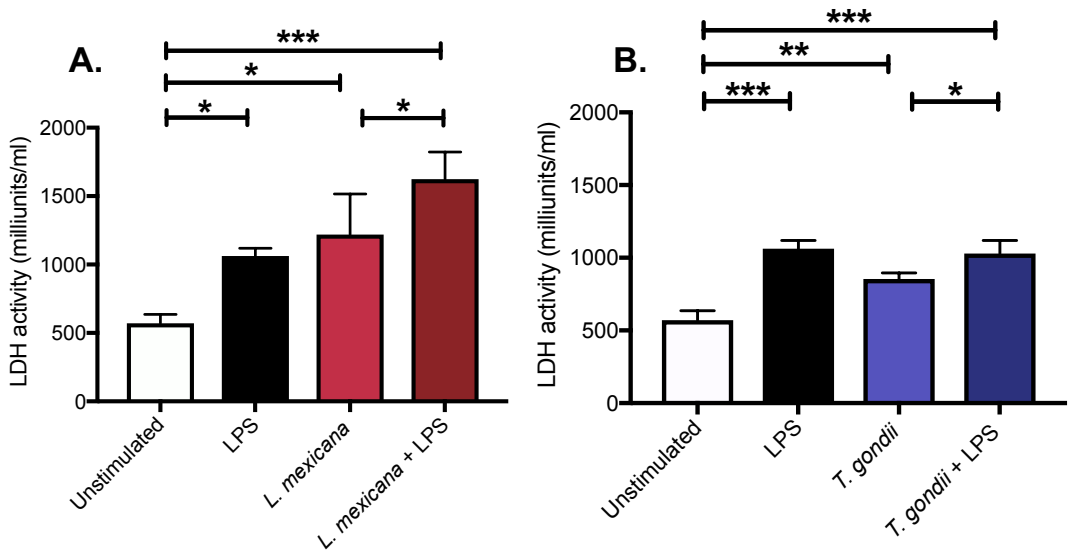

Figure 4.10. *L. mexicana* and *T. gondii* modulate Lactate dehydrogenase activity (LDH) in BMDCs. Bone marrow derived DCs were exposed to *L. mexicana* (5:1 ratio) or *T. gondii* (1:1 ratio), 4 hours prior to LPS stimulation. After 24 hours, supernatant from homogenised cells was used to calculated the LDH activity based on LDH reducing NAD to NADH. Results are representative of three independent experiments (n = 3) and show the mean +/- SEM. Statistical analysis performed using 1-way ANOVA with Bonferroni post-test. Significant differences were identified where P*<0.05, **P< 0.01 and ***P<0.001.

4.2.8. Mitochondrial morphology and mitochondrial membrane potential changes during BMDC activation and parasite infection.

4.2.8.1 Mitochondrial morphology

To investigate the extent to which OXPHOS is suppressed within BMDCs, it was of interest to visualise the changes in mitochondrial morphology as well as the difference in mitochondrial membrane potential between naïve, activated and infected BMDCs. Cells were stained with Mitotracker Green or Mitotracker Red ROX, a fluorescent dye that localises to the mitochondria regardless of mitochondrial membrane potential. From the image (Figure 4.11), there are clear distinctions in the mitochondrial morphology of unstimulated, LPS activated and parasite infected BMDCs. In comparison to naïve BMDCs that had smaller, punctuated mitochondria, LPS activated BMDCs exhibited elongated spindle-like mitochondria that are extremely motile (video data not shown). The mitochondria of BMDCs infected with either CFSE labelled *L. mexicana* or *T. gondii* were similar to that of naïve BMDCs.

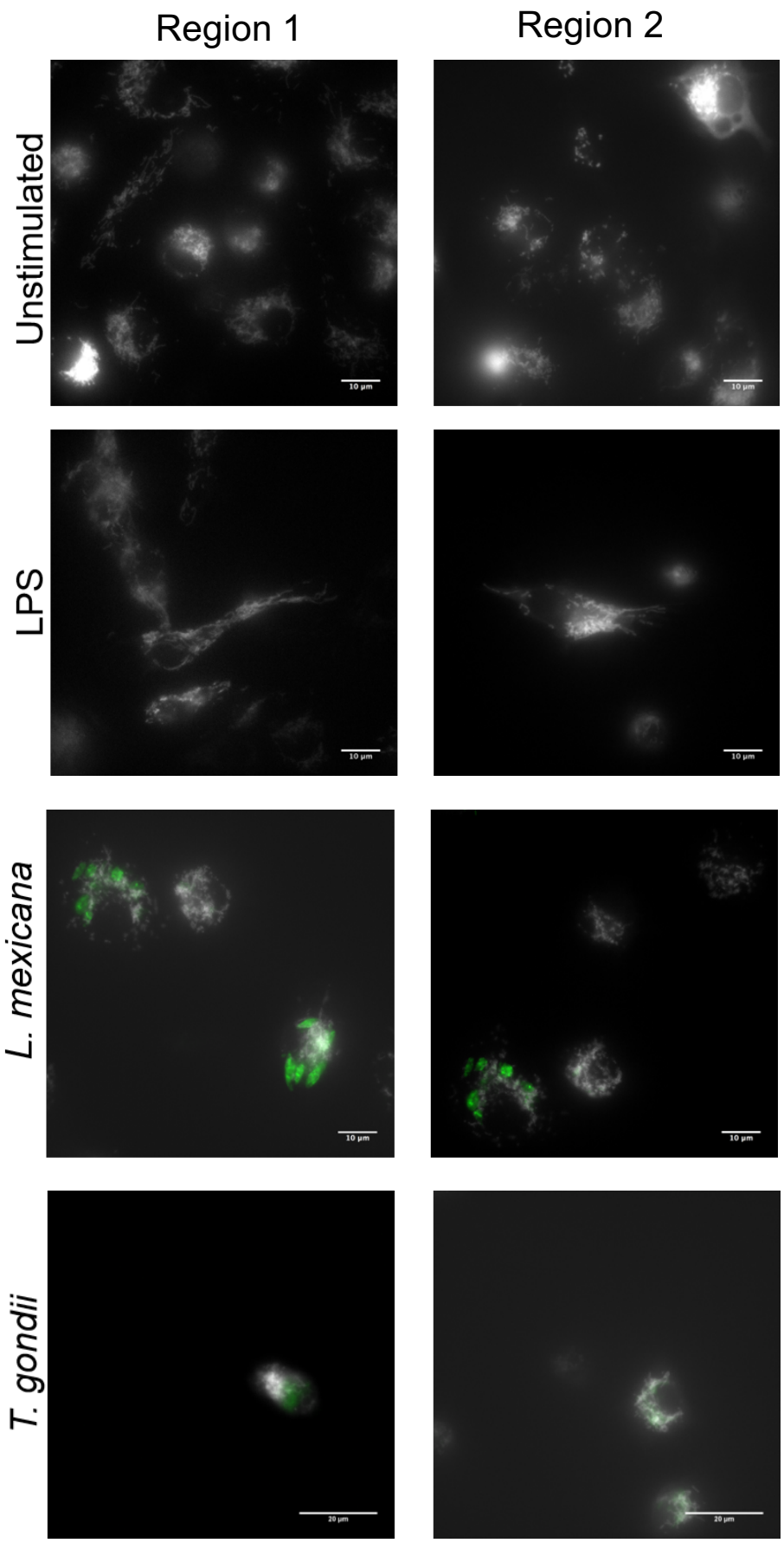
Region 1
Region 2
Unstimulated
LPS
L. mexicana
T. gondii
10 µm
10 µm
10 µm
10 µm
10 µm
10 µm
20 µm
20 µm

Figure 4.11. LPS activation but not parasite infection alters mitochondria morphology within BMDCs. Bone marrow derived DCs were activated with LPS or co-cultured with either CFSE labelled *L. mexicana* (5:1 ratio) or *T. gondii* (1:1 ratio). After 24 hours, the cells were stained with either 100nM of Mitotracker Green (UN, LPS) or Mitotracker Red ROX (*L. mexicana*, *T. gondii*) for 30 minutes to determine mitochondrial morphology. The images show two regions of interest which are representative of 3 independent experiments (n = 3).

4.2.8.2. Mitochondrial membrane potential

Mitochondrial membrane potential was also assessed in these cells. By overlaying Mitotracker Green with TMRM, active mitochondria were visualised. TMRM (red) is a dye that will only accumulate in active mitochondria with an intact membrane potential (Figure 4.12). The signal is bright in healthy functioning mitochondria but this signal dims when the mitochondria membrane potential ceases. This was visualised by a colour change from red/ orange to yellow/ green due to merging with the Mitotracker green. A shift from orange to yellow was seen when comparing naïve BMDCs (orange) with those activated with LPS (yellow), showing a loss in mitochondrial membrane potential. This change in colour was also visualised between naïve BMDCs (orange) and BMDCs infected with *L. mexicana* or *T. gondii* (yellow), indicating less active mitochondria.

Unstimulated BMDCs

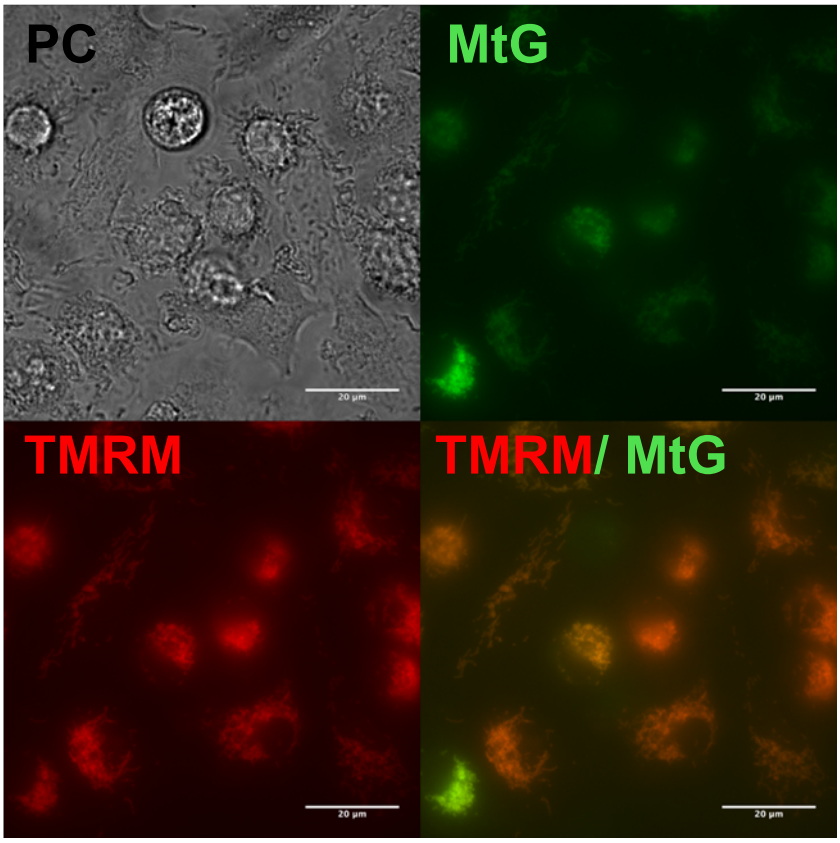

LPS Stimulated BMDCs

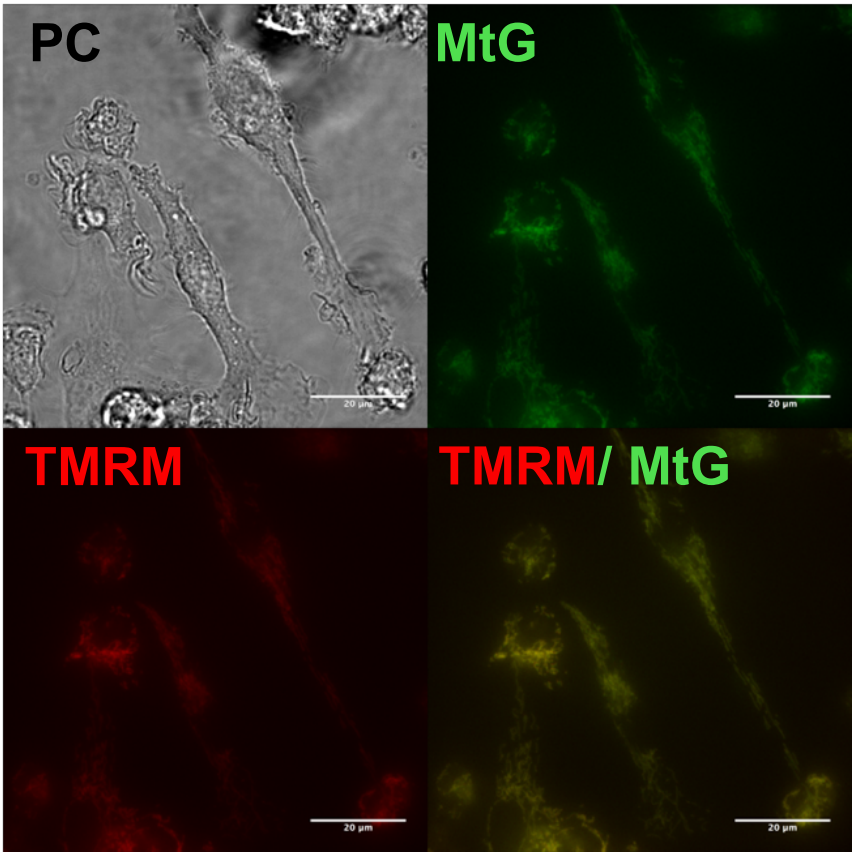

L. mexicana infected BMDCs

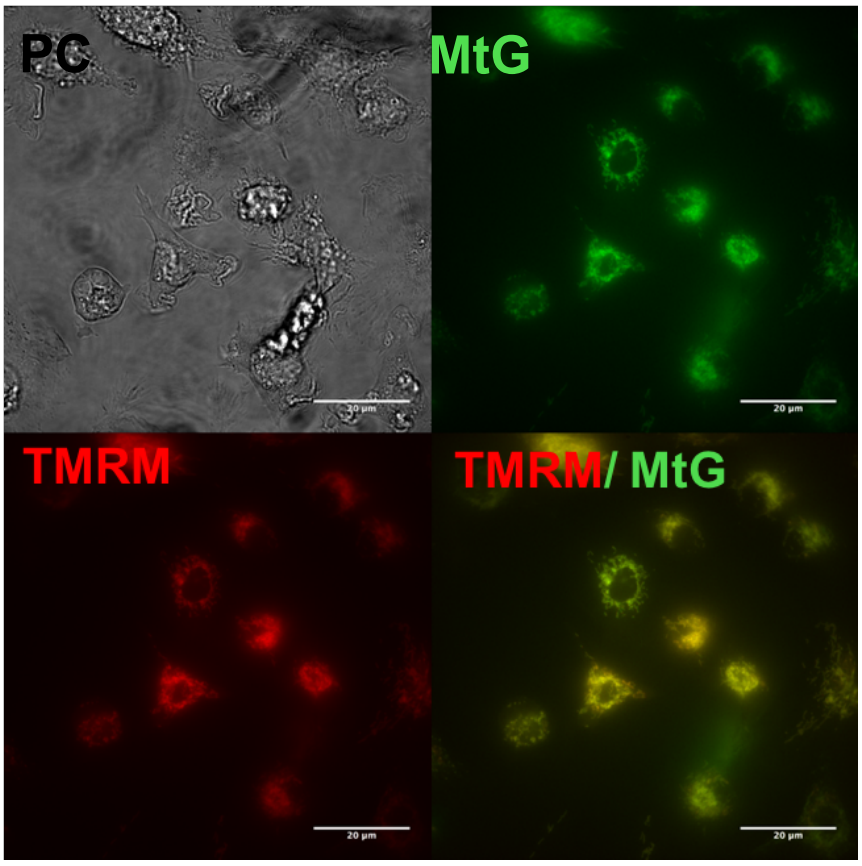

T. gondii infected BMDCs

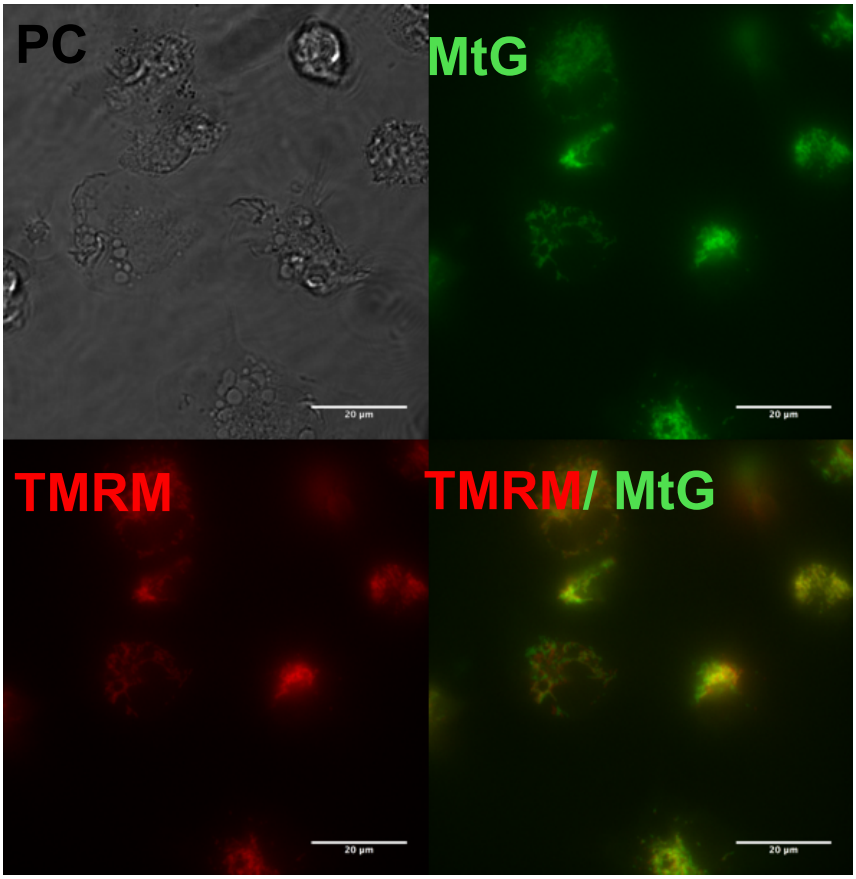

Figure 4.12. LPS activation and parasite infection decreases mitochondria membrane potential within BMDCs. Bone marrow derived DCs were activated with LPS or co-cultured with either *L. mexicana* (5:1 ratio) or *T. gondii* (1:1 ratio), 4 hours prior to LPS stimulation. After 24 hours, the cells were stained with 100nM of Mitotracker Green or 100nM TMRM for 30 minutes to determine mitochondrial morphology. The images show separate images for Phase Contrast (PC), Mitotracker green (MtG), TMRM and then MtG and TMRM merged (TMRM/ MTG). n = 3.

4.2.9. *L. mexicana* and *T. gondii* direct BMDC arginine metabolism toward different metabolic 'end goals' to LPS stimulation

In order to characterise the effect *L. mexicana* or *T. gondii* has on arginine metabolism within BMDCs, the expression of the enzymes, iNOS and Arg-1 was investigated. Moreover, the relative intensity of the end-products citrulline, ornithine, proline (via LCMS) and nitric oxide generation (via Griess assay) was also measured.

4.2.9.1 Intracellular iNOS expression is not altered in BMDCs cultures infected with *T. gondii* or *L. mexicana.*

BMDCs stimulated with LPS resulted in significant up-regulation of iNOS expression compared to resting BMDCs (Figure 4.13) ($p=<0.0001$). No significant difference in the percentage of cells expressing iNOS was seen in BMDCs cultures infected with *L. mexicana* or *T. gondii* alone when compared to naïve cells. However, when BMDCs were infected with *L. mexicana* and then re-stimulated with LPS, a significant increase in iNOS expression was observed in comparison to LPS activated BMDCs ($p=<0.0001$). This change was not observed in *T. gondii* + LPS stimulated BMDCs.

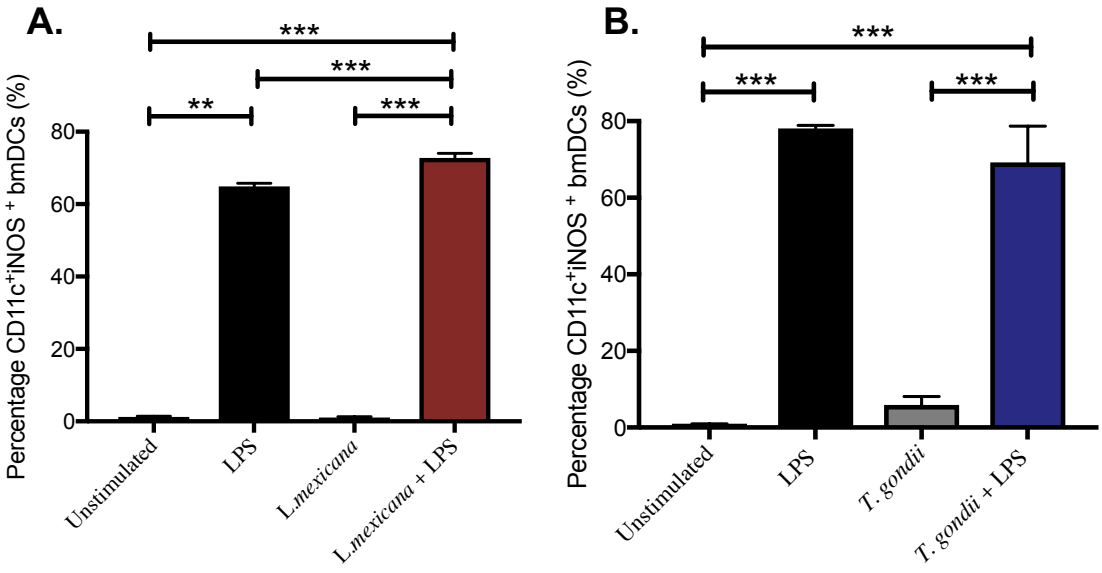

Figure 4.13. Intracellular iNOS expression is not altered in BMDCs infected with *L. mexicana* or *T. gondii*. Bone marrow derived DCs were exposed to (A) *L. mexicana* (5:1 ratio) or (B) *T. gondii* (1:1 ratio), 4 hours prior to LPS stimulation. After 24 hours, CD11c+ cells were analysed for iNOS expression by flow cytometry. Results are representative of three independent experiments (n = 3) and show the mean +/- SEM. Statistical analysis performed using 1-way ANOVA with Bonferroni post-test. Significant differences were identified where P*<0.05, **P< 0.01 and P<0.001.

4.2.9.2. BMDCs upregulate arginase-1 activity in response to *T. gondii* but not *L. mexicana*.

To observe arginase-1 activity within parasite infected BMDCs, the by-product urea was measured. In comparison to unstimulated BMDCs, it can be seen that there was a significant increase in arginase-1 activity in LPS stimulated BMDCs (Figure 4.14) ($p=<0.001$). This increase in activity was not seen in *L. mexicana* infected BMDCs alone but those reactivated with LPS treatment ($p=0.0212$). In comparison, arginase-1 activity was significantly enhanced in BMDCs infected with *T. gondii* tachyzoites alone ($p=0.0002$) or re-stimulated with LPS ($p= 0.0010$).

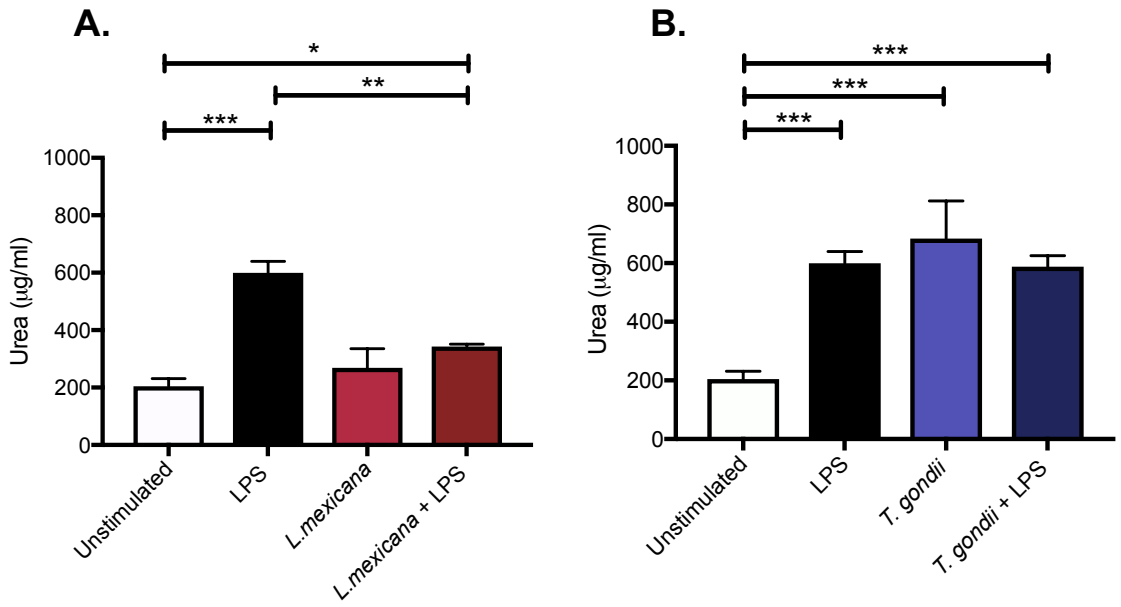

Figure 4.14. BMDCs up-regulate Arginase-1 activity in response to *T. gondii* but not *L. mexicana*. Bone marrow derived DCs were exposed to (A) *L. mexicana* (5:1 ratio) or (B) *T. gondii* (1:1 ratio), 4 hours prior to LPS stimulation. After 24 hours, Urea (µg/ml) was measured from homogenised cells. This is indicator of Arginase-1 activity. Results are representative of three independent experiments (n = 3) and show the mean +/- SEM. Statistical analysis performed using 1-way ANOVA with Bonferroni post-test. Significant differences were identified where P*<0.05, **P< 0.01 and P<0.001.

4.2.9.3. Both *L. mexicana* and *T. gondii* alter the relative intensity of arginine metabolism intermediates but not NO production.

Unlike the enzymatic assays, LCMS and NO data give a true representative of end-goal metabolic changes within the cell. Arginine metabolites detected by LCMS include L-arginine, L-citrulline, N-(L-Arginino) succinate, L-ornithine, L-proline, L-1-pyrroline-3-hydroxy-5-carboxylate and L-glutamate (Figure 4.15). In comparison to naïve cells, BMDCs activated with LPS significantly induced the metabolism of arginine ($p=<0.05$) to citrulline ($p=0.0009$) and N-(L-Arginino) succinate ($p=<0.05$). Proline and L-1-pyrroline-3-hydroxy-5-carboxylate were also significantly increased in LPS stimulated BMDC whilst L-glutamate was significantly decreased compared to naïve BMDCs ($p=<0.05$). In comparison, *T. gondii* and *L. mexicana* infected BMDCs had significantly increased L-ornithine, L- proline, L-1-pyrroline-3-hydroxy-5-carboxylate ($p=<0.01$) compared to control cells. L-citrulline and N-(L-Arginino) succinate ($p=0.045$) was also significantly elevated in in *L. mexicana* infected BMDCs. In addition, L-glutamate was significantly down-regulated in *L. mexicana* infected BMDC cultures but significantly increased in *T. gondii* infected BMDC cultures.

Moreover, BMDCs cultures infected with *L. mexicana* or *T. gondii* alone did not alter nitrite levels compared to controls cells. This is in comparison to LPS stimulated DCs which significantly increased nitrite levels compared to naïve BMDCs ($p=<0.0001$).

A.

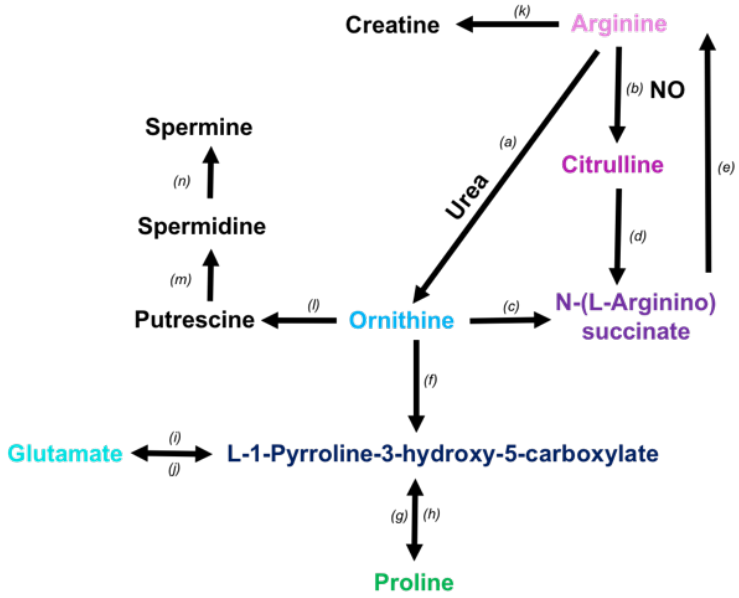
Creatine
(k)
Arginine
(b) NO
(a)
Urea
Citrulline
(e)
(d)
Spermine
(n)
Spermidine
(m)
Putrescine
(l)
Ornithine
(c)
N-(L-Arginino) succinate
(f)
Glutamate
(i)
(j)
L-1-Pyrroline-3-hydroxy-5-carboxylate
(g)
(h)
Proline

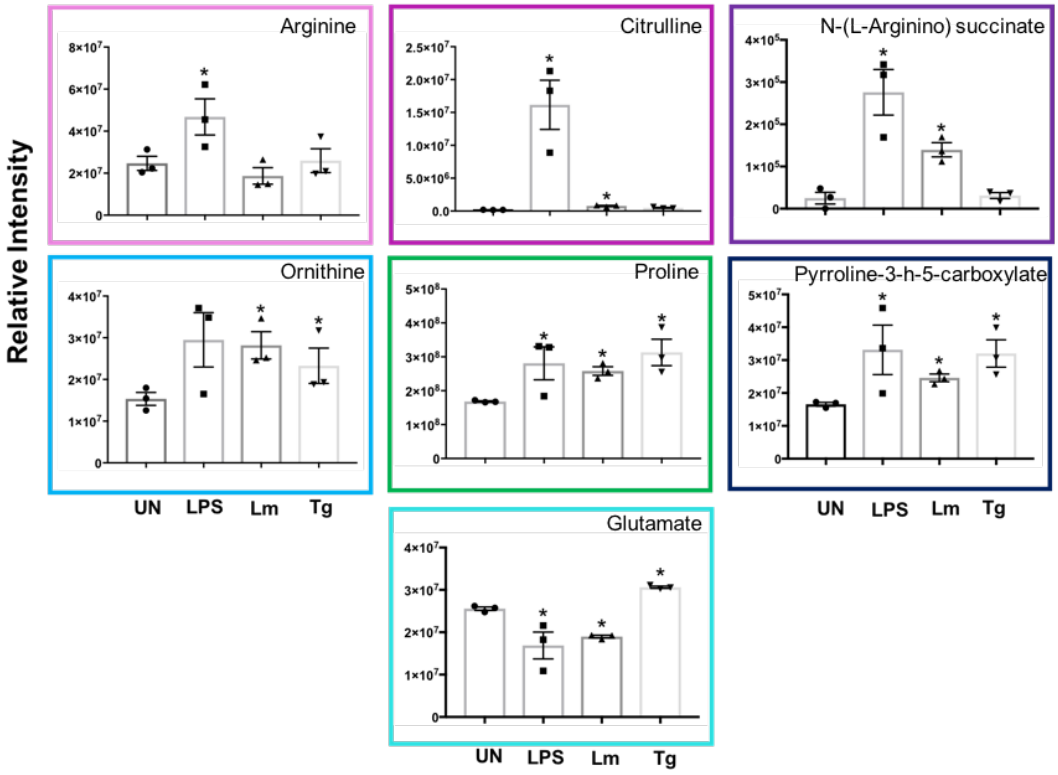
Relative Intensity
Arginine
Citrulline
N-(L-Arginino) succinate
Ornithine
Proline
Pyrroline-3-h-5-carboxylate
Glutamate
UN
LPS
Lm
Tg

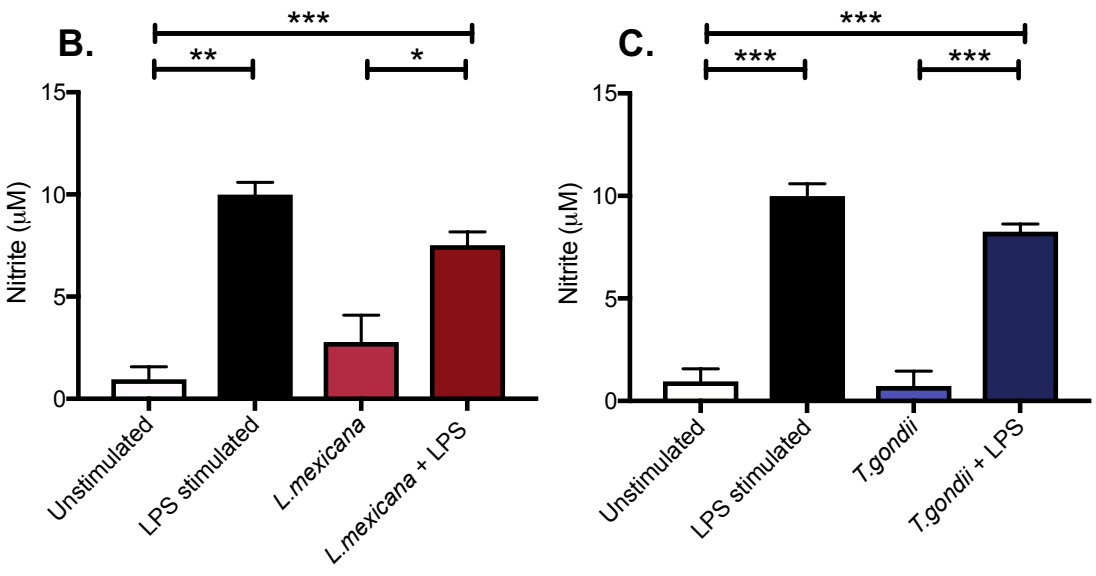

Figure 4.15. Arginine metabolism and Nitric oxide changes in parasite treated dendritic cells. Bone marrow derived DCs were co-cultured with either *L. mexicana* or *T. gondii* as indicated for 24 hours. After this time, the metabolites of the BMDCs were extracted and analysed by (A) Liquid Chromatography Mass Spectroscopy (LCMS) while the supernatants were used to measure (B + C) NO by Griess assay. For clarity, the diagram A focuses on relevant metabolites (shown by the graphs) and enzymes (depicted (a) through to (n)) only are only mentioned in this legend. (a) arginase; (b) NOS; (c) ornithine transcarbamylase; (d) argininosuccinate synthase; (e) argininosuccinate lyase; (f) ornithine aminotransferase; (g) pyrroline-5-carboxylate reductase; (h) proline dehydrogenase; (i) pyrroline-5-carboxylate synthase; (j) P5C dehydrogenase (k) arginine: glycine aminotransferase; (l) ornithine decarboxylase; (m) spermidine synthase and (n) spermine synthase. (A) Statistical analysis was performed using a non-parametric Mann-Whitney test. Significant differences are $p < 0.05$ where * is compared to unstimulated BMDCs. (B+C) Statistical analysis was performed using a One-way ANOVA with Bonferroni post-test. Significant differences were identified where P*<0.05, **P< 0.01 and P<0.001. Results are representative of three independent runs. N = 3.

Figure 4.2 Summary	**LPS**	***L. mexicana***	***T. gondii***
DC Characteristics			
Internalisation rate	N/A	40%	80%
Activation marker upregulation	CD40 & CD80	CD40 & CD86	CD40, CD80 & CD86
IL-12 production	Yes	No	No
Global changes			
OPLS-DA Separation	Yes	Yes	Yes
Metabolism changes			
Upregulated Glycolysis metabolites	G6P, F6P, 2-Phosphoglycerate & Lactate	Glucose, G6P, F6P, 2-Phosphoglycerate, Pyruvate & Lactate	Glucose, G6P, F6P, 2-Phosphoglycerate, Pyruvate & Lactate
Up-regulated TCA intermediates	Citrate, Ketoglutarate, Fumarate & Malate	Citrate, Succinate, Malate & Itaconate	Citrate & Malate
Glucose uptake	Increased	No change	Increased
LDH activity	Increased	Increased	Increased
Mito membrane potential	Reduced	Reduced	Reduced
Intracellular iNOS and NO production	Increased	No change	No change
Arginase-1 activity	Increased	No change	Increased
Up-regulated Arginine metabolism intermediates	Arginine, Citrulline, N-(L Arginino) succinate, Proline, Pyrroline-3-hydroxy-5-carboxylate	Citrulline and N-(L-Arginino) succinate, Ornithine, Proline, Pyrroline-3-hydroxy-5-carboxylate,	Ornithine, Proline, Pyrroline-3-hydroxy-5-carboxylate,

4.3. Discussion

The metabolic crosstalk between intracellular parasites and their host cells have been shown to be essential for pathogens to survive and evade the immune response. Parasites are completely dependent on their host for a wide variety of different nutrients including carbon sources and amino acids (Fox *et al*., 2004; Xu *et al*, 2010). However, the host immune system has evolved to respond to this pathogen invasion by restricting the availability of essential nutrients (Munder *et al*., 2009). These immune-cell mediated changes can be rapid and thus prevent intracellular parasite multiplication before the development of an effective adaptive immune response. Furthermore, different species of parasites reside in separate niches within immune cells and this will ultimately determine what nutrients are available to a pathogen for salvage (Sibley *et al*., 2011). Two intracellular obligate parasites that survive in distinct niches include *Leishmania mexicana* and *Toxoplasma gondii*. Extensive studies have focused on the characterisation of *Leishmania* or *Toxoplasma* virulence factors and strategies the parasites have developed to modulate host intracellular signalling pathways (Alexander, 1981; Butcher *at al*., 2011 Sibley *et al*., 2012; Canonne-Hergaux *et al*., 1999). Yet, how the host and parasite compete for identical nutrients and energy sources has not been extensively studied. Studying the metabolic interplay between these parasites and host cells is complex, but necessary in order to understand how this host-pathogen relationship is regulated and how this influences the outcome of disease. The work described in this chapter has highlighted the extent to which live *L. mexicana* and *T. gondii* parasites influence dendritic cell metabolism. However, whether these changes serve to protect the host through initiating

appropriate immune countermeasures or are instead parasite-evolved mechanisms to evade these countermeasures remains unclear.

To validate that BMDCs internalise these parasites and become activated during infection, key immunological parameters of BMDCs were measured. In keeping with the literature, *L. mexicana* internalisation by BMDC appeared to be dependent on DC cellular processes as both live and fixed parasites were internalised at the same rate (Rittig *et al*., 2000). In contrast, fixed *T. gondii* internalisation was greatly reduced compared with live parasites confirming that they actively invade BMDCs (Subauste *et al*., 2000; Zhao *et al*., 2014; Carruthers *et al*., 1999). BMDCs infected with *L. mexicana* were also found to up-regulate CD40 and CD86 expression whilst those cells infected with *T. gondii* had elevated levels of CD40, CD80 and CD86. The expression of all three activation markers was augmented upon subsequent LPS exposure (Andrade *et al*., 2006; Morgado *et al*., 2014; Verhasselt *et al*., 1997). These data validate the experimental approach and demonstrate that *L. mexicana* and *T. gondii* influence the phenotype of BMDCs and set the foundation to establish how these intracellular pathogens modulate global changes in BMDC metabolism, specifically glycolysis, TCA and arginine metabolism.

Initial results demonstrated elevated levels of glycolysis intermediates (glucose 6 phosphate, fructose 6 phosphate, 2-phosphoglycerate and pyruvate) detected by LCMS in BMDCs infected with *L. mexicana* or *T. gondii*. This was similar to the metabolic profile observed in LPS activated BMDCs and may indicate that BMDCs infected with *L. mexicana* or *T. gondii* adopt a 'Warburg-like' profile (Krawcyzk *et*

al., 2010; Everts *et al*., 2012). To validate the above theory, glucose uptake and lactate dehydrogenase activity was measured. Results showed increased uptake of glucose in BMDCs co-cultured with *T. gondii* but not *L. mexicana* (Nitzsche *et al*., 2016). In addition, a novel finding demonstrated that LDH activity was elevated in BMDCs co-cultured with both *T. gondii* or *L. mexicana*. In comparison to glucose uptake, LDH activity is more indicative of the Warburg effect in cells. Glucose uptake can be seen as time-dependent whereas LDH activity will be indicative of lactate accumulation over time - suggestive of a switch to aerobic glycolysis. In addition, lactate was also increased in these parasite infected BMDCs. The effect of LPS on BMDC activation is broadly in agreement with that previously reported for macrophages and dendritic cells (Fukuzumi *et al*., 1996; Jantsch *et al*., 2008; Krawczyk *et al*., 2010). However, the findings here that *T. gondii* and *L. mexicana* have similar effects on glycolysis in dendritic cells is novel.

In addition to the up-regulation of glycolysis intermediates and elevated LDH activity, the data also demonstrates an accumulation of TCA intermediates and a concomitant decrease in mitochondrial function in parasite infected BMDCs. A similar observation has been reported in macrophages and BMDCs stimulated with LPS (Everts *et al*., 2012; Van den Bossche *et al*., 2016; Krawczyk *et al*., 2010; Panpandreou *et al*., 2006). This further suggests a shift to the Warburg effect in *T. gondii* and *L. mexicana* infected dendritic cells. Elevated TCA intermediates in *L. mexicana* infected BMDC cultures include citrate, succinate, malate and itaconate, whereas citrate and malate accumulation were observed in BMDCs co-cultured with *T. gondii*. Previous studies have demonstrated the accumulation of these intermediates influence the effector

function of LPS-stimulated dendritic cells and macrophages (Tannahill *et al*., 2013; Jha *et al*., 2015; Infantino *et al*., 2011). Thus, succinate accumulation in macrophages stimulated with LPS can enhance the expression of pro-inflammatory genes (via HIF-1 α activation) and ROS (via reverse electron transport) (Mills *et al*., 2016).

Further studies are necessary to understand the role this metabolic remodelling plays in *L. mexicana* or *T. gondii* infected BMDC cultures. A novel finding is that itaconate was significantly up-regulated in *L. mexicana* exposed BMDCs, but not those infected with *T. gondii* or activated with LPS. Seminal studies have demonstrated that itaconate is one molecule that has anti-inflammatory properties by inhibiting succinate dehydrogenase (Strelko *et al*., 2011; Nemeth *et al*., 2015). This would reduce the generation of ROI and pro-inflammatory cytokines e.g. IL-1β elevated during succinate accumulation and succinate dehydrogenase activation (Lampropoulou *et al*. 2016; Mills *et al*., 2016; Strelko *et al*., 2011). In contrast, itaconate has been demonstrated to block the glycoxylate shunt in some pathogen infections limiting viability (Michelucci *et al*., 2013; McFadden *et al*., 1977). Therefore, future studies should further investigate if an increase in itaconate in *L. mexicana* infected BMDCs may be a possible mechanism for these parasites to avoid an inflammatory phenotype in BMDCs or a tactic used by the BMDC to suppress *L. mexicana* intracellular growth.

Mitochondria which are the of site of the TCA cycle can also be used as an indicator of the Warburg effect in cells. Mitochondria are dynamic organelles that re-arrange morphology and alter membrane potential in response to stress, nutrient availability and energy demands (Rambold *et al*., 2017). Herein, for the first time we demonstrate

that LPS stimulation alters BMDC mitochondria morphology and decreases membrane potential. Furthermore, a reduction in membrane potential is also observed in *L. mexicana* or *T. gondii* infected BMDCs, although this does not correlate with morphological changes seen in LPS stimulated BMDCs. This demonstrates that LPS activated BMDCs and those infected with *L. mexicana* or *T. gondii* have a less active mitochondria in comparison to naïve BMDCs. This is consistent with previous studies that observed changes to oxidative metabolism including suppression of the respiratory burst in *T. gondii* infected macrophages (O'Neill *et al*., 2013; Chang *et al*., 1989).

Previous studies have examined murine macrophages infected with *Leishmania infantum* for functional changes to their metabolism. In these studies, a metabolic switch similar to the Warburg effect was observed (peaking at 6 hours post infection), but reversion was noted as early as 18 hours post infection (Moreira *et al*., 2015). Apparent differences in the timing and potential duration of the Warburg effect could be due to differences in the type of immune cell or the species of parasite examined. Alternatively, differences might reflect the discrepancy between detecting enzyme activities (using the Seahorse platform) versus their substrates and products as achieved by LCMS.

The ability of LPS stimulation to induce changes to the arginine metabolism of macrophages and dendritic cells is well described (Reviewed in O'Neill *et al*., 2016). Consistent with these studies LPS-stimulated dendritic cells had elevated levels of citrulline, up-regulation of iNOS expression and were able to generate NO. However,

Toxoplasma infected BMDCs had increased arginase-1 activity and augmented levels of ornithine and proline relative to control cells. This could be interpreted in 2 ways (i) a parasite-mediated strategy whereby *T. gondii* induces a phenotype in dendritic cells akin to what is referred to as 'M2 macrophages'. This would be commensurate with the literature that demonstrates *T. gondii* can induce Arg1 expression in a STAT6 dependent (via *T. gondii* specific ROP16 molecule) and independent manner (via TLR-4 ligands; GPI anchors and HSP70) (El-Kasmi *et al*., 2008; Butcher *et al*., 2011; Marshall *et al*., 2011) This has been suggested to function as a means to reduce NO production by infected cells and thus promote parasite survival. (ii) A host mediated mechanism to deprive *T. gondii* of arginine for which it is auxotrophic and must therefore acquire from the host (Fox *et al*., 2004). In support of this interpretation, studies have demonstrated that *arg1* induction can limit parasite growth and be host protective too, presumably by depriving *T. gondii* of arginine (Woods *et al*., 2013). In all likelihood, these two opposing scenarios are evolutionary counter measures.

BMDCs infected with *Leishmania* were found to have increased levels of ornithine and proline relative to control cells. Arginase-1 activity was not elevated in BMDCs in response to *Leishmania* infection and supports previous data describing polyamine biosynthesis in *Leishmania* itself (Roberts *et al*., 2004; Reviewed in Gianni *et al*., 2011). Host arginine is known to be used in polyamine biosynthesis and to be the sole source of spermidine necessary to synthesise the anti-oxidant trypanothione, necessary for amastigotes survival by neutralising ROS (Pinkovich *et al*., 2016). In addition, citrulline and argininosuccinate were increased in *L. mexicana* infected BMDC cultures whilst NO production and iNOS protein levels were not. Studies by

Westrop *et al*., show that a major route of arginine catabolism in *L. mexicana* parasites is to arginic acid, argininosuccinate and ultimately polyamines in these infected BMDCs (Westrop *et al*., 2015).

The data in this chapter has highlighted that intracellular parasites such as *L. mexicana* or *T. gondii* can influence dendritic cell metabolism. While certain changes to the metabolism (e.g. arginine metabolism in *T. gondii* infected BMDCs) would appear to be instigated by the parasite to promote growth and survival, other changes (e.g. to glycolysis and the TCA cycle) would appear to be general host evolved strategies to augment immunity and parasite control. Understanding how parasites affect cellular metabolism is a potential important step in the production of new drugs and might also inform vaccine design against *L. mexicana* and *T. gondii*. In addition, a fuller understanding of metabolic changes in disease could aid in the development of new treatments for other chronic conditions.

Chapter 5

Leishmania mexicana and *Toxoplasma gondii* alter the transcriptome of dendritic cells

5.1 Introduction

Transcriptomics is the study of mRNA expression within cells and allows an understanding of the genes that are being actively expressed at any given time. This was previously achieved through microarray analysis, but advances in DNA sequencing technology have given rise to whole transcriptome shotgun sequencing (WTSS) often referred to as RNAseq. These analyses have revolutionised many fields of study including immunology and it is possible to obtain an overview of changes in gene expression during an ongoing immune response.

Like metabolomics, transcriptomics has allowed researchers to take a complete uninterrupted snapshot of the relationship between parasite and host cells at one or more particular time points. Understanding regulation of mRNA transcripts encoding receptors, metabolic enzymes and transcription factors in conjunction with LCMS and functional studies (as described in previous chapters of this thesis) can provide insight into the flux of metabolites through a metabolic pathway and how this is influenced by parasites. In addition, transcriptomics indicate other immune-related genes that are influenced during infection and in relation to the overall aims of the work described in this thesis can help establish not just how parasites alter the mechanism regulating host metabolism e.g. mTOR/AMPK axis, but also how they modulate immune cell effector function. Therefore, this chapter uses transcriptomic analyses to confirm parasite induced, metabolic reprogramming of dendritic cells (as described in the previous two chapters) and provide mechanistic insight into this process.

5.2. Results

5.2.1. High quality transcriptomic data was obtained for BMDCs activated with LPS or co-cultured with either *L. mexicana* or *T. gondii*

Each individual replicate DC culture produced between 32 190 355 and 51 515 394 total reads of which between 32 025 937 and 51 319 651 were clean reads (Table 5.1). Between 97.8 and 98.2% clean reads from unstimulated DCs and between 97.9 and 98.3% clean reads from LPS-stimulated DCs were mapped onto the *Mus musculus* reference genome. In contrast, between 84.8 and 86.2 clean reads for DCs co-cultured with *L. mexicana* and between 88.5 and 91.2 clean reads for DCs co-cultured with *T. gondii* were mapped onto the *Mus musculus* reference genome. The lower percentage of mapped reads in the parasite infected cultures likely reflected the presence of parasite transcripts that were not positively mapped.

Table 5.1. High quality transcriptomic data was obtained for BMDC activated with LPS or co-cultured with either *L. mexicana* or *T. gondii* [1]

Sample	Total Reads	Discarded Reads	Clean Reads	Mapped Reads[2]	% Mapped
UN1	46, 050, 349	0.4%	45, 874, 907	44, 913, 488	97.9
UN2	42, 960, 078	0.4%	42, 770, 393	41, 849, 911	97.8
UN3	51, 319, 651	0.4%	51, 319, 651	50, 388, 676	98.2
LPS1	40, 239, 286	0.4%	40, 072, 860	39,229, 554	97.9
LPS2	43, 550, 476	0.4%	43, 388, 004	42, 273, 359	97.4
LPS3	47, 700, 318	0.4%	47, 517, 704	46, 701, 407	98.3
Lm1	32, 190, 355	0.5%	32, 025, 937	27, 155, 308	84.8
Lm2	35, 802, 031	0.4%	35, 663, 328	30, 417, 387	85.3
Lm3	48, 535, 073	0.3%	48, 369, 328	41, 680, 898	86.2
Tg1	44, 610, 461	0.5%	44, 401, 746	40, 497, 402	91.2
Tg2	36, 114, 699	0.5%	35, 937, 718	41, 849, 911	90.0
Tg3	43, 868, 055	0.5%	43, 660, 931	50, 388, 676	88.5

[1]Bone marrow derived dendritic cells were stimulated with LPS or infected with *L. mexicana* or *T. gondii,* 6 hours before mRNA was extracted.

[2]Clean reads were mapped to the *Mus musculus* reference genome.

5.2.2. Dendritic cells undergo distinct but overlapping holistic transcript changes when activated with LPS or co-cultured with either *L. mexicana* or *T. gondii*

Holistic changes in the transcriptome of naïve BMDCs, LPS activated BMDCs and those infected with *L. mexicana* or *T. gondii* were observed. Orthogonal partial least squares discriminant analysis (OPLS-DA) found distinct separation between naïve BMDC cultures, LPS activated BMDCs and *L. mexicana* infected BMDC cultures (Figure 5.1). Separation was also observed between naïve BMDCs and those co-cultured with *T. gondii* but to a lesser degree that the other sample groups (LPS or *L. mexicana*). The holistic changes in transcript expression (based on fragments per kilobase of transcript per million mapped reads; FPKM) are fully detailed in a VIP score list which order the most important variables across the model as a whole (VIP score ≥ 2.00) (Table 5.2). Separate pairwise comparisons of LPS activated, *L. mexicana* infected or *T. gondii* infected cultures compared to naïve cells are shown in Table 8.13 – 8.15.

Notably, most transcripts are immune-related (shaded blue). However, transcripts associated with glycolysis, TCA cycle, OXPHOS, arginine (shaded green) or signalling molecule/transcription factors (shaded orange) are evident. These will be discussed detail later in the chapter.

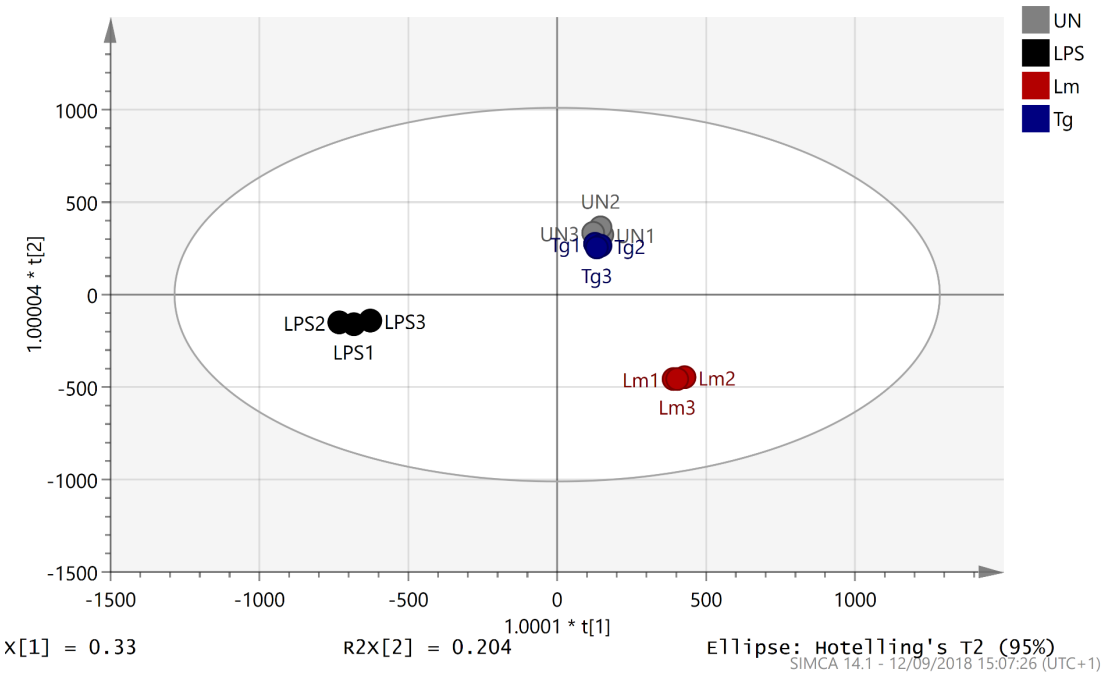

Figure 5.1. Orthogonal Projections to Latent Structures Discriminant Analysis of transcript changes in BMDCs activated with LPS or co-cultured with *L. mexicana* or *T. gondii*. Bone marrow derived DCs were either stimulated with LPS or co-cultured with *L. mexicana* or *T. gondii* as indicated for 6 hours. After this time, mRNA was subsequently extracted and then quantified using RNA-seq. The data was analysed on SIMCA and an Orthogonal Projections to Latent Structures Discriminant Analysis (OPLS-DA) plot for mRNA of BMDC activated with LPS or influenced by *L. mexicana* or *T. gondii* was generated. OPLS based on FPKM values. Key: Grey, unstimulated; Black, LPS; Red, *L. mexicana*; Blue, *T. gondii*. The confidence ellipses are based on Hotelling's $T^2 = 95$. N = 1.

Table 5.2. VIP Score of transcript expression changes in LPS activated BMDC cultures or infected with *L. mexicana* or *T. gondii*.

Transcript abbreviation	M1.VIP [3+3+0][1]	2.44693 * M1.VIP [3]cvSE[2]	Gene name or Role[3]
Gm7204	44.2085	49.8178	Peroxiredoxin 1 pseudogene
Bbx	29.7071	23.2165	Bobby sox homolog
Gm7665	19.4834	10.3706	Calcium binding protein A11 pseudogene
Pde1c	19.4217	15.3233	Calcium/ calmodulin dependent 3'-5' cyclic nucleotide phosphodiesterase
Il1rapl1	18.9698	6.08534	IL-1 receptor
Rps28	17.6718	9.52939	Ribosomal protein 28
Mir6236	17.4435	6.21069	MicroRNA
Mctp2	15.93	5.7897	Transmembrane protein
Lyz2	14.4366	6.01477	Lysozyme
Mir6240	12.9639	11.8687	MicroRNA
Gm23374	11.0565	3.19298	Unknown
Gm7897	9.67639	3.31907	Unknown
Ftl1	9.39644	5.53485	Ferritin light chain
Tpt1-ps3	9.30818	5.6012	Tumour protein, translationally controlled pseudogene 3
Gm15487	9.2339	3.80037	Atp6v0c pseudogene
Ptprb	8.94186	2.92149	Protein tyrosine phosphatase
Cntnap2	8.79279	7.7387	Contactin associated like protein
Gm8909	8.75667	2.93273	MHC class I
Il1b	8.59456	2.69467	IL-1b
Fth1	8.27369	7.49851	Ferritin heavy chain
Txlnb	7.83952	2.96871	Beta-taxilin
Hmox1	7.83303	4.69604	Heme oxygenase 1
Saa3	7.41373	3.03835	Serum amyloid A 3
Gm14303	7.2885	2.38975	Unknown
Gm8984	7.16659	5.74524	Glyceraldehyde 3 phosphate dehydrogenase pseudogene
Chd2	7.15314	3.36652	Chromo domain helicase
Ctcf	7.11585	5.57589	Translational repressor
Slc8a3	6.88953	5.29358	Sodium/ calcium exchanger precursor
Cacna2d4	6.67204	2.53635	Calcium voltage-gated channel subunit
Fam19a3	6.66967	4.38416	TAFA family and associated with MIP-1a

Bach2	6.65045	1.78612	Transcription regulator
Vmn2r-ps54	6.57506	2.46707	Vomeronasal receptor 2 psudogene
Gm26825	6.45373	2.72707	iNOS pseudogene
Gm37361	6.39463	3.4686	Unknown
Ccl3	6.32234	2.03812	MIP-1a
Uqcrh-ps2	6.19407	4.23454	Ubinquinol cytochrome c reductase hinge protein psudogene
Negr1	6.14925	4.08793	Neuronal growth factor
Mt1	6.13941	3.82135	Metallothionein 1
9330179D12Rik	6.13517	4.07526	cDNA
Ctsd	6.12457	2.50499	Cathepsin D
Hormad2	6.05553	3.11821	HORMA domain containing protein
Rpl27a-ps2	6.01029	4.42841	Ribosomal protein L27A
Gm12111	5.95354	2.8035	Unknown
Il1a	5.8656	1.85936	IL-1a
Gm26981	5.86067	3.28727	Unknown
Ccl5	5.68762	2.56484	RANTES (T cell activation)
Gm11560	5.57199	3.95428	Unknown
Gm16418	5.57179	2.40291	Ubiquinol cytochrome c reductase subunit precursor pseudogene
Lgals3	5.56498	3.03123	Lectin galactose binding
Gm26615	5.5524	3.0258	Unknown
Gm26745	5.52957	2.13365	Unknown
Gm7846	5.52724	2.22687	Unknown
Rsad2	5.50725	1.8977	Radical 2-adenosyl methionine domain
Rnf24	5.50142	2.29814	Ring finger protein
Lhx9	5.47962	2.60916	Lim homeobox 9 (transcription)
Gm6682	5.41961	6.86182	Tubulin, alpha 1c pseudogene
Cdk8	5.40382	1.79713	Cyclin dependent kinase 8
Gm5870	5.40291	2.94756	Unknown
Grm8	5.40177	1.66426	Glutamate metabotropic receptor
Prdx1	5.40043	3.46901	Peroxiredoxin
Gm8529	5.34486	4.65298	Unknown
Cxcl3	5.3351	1.67238	MIP-2a (Macrophage inflammatory protein)
Gm12864	5.32763	4.3968	Glyceraldehyde 3 phosphate dehydrogenase pseudogene
Cd74	5.32338	3.63849	CD74
Gm43841	5.28575	8.10154	Unknown
Mt2	5.20012	2.49981	Metallothionein 2
Gm9575	5.18673	1.65272	Unknown
Tcea1	5.18172	5.75672	Transcription elongation factor

RP23-166L22.1	5.17073	4.32575	
Marcksl1	5.1663	1.56085	Associated with cytoskeleton
Pcsk5	5.04365	2.92344	Proprotein convertase
Ldha	4.98461	2.98736	Lactate dehydrogenase
RP23-183A4.1	4.98368	6.88956	
Gm19963	4.90874	1.66453	Unknown
Ccl22	4.8788	1.23599	Chemokine 22
Gm14130	4.87214	4.16602	Unknown
Gm10180	4.84417	2.82733	Unknown
Gm609	4.81031	4.35129	Unknown
Oaz1-ps	4.79489	1.25781	Ornithine decarboxylase antizyme pseudogene
Batf2	4.7849	1.89122	Basic leucine zipper transcriptional factor
Eif4a-ps4	4.72796	5.51477	Eukaryotic translation initiation factor
Eif1ax	4.72568	3.75652	Eukaryotic translation initiation factor 1A X-linked
Timp4	4.70114	3.64862	Metallopeptidase inhibitor
Gm8304	4.68731	3.57625	Ribosomal protein L17 pseudogene
Gm16505	4.67865	2.53826	Unknown
Gm10425	4.63162	1.52843	Unknown
Gm6394	4.62072	3.15222	Ribosomal protein L11 pseudogene
Il1rn	4.60949	1.77363	IL-1 receptor antagonist
Cntnap5b	4.59925	2.94658	Contactin-associated protein like 5 precursors
Gm7676	4.59312	4.85332	Interferon induced transmembrane protein pseudogene
Gm13450	4.58191	3.49487	Unknown
Gm15173	4.53337	3.95111	Unknown
Txnrd1	4.52112	1.27724	Thioredoxin reductase 1
Clec4n	4.49329	1.55138	C-type lectin domain family
G6pd2	4.48836	4.06188	Glucose 6 phosphate dehydrogenase 2
Usp32	4.46446	1.72622	Ubiquitin carboxyl-terminal hydrolase 32 precursor
Gm32444	4.45708	3.56587	Unknown
Gm18957	4.42228	3.8403	Unknown
Rpl3-ps1	4.39688	2.6593	Ribosome protein L3 pseudogene
Gm24951	4.32838	1.37497	Unknown
Gm5809	4.28118	4.99539	Transmembrane protein
Gm11822	4.26878	2.53804	Unknown
Tmcc1	4.23927	1.38366	Transmembrane and coiled coil domain
S100a16	4.2276	3.0665	S100 calcium binding protein
Zfp36l1-ps	4.22219	3.88201	Zinc finger protein pseudogene

Hp	4.21775	1.17499	Haptoglobin (binds free haemoglobin)
Ryr3	4.20421	6.39889	Ryanodine receptor
Mvp	4.1972	4.9343	Major vault protein
Sh3gl3	4.16681	4.54661	Endophilin A3
Gm9840	4.12565	1.21806	Rbx-1 MGI pseudogene
Gm12497	4.12182	3.50395	Unknown
Gm17638	4.09674	2.46976	Unknown
Rn18s-rs5	4.08829	5.01579	18s RNA
Gm19587	4.07276	4.45993	Unknown
Mmp12	4.05839	2.82008	Matrix metallopeptidase
Il31ra	4.05653	2.38591	IL-31 receptor a
Anks1b	4.04838	3.16071	Ankyrin repeat and sterile alpha motif domain
Rpl10l	4.02909	1.40661	Ribosomal protein L10
H3f3a-ps2	4.01144	2.6302	Histone family psudogene 2
Macrod2	3.97799	4.80149	MACRO domain containing 2
Mir703	3.87729	1.93209	microRNA
Gm7332	3.83326	1.72852	Protein phosphatase 1 regulator pseudogene
Acod1	3.81152	1.22796	Cis-aconitate dehydrogenase
Gm2522	3.80503	2.74038	KOMP
Gm13453	3.79675	2.04927	Unknown
Gm11258	3.79553	2.04059	Unknown
Gm15925	3.78863	1.70123	Unknown
Gm38187	3.78162	2.66061	Unknown
Pkm	3.7804	1.91925	Pyruvate kinase
Vim	3.76393	1.92874	Vimentin
Gm42989	3.74389	2.76842	Unknown
Gm12892	3.73458	2.26162	Unknown
4930552N02Rik	3.72834	2.56903	cDNA
Gm7984	3.72533	2.25894	Unknown
Zfp839	3.71077	3.71903	Zinc finger protein
Gm16372	3.70445	1.45632	Unknown
Cxcl2	3.70259	1.29524	MIP-2alpha
Pou2f3	3.69632	1.31047	Transcription factor
Gm5548	3.69327	3.40019	Leptin receptor gene related protein pseudogene
Gm6180	3.6727	3.52703	COL3A1
Serpina3n	3.66639	1.16331	Serine or cysteine peptidase inhibitor
Isg15	3.66017	1.30077	Interferon stimulated gene 15
Adgrl3	3.66001	5.51186	Adhesion G protein coupled receptor L3
Ccl4	3.65419	1.14436	MIP-1b

Gm1840	3.6351	1.3381	Glucose phosphate isomerase 1 pseudogene
Rit2	3.61694	2.88225	GTP binding protein Rit2
Antxr1	3.61018	4.68996	Cell adhesion molecule
Actg1	3.59712	1.27312	Actin-gamma 1
Camk1d	3.58562	4.06335	Calcium/ calmodulin dependent protein kinase 1D
Gm8814	3.58406	1.62611	Ferritin light chain 2 pseudogenes
Il12b	3.58325	1.16643	IL-12b
Aldoart1	3.55018	3.73211	Fructose-bisphosphate aldolase
Gm5560	3.5332	2.68933	Unknown
Gm15482	3.52754	3.76918	Unknown
Ctss	3.51508	1.76218	Cathepsin S
2410017I17Rik	3.50809	1.10672	cDNA
Gm2199	3.4877	2.75154	Mitochondrial carrier homolog 2 pseudogenes
B830042I05Rik	3.48074	1.70146	cDNA
Cmpk2	3.47324	1.14177	Cytidine/ uridine monophosphate kinase 2
Hs6st3	3.46662	4.09728	Heparan sulfate 6-O-sulfotransferease
Gm35106	3.46112	3.59215	Unknown
Gm5578	3.45964	2.82373	CAAX motif
Prdx5	3.45945	1.39397	Peroxiredoxin-5 mitochondrial
Gm45211	3.45839	1.30878	Unknown
Gpx1	3.4569	0.899701	Glutathione peroxidase
Tpi1	3.40848	2.00166	Triose phosphate isomerase 1
S100a9	3.39661	2.07098	Calcium binding protein
Gm16407	3.39498	1.3402	Unknown
AA467197	3.38638	1.27242	
Spp1	3.38003	2.15907	Secreted phosphoprotein 1
Gm6987	3.36848	2.42387	Unknown
Lcn2	3.36792	1.10833	Lipocalin-1 (sequesters iron)
Gm12428	3.36759	3.13529	Unknown
Sh2d2a	3.35684	2.12569	SH2 domain containing 2A
Plxdc1	3.35373	1.26385	Plexin domain containing protein
Fscn1	3.3432	0.993499	Fascin actin bundling protein
Eef1a1	3.33943	0.849815	Eukaryotic translation factor
Gm3145	3.32693	1.71674	Unknown
Tmsb4x	3.31965	1.64516	Thymosin beta 4
6030443J06Rik	3.31929	3.21011	cDNA
Gm6863	3.31826	1.31015	Unknown
Scp2-ps2	3.31297	5.00169	Sterol carrier protein 2
Gm7634	3.30462	3.21838	Unknown

Gm14877	3.28836	1.97987	Unknown
Gm44090	3.27596	3.20955	Unknown
Ctsb	3.25649	1.86527	Cathepsin B
Cxcl10	3.23261	1.01128	Chemokine – Interferon gamma induced protein
H2-Eb1	3.20236	1.83325	MHC class II antigen E beta
Lrp1b	3.20091	4.2564	LDL receptor related protein 1B
Gm11951	3.20018	2.34609	Unknown
Gm12158	3.19943	2.75503	Unknown
Crocc	3.19156	1.8337	Rootletin (centrosome cohesion)
Clec4e	3.17038	1.14504	Macrophage inducible Ca^{2+} dependent lectin receptor
Gm7816	3.17004	0.994889	Unknown
Gm43972	3.16533	3.72883	Unknown
Tmem232	3.1647	2.07077	Transmembrane protein
Gm16111	3.13841	3.0216	Unknown
Ptgs2	3.13247	1.04156	Prostaglandin endoperoxide synthase 2
Tpt1-ps6	3.12847	1.31197	Tumour protein translationally controlled pseudogene
Ebf1	3.12637	1.07009	Early B cell factor (Transcription factor)
Ifitm1	3.12337	1.17191	Fat storage transmembrane protein
H2-Q3	3.12224	1.29909	MHC class II
H2-Aa	3.1041	2.35567	MHC Class II
Gm8048	3.0953	2.06611	Glyceraldehyde 3 phosphate dehydrogenase pseudogene
Usp37	3.08695	2.17785	Ubiquitin carboxyl terminal hydrolase 37
Trim30e-ps1	3.06643	1.91924	Tripartite motif containing 30E pseudogene
Gm13736	3.05138	1.6354	Unknown
Gm2824	3.01795	2.93679	Unknown
Gm16755	3.01565	1.51052	Unknown
4833427G06Rik	3.01557	1.55453	cDNA
Gm8979	3.00755	1.97046	Unknown
Lipa	2.97273	1.42313	
Il6	2.97071	0.999891	Pro-inflammatory cytokine
Gm29610	2.96908	0.790122	
Mmp13	2.96648	1.03287	
Angel1	2.96411	2.55772	
P4hb	2.96321	1.46409	
Cstb	2.96077	1.98271	
Gm9824	2.95356	2.77919	
Gm9025	2.95171	4.54248	
Gm12906	2.94896	2.15749	

Gm15703	2.94474	1.63937	
Gm26852	2.93931	2.54419	
Fcrla	2.93615	3.34901	
Gapdh	2.92616	1.70483	Glyceraldehyde 3 dehydrogenase
Tcp1	2.92477	1.1163	
Acyp2	2.92142	1.54114	
Gnaq	2.91635	1.97142	
Slk	2.91568	2.7238	
Gm16589	2.90862	3.07	
Serpina3g	2.90451	0.983249	
Nckap5	2.8977	4.58715	
Gm36551	2.89467	1.77945	
Cep72	2.89354	1.55553	
AW112010	2.88941	0.913458	
Slc39a1-ps	2.88774	2.43184	
Lrrc20	2.87994	4.17774	
Gbp2	2.87752	0.927666	
Gm5607	2.87507	1.05523	
Cd40	2.87498	0.959689	Co-stimulatory molecule
Gm15529	2.87162	1.12345	
Sepw1	2.86584	4.04917	
RP23-96L20.1	2.86146	4.01667	
Gm28343	2.85637	1.52808	
Gm5615	2.85577	1.04249	
Coro1a	2.85222	0.682716	Associated with T cell activation
Mup-ps16	2.8506	2.65736	
Fn1	2.84998	2.20024	
Dmd	2.84894	3.06996	
Gm13082	2.8417	2.0879	
Itfg1	2.83902	1.47536	T cell immunomodulatory protein precursor
Tyrobp	2.83852	1.10876	
Gbp2b	2.83609	0.939693	
Gm7964	2.83073	1.7362	
Rpl9-ps8	2.82813	1.41108	
Gm42418	2.82666	2.90494	
4930509G22Rik	2.82523	1.29574	
H2-Bl	2.82044	4.06051	MHC Class II
Cotl1	2.81936	0.980817	
Eef2	2.81659	0.956652	Eukaryotic elongation protein
Gm4852	2.81551	3.07575	
Oasl1	2.81267	0.892338	
Gm11970	2.81187	2.69461	
Gm37945	2.80977	1.48573	

Ccl9	2.80684	1.72971	MIP-1g
Rplp1	2.80011	1.32611	
RP23-74O12.6	2.79879	1.60449	
Sepp1	2.78453	0.739246	
Cd36	2.77948	1.09842	Imports fatty acids
Gm44737	2.76729	1.70146	
Gm44209	2.754	1.35501	
Cpa6	2.74598	1.81355	
Sema3a	2.74111	2.26863	
Crb1	2.73203	1.44285	
Gm13392	2.72885	4.09791	
Lpl	2.72571	2.43505	
Ralgps2	2.72529	1.92538	
Cntnap2	2.72239	2.36004	
Gm9089	2.71617	1.28077	
Fry	2.71523	0.847516	
Gm10698	2.71443	3.4158	
Rnft2	2.71386	2.71574	
Cd9	2.70812	2.00359	
Txnrd1	2.70007	1.37671	
Gm4585	2.68053	2.55722	
Asap2	2.67469	0.763283	
Rps5	2.67383	0.66643	
Oca2	2.67195	3.43979	
Gm5940	2.657	3.93047	
Fxyd5	2.65136	0.921018	
Myo9a	2.6404	4.56671	
Rps18	2.64023	1.01036	
Gm6913	2.63369	2.29617	
Rps14	2.62828	1.45367	
Gm28539	2.62096	2.67287	
Irf7	2.60983	0.949531	Interferon regulatory factor
Gm5244	2.59575	1.69218	
Gm19087	2.58941	3.8544	
RP23-297C11.2	2.5889	0.897308	
Pnp	2.58727	1.01816	
Cebpb	2.57975	1.17812	
Gm20470	2.57962	0.878436	
Gm8545	2.57766	2.31003	
Txnrd1	2.57413	0.787497	
Txnrd1	2.55853	1.3278	
Zfp280c	2.5543	3.04528	
Clic4	2.55175	0.770052	
Anxa2	2.54593	1.42891	

Slc28a1	2.53171	1.45135	
Gm4374	2.53165	2.94227	
Plek	2.52748	0.916156	
Csf1r	2.52369	0.508098	
Trim2	2.51368	1.4534	
Socs3	2.5091	0.802806	Suppressor of cytokine signalling 3
Cxcl1	2.50579	0.790183	Neutrophil activating protein
Prex2	2.5045	1.62312	Phosphatidylinositol-3,4,5-trisphosphate-dependent Rac exchange factor 2
Serpine1	2.50155	0.816554	
Ccl6	2.50139	1.26289	Chemokine
Rpl32	2.4996	1.22562	
Rpl36a-ps1	2.49889	4.35919	
Frem1	2.49541	1.67031	
H2-Ab1	2.49228	1.43858	MHC Class II
Magee2	2.49108	2.58078	
Gm37103	2.48185	1.44686	
Sqstm1	2.47422	1.51019	
Eno1	2.47017	1.32304	Enolase 1
Tpt1	2.46839	0.952131	Cell differentiation
Gm44978	2.46811	2.0771	
Gm7335	2.46767	1.04875	
Ms4a6d	2.46541	0.789284	
Rps19-ps10	2.46365	2.28486	
RP24-285L8.3	2.45364	1.55781	
Txn1	2.45079	1.13627	
Gm6265	2.44711	3.45829	
H2-Ea-ps	2.44069	2.13868	MHC Class II
Rps9	2.44005	0.605959	
Slc2a6	2.43221	0.754842	GLUT
Mmp9	2.4301	0.841069	
Ccdc7b	2.42361	1.54257	
H3f3b	2.42189	0.760959	
Gm13502	2.41805	1.16371	
Ifitm3	2.41334	0.753316	
Lamp1	2.41213	0.780571	Lysosomal fusion and cell adhesion
Zfyve28	2.40836	2.39422	
Cd14	2.40534	0.753208	Ligand for LPS
Tubb5	2.40273	0.688543	
Gm6421	2.4014	2.68199	
mt-Nd6	2.39471	2.81663	NADH: Ubiquinone oxidoreductase
Pfn1	2.3946	1.2148	
Gm43083	2.38681	0.632823	

Syngr2	2.3838	0.861259	
Gm18848	2.37892	1.36502	
Gm2670	2.37225	1.71996	
Rps29	2.36975	1.52444	
Gm10221	2.36769	1.46594	
Gm20589	2.35861	1.59396	
Gm7293	2.35704	2.18924	
Upp1	2.35376	0.950335	
Esd	2.3507	1.80216	
mt-Cytb	2.3506	2.58004	Cytochrome B
Slc15a3	2.34609	0.830972	
Pnp	2.34475	0.784194	Purine nucleoside phosphorylase
Gm9159	2.34334	1.68582	
Atp5e	2.33819	1.38728	ATP synthase
Rnh1	2.33569	1.36643	
Zfp956	2.33496	0.910862	
Gm26659	2.32523	2.08351	
Clec7a	2.3182	0.642864	
Ifit2	2.30683	0.814466	
F10	2.30151	0.82416	
Rpl8	2.30082	0.975772	
Rack1	2.28714	0.788143	Receptor of activated protein kinase C
Laptm5	2.28708	0.519746	
Id2	2.28389	0.97886	
Gm17275	2.28004	0.982365	
Lgals1	2.27584	1.33594	
Fpr2	2.26866	0.757618	
Gm42522	2.26002	1.65126	
Acsl1	2.25952	0.730644	Acyl-CoA synthetase
Erbb4	2.24865	2.15982	
Pgam1	2.24848	1.45792	Phosphoglycerate mutase 1
BC048502	2.24808	1.00782	
Psme2	2.24344	0.836681	
Tnfaip2	2.24204	0.683525	TNF alpha induced protein 2
Cks1brt	2.24193	1.84755	
Ifi47,Olfr56	2.23844	0.842325	Interferon gamma inducible protein 47
Gm20412	2.23332	0.838324	
Gbp3	2.22586	0.742214	
Gm26561	2.22565	0.946603	
Apoe	2.22457	0.645847	Fat metabolism
Capg	2.22185	1.39339	Macrophage capping protein
Rps17	2.21942	0.944689	

Gm38305	2.21737	1.83086	
Mmp8	2.21318	0.700046	
Rps21	2.20775	1.41111	
Vat1	2.20073	1.26234	
Cst3	2.20042	1.52296	
Ehd1	2.19916	0.664297	
Gm28196	2.19743	3.35371	
Gm16907	2.19654	1.1111	
Fshr	2.19434	0.876521	
Retnla	2.19179	0.991128	
Fam227b	2.18031	0.837044	
Lcp1	2.17793	0.87712	
Tagln2	2.17406	0.945533	
Gm43495	2.16859	1.40965	
Sirpb1b	2.16576	1.65916	
Wfdc21	2.1494	0.768147	
Kcp	2.14785	1.72111	
Gpi1	2.14696	0.785192	Glucose-6-phosphate isomerase
Slc25a5-ps	2.14625	1.45787	
Slfn2	2.1461	0.826289	
Gm13132	2.14532	2.55951	
Itm2b	2.13942	0.741115	
Hck	2.13887	0.682008	
Ifi44	2.13855	0.736236	
Rpl18a	2.13765	0.622259	
Rps19	2.1348	0.693413	
Rps26	2.13213	0.819547	
Slc7a2	2.12744	0.768568	
Hhat	2.12731	1.3128	
Gm16505	2.12518	1.35994	
Rps16	2.12057	0.940359	
Usp18	2.1167	0.674779	
Pla2g7	2.11611	0.390871	
Tnfrsf1b	2.11446	0.674894	TNF receptor
Tcf12	2.11273	0.853842	Transcription factor
Mapkapk2	2.1093	0.646049	MAP kinase activated protein kinase 2
Rps11	2.10649	1.00544	
Txnrd1	2.10138	0.649982	
Ctsz	2.10121	1.83203	
Ndrg1	2.0998	1.29449	
Gpnmb	2.09937	0.900917	
Trim28	2.09224	2.51622	Transcription intermediator factor
Gm26530	2.08727	0.879248	

Sdc4	2.08722	0.669649	
Tapbp,Zbtb22	2.08637	0.658537	
Tnf	2.08291	0.795961	TNF-a
Gm12352	2.08238	0.917699	
Gm22553	2.07661	2.01571	
Tspo	2.07429	0.644657	
Txnrd1	2.07307	0.581774	
Gm5124	2.0726	0.94677	
Ass1	2.07066	0.983894	Argininosuccinate synthase
Basp1	2.06647	1.50293	
Sh3bgrl	2.06505	0.871536	
S100a11	2.06486	0.75245	
Spock3	2.06131	1.22908	
Ptma	2.06091	0.822367	
Ctsa	2.05782	0.751184	
Nfkbia	2.05658	0.600731	NFkB inhibitor alpha
Arg1	2.05531	0.587735	Arginase-1
Cacng4	2.05465	1.4067	
Cd68	2.05291	1.05178	Associated with monocyte activation
Gm5997	2.05268	1.60673	
Gm7935	2.04719	2.15618	
Rps10	2.04528	1.08729	
Rps12	2.02669	0.794079	
Rps15	2.02603	0.934912	
Mmp14	2.02271	0.708681	
Rps4x	2.02146	0.636679	
EU599041	2.01804	1.95393	
Gm10814	2.01788	2.16455	
Ctnnb1	2.01405	0.7303	
Lgals9	2.01332	0.686127	
Gm12060	2.00628	2.6311	
Cdkn1a	2.00477	0.620973	
Gm12017	2.00158[4]	1.13323	

[1]The data was analysed on SIMCA. The value represents the difference between the distinct groups.

[2] The value highlights variety within each sample groups

[3] Transcripts that are immune related (blue), associated with metabolic pathways (green), regulatory/ signalling (orange)

[4] The VIP list was limited to a VIP score of ≥ 2.00

5.2.3. Using the cytokine profile of BMDCs stimulated with LPS or co-cultured with *L. mexicana* and *T. gondii* to further validate the reliability of the transcriptomic data.

Cytokine production by BMDCs stimulated with LPS or co-cultured with *L. mexicana* or *T. gondii* was measured in culture supernatants and compared with the transcriptomic data. Compared to naïve BMDCs, stimulation with LPS significantly increased the mRNA and protein levels of IL-1α (*Il1a)*, IL-1β (*Il1b)*, IL-12p70 (*Il12a, Il12b)*, TNF-α (*Tnfa)*, IL-6 (*Il6),* MCP-1(*ccl2)*, IL-10 (*Il10*), IFN-β (*Infb)* and IL-23 (*Il23)* ($p = <0.001$) (Figure 5.2).

L. mexicana infected BMDC cultures, significantly down-regulated IL-1β and up-regulated TNF-α protein levels in comparison to naïve cells. These changes were also observed in the transcriptomic analysis with significantly increased *Il1a, Il12b, Tnfa, Il6* and *Il10* mRNA transcripts and significantly decreased *Il1b* and *ccl2* mRNA levels ($p = 0.0005$) (Figure 6.1). In addition, the protein level of IL-1α, IL-12p70, IL-6 and IL-10 was significantly increased in *T. gondii* co-cultured BMDCs. This was concurrent to the findings observed in the transcriptomics with significant up-regulated Il1a, Il12a and Il6 ($p = 0.0013$) transcripts. This validates the reliability and robustness of this data.

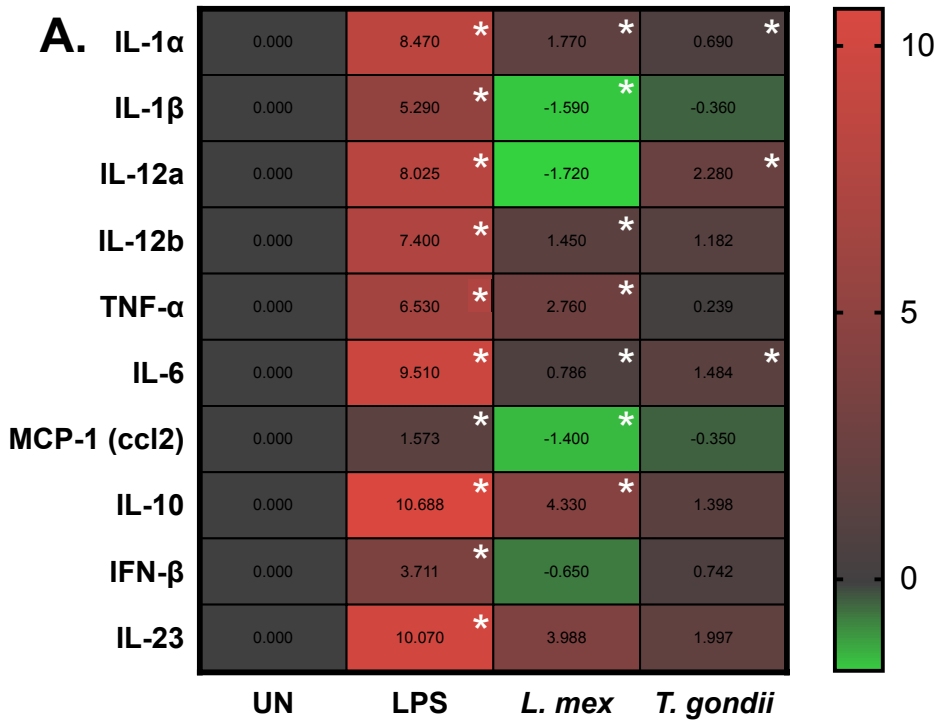
A.
IL-1α
IL-1β
IL-12a
IL-12b
TNF-α
IL-6
MCP-1 (ccl2)
IL-10
IFN-β
IL-23
0.000 8.470 * 1.770 * 0.690 *
0.000 5.290 * -1.590 * -0.360
0.000 8.025 * -1.720 2.280 *
0.000 7.400 * 1.450 * 1.182
0.000 6.530 * 2.760 * 0.239
0.000 9.510 * 0.786 * 1.484 *
0.000 1.573 * -1.400 * -0.350
0.000 10.688 * 4.330 * 1.398
0.000 3.711 * -0.650 0.742
0.000 10.070 * 3.988 1.997
UN
LPS
L. mex
T. gondii
10
5
0

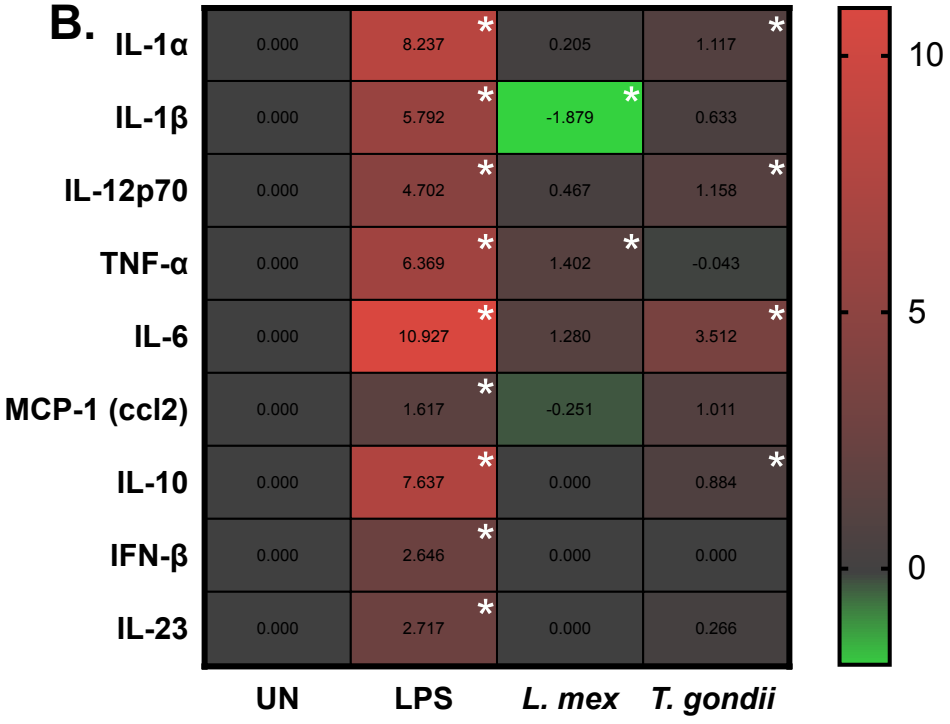
B.
IL-1α
IL-1β
IL-12p70
TNF-α
IL-6
MCP-1 (ccl2)
IL-10
IFN-β
IL-23
0.000 8.237 * 0.205 1.117 *
0.000 5.792 * -1.879 * 0.633
0.000 4.702 * 0.467 1.158 *
0.000 6.369 * 1.402 * -0.043
0.000 10.927 * 1.280 3.512 *
0.000 1.617 * -0.251 1.011
0.000 7.637 * 0.000 0.884 *
0.000 2.646 * 0.000 0.000
0.000 2.717 * 0.000 0.266
UN
LPS
L. mex
T. gondii
10
5
0

Figure 5.2. mRNA and protein levels of cytokines expressed by BMDCs when stimulated with LPS or co-cultured with *L. mexicana* or *T. gondii*. Bone marrow derived DCs were either stimulated with LPS or co-cultured with *L. mexicana* or *T. gondii* as indicated for 6 hours or 24 hours. After this time, (A) mRNA was subsequently extracted and then quantified using RNA-seq. Data shows the log2(fold change) as normalised to unstimulated controls. Red indicates an increase in mRNA expression, green indicates a decrease in transcript expression and grey shows no changes from the control cells. (B) a cytokine bead array was performed on the supernatant to obtain cytokine protein levels. Statistical analysis was performed (A) using Cuffdiff (Eurofin) to determine the differential expression levels at the transcript level including a measure of significance between samples. (B) One-way ANOVA with Dunnett post-test. Significant differences are $p < 0.05$ where * is compared to unstimulated. N = 1.

5.2.4. The activation profile of LPS activated BMDCs is different to that of *L. mexicana* or *T. gondii* infected BMDC cultures.

LPS stimulated DCs had significantly increased mRNA levels of *cd40, cd80, cd86* and the majority of subunits associated with the MHC class I and II complexes (*H2-D1, Q1, Q2, Q3, Q4, Q5, Q5, Q6, Q7, Q10, M3, K2, K2, K1, T24, T23, T22, M2*) ($p = 0.00015$). Notably, one subunit associated with the MHC Class II complex (*H2-DMa*) was significantly down-regulated ($p = 0.00015$) in LPS-stimulated cells.

Compared to naïve BMDCs, *L. mexicana* infected BMDC cultures had significantly increased levels of *cd40* and MHC Class I and II associated molecules *H2-Q5* ($p = 0.00015$), *Q5* ($p = 0.014$), *Q7* ($p = 0.00053$) and *K2* (0.009). Similar to LPS activation, *L. mexicana* infected BMDC cultures had significant down-regulation of *H2-DMa* (0.00053) and *H2-DMb2* ($p = 0.006$).

In comparison, BMDC co-cultured with *T. gondii* had numerous significantly reduced MHC class I and II molecules (*H2-Oa* ($p = 0.01$), *DMa* ($p = 0.0013$), *DMb2* ($p = 0.0013$), *Ab1* ($p = 0.01$), *Eb1* (0.006), *Aa* ($p = 0.002$) and *M2* ($p = 0.0013$)). However, mRNA levels of *cd80* ($p = 0.0013$) and *cd86* ($p = 0.02$) were up-regulated in these *Toxoplasma* infected BMDC cultures when compared to control cells.

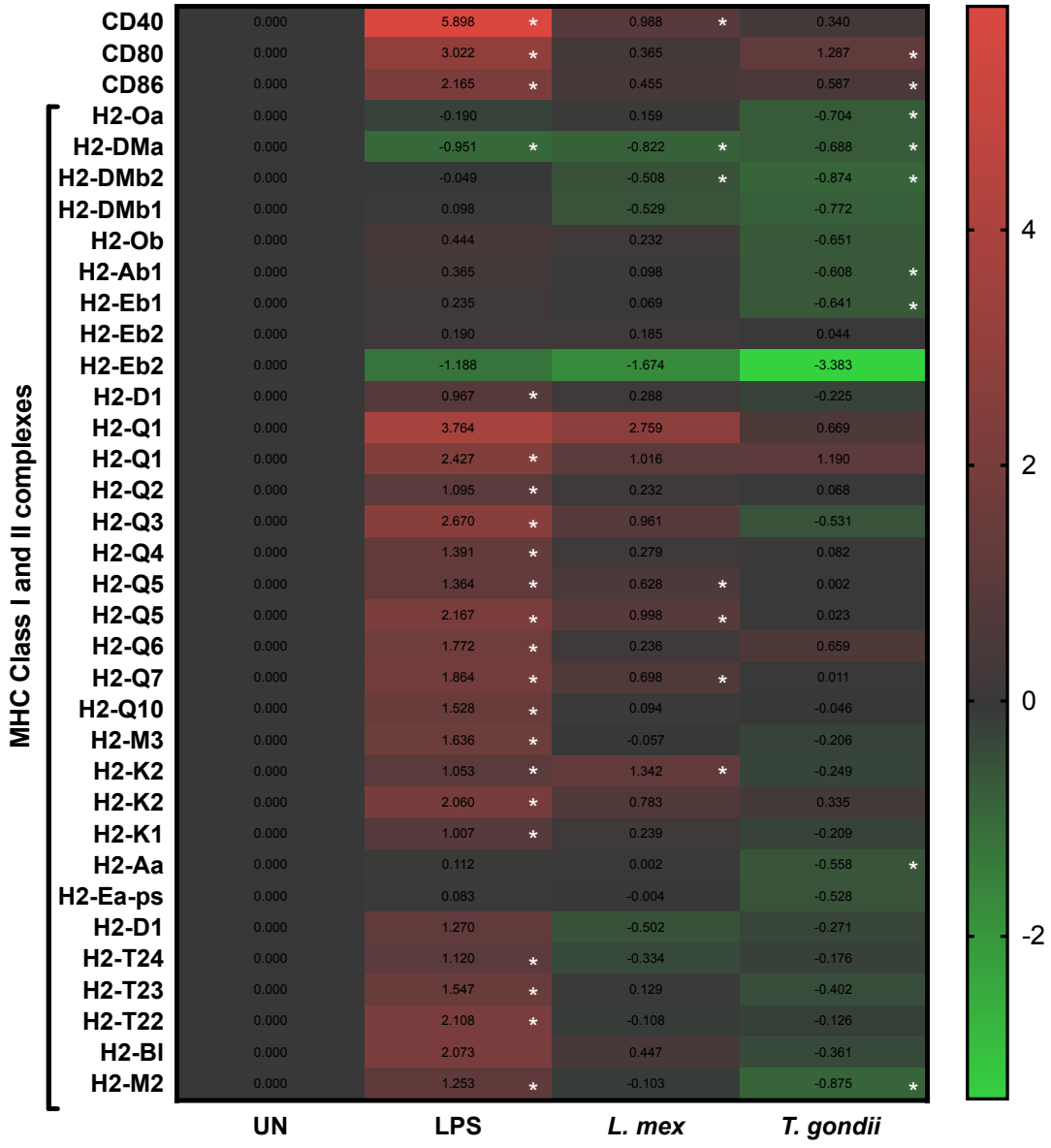
MHC Class I and II complexes
CD40 0.000 5.898 * 0.988 * 0.340
CD80 0.000 3.022 * 0.365 1.287 *
CD86 0.000 2.165 * 0.455 0.587 *
H2-Oa 0.000 -0.190 0.159 -0.704 *
H2-DMa 0.000 -0.951 * -0.822 * -0.688 *
H2-DMb2 0.000 -0.049 -0.508 * -0.874 *
H2-DMb1 0.000 0.098 -0.529 -0.772
H2-Ob 0.000 0.444 0.232 -0.651
H2-Ab1 0.000 0.365 0.098 -0.608 *
H2-Eb1 0.000 0.235 0.069 -0.641 *
H2-Eb2 0.000 0.190 0.185 0.044
H2-Eb2 0.000 -1.188 -1.674 -3.383
H2-D1 0.000 0.967 * 0.288 -0.225
H2-Q1 0.000 3.764 2.759 0.669
H2-Q1 0.000 2.427 * 1.016 1.190
H2-Q2 0.000 1.095 * 0.232 0.068
H2-Q3 0.000 2.670 * 0.961 -0.531
H2-Q4 0.000 1.391 * 0.279 0.082
H2-Q5 0.000 1.364 * 0.628 * 0.002
H2-Q5 0.000 2.167 * 0.998 * 0.023
H2-Q6 0.000 1.772 * 0.236 0.659
H2-Q7 0.000 1.864 * 0.698 * 0.011
H2-Q10 0.000 1.528 * 0.094 -0.046
H2-M3 0.000 1.636 * -0.057 -0.206
H2-K2 0.000 1.053 * 1.342 * -0.249
H2-K2 0.000 2.060 * 0.783 0.335
H2-K1 0.000 1.007 * 0.239 -0.209
H2-Aa 0.000 0.112 0.002 -0.558 *
H2-Ea-ps 0.000 0.083 -0.004 -0.528
H2-D1 0.000 1.270 -0.502 -0.271
H2-T24 0.000 1.120 * -0.334 -0.176
H2-T23 0.000 1.547 * 0.129 -0.402
H2-T22 0.000 2.108 * -0.108 -0.126
H2-Bl 0.000 2.073 0.447 -0.361
H2-M2 0.000 1.253 * -0.103 -0.875 *
UN
LPS
L. mex
T. gondii
4
2
0
-2

Figure 5.3. Changes in expression in the mRNA levels of co-stimulatory molecules when stimulated with LPS or co-cultured with *L. mexicana* or *T. gondii.* Bone marrow derived DCs were either stimulated with LPS or co-cultured with *L. mexicana* or *T. gondii* as indicated for 6 hours. After this time, mRNA was subsequently extracted and then quantified using RNA-seq. Data shows the log2(fold change) as normalised to unstimulated controls. Red indicates an increase in mRNA expression, green indicates a decrease in transcript expression and grey shows no changes from the control cells. For clarity, relevant gene abbreviates are shown in the diagram where *Cd40, Cd80* and *Cd86* are co-stimulatory molecules and *H2-oa* to *H2-m2* are associated with the major histocompatibility complex I and II (MHC Class I and II) Statistical analysis was performed using Cuffdiff (Eurofin) to determine the differential expression levels at the transcript level including a measure of significance between samples. Significant differences are $p < 0.05$ where * is compared to unstimulated. N = 1.

5.2.5. Metabolic pathways of interest

5.2.5.1 Glycolysis

Glut, Hk, gck, gpi, pfkfb, pfkl, pfkm, pfkp, aldo, gadph, pgk, pgam, eno, pkm, pklr and *ldh* are all mRNA transcripts that encode enzymes or transporters of the glycolysis pathway (Figure 5.4). Distinct differences in transcript levels were observed in BMDCs following LPS stimulation or infection with *L. mexicana* or *T. gondii*. In comparison to naïve BMDCs, those stimulated with LPS had significantly increased levels of *glut1* ($p = 0.00029$), *hk1*, *hk2* ($p = 0.00015$), *hk3* ($p = 0.003$), *pfkfb3* ($p = 0.007$), *ldha* and significantly decreased levels of *gpi* ($p = 0.00015$), *pfkm* ($p = 0.00015$), *eno3 aldoc* ($p = 0.01$) *pgam2* ($p = 0.016$) and *ldhb*. Significantly increased levels of *glut1* ($p = 0.00053$), *hk1* ($p = 0.0005$), *hk2* ($p = 0.006$), *gpi* (0.0002), *pgk1*, *pfkl* ($p = 0.0018$), *pgam*, *tpi1* ($p = 0.00053$), *gapdh* ($p = 0.00015$), *eno1, 2, 3* ($p = 0.00053$) and *ldha* ($p = 0.00053$) were observed in BMDCs co-cultured with *L. mexicana* when compared to unstimulated BMDCs. A significant decrease in *pfkm* ($p = 0.015$) and *pgam2* ($p = 0.063$) was also observed in *L. mexicana*-infected BMDCs. *T. gondii*-infected BMDC cultures had significantly decreased levels of *glut1* ($p = 0.028$), *pgam2* ($p = 0.024$) and *eno3* ($p = 0.0013$).

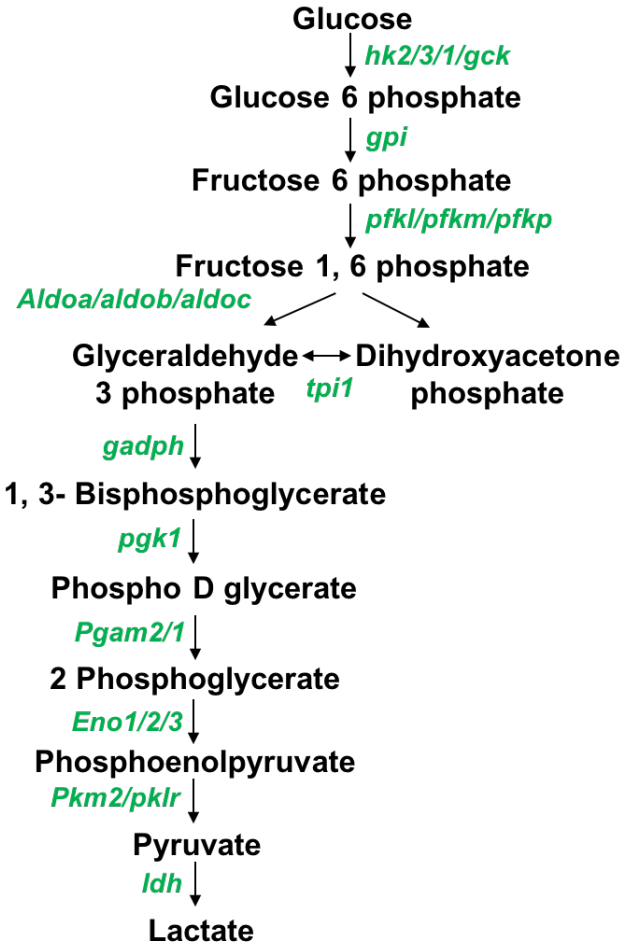
Glucose
hk2/3/1/gck
Glucose 6 phosphate
gpi
Fructose 6 phosphate
pfkl/pfkm/pfkp
Fructose 1, 6 phosphate
Aldoa/aldob/aldoc
Glyceraldehyde 3 phosphate
tpi1
Dihydroxyacetone phosphate
gadph
1, 3- Bisphosphoglycerate
pgk1
Phospho D glycerate
Pgam2/1
2 Phosphoglycerate
Eno1/2/3
Phosphoenolpyruvate
Pkm2/pklr
Pyruvate
ldh
Lactate

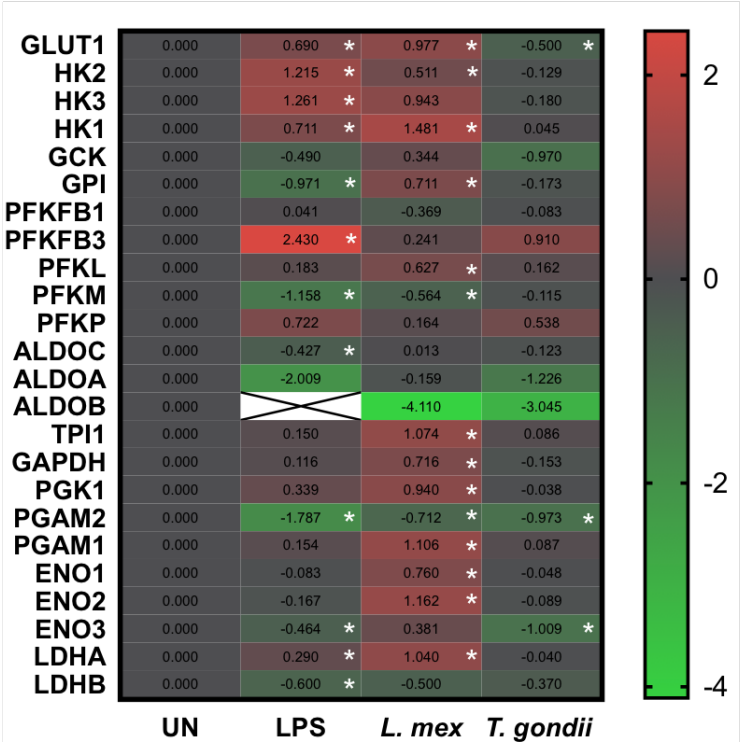
GLUT1 0.000 0.690 * 0.977 * -0.500 *
HK2 0.000 1.215 * 0.511 * -0.129
HK3 0.000 1.261 * 0.943 -0.180
HK1 0.000 0.711 * 1.481 * 0.045
GCK 0.000 -0.490 0.344 -0.970
GPI 0.000 -0.971 * 0.711 * -0.173
PFKFB1 0.000 0.041 -0.369 -0.083
PFKFB3 0.000 2.430 * 0.241 0.910
PFKL 0.000 0.183 0.627 * 0.162
PFKM 0.000 -1.158 * -0.564 * -0.115
PFKP 0.000 0.722 0.164 0.538
ALDOC 0.000 -0.427 * 0.013 -0.123
ALDOA 0.000 -2.009 -0.159 -1.226
ALDOB 0.000 -4.110 -3.045
TPI1 0.000 0.150 1.074 * 0.086
GAPDH 0.000 0.116 0.716 * -0.153
PGK1 0.000 0.339 0.940 * -0.038
PGAM2 0.000 -1.787 * -0.712 * -0.973 *
PGAM1 0.000 0.154 1.106 * 0.087
ENO1 0.000 -0.083 0.760 * -0.048
ENO2 0.000 -0.167 1.162 * -0.089
ENO3 0.000 -0.464 * 0.381 -1.009 *
LDHA 0.000 0.290 * 1.040 * -0.040
LDHB 0.000 -0.600 * -0.500 -0.370
UN
LPS
L. mex
T. gondii
2
0
-2
-4

Figure 5.4. LPS activation or infection with *L. mexicana* or *T. gondii* changes the expression of genes encoding enzymes of the glycolysis pathway. Bone marrow derived DCs were either stimulated with LPS or co-cultured with *L. mexicana* or *T. gondii* as indicated for 6 hours. After this time, mRNA was subsequently extracted and then quantified using RNA-seq. Data shows the log2(fold change) as normalised to unstimulated controls. Red indicates an increase in transcript expression, green indicates a decrease in transcript expression and grey shows no changes from the control cells. For clarity, the diagram focuses on gene abbreviations encoding the enzymes, *hk1,2,3* (hexokinases); *gpi* (phosphoglucose isomerase); *pfkl, pfkm, pfkp* (phosphofructokinases); *aldoa, aldob, aldoc* (fructose bisphosphate aldoses); *tpi* (triose phosphate isomerase); *gapdh* (glyceraldehyde 3-phosphate dehydrogenase); *pgk1* (phosphoglycerate kinase); *pgam1,2* (phosphoglycerate mutase) *eno1,2,3* (enolase) and *ldha/b* (lactate dehydrogenase). Statistical analysis was performed using Cuffdiff (Eurofin) to determine the differential expression levels at the transcript level including a measure of significance between samples. Significant differences are $p < 0.05$ where * is compared to unstimulated. N = 1.

5.2.5.2 TCA cycle

From the transcriptomic data, it is possible to identify 18 mRNA transcripts associated with enzymes or transporters linked with the TCA cycle including *Acc, aco2, acly idh3g, b, a, ogdh, dlst, sucla2/1, sdhb/a/c, fh, mdh1/2* and *acod1* (Figure 5.5). Transcript levels of at least one of more of these were affected in BMDCs whether they were LPS stimulated, *L. mexicana*-infected or *T. gondii*-infected. Significant down-regulation of *acc* ($p = 0.01$), *idh3g* ($p = 0.00015$), *idh3b* ($p = 0.00043$), *idha* ($p = 0.00015$), *ogdh* ($p = 0.012$), *suclg1* ($p = 0.0029$) and *fh* ($p = 0.00015$) levels were evident in LPS activated BMDCs in comparison to unstimulated BMDCs. Significant upregulation of *acly* ($p = 0.022$), *dlst* ($p = 0.039$) and *acod1* ($p = 0.00015$) transcripts were observed in LPS-stimulated BMDCs. In comparison to naïve DCs, those co-cultured with *L. mexicana* demonstrated increased *ogdh* ($p = 0.001$) and *acod1* ($p = 0.00053$) and decreased *acc* ($p = 0.01$), *acly* ($p = 0.013$), *idh3g* ($p = 0.00053$) and *fh* ($p = 0.00053$) transcripts. Significant down-regulation of *sdhb* ($p = 0.004$) could also be observed in *T. gondii* exposed BMDCs compared to control cells.

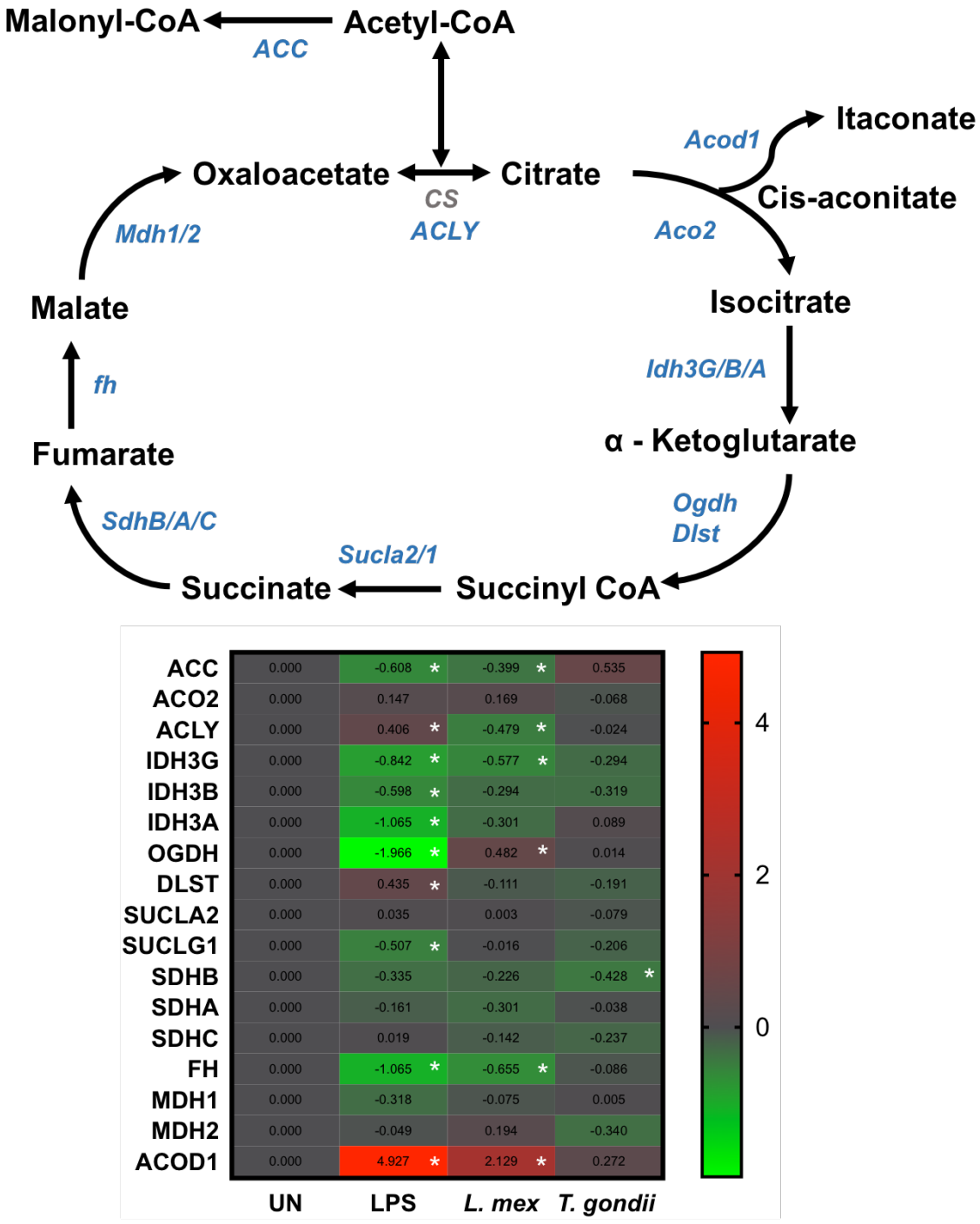
Malonyl-CoA
Acetyl-CoA
ACC
Oxaloacetate
Citrate
CS
ACLY
Acod1
Itaconate
Cis-aconitate
Aco2
Isocitrate
Idh3G/B/A
α - Ketoglutarate
Ogdh
Dlst
Succinyl CoA
Sucla2/1
Succinate
SdhB/A/C
Fumarate
fh
Malate
Mdh1/2
ACC 0.000 -0.608 * -0.399 * 0.535
ACO2 0.000 0.147 0.169 -0.068
ACLY 0.000 0.406 * -0.479 * -0.024
IDH3G 0.000 -0.842 * -0.577 * -0.294
IDH3B 0.000 -0.598 * -0.294 -0.319
IDH3A 0.000 -1.065 * -0.301 0.089
OGDH 0.000 -1.966 * 0.482 * 0.014
DLST 0.000 0.435 * -0.111 -0.191
SUCLA2 0.000 0.035 0.003 -0.079
SUCLG1 0.000 -0.507 * -0.016 -0.206
SDHB 0.000 -0.335 -0.226 -0.428 *
SDHA 0.000 -0.161 -0.301 -0.038
SDHC 0.000 0.019 -0.142 -0.237
FH 0.000 -1.065 * -0.655 * -0.086
MDH1 0.000 -0.318 -0.075 0.005
MDH2 0.000 -0.049 0.194 -0.340
ACOD1 0.000 4.927 * 2.129 * 0.272
UN
LPS
L. mex
T. gondii
4
2
0

Figure 5.5. mRNA changes to enzymes regulating TCA cycle in LPS activated and parasite co-cultured BMDCs. Bone marrow derived DCs were either stimulated with LPS or co-cultured with *L. mexicana* or *T. gondii* as indicated for 6 hours. After this time, mRNA was subsequently extracted and then quantified using RNA-seq. Data shows the log2(fold change) as normalised to unstimulated controls. Red indicates an increase in transcript expression, green indicates a decrease in transcript expression and grey shows no changes from the control cells. For clarity, relevant gene abbreviates are shown in the diagram where *cs* (citrate synthase); *aco2* (aconitase); *Idh3a/b/g* (isocitrate dehydrogenases); *ogdh/ dlst* (α-ketoglutarate dehydrogenases); *sucla2/g1* (succinyl-CoA synthetases); *sdha/b/c* (succinate dehydrogenase); *fh* (fumarase); *mdh1/2* (malate dehydrogenase). Statistical analysis was performed using Cuffdiff (Eurofin) to determine the differential expression levels at the transcript level including a measure of significance between samples. Significant differences are $p < 0.05$ where * is compared to unstimulated. n = 1.

5.2.5.3 Oxidative phosphorylation

Transcripts encoding components of the electron transport chain (ETC) include NADH dehydrogenase, succinate dehydrogenase and cytochrome c oxidase. Evidence of down regulation of components of the ETC was observed in BMDCs stimulated with LPS, infected with *L. mexicana* or *T. gondii* (Figure 5.6). In comparison to naïve BMDCs, LPS activated BMDCs had significant down-regulation of the majority of subunits associated with NADH dehydrogenase (*ndufs1* ($p = 0.014$), *ndufs7* ($p = 0.00015$), *ndufs8* (0.0009), *ndufa6* ($p = 0.00025$), *ndufa8* ($p = 0.00015$), *ndufb11* ($p = 0.0019$), *ndufb10* ($p = 0.0014$), *ndufb5* ($p = 0.021$)) and *cox10* (0.0057). Other mRNA transcripts were significantly up-regulated in LPS-stimulated BMDCs including *ndufs4* ($p = 0.00015$), *cox11* ($p = 0.003$) and *cox15* ($p = 0.00015$). BMDC cultures infected with *L. mexicana* had significantly decreased levels of *ndufs7* ($p = 0.041$) and *ndufa6* ($p = 0.028$) compared to naïve BMDCs. BMDCs co-cultured with *T. gondii* had significantly down-regulated expression of *ndufa6* ($p = 0.045$) and *sdhb* ($p = 0.046$) compared to control cells.

Transcripts encoding subunits of complex V (ATP synthase) were generally found to downregulated in BMDCs following LPS stimulation, but increased following exposure to *T. gondii* or *L. mexicana* (Figure 5.7). In comparison to naïve BMDCs, LPS activated BMDCs has significant down-regulation of *atp2b1, atp6v0a1, atp13a3, atp6v0c, atp8b4, atp9a, atpaf1, atp13a2* and *atp6v0b* ($p \leq 0.001$). mRNA transcripts significantly up-regulated in this phenotype include *atp6v1h, atp6v1d, atp9b, atp11b, atp8b2, atp2b4, atp5b, atp6vlg1* and *atp6v0b* ($p \leq 0.001$). BMDC cultures infected

with *L. mexicana* has significantly increased levels of *atp6ap2, atp2b4, atp2b1, atp6v1d, atp6v1c1, atp13a3, atp6v1a, atp6v0e, atp6v0c, atp9a, atp1a1, atp6v0d2, atp6v0b* ($p \leq 0.0015$) compared to control cells. These parasite infected BMDCs also had significantly decreased mRNA levels of *atp11c, atp2a3, atp8b4* and *atp10d* ($p = 0.0015$). *T. gondii* infected BMDC cultures had significantly upregulated *atp2b4* and significantly down-regulated *atp6v0a1*and *atp6v0d* ($p = 0.01$).

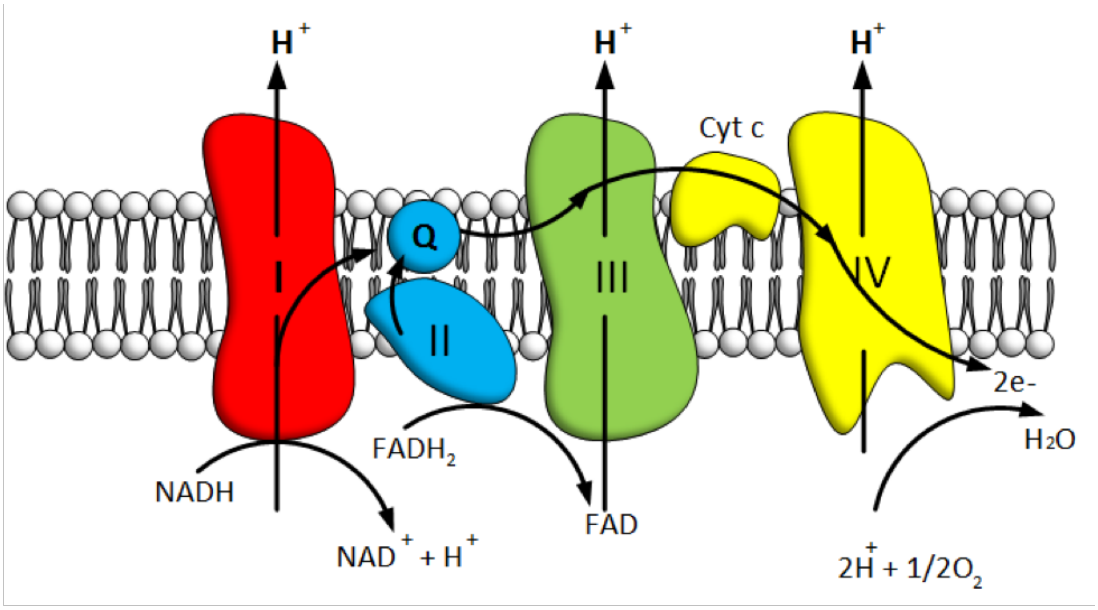
H+
H+
H+
Cyt c
Q
I
II
III
IV
2e-
H2O
FADH2
NADH
FAD
NAD+ + H+
2H+ + 1/2O2

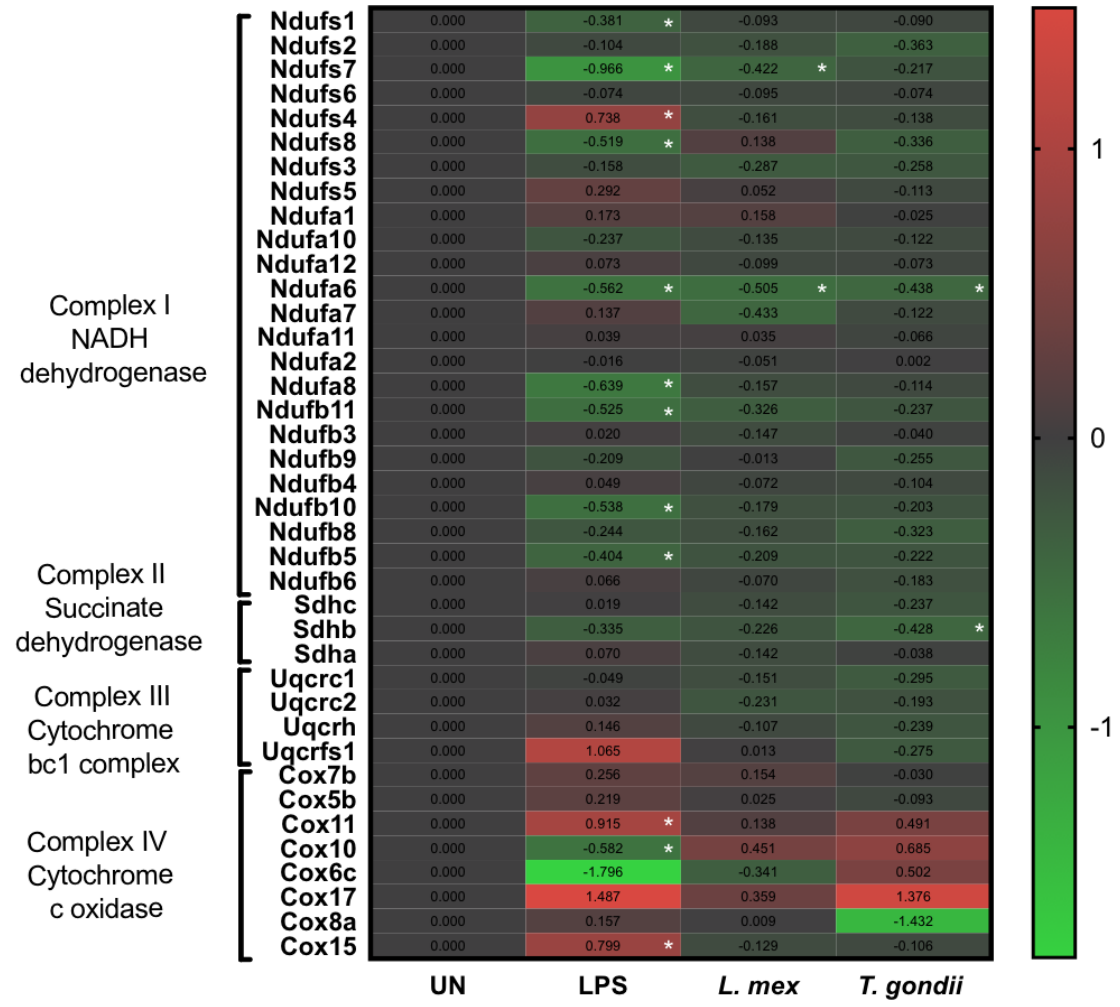
Complex I NADH dehydrogenase
Complex II Succinate dehydrogenase
Complex III Cytochrome bc1 complex
Complex IV Cytochrome c oxidase
Ndufs1 0.000 -0.381 * -0.093 -0.090
Ndufs2 0.000 -0.104 -0.188 -0.363
Ndufs7 0.000 -0.966 * -0.422 * -0.217
Ndufs6 0.000 -0.074 -0.095 -0.074
Ndufs4 0.000 0.738 * -0.161 -0.138
Ndufs8 0.000 -0.519 * 0.138 -0.336
Ndufs3 0.000 -0.158 -0.287 -0.258
Ndufs5 0.000 0.292 0.052 -0.113
Ndufa1 0.000 0.173 0.158 -0.025
Ndufa10 0.000 -0.237 -0.135 -0.122
Ndufa12 0.000 0.073 -0.099 -0.073
Ndufa6 0.000 -0.562 * -0.505 * -0.438 *
Ndufa7 0.000 0.137 -0.433 -0.122
Ndufa11 0.000 0.039 0.035 -0.066
Ndufa2 0.000 -0.016 -0.051 0.002
Ndufa8 0.000 -0.639 * -0.157 -0.114
Ndufb11 0.000 -0.525 * -0.326 -0.237
Ndufb3 0.000 0.020 -0.147 -0.040
Ndufb9 0.000 -0.209 -0.013 -0.255
Ndufb4 0.000 0.049 -0.072 -0.104
Ndufb10 0.000 -0.538 * -0.179 -0.203
Ndufb8 0.000 -0.244 -0.162 -0.323
Ndufb5 0.000 -0.404 * -0.209 -0.222
Ndufb6 0.000 0.066 -0.070 -0.183
Sdhc 0.000 0.019 -0.142 -0.237
Sdhb 0.000 -0.335 -0.226 -0.428 *
Sdha 0.000 0.070 -0.142 -0.038
Uqcrc1 0.000 -0.049 -0.151 -0.295
Uqcrc2 0.000 0.032 -0.231 -0.193
Uqcrh 0.000 0.146 -0.107 -0.239
Uqcrfs1 0.000 1.065 0.013 -0.275
Cox7b 0.000 0.256 0.154 -0.030
Cox5b 0.000 0.219 0.025 -0.093
Cox11 0.000 0.915 * 0.138 0.491
Cox10 0.000 -0.582 * 0.451 0.685
Cox6c 0.000 -1.796 -0.341 0.502
Cox17 0.000 1.487 0.359 1.376
Cox8a 0.000 0.157 0.009 -1.432
Cox15 0.000 0.799 * -0.129 -0.106
UN
LPS
L. mex
T. gondii
1
0
-1

Figure 5.6. mRNA changes to enzymes regulating ETC in LPS activated and parasite co-cultured BMDCs. Bone marrow derived DCs were either stimulated with LPS or co-cultured with *L. mexicana* or *T. gondii* as indicated for 6 hours. After this time, mRNA was subsequently extracted and then quantified using RNA-seq. Data shows the log2(fold change) as normalised to unstimulated controls. Red indicates an increase in transcript expression, green indicates a decrease in transcript expression and grey shows no changes from the control cells. For clarity, relevant gene abbreviates are shown in the diagram where Complex I is NADH dehydrogenase (*ndufs1* – *bdufb6*), Complex II is Succinate dehydrogenase (*sdhc* – *sdha*), Complex III is Cytochrome bc1 complex (*uqcrc1* – *uqcrfs1*) and Complex IV is Cytochrome C oxidase (*cox7b* – *cox15*). Statistical analysis was performed using Cuffdiff (Eurofin) to determine the differential expression levels at the transcript level including a measure of significance between samples. Significant differences are $p < 0.05$ where * is compared to unstimulated. n = 1.

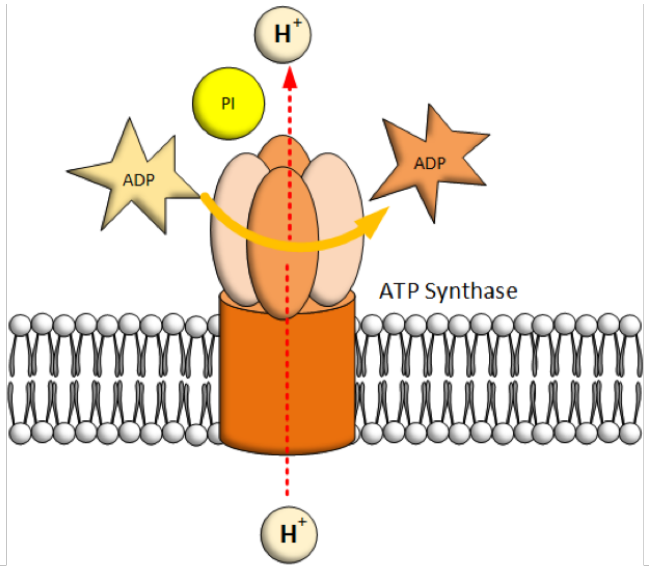
H+
PI
ADP
ADP
ATP Synthase
H+

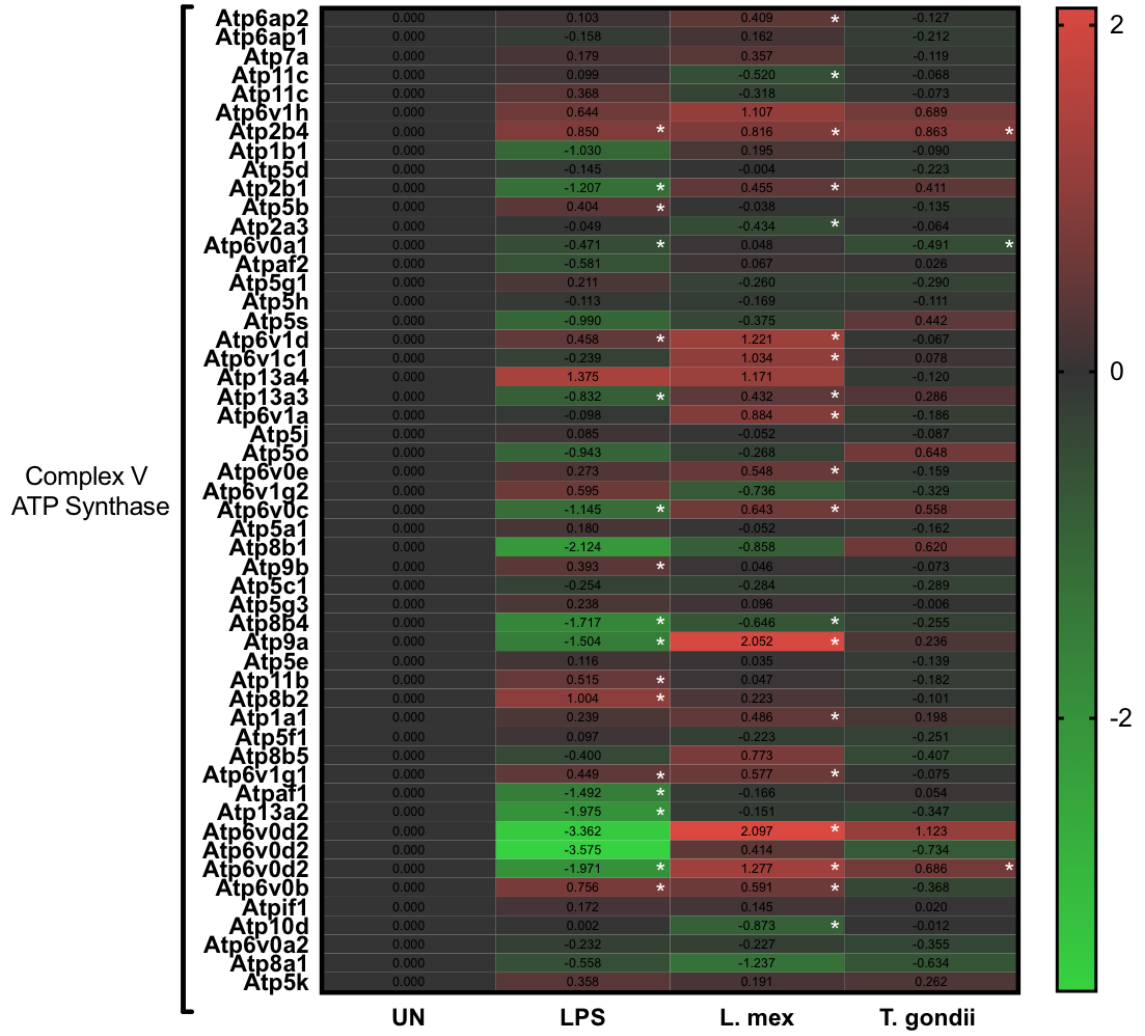
Complex V
ATP Synthase
Atp6ap2 0.000 0.103 0.409 * -0.127
Atp6ap1 0.000 -0.158 0.162 -0.212
Atp7a 0.000 0.179 0.357 -0.119
Atp11c 0.000 0.099 -0.520 * -0.068
Atp11c 0.000 0.368 -0.318 -0.073
Atp6v1h 0.000 0.644 1.107 0.689
Atp2b4 0.000 0.850 * 0.816 * 0.863 *
Atp1b1 0.000 -1.030 0.195 -0.090
Atp5d 0.000 -0.145 -0.004 -0.223
Atp2b1 0.000 -1.207 * 0.455 * 0.411
Atp5b 0.000 0.404 * -0.038 -0.135
Atp2a3 0.000 -0.049 -0.434 * -0.064
Atp6v0a1 0.000 -0.471 * 0.048 -0.491 *
Atpaf2 0.000 -0.581 0.067 0.026
Atp5g1 0.000 0.211 -0.260 -0.290
Atp5h 0.000 -0.113 -0.169 -0.111
Atp5s 0.000 -0.990 -0.375 0.442
Atp6v1d 0.000 0.458 * 1.221 * -0.067
Atp6v1c1 0.000 -0.239 1.034 * 0.078
Atp13a4 0.000 1.375 1.171 -0.120
Atp13a3 0.000 -0.832 * 0.432 * 0.286
Atp6v1a 0.000 -0.098 0.884 * -0.186
Atp5j 0.000 0.085 -0.052 -0.087
Atp5o 0.000 -0.943 -0.268 0.648
Atp6v0e 0.000 0.273 0.548 * -0.159
Atp6v1g2 0.000 0.595 -0.736 -0.329
Atp6v0c 0.000 -1.145 * 0.643 * 0.558
Atp5a1 0.000 0.180 -0.052 -0.162
Atp8b1 0.000 -2.124 -0.858 0.620
Atp9b 0.000 0.393 * 0.046 -0.073
Atp5c1 0.000 -0.254 -0.284 -0.289
Atp5g3 0.000 0.238 0.096 -0.006
Atp8b4 0.000 -1.717 * -0.646 * -0.255
Atp9a 0.000 -1.504 * 2.052 * 0.236
Atp5e 0.000 0.116 0.035 -0.139
Atp11b 0.000 0.515 * 0.047 -0.182
Atp8b2 0.000 1.004 * 0.223 -0.101
Atp1a1 0.000 0.239 0.486 * 0.198
Atp5f1 0.000 0.097 -0.223 -0.251
Atp8b5 0.000 -0.400 0.773 -0.407
Atp6v1g1 0.000 0.449 * 0.577 * -0.075
Atpaf1 0.000 -1.492 * -0.166 0.054
Atp13a2 0.000 -1.975 * -0.151 -0.347
Atp6v0d2 0.000 -3.362 2.097 * 1.123
Atp6v0d2 0.000 -3.575 0.414 -0.734
Atp6v0d2 0.000 -1.971 * 1.277 * 0.686 *
Atp6v0b 0.000 0.756 * 0.591 * -0.368
Atpif1 0.000 0.172 0.145 0.020
Atp10d 0.000 0.002 -0.873 * -0.012
Atp6v0a2 0.000 -0.232 -0.227 -0.355
Atp8a1 0.000 -0.558 -1.237 -0.634
Atp5k 0.000 0.358 0.191 0.262
UN
LPS
L. mex
T. gondii
2
0
-2

Figure 5.7. mRNA levels of the subunits of the ATP synthase complex in LPS activated and parasite co-cultured BMDCs. Bone marrow derived DCs were either stimulated with LPS or co-cultured with *L. mexicana* or *T. gondii* as indicated for 6 hours. After this time, mRNA was subsequently extracted and then quantified using RNA-seq. Data shows the log2(fold change) as normalised to unstimulated controls. Red indicates an increase in transcript expression, green indicates a decrease in transcript expression and grey shows no changes from the control cells. For clarity, relevant gene abbreviates are shown in the diagram where Complex V is ATP synthase (*atp6ap2* – *atp5k*). Statistical analysis was performed using Cuffdiff (Eurofin) to determine the differential expression levels at the transcript including a measure of significance between samples. Significant differences are $p < 0.05$ where * is compared to unstimulated. n = 1.

5.2.5.4 Pentose phosphate pathway

mRNA transcripts encoding enzymes and transporters of the PPP detected by RNA-seq include *g6pd2, pgls, pgd, rpia, rpe, tkt, taldo*1 and *carkl* (Figure 5.8). In general transcripts were down regulated at multiple points in BMDCs stimulated with LPS or infected with *L. mexicana* or *T. gondii* although not always significantly. In comparison to naïve BMDCs, LPS stimulated BMDCs had significant down-regulation of *pgd* ($p = 0.032$), *rpia* ($p = 0.00015$) and *carkl* ($p = 0.00015$), but significant up-regulation of *rpe* ($p = 0.00015$). BMDCs co-cultured with *L. mexicana* had significantly decreased levels of *rpia* ($p= 0.00053$), *rpe* ($p = 0.0072$) and *taldo1* ($p = 0.011$) gene transcripts compared to unstimulated cells. The mRNA expression of *pgd* ($p = 0.0047$) was significantly increased in *L. mexicana* infected BMDCs.

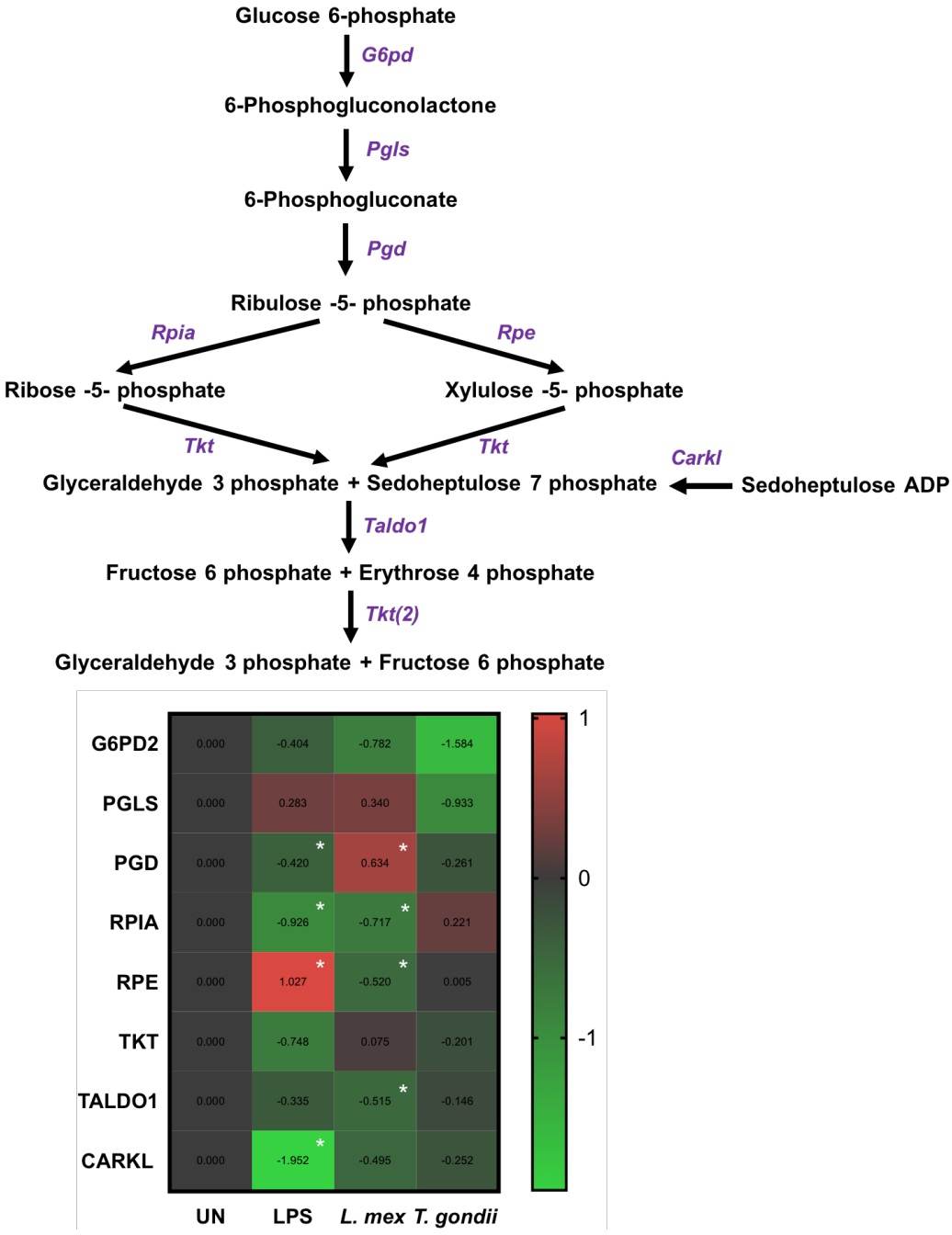
Glucose 6-phosphate
G6pd
6-Phosphogluconolactone
Pgls
6-Phosphogluconate
Pgd
Ribulose -5- phosphate
Rpia
Rpe
Ribose -5- phosphate
Xylulose -5- phosphate
Tkt
Tkt
Carkl
Glyceraldehyde 3 phosphate + Sedoheptulose 7 phosphate
Sedoheptulose ADP
Taldo1
Fructose 6 phosphate + Erythrose 4 phosphate
Tkt(2)
Glyceraldehyde 3 phosphate + Fructose 6 phosphate
G6PD2
PGLS
PGD
RPIA
RPE
TKT
TALDO1
CARKL
0.000 -0.404 -0.782 -1.584
0.000 0.283 0.340 -0.933
0.000 -0.420 * 0.634 * -0.261
0.000 -0.926 * -0.717 * 0.221
0.000 1.027 * -0.520 * 0.005
0.000 -0.748 0.075 -0.201
0.000 -0.335 -0.515 * -0.146
0.000 -1.952 * -0.495 -0.252
UN
LPS
L. mex
T. gondii
1
0
-1

Figure 5.8. LPS activation or infection with *L. mexicana* or *T. gondii* changes the expression of mRNA levels encoding enzymes of the PPP. Bone marrow derived DCs were either stimulated with LPS or co-cultured with *L. mexicana* or *T. gondii* as indicated for 6 hours. After this time, mRNA was subsequently extracted and then quantified using RNA-seq. Data shows the log2(fold change) as normalised to unstimulated controls. Red indicates an increase in transcript expression, green indicates a decrease in transcript expression and grey shows no changes from the control cells. For clarity, the diagram shows the gene abbreviations where *g6pd2* (Glucose 6 phosphate dehydrogenase); *pgls* (Gluconolactonase); *pgd* (6-phosphogluconate dehydrogenase); *rpia* (ribulose 5 phosphate isomerase); *rpe* (ribulose 5 phosphate 3 epimerase); *tkt* (transketolase); *taldo1* (transaldolase). Statistical analysis was performed using Cuffdiff (Eurofin) to determine the differential expression levels at the transcript level including a measure of significance between samples. Significant differences are $p < 0.05$ where * is compared to unstimulated. n = 1.

5.2.5.5. Arginine metabolism

The mRNA transcripts of enzymes associated with arginine metabolism detected by transcriptomics include *nos2, ass, asl, arg1/2, oat, odc, srm* and *sms* (Figure 5.9). In comparison to naïve cells, BMDCs activated with LPS significantly up-regulated the expression of *ass* ($p = 0.00015$), *arg2* ($p = 0.00015$), *odc* ($p = 0.0033$) and *sms* ($p = 0.0007$). Levels of *asl* ($p = 0.00057$), *arg1* ($p = 0.00015$) and *srm* ($p = 0.00015$) were significantly down-regulated in these cells. BMDCs cultures infected with *L. mexicana* significantly increased the mRNA expression of *nos2* ($p = 0.00053$) and *ass* ($p = 0.00053$), but decreased the mRNA levels of *srm* ($p = 0.00053$) when compared to control cells. *T. gondii* co-cultured BMDCs compared to unstimulated BMDCs, significantly up-regulated *nos2* ($p = 0.0013$) and *srm* ($p = 0.045$) mRNA expression.

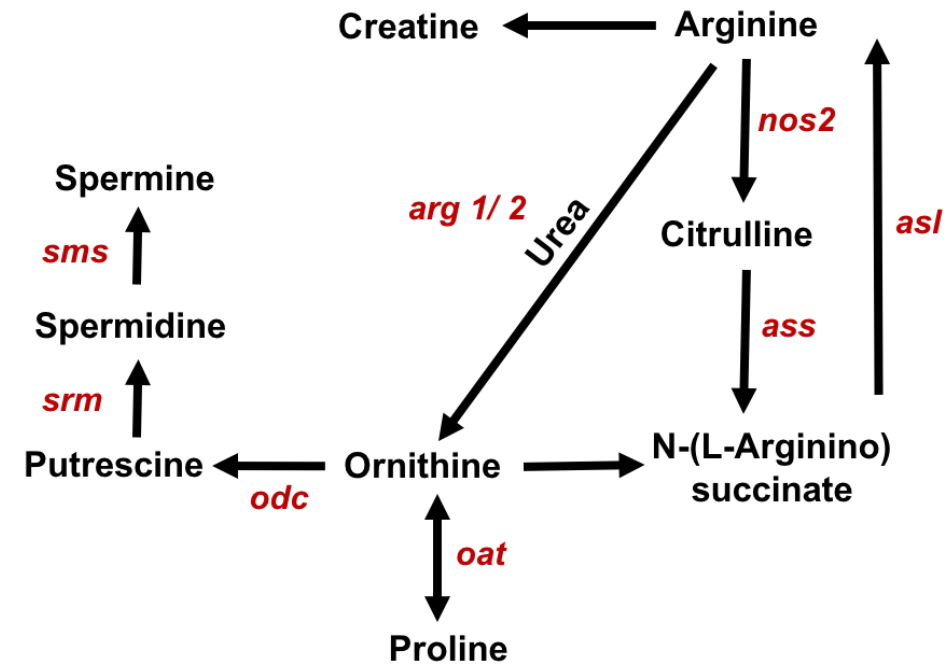
Creatine
Arginine
nos2
Spermine
arg 1/ 2
Urea
Citrulline
asl
sms
Spermidine
ass
srm
Putrescine
Ornithine
N-(L-Arginino)
succinate
odc
oat
Proline

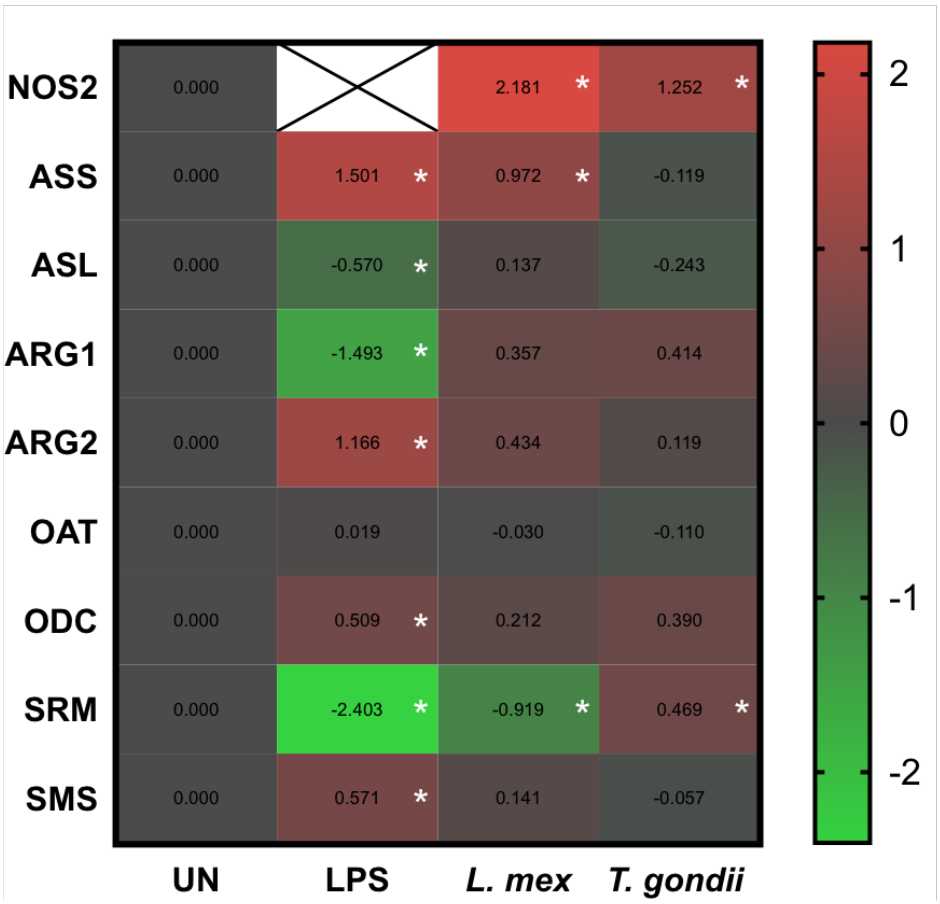
NOS2
ASS
ASL
ARG1
ARG2
OAT
ODC
SRM
SMS
0.000
2.181 *
1.252 *
0.000
1.501 *
0.972 *
-0.119
0.000
-0.570 *
0.137
-0.243
0.000
-1.493 *
0.357
0.414
0.000
1.166 *
0.434
0.119
0.000
0.019
-0.030
-0.110
0.000
0.509 *
0.212
0.390
0.000
-2.403 *
-0.919 *
0.469 *
0.000
0.571 *
0.141
-0.057
UN
LPS
L. mex
T. gondii
2
1
0
-1
-2

Figure 5.9. Changes in arginine metabolism mRNA transcripts in LPS activated or parasite treated BMDCs. Bone marrow derived DCs were either stimulated with LPS or co-cultured with *L. mexicana* or *T. gondii* as indicated for 6 hours. After this time, mRNA was subsequently extracted and then quantified using RNA-seq. Data shows the log2(fold change) as normalised to unstimulated controls. Red indicates an increase in transcript expression, green indicates a decrease in transcript expression and grey shows no changes from the control cells. For clarity, the diagram shows the gene abbreviations were *nos2* (nitric oxide synthase 2); *ass* (argininosuccinate synthase); *asl* (argininosuccinate lyase); *arg1/2* (arginase 1 or 2); *oat* (ornithine aminotransferase); *odc* (ornithine decarboxylase); *srm* (spermidine synthase) and *sms* spermine synthase. Statistical analysis was performed using Cuffdiff (Eurofin) to determine the differential expression levels at the transcript level including a measure of significance between samples. Significant differences are $p < 0.05$ where * is compared to unstimulated. n = 1.

5.2.6. Transcriptomic analysis of signalling pathways in LPS activated and parasite infected BMDC cultures.

5.2.6.1. PI3K-AKT-mTOR signalling pathway

RNA-seq results demonstrate significantly increased expression of PI3K complex subunits (*pik3r5* (p = 0.00015), *pik3r6* (p = 0.0029), *pik3r1* (p = 0.00015), *pik3ap1* (p = 0.00015), *pik3ca (*p = 0.0083)), *akt2* (p = 0.00015), *akt3* (p = 0.00015), *mTOR* (p=0.018), subunits of the S6K complex (*Rps6kc1*(p = 0.0015), *Rps6ka2 (*p = 0.00015), *Rps6kb2* (p = 0.041), *Rps6ka4* (p = 0.000154)) in LPS stimulated BMDCs compared to naïve BMDCs (Figure 5.10). A significant decrease in mRNA levels were observed in *pik3cg* (p = 0.00015), *prkag2* (p = 0.00015), *tsc1* (p = 0.02), *tsc2* (p = 0.00015) *rheb* (p = 0.048), *rps6ka1* (p = 0.00015) and *eif4ebp2* (p = 0.00015).

BMDC cultures infected with *L. mexicana* had significantly increased mRNA expression levels of *pik3r5 (p = 0.00018)* and *rps6ka2* (0.00053) compared to control cells. In addition, these cells had significant down-regulation of *pik3r6* (p= 0.021), *pik3cg* (p = 0.00053), *pik3cd* (p=0.00053), *rps6ka5* (p = 0.0050), *hif1a* and *eif4ebp2* (p = 0.033) when compared to naïve BMDCs.

BMDCs co-cultured with *T. gondii* had significantly up-regulated expression of *pik3r1* (p = 0.031) and *pik3r3* (p = 0.0077) and significantly down-regulated *pik3cd* (p = 0.024) mRNA levels when compared to unstimulated BMDC.

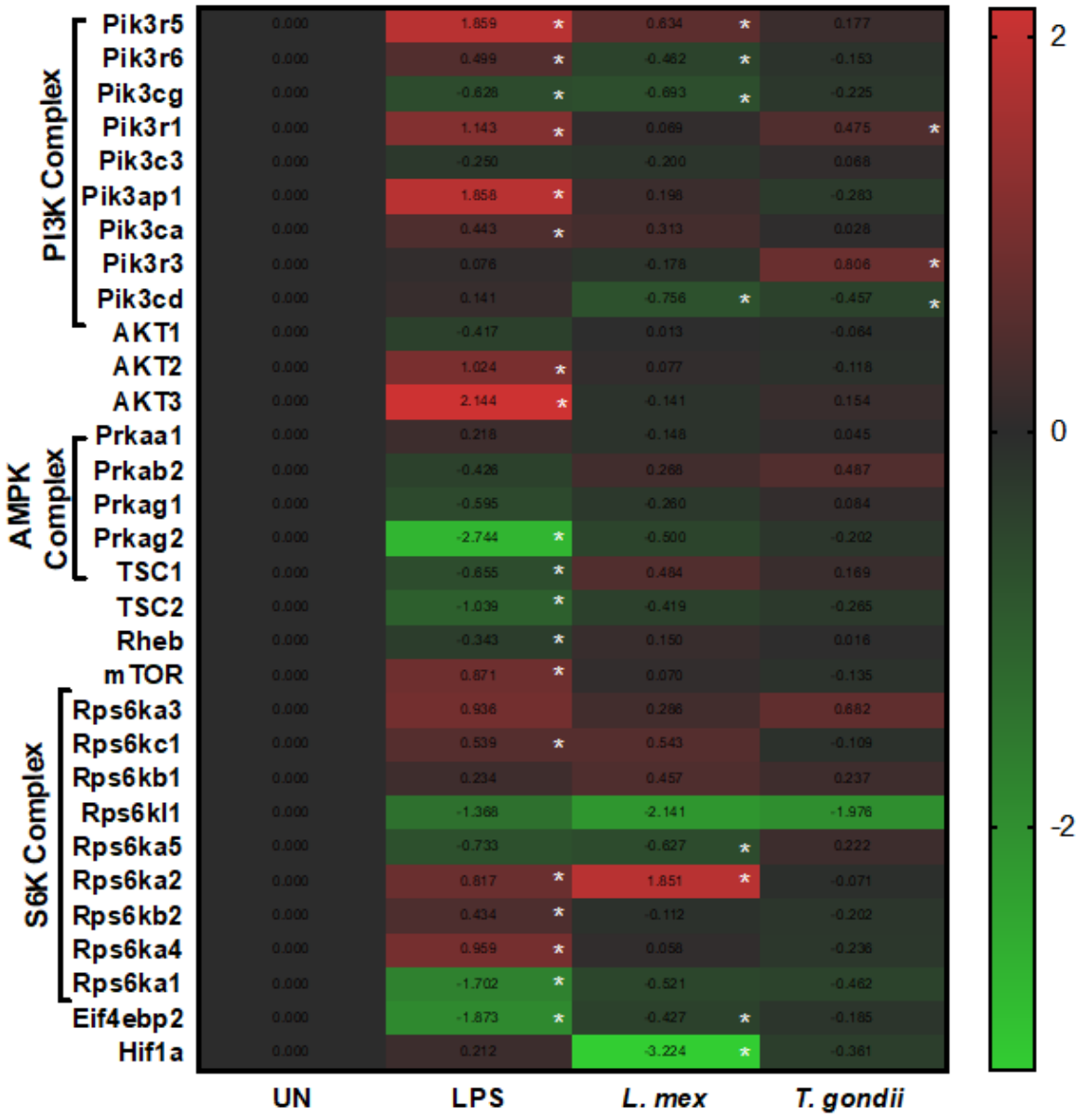
PI3K Complex
Pik3r5
Pik3r6
Pik3cg
Pik3r1
Pik3c3
Pik3ap1
Pik3ca
Pik3r3
Pik3cd
AKT1
AKT2
AKT3
AMPK Complex
Prkaa1
Prkab2
Prkag1
Prkag2
TSC1
TSC2
Rheb
mTOR
S6K Complex
Rps6ka3
Rps6kc1
Rps6kb1
Rps6kl1
Rps6ka5
Rps6ka2
Rps6kb2
Rps6ka4
Rps6ka1
Eif4ebp2
Hif1a
0.000 1.859 * 0.634 * 0.177
0.000 0.499 * -0.462 * -0.153
0.000 -0.628 * -0.693 * -0.225
0.000 1.143 * 0.089 0.475 *
0.000 -0.250 -0.200 0.068
0.000 1.858 * 0.198 -0.283
0.000 0.443 * 0.313 0.028
0.000 0.076 -0.178 0.806 *
0.000 0.141 -0.756 * -0.457 *
0.000 -0.417 0.013 -0.064
0.000 1.024 * 0.077 -0.118
0.000 2.144 * -0.141 0.154
0.000 0.218 -0.148 0.045
0.000 -0.426 0.268 0.487
0.000 -0.595 -0.260 0.084
0.000 -2.744 * -0.500 -0.202
0.000 -0.655 * 0.484 0.169
0.000 -1.039 * -0.419 -0.265
0.000 -0.343 * 0.150 0.016
0.000 0.671 * 0.070 -0.135
0.000 0.936 0.286 0.682
0.000 0.539 * 0.543 -0.109
0.000 0.234 0.457 0.237
0.000 -1.368 -2.141 -1.976
0.000 -0.733 -0.627 * 0.222
0.000 0.817 * 1.851 * -0.071
0.000 0.434 * -0.112 -0.202
0.000 0.959 * 0.058 -0.236
0.000 -1.702 * -0.521 -0.462
0.000 -1.873 * -0.427 * -0.165
0.000 0.212 -3.224 * -0.361
UN
LPS
L. mex
T. gondii
2
0
-2

Figure 5.10. Transcriptomic analysis of PI3K-AKT-mTOR pathway in LPS activated and parasite infected BMDC cultures. Bone marrow derived DCs were either stimulated with LPS or co-cultured with *L. mexicana* or *T. gondii* as indicated for 6 hours. After this time, mRNA was subsequently extracted and then quantified using RNA-seq. Data shows the log2(fold change) as normalised to unstimulated controls. Red indicates an increase in mRNA transcript expression, green indicates a decrease in mRNA expression and grey shows no changes from the control cells. For clarity, the heat map shows the gene abbreviations were *Pik3r5-Pik3cd* are associated with the phosphoinositide-3-kinase (PI3K) complex, Akt1-3 are associated with protein kinase B (AKT), *Prkaa1-Prkag2* are associated with AMP-activated protein kinase (AMPK) complex, *TSC1/2* is the abbreviation for tuberous sclerosis complex, *Rheb* is the acronym for Ras homolog enriched in brain, *mTOR* is the abbreviation of mammalian target of rapamycin, Rps6ka3-Rps6ka1 is associated with P70-S6 Kinase 1 (S6K) and *Eif4ebp4* is the mRNA name for eukaryotic translation initiation factor 4E. Statistical analysis was performed using Cuffdiff (Eurofin) to determine the differential expression levels at the transcript levels including a measure of significance between samples. Significant differences are $p < 0.05$ where * is compared to unstimulated. n = 1.

5.2.6.2. Nuclear receptor Nur77 (nr4a1 transcript) as a key transcriptional regulator during BMDC metabolic reprogramming with intracellular protozoan parasites.

Compared to naïve BMDCs, activation with LPS significantly up-regulated the mRNA transcript level of *myd88* ($p = 0.00015$), *tnfa* ($p = 0.00015$), *ikbkb* ($p = 0.00015$), *nfkb2* ($p = 0.00015$), *nfkb1* ($p = 0.00015$), *nfkbia* ($p = 0.00015$) and *nr4a1* ($p = 0.0067$). *L. mexicana* infected BMDC cultures had significantly increased *tnfa* ($p = 0.00053$) and *nfkbia* ($p = 0.0063$), but significantly decreased mRNA levels of *nr4a1* ($p = 0.023$) compared to control cells. In addition, BMDCs co-cultured with *T. gondii* significantly up-regulated *nfkb1* ($p = 0.019$) and *nfkbia* ($p = 0.012$) mRNA transcript expression compared to naïve BMDCs.

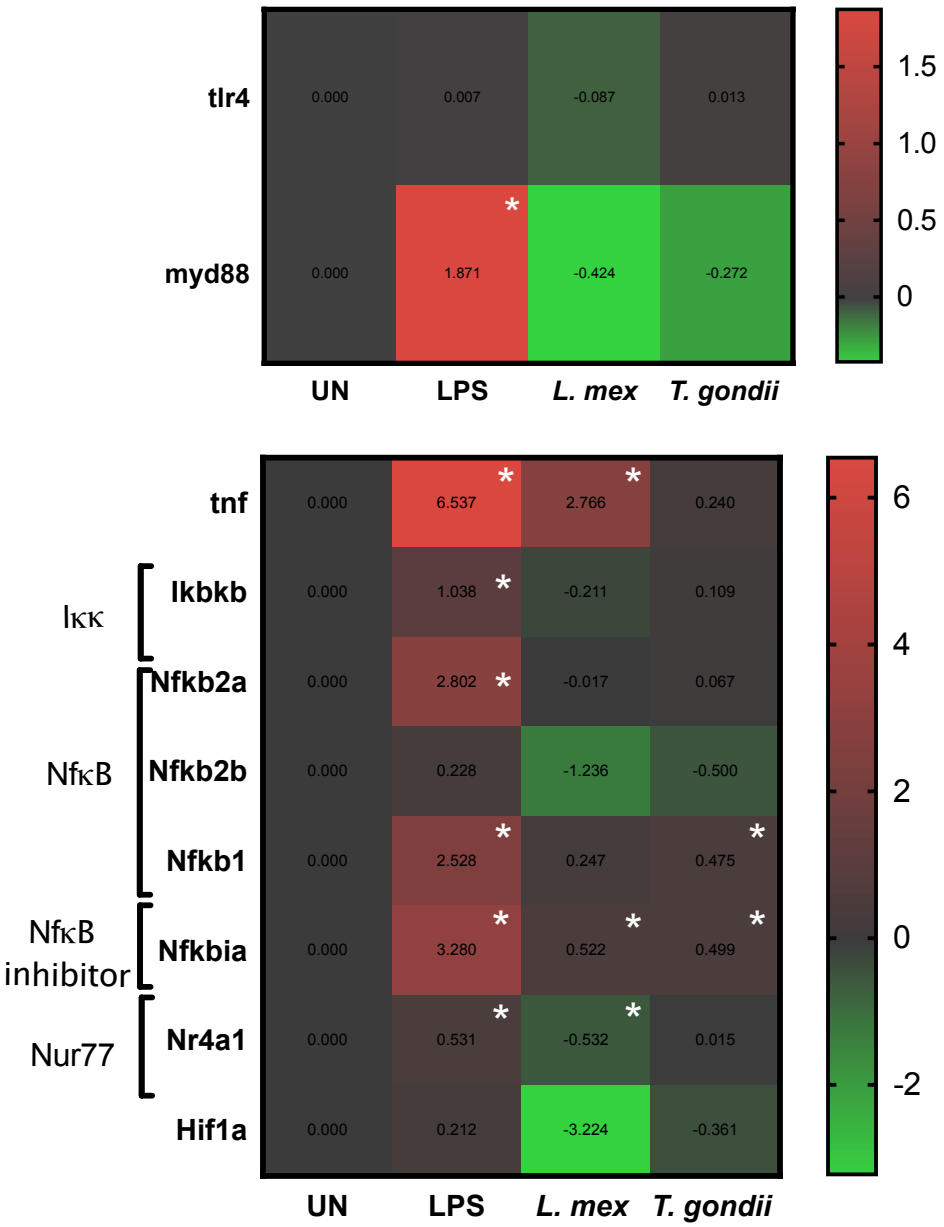
tlr4
myd88
0.000
0.007
-0.087
0.013
0.000
1.871
-0.424
-0.272
*
1.5
1.0
0.5
0
UN
LPS
L. mex
T. gondii
tnf
Ikbkb
Nfkb2a
Nfkb2b
Nfkb1
Nfkbia
Nr4a1
Hif1a
IκK
NfκB
NfκB inhibitor
Nur77
0.000
6.537
2.766
0.240
1.038
-0.211
0.109
2.802
-0.017
0.067
0.228
-1.236
-0.500
2.528
0.247
0.475
3.280
0.522
0.499
0.531
-0.532
0.015
0.212
-3.224
-0.361
6
4
2
0
-2

Figure 5.11. Transcriptomic analysis of Nur77 as a key transcriptional regulator during BMDC metabolic reprogramming with parasites. Bone marrow derived DCs were either stimulated with LPS or co-cultured with *L. mexicana* or *T. gondii* as indicated for 6 hours. After this time, mRNA was subsequently extracted and then quantified using RNA-seq. Data shows the log2(fold change) as normalised to unstimulated controls. Red indicates an increase in mRNA transcript expression, green indicates a decrease in mRNA expression and grey shows no changes from the control cells. For clarity, the heat map shows the gene abbreviations where are *ikbkb* is Ikk, *nfkb2a*, *2b* and *1* are NFkB subunits, *nfkbia* is NFkb inhibitor and *nr4a1* is Nur77. Statistical analysis was performed using Cuffdiff (Eurofin) to determine the differential expression levels at the transcript levels including a measure of significance between samples. Significant differences are $p < 0.05$ where * is compared to unstimulated. n = 1.

Table 5.3. Summary of Findings	**LPS**	***L. mexicana***	***T. gondii***
Global changes			
OPLS-DA Separation	Yes	Yes	Minimal
DC Characteristics			
Cytokine profile (Transcripts)	All up-regulated	**Up-regulated:** *Il1a, Il12b, Tnfa, Il6 & Il10* **Down-regulated:** *Il1b & ccl2*	**Up-regulated:** *Il1a, Il12a &Il6*
Cytokine profile (Protein)	All up-regulated	**Up-regulated:** TNF-a **Down-regulated:** IL-1b	**Up-regulated:** IL-1a, IL-12p70, IL-6 and IL-10
Activation profile (Transcript)	CD40, CD80, CD86 & MHC subunits all up-regulated	CD40 and some MHC subunits up-regulated	CD80 and CD86 up-regulated and many MHC subunits down-regulated
Metabolism changes			
Glycolysis	**Up-regulated:** *Glut1, Hk, pfkfb3 & ldha*	**Up-regulated***: Glut1, Hk, gpi, Pfkl, tpi, gadph, pgk1, pgam1, eno & ldha*	**Down-regulated:** *Glut1, pgam2, eno3*
TCA metabolites	**Up-regulated:** *Acly & Acod* **Down-regulated:** *acc, idh, ogdh, sucl & fh*	**Up-regulated:** *Ogdh & Acod* **Down-regulated:** *Acc, acly, idh3g, fh*	**Down-regulated:** *sdhb*
Oxidative phosphorylation	Most subunits of the electron transport chain are down-regulated whilst sub-units that are up-regulated have other functions un-related to ATP production		

Arginine metabolism	**Up-regulated:** *Ass, arg2 & sms* **Down-regulated:** Asl, arg1, srm	**Up-regulated:** *Nos2, ass* **Down-regulated:** Srm	**Up-regulated:** *Nos2 & Srm*
Signalling pathway changes			
Pi3k-Akt-mTOR pathway	**Up-regulated:** *Pik3r, pik3ap, pik3ca, akt2, mtor, rsp6kc, rsp6ka & rsp6kb* **Down-regulated:** *Pik3cg, Prkag, tsc, rheb, rps6ka & eif4ebp2*	**Up-regulated:** *Pik3r & rps6ka2* **Down-regulated:** *Pik3r, pik3cg, pik3cd, rps6ka5*	**Up-regulated:** *Pik3r1 & Pik3r3* **Down-regulated:** *Pik3cd*
Nur 77 pathway	**Up-regulated:** *Ikbkb, nfkb2a, nfkb1, nfkbia, nur77*	**Up-regulated:** Nfkbia **Down-regulated:** nur77	**Up-regulated:** Nfkbia & Nfkb1

5.3. Discussion

Liquid chromatography mass spectroscopy is an ideal method to investigate cellular metabolism and metabolite accumulation within a cell (Cambiaghi *et al*., 2017). However, as this is an end-point technique, understanding the flux of metabolites through a specific pathway is extremely difficult. Therefore, other methods must be used in conjugation with LCMS to gain a different perspective on the intricacies of metabolic reprogramming within an immune cell. Thus, for example in previous chapters the LCMS data has been bolstered and validated using glucose uptake assays, LDH and arginase enzyme activities, nitrite production and iNOS protein expression. However, these methods do not provide a holistic view of events in a cell and do not deconvolute host and parasite contributions. Towards this goal, the work described in this chapter used a transcriptomic approach to quantify the mRNA transcripts of metabolic enzymes, metabolite transporters and nutrient regulators within a cell (Kircher *et al*., 2010). In parallel with the transcriptomic studies a multiplex bead array system was used to partially immunologically phenotype each host cell condition to quality control the experiment.

BMDCs activated with LPS, *L. mexicana* infected BMDC cultures and BMDCs co-cultured with *T. gondii* all had up-regulated DC activation marker expression (e.g. CD40, CD80 and CD86). This is consistent with work described in chapter 4 and the literature that observed similar changes in surface expression of these molecules using flow cytometry (Andrade *et al*., 2006; Morgardo *et al*., 2014; Verhasselt *et al*., 1997). LPS stimulated BMDCs and those infected with *L. mexicana* also had elevated levels of many transcripts associated with the MHC class I and II complex. In keeping with

the literature that demonstrates the ability of *T. gondii* infection to inhibit MHC expression in macrophages, the majority of MHC class I and II transcripts were down-regulated in *T. gondii* co-cultured BMDCs (Luder *et al*., 1999). Congruence was found between transcript and protein induction using the multiplex cytokine bead array in parallel with the transcriptomics study. Thus *L. mexicana* and *T. gondii* infected BMDC cultures had elevated expression of both mRNA and protein levels of pro-inflammatory cytokines IL-1α, IL-12α (*L. mexicana*), IL-12β (*T. gondii*), TNF-α and IL-6. In contrast, IL-1β mRNA levels and protein expression was down-regulated in both BMDC infected with *L. mexicana*. These data demonstrate RNA-sequencing as a complimentary technique to add value to metabolomics and functional data shown in this thesis. This provided confidence for further analysis of metabolic associated transcripts and the associated signalling pathways (Contreras *et al*., 2014; Nam *et al*., 2011).

Initial results demonstrated elevated expression of the mRNA transcripts encoding the glucose transporter (glut1) and glycolytic enzymes in LPS activated BMDCs and *L. mexicana* infected BMDC cultures. These data are in agreement with other transcriptomic studies that observed increased mRNA levels of glucose transporters and the majority of genes associated with glycolysis and lactate dehydrogenase in LPS stimulated and *L. major* infected murine macrophages (Jantsch *et al*., 2008; Krawczyk *et al*., 2010; Rabhi *et al*., 2012). In contrast, a novel finding is that glut1 was down-regulated in *T. gondii* infected BMDC cultures. Further studies are necessary to investigate why this might be the case.

In addition, transcripts for all hexokinase isoforms were increased in LPS activated BMDCs and those co-cultured with *L. mexicana*. Studies have demonstrated that inhibiting hexokinase by 2-DG effectively prevents LPS-induced dendritic cell activation (Everts *et al*., 2014). Furthermore, phosphofructokinase pfkfb3 mRNA levels were elevated in BMDCs stimulated with LPS and BMDCs exposed to *T. gondii* compared to naïve BMDCs. Previous studies have observed that different isoforms of phosphofructokinase are associated with the phenotype of macrophages. The highly active isoform of phosphofructokinase, pfkfb3, that promotes glycolysis is known to be upregulated in macrophages stimulated with LPS, while the less active isoform pfkfb1 is associated with resting metabolism (Rodriquez–Prados *et al*., 2010; Kelly and O'Neill., 2015). Herein, LPS and *T. gondii* infection are found to induce pfkfb3 rather than pfkfb1 in keeping with aerobic glycolysis and the Warburg effect.

The mRNA level of sedoheptulokinase (CARKL transcript) was decreased in *L. mexicana, T. gondii* infected and LPS activated BMDCs. Decreased CARKL expression is characteristic of the Warburg effect as this molecule limits flux of glucose-6-phosphate into the PPP, decreasing NADPH and glutathione (Haschemi *et al*., 2012).

The majority of mRNA transcripts associated with the TCA cycle were down-regulated in LPS activated BMDCs, *L. mexicana* infected BMDC cultures and BMDCs co-cultured with *T. gondii* compared to naïve BMDCs at 6 hours' post-infection. Notably, similar downregulation of the transcripts has been observed in macrophages stimulated with LPS (Jha *et al*., 2015). Transcripts for *acly*, *dlst* and *acod1* expression

were increased in LPS activated BMDCs as previously reported in LPS-stimulated macrophages (Infantino *et al*., 2013). In contrast, *L. mexicana* infected BMDC cultures had increased levels of *ogdh* and *acod1* transcripts compared to control cells. The overlapping, but distinct pattern of transcript expression could have important consequences for cellular metabolism. The *acly* transcript (upregulated following LPS stimulation) encodes ATP citrate lyase, the enzyme that promotes fatty acid, lipid and prostaglandin synthesis by converting citrate back to acetyl co-A (Infantino *et al*., 2013). The *acod1* transcript (upregulated by both LPS and *L. mexicana* infection) encodes cis-aconitate decarboxylase, the enzyme that metabolises cis-aconitate (from citrate) into the anti-inflammatory mediator itaconate. In macrophages itaconate has been shown to both, suppress succinate dehydrogenase (complex II of ETC) and thereby decrease ROS production and pro-inflammatory cytokine expression (Nemeth *et al*., 2015; Lampropoulou *et al*., 2016; Michelucci *et al*., 2013) and to block the glyoxylate shunt of some pathogens (McFadden *et al*., 1977, Patel *et al*., 1997). Further studies are necessary to investigate the importance of itaconate as an anti-inflammatory mediator in parasite infected BMDCs.

The majority of transcripts encoding the electron transport chain (but not complex IV and V subunits) were also down-regulated in LPS activated BMDCs, *L. mexicana* infected BMDC cultures and those co-cultured with *T. gondii*. Although decreased oxygen consumption has been observed in LPS stimulated macrophages, it is a novel finding for parasite-infected BMDCs (Van den Bossche *et al*., 2016; Zhu *et al*., 2015). Given the previous observations and way that the electron transport chain is linked to the TCA cycle and oxidative phosphorylation this is not surprising. This is also in

keeping with the Warburg-like phenotype. Transcripts encoding complex IV and V subunits were increased in these phenotypes but it has been observed in the literature in other cell types and species that specific components of the ETC have additional roles other than generating energy. These include Cox11 and Cox 15 used in heme A biosynthesis, Atp2b4 and Atp11b that are necessary to support ion transport and calcium homeostasis and Atp6v1d, Atp6v1g1, Atp6v0b and Atp8b2 that aid vesicle formation and lipid signalling (Antonicka *et al*., 2003; Sharma *et al*., 2019). Overall the transcriptomics reported in this chapter together with the observations made in previous chapters agree that like LPS activated BMDCs, cultures infected with *L. mexicana* or *T. gondii* exhibit a Warburg-like phenotype.

To investigate potential common mechanisms and to elucidate unique aspects of metabolic re-programming under the 3 conditions used an analysis of signalling pathways including the PI3K-AKT-mTOR pathway was performed. Firstly, the data demonstrates that BMDCs behave similar to macrophages following LPS stimulation (Choo *et al*., 2008). Thus, the PI3K-AKT-mTOR pathway is increased in BMDCs following LPS stimulation. Significant up-regulation could be observed in the majority of transcripts associated with PI3K and AKT cascade including *mTOR* and the S6K complex. Down-regulation could be seen in inhibitory molecule transcripts including *TSC1*, *TSC2*, *AMPK* and *Eif4ebp*. Furthermore, and as previously reported in macrophages, *HIF-1α* expression was elevated in BMDCs following LPS stimulation. Studies show the importance of this molecule in regulating *glut1* expression and the activity of glycolytic enzymes (Palsson-McDermott *et al*., 2015; Weinhart *et al*., 2008; Weinhart *et al*., 2009).

Secondly, the PI3K-AKT-mTOR pathway in *L. mexicana* and *T. gondii* infected BMDCs is altered compared to naïve BMDCs. However, subtle differences in the extent of these alterations compared with LPS were noted. For example, *AMPK* expression was elevated, rather than reduced in *T. gondii* infected BMDCs. AMPK is activated in during periods of low cellular energy and promotes pathways that generate energy including glucose uptake and aerobic glycolysis. This might reflect the increased energy requirements of a parasitized cell. Whether this is driven by the parasite or the host cell remains to be determined (Reviewed in Moreira *et al*., 2015; Moreira *et al*., 2016; O'Neill and Hardie, 2013).

Recently, Nur77 mediated NF-kB suppression has been described as important in regulating metabolic pathways. Nur 77 (*Nr4a1*) is a nuclear receptor that can function as an activator or repressor of transcription, depending on post-translational modifications (Hamers *et al*., 2016). LPS activated BMDCs and those co-cultured with *T. gondii* were found to have increased transcripts for the Nur77 and decreased transcripts for *HIF-1α*. Current studies in LPS stimulated macrophages have demonstrated that Nur77 can exert its anti-inflammatory effects via suppression of NF-kB signalling or by inhibition of succinate dehydrogenase (Bonta *et al*., 2006; Pei *et al*., 2005; Koenis *et al*., 2018). In these studies, it was observed that Nur 77 suppresses succinate accumulation, NO generation, HIF-1α expression and pro-inflammatory cytokine production in LPS activated macrophages. Interestingly, both Nur 77 transcript *Nr4a1* and *Hif1α* were down-regulated in *L. mexicana* infected BMDC co-cultures.

The transcriptomic studies in this chapter provide compelling support for the metabolomic and functional studies demonstrating that intracellular parasites such as *L. mexicana* or *T. gondii* reprogram BMDCs. Consistent with metabolomic studies, RNA sequencing has demonstrated that certain changes to the metabolism appear to be general host evolved strategies to augment immunity and parasite control whilst other changes appear to be instigated by the parasite to promote growth. Further understanding is still necessary to determine the extent of this bi-directional interplay between parasite and host.

Chapter 6

General Discussion

6. General Discussion

Metabolic changes associated with the immune response have recently received a lot of attention and this field is often referred to as 'immunometabolism'. Some metabolic changes occurring during an immune response can be considered physiological and serve to provide additional energy or precursors for synthesis of proteins, fatty acids or lipids (Krawcyzk *et al*., 2010; Kelly *et al*., 2015). In some cases, changing levels of metabolites in the local environment can influence or even regulate the developing immune response (Infantino *et al*., 2011; Mills *et al*., 2016; Michelucci *et al*., 2013). Other metabolic changes can directly target pathogens by producing effector molecules including RNI and ROI (Wei *et al,* 1995; Calegani-silva *et al*., 2015). Lastly, metabolic changes can prevent parasite multiplication through the depletion of metabolites that the parasite is required to scavenge from the host (Fox *et al*., 2004; Silva *et al*., 2002; Westrop *et al*., 2015; Green *et al*., 1990).

Ultimately, the activation stimuli received by the cell will determine the nature of these metabolic changes. Within the literature, metabolic reprogramming within a LPS stimulated or IL-4 treated macrophage has been well documented. LPS stimulation is associated with numerous metabolic changes culminating in a shift from oxidative phosphorylation to aerobic glycolysis. This is often to referred to as the 'Warburg effect'.

In contrast, IL-4 stimulation is associated with augmented OXPHOS and ATP production (Pearce *et al*., 2013; Palsson-McDermott *et al*., 2013; Jha *et al*., 2015; Reviewed in O'Neill *et al*., 2016; Rattigan *et al*., 2018;).

BMDCs are known to be responsive to many of the same mediators as macrophages and share a number of functions (Chaussabel *et al*., 2003). The role of BMDCs as primary antigen presenting cells and their provision of a bridge from the innate to adaptive immune response makes their characterisation essential (Reviewed in Pearce *et al*., 2015). The findings documented in chapter 1 of this thesis demonstrates that like macrophages and other studies involving dendritic cells, BMDCs adopt a spectrum of activation states when stimulated with a variety of stimuli and this can alter their functional phenotype. (Figure 6.2) (Pearce *et al*., 2015; Everts *et al*., 2012; Krawcyzk *et al*., 2010). Thus, the studies in chapter 1 demonstrate that TLR-stimulation of BMDCs with LPS induces increased glucose uptake, aerobic glycolysis and augmentation of the pentose phosphate pathway while supressing oxidative phosphorylation (encompassing both the TCA cycle and electron transport chain). Previous studies in macrophages have noted that LPS activation leads to 'breaks' within the TCA cycle resulting in accumulation of intermediates including citrate and succinate (Lampropoulou *et al*., 2016; Mills *et al*., 2016; Tannahill *et al*., 2013; O'Neill *et al*., 2011). In BMDC stimulated with LPS accumulation of citrate, α-ketoglutarate, fumarate and malate can be observed. In addition, LPS stimulation of BMDCs was found to promote increased arginine metabolism evidenced by an increase in both iNOS and arginase activity and the production of citrulline, argininosuccinate and ornithine.

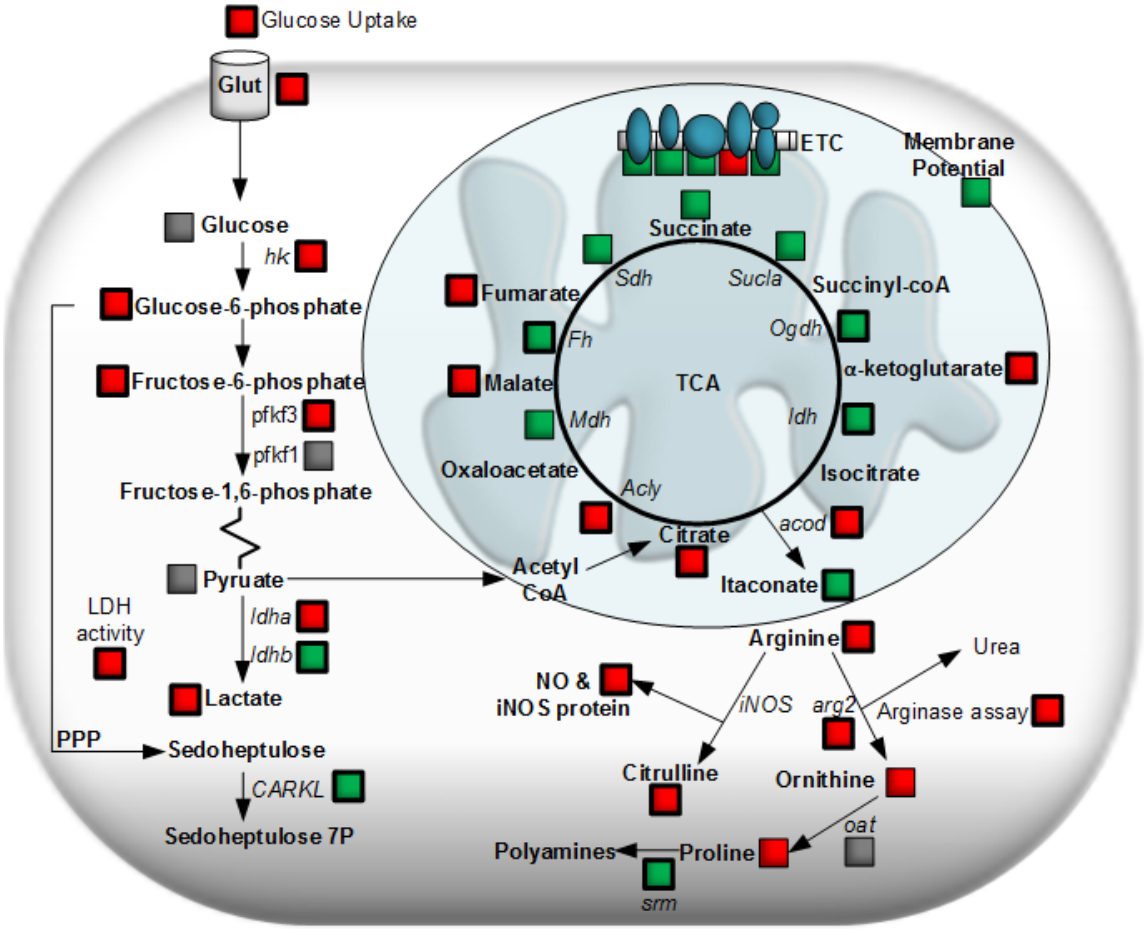

Figure 6.1. BMDC metabolic reprogramming upon LPS stimulation. Upon LPS activation, BMDCs switch from OXPHOS to aerobic glycolysis and PPP. The accumulation of TCA intermediates is also observed, necessary for immune cell effector function. Metabolism of arginine is generally diverted towards citrulline and NO production. Using metabolomics, transcriptomics and functional studies this diagram depicts metabolic reprogramming in BMDCs stimulated with LPS. Red squares show metabolites, transcripts or functional activity that were up-regulated compared to naïve BMDCs whilst green squares were down-regulated. Grey squares had no change in metabolites, transcripts or functional activity compared to unstimulated BMDCs. Squares shown in bold are significantly altered.

In chapter 1, IL-4 treatment of BMDCs was found to promote glucose uptake, glycolysis, PPP, TCA intermediate accumulation and elevated ornithine. These results are in contrast with what has been reported in the literature, where macrophages been shown to increase OXPHOS and ATP production following IL-4 stimulation (via the Seahorse Extracellular Flux Analyser) (Wu *et al*., 2007; Odegaard *et al*., 2011; Rattigan *et al*., 2018). Similar studies will be required in BMDCs to determine if this is also the case.

The exciting foundational data in chapter 1 provided a baseline to study how other virulence factors and pathogens may differentially metabolically reprogram BMDCs. The body of this thesis focused on two protozoan parasites, *Toxoplasma gondii* and *Leishmania mexicana*. Although both are obligate intracellular protozoan parasites they each have unique survival strategies and reside in different intracellular niches (Sibley *et al*., 2011; Sibley *et al*., 2012). These two parasites are important human pathogens and are worthy of study for this alone. However, they also provide valuable case studies to investigate how intracellular parasites have evolved mechanisms to alter host metabolism and evade the immune response and of course how hosts have responded.

Using a combination of metabolomics, transcriptomics and functional studies, this thesis has demonstrated that live *L. mexicana* and *T. gondii* reprogram dendritic cell metabolism (Figure 6.2 and 6.3). The combination of all these techniques were necessary to unravel the complexity of the metabolic changes and to gain insight into whether these changes were occurring in host BMDCs or a reflection of parasite

metabolites. Thus, while LCMS provided an overview of the metabolites in both host and parasites, augmentation of this data with transcriptomics corroborated the results by looking for changes in the levels of associated enzyme transcripts. The data can be further enriched by the detection of enzyme proteins or activity.

L. mexicana and *T. gondii* were found to reprogram BMDC cultures in a similar way to that observed for LPS stimulation by inducing a 'Warburg-like' profile. Notably, the majority of glycolytic enzyme transcripts, glycolysis intermediates and lactate dehydrogenase activity were increased in LPS stimulated BMDCs, *L. mexicana* infected BMDC cultures and BMDCs co-cultured with *T. gondii* compared to control cells. It was note-worthy that CARKL transcripts were down-regulated in BMDC cultures following LPS stimulation, *T. gondii* infection or *L. mexicana* infection. Downregulation of CARKL is a key event associated with the Warburg effect as the down-regulation of this transcript allows glucose-6-phosphate to enter the pentose phosphate pathway providing NADPH (Haschemi *et al*., 2012). Moreover, in all of these BMDC cultures there was down-regulation of transcripts associated with the TCA cycle and oxidative phosphorylation. These results were consistent with mitochondrial function as a distinct reduction in mitochondrial membrane potential was observed in LPS stimulated BMDCs, *L. mexicana* infected BMDC cultures and BMDCs co-cultured with *T. gondii* when compared to naïve BMDC cultures. In keeping with the literature, this again was found to result in TCA intermediate accumulation, a hall-mark of the Warburg effect (Lampropoulou *et al*., 2016; Mills *et al*., 2016; O'Neill *et al*., 2011; Tannahill *et al*., 2013).

Distinct differences between LPS stimulated BMDCs and cultures infected with parasites were observed and could either reflect (i) a host evolved strategy used to restrict nutrient availability to the parasite (ii) a parasite evolved mechanism to alter host metabolism or (iii) simply reflect a limitation of a single time-point metabolic snap-shot in a potentially dynamic host parasite relationship (Nagy *et al*., 2015). The studies described in this thesis support all 3 of these possibilities occurring simultaneously.

Arginine metabolism in *T. gondii* infected BMDCs was extensively discussed in chapter 4 where opposing hypotheses can be formed as to whether these changes benefit the host or the parasite. Viewing the alteration in arginine metabolism as a host evolved strategy, arginine depletion has the potential to restrict *T. gondii* growth as it is an arginine auxotroph (Fox *et al*., 2004). BMDCs infected with *T. gondii* appear to instigate the diversion of arginine to ornithine and proline. This was observed by an increase in arginase activity as well as ornithine and proline levels in *T. gondii* infected BMDC cultures. In addition, *srm* which encodes spermidine synthesis was elevated in these infected cells suggesting further metabolism of proline to polyamines. The importance of host arginine for *T. gondii* growth has also been demonstrated by Woods *et al*., 2013. In contrast, alteration to arginine metabolism can also be viewed as a parasite evolved strategy. *T. gondii* has actively evolved a mechanism to subvert arginine metabolism towards arginase degradation reducing the ability of iNOS to produce nitric oxide. Other studies have demonstrated that ROP16 (released from the rhoptry organelles during invasion) induces *Arg* expression in a STAT6 dependent (El-Kasmi *et al*., 2008; Butcher *et al*., 2011; Marshall *et al*., 2011)

manner. In all reality, it is probable that parasites and hosts evolve together and both these hypotheses can coexist.

The results in this thesis also uncovered a potential parasite mediated mechanism to ameliorate the host immune response. *L. mexicana* induces two breaks in the TCA cycle (resulting in increased aconitase and α-ketoglutarate dehydrogenase levels) leading to the net accumulation of citrate, succinate and itaconate. Itaconate is a known anti-inflammatory mediator. This important function of itaconate was previously observed in LPS-stimulated macrophages where succinate accumulation was found to promote succinate oxidation (via succinate dehydrogenase reversing the electron transport chain) driving pro-inflammatory changes (IL-1β and HIF-α). Itaconate inhibits this process by inhibiting succinate dehydrogenase (Michelucci *et al*., 2013; Lampropoulou *et al*., 2016; Mills *et al*., 2016). Itaconate can also affect some pathogens by blocking the glyoxylate shunt (McFadden *et al*., 1977; Patel, 1997). Further studies will be necessary to understand if itaconate production is induced by the parasite to suppress inflammation or by the host cell to block parasite growth.

Parasites also have immunomodulatory effects on specific signalling pathways and these have been mostly studied in terms of the immune response. This is observed during the release of rhoptries and dense granule proteins in *T. gondii* infection (Carruthers *et al*., 1997). Recently, it has been demonstrated that Nur77 mediates the suppression of NFkb signalling and succinate dehydrogenase (Koenis *et al*., 2018; Bonta, 2006). In chapter 5, nur77 transcript was only subtly increased in *T. gondii*

infected BMDC cultures, but nonetheless a significant increase in *Nfkbia* (an inhibitor of NFkB) was noted. Further studies will be necessary to determine if this immunomodulatory mechanism is Nur77 or NFkBia-dependent and utilised by *T. gondii* to limit inflammation, promoting parasite survival.

Secondly, the PI3K-AKT-mTOR pathway in *L. mexicana* and *T. gondii* infected BMDCs is altered compared to naïve BMDCs. Transcripts for multiple components of the PI3K/AKT/mTOR pathway were altered in LPS-stimulated BMDCs, *L. mexicana* and *T. gondii* infected BMDC cultures. This pathway culminates in the activation of S6K and the suppression of 4EBP1 (Covarrubias *et al*., 2015). In the studies herein, LPS was noted to upregulate transcripts for RPS6Kc1, RPS6Ka2, RPS6Kb2 and RPS6Ka4. In contrast, *L mexicana* only significantly upregulated the RPS6Ka2 transcript and no upregulation of any S6K complex components was observed in *T. gondii* infected BMDC cultures. Transcripts for *Eif4ebp2* (Part of 4EBP1 complex) were significantly downregulated in LPS-stimulated and *L. mexicana*-infected BMDCs. This was not observed in *T. gondii*-infected BMDC cultures. Previous studies of LPS-stimulated macrophages and BMDCs observed elevated *Hif1α* expression (Kim *et al*., 2006; Papandreou *et al*., 2006; Tannahill *et al*., 2013). This was also consistently demonstrated in BMDCs within this thesis. However, *Hif1α* transcript levels was reduced in *L. mexicana* and *T. gondii* infected BMDC cultures. The differences noted between LPS stimulated and parasite infected BMDC cultures might point to (i) a specific parasite mediated interference or (ii) differences in the timing of these transcripts in the conditions examined.

A potential limitation of many metabolomic and transcriptomic studies including the current analyses, is the use of a single time-point metabolic snap-shot in a potentially dynamic host parasite relationship (Nagy *et al*., 2015). Apparent contradictions in the data might be due to this shortfall. For example, glucose uptake and glycolysis intermediates were increased in *T. gondii* infected BMDC cultures whilst *glut1* and hexokinase transcripts were down-regulated. Similarly, glucose uptake and the highly active *pfkfb3* (phosphofructokinase) isoform remained un-changed in *L. mexicana* infected BMDC cultures compared to naïve BMDCs. It is plausible that *L. mexicana* and *T. gondii* may switch to the Warburg effect at different times over a 24-hour period.

Using metabolomics, transcriptomics and functional studies the data in this thesis has highlighted that intracellular parasites such as *L. mexicana* or *T. gondii* can influence both transcripts and metabolites to reprogram dendritic cell metabolism. While certain changes to metabolism (e.g. arginine metabolism in *T. gondii* infected BMDCs) could appear to be instigated by the parasite to promote growth and survival, other changes (e.g. to glycolysis, the TCA cycle and arguably arginine metabolism) would appear to be general host evolved strategies to augment immunity and parasite control. Understanding how parasites affect cellular metabolism is a potentially important step in the production of new drugs and might also inform vaccine design against *L. mexicana* and *T. gondii*.

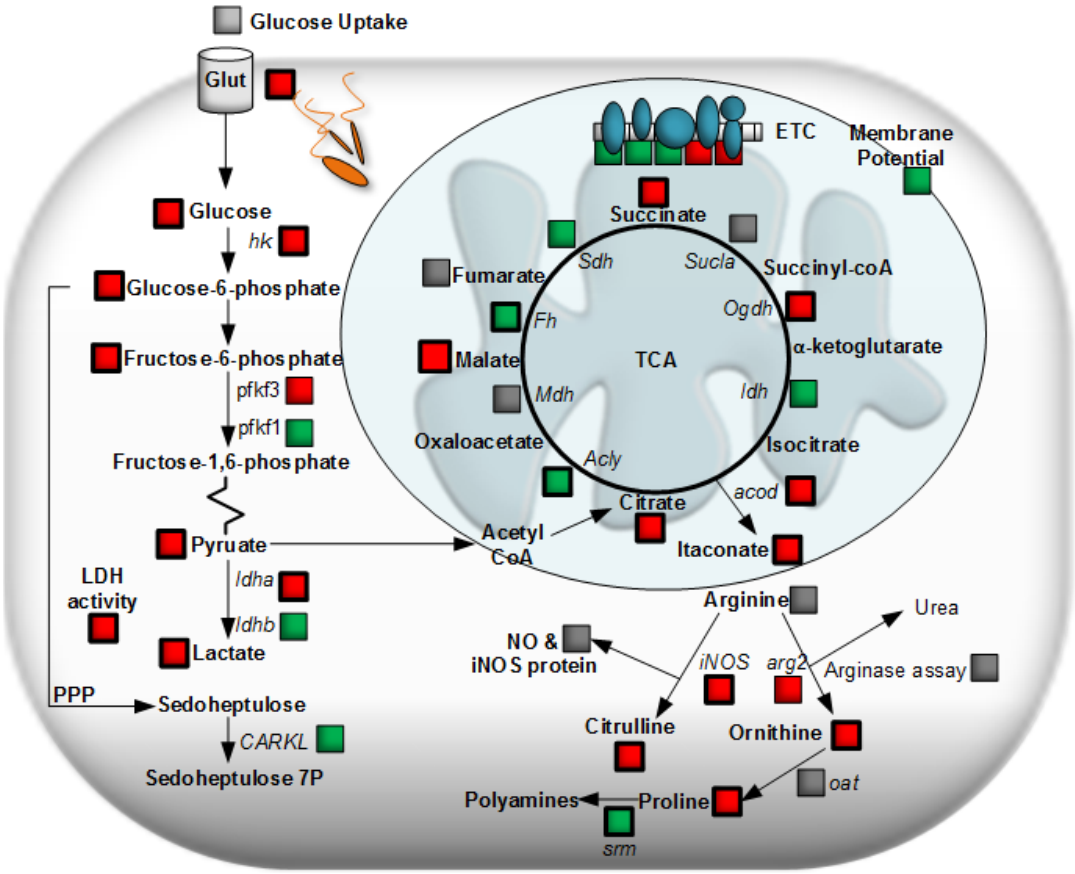

Figure 6.2. BMDC metabolic reprogramming during *L. mexicana* infection. Upon *L. mexicana* infection, BMDCs switch to a Warburg like profile. The accumulation of TCA intermediates was also observed, necessary for immune cell effector function. Metabolism of arginine is generally diverted towards both citrulline and ornithine production with no NO expression. Using metabolomics, transcriptomics and functional studies this diagram depicts metabolic reprogramming in BMDCs cultures infected with *L. mexicana*. Red squares show metabolites, transcripts or functional activity that were up-regulated compared to naïve BMDCs whilst green squares were down-regulated. Grey squares had no change in metabolites, transcripts or functional activity compared to unstimulated BMDCs. Squares shown in bold were significantly altered.

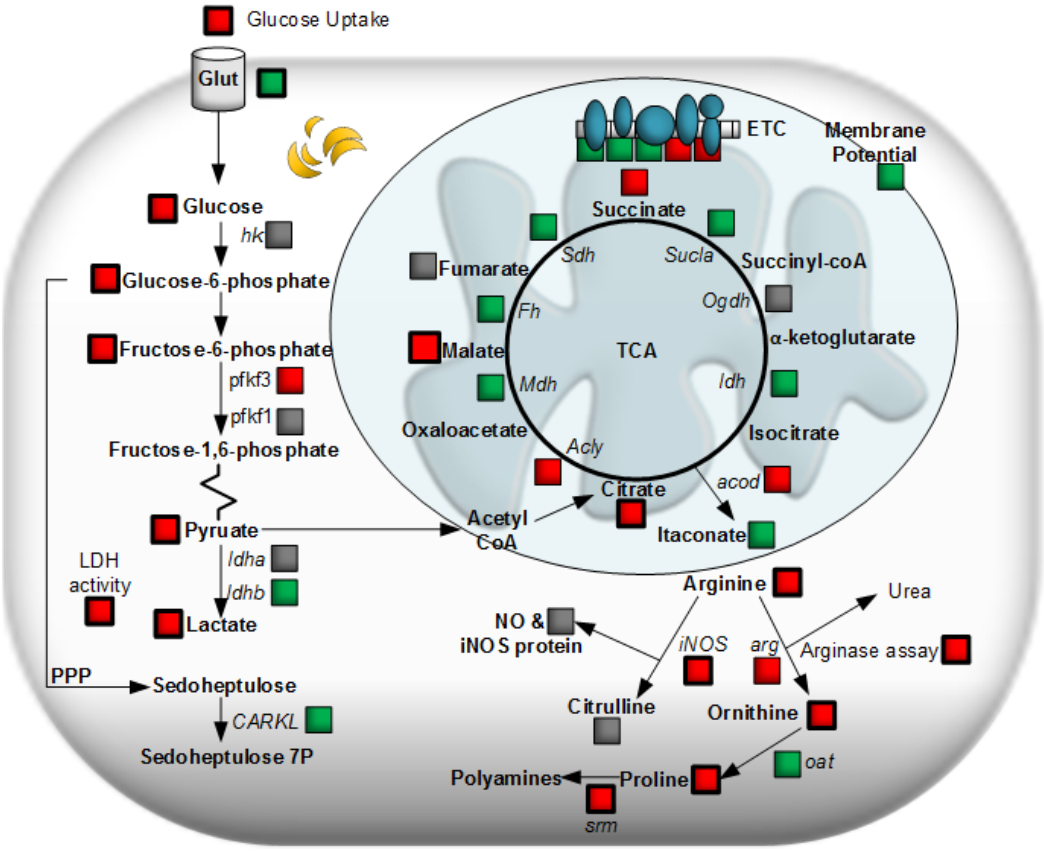

Figure 6.3. BMDC metabolic reprogramming during *T. gondii* infection. Upon *T. gondii* infection, BMDCs switch to a Warburg like profile. The accumulation of TCA intermediates was also observed, necessary for immune cell effector function. Metabolism of arginine is generally diverted towards ornithine, proline and polyamines. Using metabolomics, transcriptomics and functional studies this diagram depicts metabolic reprogramming in BMDCs cultures infected with *T. gondii*. Red squares show metabolites, transcripts or functional activity that were unregulated compared to naïve BMDCs whilst green squares were down-regulated. Grey squares had no change in metabolites, transcripts or functional activity compared to unstimulated BMDCs. Squares shown in bold were significantly altered.

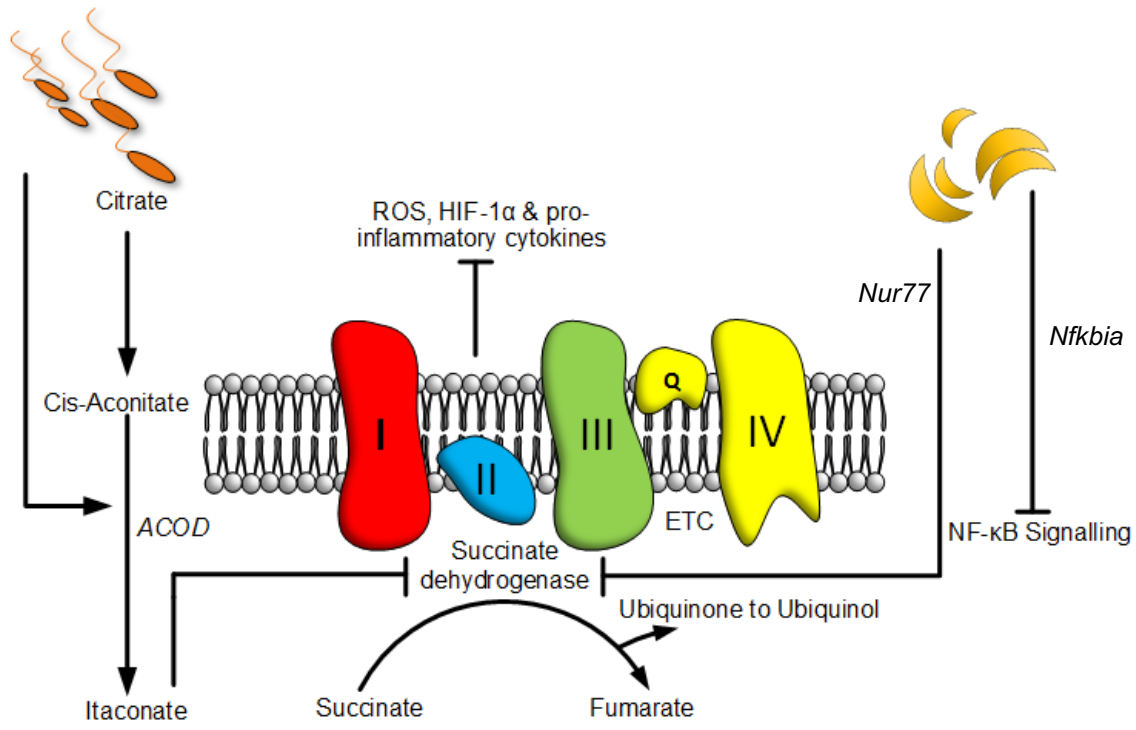

Figure 6.4. Using metabolomics and transcriptomics to inform a proposed anti-inflammatory mechanism of *L. mexicana* or *T. gondii* infection in BMDC *L. mexicana* up-regulates *ACOD* converting citrate into itaconate (increased levels). Itaconate is known to suppress succinate dehydrogenase and inhibit the activity ROS, HIF-1α and pro-inflammatory cytokines. In addition to significantly up-regulating *Nfkbia* (an inhibitor of NF-kB), *T. gondii* can subtly up-regulates Nur77 that can mediate the inhibition of NF-kB and succinate dehydrogenase. This can lead to suppression of pro-inflammatory mediators. LPS stimulation can possibly utilise both anti-inflammatory mechanisms.

Chapter 7

References

Abi Abdallah, D. S., Egan, C. E., Butcher, B. A., & Denkers, E. Y. (2011). Mouse neutrophils are professional antigen-presenting cells programmed to instruct Th1 and Th17 T-cell differentiation. *International Immunology*, *23*(5), 317–326. http://doi.org/10.1093/intimm/dxr007

Aderem, A., & Ulevitch, R. J. (2000). Toll-like receptors in the induction of the innate immune response. *Nature*, *406*(6797), 782–787. http://doi.org/10.1038/35021228

Alexander, J. (1981). Leishmania mexicana: inhibition and stimulation of phagosome-lysosome fusion in infected macrophages. *Experimental Parasitology*, *52*(2), 261–270.

Alexander, J., & Vickerman, K. (1975). Fusion of Host Cell Secondary Lysosomes with the Parasitophorous Vacuoles of Leishmania mexicana-inlected Macrophages. *The Journal of Protozoology*, *22*(4), 502–508. http://doi.org/10.1111/j.1550-7408.1975.tb05219.x

Alexander, J., Brombacher, F., McGachy, H. A., McKenzie, A. N. J., Walker, W., & Carter, K. C. (2002). An essential role for IL-13 in maintaining a non-healing response following Leishmania mexicana infection. *European Journal of Immunology*, *32*(10), 2923–2933. http://doi.org/10.1002/1521-4141(2002010)32:10<2923::AID-IMMU2923>3.0.CO;2-E

Alexander, J., Coombs, G. H., & Mottram, J. C. (1998). Leishmania mexicana Cysteine Proteinase-Deficient Mutants Have Attenuated Virulence for Mice and Potentiate a Th1 Response. *The Journal of Immunology*, *161*(12), 6794–6801. http://doi.org/10.1084/jem.177.5.1505

Alexander, J., Satoskar, A. R., & Russell, D. G. (1999). Leishmania species: models of intracellular parasitism. *Journal of Cell Science*, *112*(18), 2993–3002.

Allain, J. P., Palmer, C. R., & Pearson, G. (1998). Epidemiological study of latent and recent infection by Toxoplasma gondii in pregnant women from a regional population in the U.K. *Journal of Infection*, *36*(2), 189–196. http://doi.org/10.1016/S0163-4453(98)80012-1

Amiel, E., Everts, B., Freitas, T. C., King, I. L., Curtis, J. D., Pearce, E. L., & Pearce, E. J. (2012). Inhibition of mechanistic target of rapamycin promotes dendritic cell activation and enhances therapeutic autologous vaccination in mice. *Journal of Immunology (Baltimore, Md. : 1950)*, *189*(5), 2151–2158. http://doi.org/10.4049/jimmunol.1103741

Andrade, R. M., Wessendarp, M., Gubbels, M.-J., Striepen, B., & Subauste, C. S. (2006). CD40 induces macrophage anti-Toxoplasma gondii activity by triggering autophagy-dependent fusion of pathogen-containing vacuoles and lysosomes. *The Journal of Clinical Investigation*, *116*(9), 2366–2377. http://doi.org/10.1172/JCI28796

Antonicka, H., Mattman, A., Carlson, C. G., Glerum, D. M., Hoffbuhr, K. C., Leary, S. C., et al. (2003). Mutations in COX15 produce a defect in the mitochondrial heme biosynthetic pathway, causing early-onset fatal hypertrophic cardiomyopathy. *American Journal of Human Genetics*, *72*(1), 101–114. http://doi.org/10.1086/345489

Ariyanayagam, M. R., & Fairlamb, A. H. (2001). Ovothiol and trypanothione as antioxidants in trypanosomatids. *Molecular and Biochemical Parasitology*, *115*(2), 189–198.

Atamna, H., & Ginsburg, H. (1997). The malaria parasite supplies glutathione to its host cell--investigation of glutathione transport and metabolism in human erythrocytes infected with Plasmodium falciparum. *European Journal of Biochemistry*, *250*(3), 670–679.

Belkaid, Y., Hoffmann, K. F., Mendez, S., Kamhawi, S., Udey, M. C., Wynn, T. A., & Sacks, D. L. (2001). The Role of Interleukin (IL)-10 in the Persistence of Leishmania major in the Skin after Healing and the Therapeutic Potential of Anti–IL-10 Receptor Antibody for Sterile Cure. *Journal of Experimental Medicine*, *194*(10), 1497–1506. http://doi.org/10.1084/jem.194.10.1497

Benichou, J., Ben-Hamo, R., Louzoun, Y., & Efroni, S. (2012). Rep-Seq: uncovering the immunological repertoire through next-generation sequencing. *Immunology*, *135*(3), 183–191. http://doi.org/10.1111/j.1365-2567.2011.03527.x

Blagih, J., & Jones, R. G. (2012). Polarizing macrophages through reprogramming of glucose metabolism. *Cell Metabolism*, *15*(6), 793–

795. http://doi.org/10.1016/j.cmet.2012.05.008

Bliss, S. K., Gavrilescu, L. C., Alcaraz, A., & Denkers, E. Y. (2001). Neutrophil Depletion during Toxoplasma gondii Infection Leads to Impaired Immunity and Lethal Systemic Pathology. *Infection and Immunity*, *69*(8), 4898–4905. http://doi.org/10.1128/IAI.69.8.4898-4905.2001

Blume, M., Rodriguez-Contreras, D., Landfear, S., Fleige, T., Soldati-Favre, D., Lucius, R., & Gupta, N. (2009). Host-derived glucose and its transporter in the obligate intracellular pathogen Toxoplasma gondii are dispensable by glutaminolysis. *Proceedings of the National Academy of Sciences of the United States of America*, *106*(31), 12998–13003. http://doi.org/10.1073/pnas.0903831106

Bogdan, C., & Röllinghoff, M. (1998). The immune response to Leishmania: mechanisms of parasite control and evasion. *International Journal for Parasitology*, *28*(1), 121–134. http://doi.org/10.1016/S0020-7519(97)00169-0

Bonta, P. I., van Tiel, C. M., Vos, M., Pannekoek, H., & de Vries, C. J. M. (2006). Nuclear orphan receptors Nur77, Nurr1 and NOR-1 expressed in atherosclerotic lesion macrophages reduce lipid loading and inflammatory responses. *Vascular Pharmacology*, *45*(3), e18. http://doi.org/10.1016/j.vph.2006.08.093

Borregaard, N., & Herlin, T. (1982). Energy Metabolism of Human Neutrophils during Phagocytosis. *The Journal of Clinical Investigation*, *70*(3), 550–557. http://doi.org/10.1172/JCI110647

Brinkmann, V. (2004). Neutrophil Extracellular Traps Kill Bacteria. *Science (New York, N.Y.)*, *303*(5663), 1532–1535. http://doi.org/10.1126/science.1092385

Buck, M. D., Sowell, R. T., Kaech, S. M., & Pearce, E. L. (2017). Metabolic Instruction of Immunity. *Cell*, *169*(4), 570–586. http://doi.org/10.1016/j.cell.2017.04.004

Butcher, B. A., Fox, B. A., Rommereim, L. M., Kim, S. G., Maurer, K. J., Yarovinsky, F., et al. (2011). Toxoplasma gondii Rhoptry Kinase ROP16 Activates STAT3 and STAT6 Resulting in Cytokine Inhibition and Arginase-1-Dependent Growth Control. *PLoS Pathogens*, *7*(9), e1002236. http://doi.org/10.1371/journal.ppat.1002236

Byles, V., Covarrubias, A. J., Ben-Sahra, I., Lamming, D. W., Sabatini, D. M., Manning, B. D., & Horng, T. (2013). The TSC-mTOR pathway regulates macrophage polarization. *Nature Communications*, *4*(1), 2834. http://doi.org/10.1038/ncomms3834

Calegari-Silva, T. C., Vivarini, Á. C., Miqueline, M., Santos, Dos, G. R. R. M., Teixeira, K. L., Saliba, A. M., et al. (2015). The human parasite Leishmania amazonensis downregulates iNOS expression via NF-κB p50/p50 homodimer: role of the PI3K/Akt pathway. *Open Biology*, *5*(9), 150118. http://doi.org/10.1098/rsob.150118

Cambiaghi, A., Ferrario, M., & Masseroli, M. (2017). Analysis of metabolomic data: tools, current strategies and future challenges for omics data integration. *Briefings in Bioinformatics*, *18*(3), 498–510. http://doi.org/10.1093/bib/bbw031

Cameron, P., McGachy, A., Anderson, M., Paul, A., Coombs, G. H., Mottram, J. C., et al. (2004). Inhibition of Lipopolysaccharide-Induced Macrophage IL-12 Production by Leishmania mexicana Amastigotes: The Role of Cysteine Peptidases and the NF-κB Signaling Pathway. *The Journal of Immunology*, *173*(5), 3297–3304. http://doi.org/10.4049/jimmunol.173.5.3297

Canonne-Hergaux, F., Gruenheid, S., Govoni, G., & Gros, P. (1999). The Nramp1 protein and its role in resistance to infection and macrophage function. *Proceedings of the Association of American Physicians*, *111*(4), 283–289.

Carruthers, V. B., & Sibley, L. D. (1997). Sequential protein secretion from three distinct organelles of Toxoplasma gondii accompanies invasion of human fibroblasts. *European Journal of Cell Biology*, *73*(2), 114–123.

Carruthers, V. B., Giddings, O. K., & Sibley, L. D. (1999). Secretion of micronemal proteins is associated with toxoplasma invasion of host cells. *Cellular Microbiology*, *1*(3), 225–235. http://doi.org/10.1046/j.1462-5822.1999.00023.x

Caspi, R., Billington, R., Fulcher, C. A., Keseler, I. M., Kothari, A., Krummenacker, M., et al. (2018). The MetaCyc database of metabolic pathways and enzymes. *Nucleic Acids Research*, *46*(D1), D633–D639. http://doi.org/10.1093/nar/gkx935

Cella, M. (1996). Ligation of CD40 on dendritic cells triggers production of high levels of interleukin-12 and enhances T cell stimulatory capacity: T-T help via APC activation. *Journal of Experimental Medicine*, *184*(2), 747–752. http://doi.org/10.1084/jem.184.2.747

Chantranupong, L., Scaria, S. M., Saxton, R. A., Gygi, M. P., Shen, K., Wyant, G. A., et al. (2016). The CASTOR Proteins Are Arginine Sensors for the mTORC1 Pathway. *Cell*, *165*(1), 153–164. http://doi.org/10.1016/j.cell.2016.02.035

Chaussabel, D., Semnani, R. T., McDowell, M. A., Sacks, D., Sher, A., & Nutman, T. B. (2003). Unique gene expression profiles of human macrophages and dendritic cells to phylogenetically distinct parasites. *Blood*, *102*(2), 672–681. http://doi.org/10.1182/blood-2002-10-3232

Choo, A. Y., Yoon, S.-O., Kim, S. G., Roux, P. P., & Blenis, J. (2008). Rapamycin differentially inhibits S6Ks and 4E-BP1 to mediate cell-type-specific repression of mRNA translation. *Proceedings of the National Academy of Sciences of the United States of America*, *105*(45), 17414–17419. http://doi.org/10.1073/pnas.0809136105

Colotti, G., & Ilari, A. (2011). Polyamine metabolism in Leishmania: from arginine to trypanothione. *Amino Acids*, *40*(2), 269–285. http://doi.org/10.1007/s00726-010-0630-3

Contreras, I., Estrada, J. A., Guak, H., Martel, C., Borjian, A., Ralph, B., Shio, M. T., Fournier, S., Krawczyk, C. M., & Olivier, M. (2014a). Impact of Leishmania mexicana Infection on Dendritic Cell Signaling and Functions. *PLoS Neglected Tropical Diseases*, *8*(9), e3202. http://doi.org/10.1371/journal.pntd.0003202

Contreras, I., Estrada, J. A., Guak, H., Martel, C., Borjian, A., Ralph, B., Shio, M. T., Fournier, S., Krawczyk, C. M., & Olivier, M. (2014b). Impact of Leishmania mexicana infection on dendritic cell signaling and functions. *PLoS Neglected Tropical Diseases*, *8*(9), e3202. http://doi.org/10.1371/journal.pntd.0003202

Cortese, M., Sinclair, C., & Pulendran, B. (2014). Translating Glycolytic Metabolism to Innate Immunity in Dendritic Cells. *Cell Metabolism*, *19*(5), 737–739. http://doi.org/10.1016/j.cmet.2014.04.012

Covarrubias, A. J., Aksoylar, H. I., & Horng, T. (2015). Control of macrophage metabolism and activation by mTOR and Akt signaling. *Seminars in Immunology*, *27*(4), 286–296. http://doi.org/10.1016/j.smim.2015.08.001

Cox, F. E. G. (2017). Glasgow encounters with tropical diseases. *Parasitology*, *144*(12), 1561–1566. http://doi.org/10.1017/S0031182017000956

Craft, N., Birnbaum, R., Quanquin, N., Erfe, M. C. B., Quant, C., Haskell, J., & Bruhn, K. W. (2014). Topical resiquimod protects against visceral infection with Leishmania infantum chagasi in mice. *Clinical and Vaccine Immunology : CVI*, *21*(9), 1314–1322. http://doi.org/10.1128/CVI.00338-14

Creek, D. J., Jankevics, A., Burgess, K. E. V., Breitling, R., & Barrett, M. P. (2012). IDEOM: an Excel interface for analysis of LC–MS-based metabolomics data. *Bioinformatics*, *28*(7), 1048–1049. http://doi.org/10.1093/bioinformatics/bts069

Cummings, H. E., Barbi, J., Reville, P., Oghumu, S., Zorko, N., Sarkar, A., et al. (2012). Critical role for phosphoinositide 3-kinase gamma in parasite invasion and disease progression of cutaneous leishmaniasis. *Proceedings of the National Academy of Sciences*, *109*(4), 1251–1256. http://doi.org/10.1073/pnas.1110339109

Daly, C., & Rollins, B. (2003). Monocyte Chemoattractant Protein-1 (CCL2) in Inflammatory Disease and Adaptive Immunity: Therapeutic Opportunities and Controversies. *Microcirculation*, *10*(3), 247–257. http://doi.org/10.1080/713773639

Das, P., Lahiri, A., Lahiri, A., & Chakravortty, D. (2010). Modulation of the Arginase Pathway in the Context of Microbial Pathogenesis: A Metabolic Enzyme Moonlighting as an Immune Modulator. *PLoS Pathogens*, *6*(6), e1000899. http://doi.org/10.1371/journal.ppat.1000899

de-la-Torre, A., Sauer, A., Pfaff, A. W., Bourcier, T., Brunet, J., Speeg-Schatz, C., et al. (2013). Severe South American Ocular Toxoplasmosis Is Associated with Decreased Ifn-γ/Il-17a and Increased Il-6/Il-13 Intraocular Levels. *PLoS Neglected Tropical Diseases*, *7*(11), e2541. http://doi.org/10.1371/journal.pntd.0002541

Denkers, E., & Abi Abdallah, D. (2012). Neutrophils cast extracellular traps in response to protozoan parasites. *Frontiers in Immunology*, *3*. http://doi.org/10.3389/fimmu.2012.00382

Dennis, E. A., & Norris, P. C. (2015). Eicosanoid storm in infection and inflammation. *Nature Reviews Immunology*, *15*(8), 511–523. http://doi.org/10.1038/nri3859

Desjeux, P. (2004). Leishmaniasis: current situation and new perspectives. *Comparative Immunology, Microbiology and Infectious Diseases*, *27*(5), 305–318. http://doi.org/10.1016/j.cimid.2004.03.004

Dubey, J. P., & Frenkel, J. K. (1976). Feline toxoplasmosis from acutely infected mice and the development of Toxoplasma cysts. *The Journal of Protozoology*, *23*(4), 537–546.

Dubey, J. P., Speer, C. A., Shen, S. K., Kwok, O. C. H., & Blixt, J. A. (1997). Oocyst-Induced Murine Toxoplasmosis: Life Cycle, Pathogenicity, and Stage Conversion in Mice Fed Toxoplasma gondii Oocysts. *The Journal of Parasitology*, *83*(5), 870. http://doi.org/10.2307/3284282

Düvel, K., Yecies, J. L., Menon, S., Raman, P., Lipovsky, A. I., Souza, A. L., et al. (2010). Activation of a metabolic gene regulatory network downstream of mTOR complex 1. *Molecular Cell*, *39*(2), 171–183. http://doi.org/10.1016/j.molcel.2010.06.022

Erecińska, M., & Wilson, D. F. (1982). Regulation of cellular energy metabolism. *The Journal of Membrane Biology*, *70*(1), 1–14.

Everts, B., Amiel, E., van der Windt, G. J. W., Freitas, T. C., Chott, R., Yarasheski, K. E., et al. (2012). Commitment to glycolysis sustains survival of NO-producing inflammatory dendritic cells. *Blood*, *120*(7), 1422–1431. http://doi.org/10.1182/blood-2012-03-419747

Filisetti, D., & Candolfi, E. (2004). Immune response to Toxoplasma gondii. *Annali dell'Istituto Superiore Di Sanita*, *40*(1), 71–80.

Flegr, J., Havlícek, J., Kodym, P., Malý, M., & Smahel, Z. (2002). Increased risk of traffic accidents in subjects with latent toxoplasmosis: a retrospective case-control study. *BMC Infectious*

Diseases, *2*(1), 11. http://doi.org/10.1186/1471-2334-2-11

Fox, B. A., Gigley, J. P., & Bzik, D. J. (2004). Toxoplasma gondii lacks the enzymes required for de novo arginine biosynthesis and arginine starvation triggers cyst formation. *International Journal for Parasitology*, *34*(3), 323–331. http://doi.org/10.1016/j.ijpara.2003.12.001

Frenkel, J. K., Ruiz, A., & Chinchilla, M. (1975). Soil survival of toxoplasma oocysts in Kansas and Costa Rica. *The American Journal of Tropical Medicine and Hygiene*, *24*(3), 439–443.

Fukuzumi, M., Shinomiya, H., Shimizu, Y., Ohishi, K., & Utsumi, S. (1996). Endotoxin-induced enhancement of glucose influx into murine peritoneal macrophages via GLUT1. *Infection and Immunity*, *64*(1), 108–112.

Gleeson, L. E., Sheedy, F. J., Palsson-McDermott, E. M., Triglia, D., O'Leary, S. M., O'Sullivan, M. P., et al. (2016). Cutting Edge: Mycobacterium tuberculosis Induces Aerobic Glycolysis in Human Alveolar Macrophages That Is Required for Control of Intracellular Bacillary Replication. *The Journal of Immunology*, *196*(6), 2444–2449. http://doi.org/10.4049/jimmunol.1501612

Gobert, A. P., McGee, D. J., Akhtar, M., Mendz, G. L., Newton, J. C., Cheng, Y., et al. (2001). Helicobacter pylori arginase inhibits nitric oxide production by eukaryotic cells: a strategy for bacterial survival. *Proceedings of the National Academy of Sciences*, *98*(24), 13844–13849. http://doi.org/10.1073/pnas.241443798

Green, S. J., Meltzer, M. S., Hibbs, J. B., & Nacy, C. A. (1990). Activated macrophages destroy intracellular Leishmania major amastigotes by an L-arginine-dependent killing mechanism. *The Journal of Immunology*, *144*(1), 278–283.

Hamers, A. A. J., Argmann, C., Moerland, P. D., Koenis, D. S., Marinković, G., Sokolović, M., et al. (2016). Nur77-deficiency in bone marrow-derived macrophages modulates inflammatory responses, extracellular matrix homeostasis, phagocytosis and tolerance. *BMC Genomics*, *17*(1), 19250. http://doi.org/10.1186/s12864-016-2469-9

Haschemi, A., Kosma, P., Gille, L., Evans, C. R., Burant, C. F., Starkl, P., et al. (2012). The Sedoheptulose Kinase CARKL Directs Macrophage Polarization through Control of Glucose Metabolism.

Cell Metabolism, *15*(6), 813–826. http://doi.org/10.1016/j.cmet.2012.04.023

Heinzel, F. P., Sadick, M. D., Holaday, B. J., Coffman, R. L., & Locksley, R. M. (1989). Reciprocal expression of interferon gamma or interleukin 4 during the resolution or progression of murine leishmaniasis. Evidence for expansion of distinct helper T cell subsets. *Journal of Experimental Medicine*, *169*(1), 59–72.

Henriquez, S. A., Brett, R., Alexander, J., Pratt, J., & Roberts, C. W. (2009). Neuropsychiatric disease and Toxoplasma gondii infection. *Neuroimmunomodulation*, *16*(2), 122–133. http://doi.org/10.1159/000180267

Howe, D. K., & Sibley, L. D. (1995). Toxoplasma gondii comprises three clonal lineages: correlation of parasite genotype with human disease. *The Journal of Infectious Diseases*, *172*(6), 1561–1566.

Humrich, J. Y., Thumann, P., Greiner, S., Humrich, J. H., Averbeck, M., Schwank, C., et al. (2007). Vaccinia virus impairs directional migration and chemokine receptor switch of human dendritic cells. *European Journal of Immunology*, *37*(4), 954–965. http://doi.org/10.1002/eji.200636230

Hunter, C. A., & Reichmann, G. (2009). Immunology of toxoplasma infection. In D. H. M. Joynson & T. G. Wreghitt (Eds.), *Toxoplasmosis* (pp. 43–57). Cambridge: Cambridge University Press. http://doi.org/10.1017/CBO9780511527005.004

Hunter, C. A., Villarino, A., Artis, D., & Scott, P. (2004). The role of IL-27 in the development of T-cell responses during parasitic infections. *Immunological Reviews*, *202*(1), 106–114. http://doi.org/10.1111/j.0105-2896.2004.00213.x

Igarashi, M., Kano, F., Tamekuni, K., Navarro, I. T., Vidotto, O., Vidotto, M. D., Garcia, J. L. (2008). Toxoplasma gondii: Evaluation of an intranasal vaccine using recombinant proteins against brain cyst formation in BALB/c mice. *Experimental Parasitology*, *118*(3), 386–392. http://doi.org/10.1016/j.exppara.2007.10.002

Infantino, V., Convertini, P., Cucci, L., Panaro, M. A., Di Noia, M. A., Calvello, R., et al. (2011). The mitochondrial citrate carrier: a new player in inflammation. *The Biochemical Journal*, *438*(3), 433–436.

http://doi.org/10.1042/BJ20111275

Infantino, V., Iacobazzi, V., Palmieri, F., & Menga, A. (2013). ATP-citrate lyase is essential for macrophage inflammatory response. *Biochemical and Biophysical Research Communications*, *440*(1), 105–111. http://doi.org/10.1016/j.bbrc.2013.09.037

Ingram, W. M., Goodrich, L. M., Robey, E. A., & Eisen, M. B. (2013). Mice Infected with Low-Virulence Strains of Toxoplasma gondii Lose Their Innate Aversion to Cat Urine, Even after Extensive Parasite Clearance. *Plos One*, *8*(9), e75246. http://doi.org/10.1371/journal.pone.0075246

Itano, A. A., McSorley, S. J., Reinhardt, R. L., Ehst, B. D., Ingulli, E., Rudensky, A. Y., & Jenkins, M. K. (2003). Distinct dendritic cell populations sequentially present antigen to CD4 T cells and stimulate different aspects of cell-mediated immunity. *Immunity*, *19*(1), 47–57.

Jantsch, J., Chakravortty, D., Turza, N., Prechtel, A. T., Buchholz, B., Gerlach, R. G., et al. (2008). Hypoxia and Hypoxia-Inducible Factor-1 Modulate Lipopolysaccharide-Induced Dendritic Cell Activation and Function. *The Journal of Immunology*, *180*(7), 4697–4705. http://doi.org/10.4049/jimmunol.180.7.4697

Jaramillo, M., Gomez, M. A., Larsson, O., Shio, M. T., Topisirovic, I., Contreras, I., et al. (2011). Leishmania Repression of Host Translation through mTOR Cleavage Is Required for Parasite Survival and Infection. *Cell Host & Microbe*, *9*(4), 331–341. http://doi.org/10.1016/j.chom.2011.03.008

Jha, A. K., Huang, S. C.-C., Sergushichev, A., Lampropoulou, V., Ivanova, Y., Loginicheva, E., et al. (2015). Network Integration of Parallel Metabolic and Transcriptional Data Reveals Metabolic Modules that Regulate Macrophage Polarization. *Immunity*, *42*(3), 419–430. http://doi.org/10.1016/j.immuni.2015.02.005

Joshi, N. S., Cui, W., Chandele, A., Lee, H. K., Urso, D. R., Hagman, J., et al. (2007). Inflammation Directs Memory Precursor and Short-Lived Effector CD8+ T Cell Fates via the Graded Expression of T-bet Transcription Factor. *Immunity*, *27*(2), 281–295. http://doi.org/10.1016/j.immuni.2007.07.010

Kaddurah-Daouk, R., Kristal, B. S., & Weinshilboum, R. M. (2008). Metabolomics: A Global Biochemical Approach to Drug Response

and Disease. *Annual Review of Pharmacology and Toxicology*, *48*(1), 653–683. http://doi.org/10.1146/annurev.pharmtox.48.113006.094715

Kaneko, Y., Takashima, Y., Xuaun, X., Igarashi, I., Nagasawa, H., Mikami, T., & Otsuka, H. (2004). Natural IgM antibodies in sera from various animals but not the cat kill Toxoplasma gondii by activating the classical complement pathway. *Parasitology*, *128*(Pt 2), 123–129.

Kasmi, El, K. C., Qualls, J. E., Pesce, J. T., Smith, A. M., Thompson, R. W., Henao-Tamayo, M., et al. (2008). Toll-like receptor-induced arginase 1 in macrophages thwarts effective immunity against intracellular pathogens. *Nature Immunology*, *9*(12), 1399–1406. http://doi.org/10.1038/ni.1671

Kassahn, K. S., Waddell, N., & Grimmond, S. M. (2011). Sequencing transcriptomes in toto. *Integrative Biology : Quantitative Biosciences From Nano to Macro*, *3*(5), 522–528. http://doi.org/10.1039/c0ib00062k

Kelly, B., & O'Neill, L. A. J. (2015). Metabolic reprogramming in macrophages and dendritic cells in innate immunity. *Cell Research*, *25*(7), 771–784. http://doi.org/10.1038/cr.2015.68

Killick-Kendrick, R. (1990). Phlebotomine vectors of the leishmaniases: a review. *Medical and Veterinary Entomology*, *4*(1), 1–24. http://doi.org/10.1111/j.1365-2915.1990.tb00255.x

Kim, J.-W., Tchernyshyov, I., Semenza, G. L., & Dang, C. V. (2006). HIF-1-mediated expression of pyruvate dehydrogenase kinase: A metabolic switch required for cellular adaptation to hypoxia. *Cell Metabolism*, *3*(3), 177–185. http://doi.org/10.1016/j.cmet.2006.02.002

Kircher, M. (2011). Analysis of High-Throughput Ancient DNA Sequencing Data. In *Ancient DNA* (Vol. 840, pp. 197–228). Totowa, NJ: Humana Press. http://doi.org/10.1007/978-1-61779-516-9_23

Kobayashi, T., Walsh, P. T., Walsh, M. C., Speirs, K. M., Chiffoleau, E., King, C. G., et al. (2003). TRAF6 Is a Critical Factor for Dendritic Cell Maturation and Development. *Immunity*, *19*(3), 353–363. http://doi.org/10.1016/S1074-7613(03)00230-9

Koenis, D. S., Medzikovic, L., van Loenen, P. B., van Weeghel, M., Huveneers, S., Vos, M., et al. (2018). Nuclear Receptor Nur77 Limits the Macrophage Inflammatory Response through Transcriptional Reprogramming of Mitochondrial Metabolism. *Cell Reports*, *24*(8), 2127–2140.e7. http://doi.org/10.1016/j.celrep.2018.07.065

Koppenol, W. H., Bounds, P. L., & Dang, C. V. (2011). Otto Warburg's contributions to current concepts of cancer metabolism. *Nature Reviews Cancer*, *11*(8), 618–618. http://doi.org/10.1038/nrc3108

Krawczyk, C. M., Holowka, T., Sun, J., Blagih, J., Amiel, E., DeBerardinis, R. J., et al. (2010). Toll-like receptor–induced changes in glycolytic metabolism regulate dendritic cell activation. *Blood*, *115*(23), 4742–4749. http://doi.org/10.1182/blood-2009-10-249540

Lachmandas, E., Boutens, L., Ratter, J. M., Hijmans, A., Hooiveld, G. J., Joosten, L. A. B., et al. (2016). Microbial stimulation of different Toll-like receptor signalling pathways induces diverse metabolic programmes in human monocytes. *Nature Microbiology*, *2*(3), 420. http://doi.org/10.1038/nmicrobiol.2016.246

Lambert, H., Vutova, P. P., Adams, W. C., Loré, K., & Barragan, A. (2009). The Toxoplasma gondii-Shuttling Function of Dendritic Cells Is Linked to the Parasite Genotype. *Infection and Immunity*, *77*(4), 1679–1688. http://doi.org/10.1128/IAI.01289-08

Lampropoulou, V., Sergushichev, A., Bambouskova, M., Nair, S., Vincent, E. E., Loginicheva, E., et al. (2016). Itaconate Links Inhibition of Succinate Dehydrogenase with Macrophage Metabolic Remodeling and Regulation of Inflammation. *Cell Metabolism*, *24*(1), 158–166. http://doi.org/10.1016/j.cmet.2016.06.004

Laskay, T., van Zandbergen, G., & Solbach, W. (2008). Neutrophil granulocytes as host cells and transport vehicles for intracellular pathogens: Apoptosis as infection-promoting factor. *Immunobiology*, *213*(3-4), 183–191. http://doi.org/10.1016/j.imbio.2007.11.010

Liu, C.-H., Fan, Y.-T., Dias, A., Esper, L., Corn, R. A., Bafica, A., et al. (2006). Cutting Edge: Dendritic Cells Are Essential for In Vivo IL-12 Production and Development of Resistance against Toxoplasma gondii Infection in Mice. *The Journal of Immunology*, *177*(1), 31–35. http://doi.org/10.4049/jimmunol.177.1.31

Lorsbach, R. B., Murphy, W. J., Lowenstein, C. J., Snyder, S. H., & Russell, S. W. (1993). Expression of the nitric oxide synthase gene in mouse macrophages activated for tumor cell killing. Molecular basis for the synergy between interferon-gamma and lipopolysaccharide. *Journal of Biological Chemistry*, *268*(3), 1908–1913.

Luder, C.G., Lang T., Beuerle B., Gross, U. (1998). Down-regulation of MHC class II molecules and inability to up-regulate class I molecules in murine macrophages after infection with Toxoplasma gondii. *Clinical & Experimental Immunology*, *112*(2), 308–316. http://doi.org/10.1046/j.1365-2249.1998.00594.x

Lyons, R. E., Lyons, K., McLeod, R., & Roberts, C. W. (2001). Construction and validation of a polycompetitor construct (SWITCH) for use in competitive RT-PCR to assess tachyzoite-bradyzoite interconversion in Toxoplasma gondii. *Parasitology*, *123*(Pt 5), 433–439.

Mandal, G., Sharma, M., Kruse, M., Sander Juelch, C., Munro, L. A., Wang, Y., et al. (2012). Modulation of Leishmania major aquaglyceroporin activity by a mitogen-activated protein kinase. *Molecular Microbiology*, *85*(6), 1204–1218. http://doi.org/10.1111/j.1365-2958.2012.08169.x

Mardis, E. R. (2017). DNA sequencing technologies: 2006-2016. *Nature Protocols*, *12*(2), 213–218. http://doi.org/10.1038/nprot.2016.182

Margulies, M., Egholm, M., Altman, W. E., Attiya, S., Bader, J. S., Bemben, L. A., et al. (2005). Genome sequencing in microfabricated high-density picolitre reactors. *Nature*, *437*(7057), 376–380. http://doi.org/10.1038/nature03959

Marshall, E. S., Elshekiha, H. M., Hakimi, M.-A., & Flynn, R. J. (2011). Toxoplasma gondii peroxiredoxin promotes altered macrophage function, caspase-1-dependent IL-1β secretion enhances parasite replication. *Veterinary Research*, *42*(1), 80. http://doi.org/10.1186/1297-9716-42-80

McConville, M. J., Saunders, E. C., Kloehn, J., & Dagley, M. J. (2015). Leishmania carbon metabolism in the macrophage phagolysosome- feast or famine? *F1000Research*, *4*.

http://doi.org/10.12688/f1000research.6724.1

McFadden, B. A., Williams, J. O., & Roche, T. E. (2002). Mechanism of action of isocitrate lyase from Pseudomonas indigofera. *Biochemistry*, *10*(8), 1384–1390. http://doi.org/10.1021/bi00784a017

McLeod, R., Eisenhauer, P., Mack, D., Brown, C., Filice, G., & Spitalny, G. (1989). Immune responses associated with early survival after peroral infection with Toxoplasma gondii. *The Journal of Immunology*, *142*(9), 3247–3255.

Menzies, F. M., Henriquez, F. L., Alexander, J., & Roberts, C. W. (2011). Selective inhibition and augmentation of alternative macrophage activation by progesterone. *Immunology*, *134*(3), 281–291. http://doi.org/10.1111/j.1365-2567.2011.03488.x

Michelucci, A., Cordes, T., Ghelfi, J., Pailot, A., Reiling, N., Goldmann, O., et al. (2013). Immune-responsive gene 1 protein links metabolism to immunity by catalyzing itaconic acid production. *Proceedings of the National Academy of Sciences*, *110*(19), 7820–7825. http://doi.org/10.1073/pnas.1218599110

Mills, E. L., Kelly, B., Logan, A., Costa, A. S. H., Varma, M., Bryant, C. E., et al. (2016). Succinate Dehydrogenase Supports Metabolic Repurposing of Mitochondria to Drive Inflammatory Macrophages. *Cell*, *167*(2), 457–470.e13. http://doi.org/10.1016/j.cell.2016.08.064

Mineo, J. R., & Kasper, L. H. (1994). Attachment of Toxoplasma gondii to host cells involves major surface protein, SAG-1 (P30). *Experimental Parasitology*, *79*(1), 11–20. http://doi.org/10.1006/expr.1994.1054

Montoya, J. G. (2012). Toxoplasmosis. In *Goldman's Cecil Medicine* (pp. e178–e186). Elsevier. http://doi.org/10.1016/B978-1-4377-1604-7.00573-X

Moreira, D., Rodrigues, V., Abengozar, M., Rivas, L., Rial, E., Laforge, M., et al. (2015). Leishmania infantum modulates host macrophage mitochondrial metabolism by hijacking the SIRT1-AMPK axis. *PLoS Pathogens*, *11*(3), e1004684. http://doi.org/10.1371/journal.ppat.1004684

Moreira, D., Silvestre, R., Cordeiro da Silva, A., Estaquier, J., Foretz, M., & Viollet, B. (2016). AMP-activated Protein Kinase As a Target

For Pathogens: Friends Or Foes? *Current Drug Targets*, *17*(8), 942–953. http://doi.org/10.2174/1389450116666150416120559

Morgado, P., Sudarshana, D. M., Gov, L., Harker, K. S., Lam, T., Casali, P., et al. (2014). Type II Toxoplasma gondii induction of CD40 on infected macrophages enhances interleukin-12 responses. *Infection and Immunity*, *82*(10), 4047–4055. http://doi.org/10.1128/IAI.01615-14

Mosmann, T. R., Cherwinski, H., Bond, M. W., Giedlin, M. A., & Coffman, R. L. (1986). Two types of murine helper T cell clone. I. Definition according to profiles of lymphokine activities and secreted proteins. *The Journal of Immunology*, *136*(7), 2348–2357

Mosser, D. M., & Edwards, J. P. (2008). Exploring the full spectrum of macrophage activation. *Nature Reviews Immunology*, *8*(12), 958–969. http://doi.org/10.1038/nri2448

Mosser, D. M., & Miles, S. A. (2013). Avoidance of Innate Immune Mechanisms by the Protozoan Parasite, Leishmania spp. In *Madame Curie Bioscience Database [Internet]*. Landes Bioscience

Mottram, J.C., Coombs, G.H., & Alexander, J. (2004). Cysteine peptidases as virulence factors of *Leishmania. Current Opinion in Microbiology*, 7: 375-381

Mukherjee, M., Basu Ball, W., & Das, P. K. (2014). Leishmania donovani activates SREBP2 to modulate macrophage membrane cholesterol and mitochondrial oxidants for establishment of infection. *The International Journal of Biochemistry & Cell Biology*, *55*, 196–208. http://doi.org/10.1016/j.biocel.2014.08.019

Muleme, H. M., Reguera, R. M., Berard, A., Azinwi, R., Jia, P., Okwor, I. B., et al. (2009). Infection with Arginase-Deficient Leishmania major Reveals a Parasite Number-Dependent and Cytokine-Independent Regulation of Host Cellular Arginase Activity and Disease Pathogenesis. *The Journal of Immunology*, *183*(12), 8068–8076. http://doi.org/10.4049/jimmunol.0803979

Munder, M. (2009). Arginase: an emerging key player in the mammalian immune system. *British Journal of Pharmacology*, *158*(3), 638–651. http://doi.org/10.1111/j.1476-5381.2009.00291.x

Muraille, E., Leo, O., & Moser, M. (2014). Th1/Th2 Paradigm Extended: Macrophage Polarization as an Unappreciated Pathogen-Driven Escape Mechanism? *Frontiers in Immunology*, *5*(7), 2348. http://doi.org/10.3389/fimmu.2014.00603

Murray, H. W., Szuro-Sudol, A., Wellner, D., Oca, M. J., Granger, A. M., Libby, D. M., et al. (1989). Role of tryptophan degradation in respiratory burst-independent antimicrobial activity of gamma interferon-stimulated human macrophages. *Infection and Immunity*, *57*(3), 845–849.

Nagy, C., & Haschemi, A. (2015). Time and Demand are Two Critical Dimensions of Immunometabolism: The Process of Macrophage Activation and the Pentose Phosphate Pathway. *Frontiers in Immunology*, *6*, 164. http://doi.org/10.3389/fimmu.2015.00164

Nam, H.-W., Ahn, H.-J., & Yang, H.-J. (2011). Pro-inflammatory cytokine expression of spleen dendritic cells in mouse toxoplasmosis. *The Korean Journal of Parasitology*, *49*(2), 109–114. http://doi.org/10.3347/kjp.2011.49.2.109

Newsholme, P., Curi, R., Gordon, S., & Newsholme, E. A. (1986). Metabolism of glucose, glutamine, long-chain fatty acids and ketone bodies by murine macrophages. *Biochemical Journal*, *239*(1), 121–125. http://doi.org/10.1042/bj2390121

Newsholme, P., Gordon, S., & Newsholme, E. A. (1987). Rates of utilization and fates of glucose, glutamine, pyruvate, fatty acids and ketone bodies by mouse macrophages. *Biochemical Journal*, *242*(3), 631–636. http://doi.org/10.1042/bj2420631

Németh, B., Doczi, J., Csete, D., Kacso, G., Ravasz, D., Adams, D., et al. (2016). Abolition of mitochondrial substrate-level phosphorylation by itaconic acid produced by LPS-induced Irg1expression in cells of murine macrophage lineage. *The FASEB Journal*, *30*(1), 286–300. http://doi.org/10.1096/fj.15-279398

Ng, L. G., Hsu, A., Mandell, M. A., Roediger, B., Hoeller, C., Mrass, P., et al. (2008). Migratory dermal dendritic cells act as rapid sensors of protozoan parasites. *PLoS Pathogens*, *4*(11), e1000222. http://doi.org/10.1371/journal.ppat.1000222

Nimri, L., Pelloux, H., & Elkhatib, L. (2004). Detection of Toxoplasma gondii DNA and specific antibodies in high-risk pregnant women. *The*

American Journal of Tropical Medicine and Hygiene, *71*(6), 831–835. http://doi.org/10.4269/ajtmh.2004.71.831

Nitric oxide and mitochondrial respiration. (1999). Nitric oxide and mitochondrial respiration. *Biochimica Et Biophysica Acta (BBA) - Bioenergetics*, *1411*(2-3), 351–369. http://doi.org/10.1016/S0005-2728(99)00025-0

Nitzsche, R., Zagoriy, V., Lucius, R., & Gupta, N. (2016). Metabolic Cooperation of Glucose and Glutamine Is Essential for the Lytic Cycle of Obligate Intracellular Parasite Toxoplasma gondii. *Journal of Biological Chemistry*, *291*(1), 126–141. http://doi.org/10.1074/jbc.M114.624619

O'Neill, L. A. J. (2011). A critical role for citrate metabolism in LPS signalling. *The Biochemical Journal*, *438*(3), e5–6. http://doi.org/10.1042/BJ20111386

O'Neill, L. A. J., & Hardie, D. G. (2013). Metabolism of inflammation limited by AMPK and pseudo-starvation. *Nature*, *493*(7432), 346–355. http://doi.org/10.1038/nature11862

O'Neill, L. A. J., & Pearce, E. J. (2016). Immunometabolism governs dendritic cell and macrophage function. *Journal of Experimental Medicine*, *213*(1), 15–23. http://doi.org/10.1084/jem.20151570

O'Neill, L. A. J., Kishton, R. J., & Rathmell, J. (2016). A guide to immunometabolism for immunologists. *Nature Reviews Immunology*, *16*(9), 553–565. http://doi.org/10.1038/nri.2016.70

Odegaard, J. I., & Chawla, A. (2011). Alternative Macrophage Activation and Metabolism. *Dx.Doi.org*, *6*(1), 275–297. http://doi.org/10.1146/annurev-pathol-011110-130138

Ohtani, M., Nagai, S., Kondo, S., Mizuno, S., Nakamura, K., Tanabe, M., et al. (2008). Mammalian target of rapamycin and glycogen synthase kinase 3 differentially regulate lipopolysaccharide-induced interleukin-12 production in dendritic cells. *Blood*, *112*(3), 635–643. http://doi.org/10.1182/blood-2008-02-137430

Olszewski, K. L., Morrisey, J. M., Wilinski, D., Burns, J. M., Vaidya, A. B., Rabinowitz, J. D., & Llinás, M. (2009). Host-Parasite Interactions Revealed by Plasmodium falciparum Metabolomics. *Cell Host & Microbe*, *5*(2), 191–199.

http://doi.org/10.1016/j.chom.2009.01.004

Oren, R., Farnham, A.E., Saito, K., Milofsky, E., & Karnovsky, M.L. (1963).Metabolic patterns in three types of phagocytizing cells. *The Journal of Cell Biology*, *17*(3), 487–501.

Palsson-McDermott, E. M., & O'Neill, L. A. J. (2013). The Warburg effect then and now: From cancer to inflammatory diseases. *BioEssays*, *35*(11), 965–973. http://doi.org/10.1002/bies.201300084

Pantel, A., Teixeira, A., Haddad, E., Wood, E. G., Steinman, R. M., & Longhi, M. P. (2014). Direct type I IFN but not MDA5/TLR3 activation of dendritic cells is required for maturation and metabolic shift to glycolysis after poly IC stimulation. *PLoS Biology*, *12*(1), e1001759. http://doi.org/10.1371/journal.pbio.1001759

Papandreou, I., Cairns, R. A., Fontana, L., Lim, A. L., & Denko, N. C. (2006). HIF-1 mediates adaptation to hypoxia by actively downregulating mitochondrial oxygen consumption. *Cell Metabolism*, *3*(3), 187–197. http://doi.org/10.1016/j.cmet.2006.01.012

Parker, S. J., Roberts, C. W., & Alexander, J. (1991). CD8+ T cells are the major lymphocyte subpopulation involved in the protective immune response to Toxoplasma gondii in mice. *Clinical & Experimental Immunology*, *84*(2), 207–212.

Patel, T. R., & McFadden, B. A. (1978). Caenorhabditis elegans and Ascaris suum: Inhibition of isocitrate lyase by itaconate. *Experimental Parasitology*, *44*(2), 262–268. http://doi.org/10.1016/0014-4894(78)90107-8

Pearce, E. J., & Everts, B. (2015). Dendritic cell metabolism. *Nature Reviews Immunology*, *15*(1), 18–29. http://doi.org/10.1038/nri3771

Pearce, E. L., & Pearce, E. J. (2013). Metabolic Pathways in Immune Cell Activation and Quiescence. *Immunity*, *38*(4), 633–643. http://doi.org/10.1016/j.immuni.2013.04.005

Pei, L., Castrillo, A., Chen, M., Hoffmann, A., & Tontonoz, P. (2005). Induction of NR4A orphan nuclear receptor expression in macrophages in response to inflammatory stimuli. *Journal of Biological Chemistry*, *280*(32), 29256–29262.

http://doi.org/10.1074/jbc.M502606200

Peters, N. C., Egen, J. G., Secundino, N., Debrabant, A., Kimblin, N., Kamhawi, S., et al. (2008). In vivo imaging reveals an essential role for neutrophils in leishmaniasis transmitted by sand flies. *Science (New York, N.Y.)*, *321*(5891), 970–974. http://doi.org/10.1126/science.1159194

Rabhi, I., Rabhi, S., Ben-Othman, R., Rasche, A., Daskalaki, A., Trentin, B., et al. (2012). Transcriptomic signature of Leishmania infected mice macrophages: a metabolic point of view. *PLoS Neglected Tropical Diseases*, *6*(8), e1763. http://doi.org/10.1371/journal.pntd.0001763

Rambold, A. S., & Pearce, E. L. (2018). Mitochondrial Dynamics at the Interface of Immune Cell Metabolism and Function. *Trends in Immunology*, *39*(1), 6–18. http://doi.org/10.1016/j.it.2017.08.006

Rattigan, K. M., Pountain, A. W., Regnault, C., Achcar, F., Vincent, I. M., Goodyear, C. S., & Barrett, M. P. (2018). Metabolomic profiling of macrophages determines the discrete metabolomic signature and metabolomic interactome triggered by polarising immune stimuli. *Plos One*, *13*(3), e0194126. http://doi.org/10.1371/journal.pone.0194126

Reiner, S. L., & Locksley, R. M. (1995). The regulation of immunity to Leishmania major. *Annual Review of Immunology*, *13*(1), 151–177. http://doi.org/10.1146/annurev.iy.13.040195.001055

Reis e Sousa, C., Yap, G., Schulz, O., Rogers, N., Schito, M., Aliberti, J., et al. (1999). Paralysis of dendritic cell IL-12 production by microbial products prevents infection-induced immunopathology. *Immunity*, *11*(5), 637–647.

Remington, J. S. (1990). The tragedy of toxoplasmosis. *The Pediatric Infectious Disease Journal*, *9*(10), 762–763.

Ribeiro-Gomes, F. L., & Sacks, D. (2012). The influence of early neutrophil-Leishmania interactions on the host immune response to infection. *Frontiers in Cellular and Infection Microbiology*, *2*, 59. http://doi.org/10.3389/fcimb.2012.00059

Roberts, S. C., Tancer, M. J., Polinsky, M. R., Gibson, K. M., Heby, O., & Ullman, B. (2004). Arginase Plays a Pivotal Role in Polyamine

Precursor Metabolism in Leishmania. *Journal of Biological Chemistry*, *279*(22), 23668–23678. http://doi.org/10.1074/jbc.M402042200

Rodriguez-Sosa, M., Monteforte, G. M., & Satoskar, A. R. (2001). Susceptibility to Leishmania mexicana infection is due to the inability to produce IL-12 rather than lack of IL-12 responsiveness. *Immunology and Cell Biology*, *79*(4), 320–322. http://doi.org/10.1046/j.1440-1711.2001.01014.x

Rodríguez-Prados, J.-C., Través, P. G., Cuenca, J., Rico, D., Aragonés, J., Martín-Sanz, P., et al. (2010). Substrate Fate in Activated Macrophages: A Comparison between Innate, Classic, and Alternative Activation. *The Journal of Immunology*, *185*(1), 605–614. http://doi.org/10.4049/jimmunol.0901698

Rolfe, D. F., & Brown, G. C. (1997). Cellular energy utilization and molecular origin of standard metabolic rate in mammals. *Physiological Reviews*, *77*(3), 731–758. http://doi.org/10.1152/physrev.1997.77.3.731

Saas, P., Varin, A., Perruche, S., & Ceroi, A. (2017). Recent insights into the implications of metabolism in plasmacytoid dendritic cell innate functions: Potential ways to control these functions. *F1000Research*, *6*, 456. http://doi.org/10.12688/f1000research.11332.2

Saeij, J. P. J., Boyle, J. P., & Boothroyd, J. C. (2005). Differences among the three major strains of Toxoplasma gondii and their specific interactions with the infected host. *Trends in Parasitology*, *21*(10), 476–481. http://doi.org/10.1016/j.pt.2005.08.001

Sanecka, A., & Frickel, E.-M. (2012). Use and abuse of dendritic cells by Toxoplasma gondii. *Virulence*, *3*(7), 678–689. http://doi.org/10.4161/viru.22833

Satoskar, A., Bluethmann, H., & Alexander, J. (1995). Disruption of the murine interleukin-4 gene inhibits disease progression during Leishmania mexicana infection but does not increase control of Leishmania donovani infection. *Infection and Immunity*, *63*(12), 4894–4899.

Saunders, E. C., Ng, W. W., Kloehn, J., Chambers, J. M., Ng, M., & McConville, M. J. (2014). Induction of a Stringent Metabolic

Response in Intracellular Stages of Leishmania mexicana Leads to Increased Dependence on Mitochondrial Metabolism. *PLoS Pathogens*, *10*(1), e1003888. http://doi.org/10.1371/journal.ppat.1003888

Sbarra, A. J., & Karnovsky, M.L. (1959). The biochemical basis of phagocytosis. I. Metabolic changes during the ingestion of particles by polymorphonuclear leukocytes. *Journal of Biological Chemistry*, *234*(6), 1355–1362.

Schaible, U. E., & Kaufmann, S. H. E. (2004). Iron and microbial infection. *Nature Reviews. Microbiology*, *2*(12), 946–953. http://doi.org/10.1038/nrmicro1046

Schmitz, F., Heit, A., Dreher, S., Eisenächer, K., Mages, J., Haas, T., et al. (2008). Mammalian target of rapamycin (mTOR) orchestrates the defense program of innate immune cells. *European Journal of Immunology*, *38*(11), 2981–2992. http://doi.org/10.1002/eji.200838761

Seabra, S. H., de Souza, W., & DaMatta, R. A. (2002). Toxoplasma gondii Partially Inhibits Nitric Oxide Production of Activated Murine Macrophages. *Experimental Parasitology*, *100*(1), 62–70. http://doi.org/10.1006/expr.2001.4675

Semenza, G. L., Jiang, B.-H., Leung, S. W., Passantino, R., Concordet, J.-P., Maire, P., & Giallongo, A. (1996). Hypoxia Response Elements in the Aldolase A, Enolase 1, and Lactate Dehydrogenase A Gene Promoters Contain Essential Binding Sites for Hypoxia-inducible Factor 1. *Journal of Biological Chemistry*, *271*(51), 32529–32537. http://doi.org/10.1074/jbc.271.51.32529

Sen, D., Forrest, L., Kepler, T. B., Parker, I., & Cahalan, M. D. (2010). Selective and site-specific mobilization of dermal dendritic cells and Langerhans cells by Th1- and Th2-polarizing adjuvants. *Proceedings of the National Academy of Sciences of the United States of America*, *107*(18), 8334–8339. http://doi.org/10.1073/pnas.0912817107

Serbina, N. V., Salazar-Mather, T. P., Biron, C. A., Kuziel, W. A., & Pamer, E. G. (2003). TNF/iNOS-producing dendritic cells mediate innate immune defense against bacterial infection. *Immunity*, *19*(1), 59–70.

Sharma, S., Oot, R. A., Khan, M. M., & Wilkens, S. (2019). Functional reconstitution of vacuolar H+-ATPase from Vo proton channel and mutant V1-ATPase provides insight into the mechanism of reversible disassembly. *Journal of Biological Chemistry*, jbc.RA119.007577. http://doi.org/10.1074/jbc.RA119.007577

Shendure, J., & Ji, H. (2008). Next-generation DNA sequencing. *Nature Biotechnology*, *26*(10), 1135–1145. http://doi.org/10.1038/nbt1486

Sibley, L. D. (2011). Invasion and intracellular survival by protozoan parasites. *Immunological Reviews*, *240*(1), 72–91. http://doi.org/10.1111/j.1600-065X.2010.00990.x

Sibley, L. D., & Boothroyd, J. C. (1992). Virulent strains of Toxoplasma gondii comprise a single clonal lineage. *Nature*, *359*(6390), 82–85. http://doi.org/10.1038/359082a0

Sibley, L. D., Howlett, B. J., & Heitman, J. (Eds.). (2012). Evolution of Virulence in Eukaryotic Microbes. Hoboken, NJ, USA: John Wiley & Sons, Inc. http://doi.org/10.1002/9781118308165

Silva, N. M. (2002). Expression of Indoleamine 2,3-Dioxygenase, Tryptophan Degradation, and Kynurenine Formation during In Vivo Infection with Toxoplasma gondii: Induction by Endogenous Gamma Interferon and Requirement of Interferon Regulatory Factor 1. *Infection and Immunity*, *70*(2), 859–868. http://doi.org/10.1128/IAI.70.2.859-868.2002

Singh, A. K., Mukhopadhyay, C., Biswas, S., Singh, V. K., & Mukhopadhyay, C. K. (2012). Intracellular Pathogen Leishmania donovani Activates Hypoxia Inducible Factor-1 by Dual Mechanism for Survival Advantage within Macrophage. *Plos One*, *7*(6), e38489. http://doi.org/10.1371/journal.pone.0038489

Stafford, J. L., Neumann, N. F., & Belosevic, M. (2002). Macrophage-mediated innate host defense against protozoan parasites. *Critical Reviews in Microbiology*, *28*(3), 187–248. http://doi.org/10.1080/1040-840291046731

Stebut, von, E. (2007). Cutaneous Leishmania infection: progress in pathogenesis research and experimental therapy. *Experimental Dermatology*, *16*(4), 340–346. http://doi.org/10.1111/j.1600-

0625.2007.00554.x

Stebut, von, E., Belkaid, Y., Jakob, T., Sacks, D. L., & Udey, M. C. (1998). Uptake of Leishmania major amastigotes results in activation and interleukin 12 release from murine skin-derived dendritic cells: implications for the initiation of anti-Leishmania immunity. *Journal of Experimental Medicine*, *188*(8), 1547–1552.

Stein, M., Keshav, S., Harris, N., & Gordon, S. (1992). Interleukin 4 potently enhances murine macrophage mannose receptor activity: a marker of alternative immunologic macrophage activation. *Journal of Experimental Medicine*, *176*(1), 287–292. http://doi.org/10.1084/jem.176.1.287

Steinman, R. M., & Hemmi, H. (2006). Dendritic Cells: Translating Innate to Adaptive Immunity. In *From Innate Immunity to Immunological Memory* (Vol. 311, pp. 17–58). Springer Berlin Heidelberg. http://doi.org/10.1007/3-540-32636-7_2

Steverding, D. (2017). The history of leishmaniasis. *Parasites & Vectors*, *10*(1), 82. http://doi.org/10.1186/s13071-017-2028-5

Stout, R. D., & Suttles, J. (2004). Functional plasticity of macrophages: reversible adaptation to changing microenvironments. *Journal of Leukocyte Biology*, *76*(3), 509–513. http://doi.org/10.1189/jlb.0504272

Strelko, C. L., Lu, W., Dufort, F. J., Seyfried, T. N., Chiles, T. C., Rabinowitz, J. D., & Roberts, M. F. (2011). Itaconic acid is a mammalian metabolite induced during macrophage activation. *Journal of the American Chemical Society*, *133*(41), 16386–16389. http://doi.org/10.1021/ja2070889

Su, C., Evans, D., Cole, R. H., Kissinger, J. C., Ajioka, J. W., & Sibley, L. D. (2003). Recent expansion of Toxoplasma through enhanced oral transmission. *Science (New York, N.Y.)*, *299*(5605), 414–416. http://doi.org/10.1126/science.1078035

Subauste, C. S., & Wessendarp, M. (2000). Human Dendritic Cells Discriminate Between Viable and Killed Toxoplasma gondii Tachyzoites: Dendritic Cell Activation After Infection with Viable Parasites Results in CD28 and CD40 Ligand Signaling That Controls IL-12-Dependent and -Independent T Cell Production of IFN-γ. *The Journal of Immunology*, *165*(3), 1498–1505.

http://doi.org/10.4049/jimmunol.165.3.1498

t'Kindt, R., Scheltema, R. A., Jankevics, A., Brunker, K., Rijal, S., Dujardin, J.-C., et al. (2010). Metabolomics to Unveil and Understand Phenotypic Diversity between Pathogen Populations. *PLoS Neglected Tropical Diseases*, *4*(11), e904. http://doi.org/10.1371/journal.pntd.0000904

Tacchini-Cottier, F., Zweifel, C., Belkaid, Y., Mukankundiye, C., Vasei, M., Launois, P., et al. (2000). An Immunomodulatory Function for Neutrophils During the Induction of a CD4+ Th2 Response in BALB/c Mice Infected with Leishmania major. *The Journal of Immunology*, *165*(5), 2628–2636. http://doi.org/10.4049/jimmunol.165.5.2628

Tait, E. D., Jordan, K. A., Dupont, C. D., Harris, T. H., Gregg, B., Wilson, E. H., et al. (2010). Virulence of Toxoplasma gondii Is Associated with Distinct Dendritic Cell Responses and Reduced Numbers of Activated CD8+ T Cells. *The Journal of Immunology*, *185*(3), 1502–1512. http://doi.org/10.4049/jimmunol.0903450

Tannahill, G. M., Curtis, A. M., Adamik, J., Palsson-McDermott, E. M., McGettrick, A. F., Goel, G., et al. (2013). Succinate is an inflammatory signal that induces IL-1[bgr] through HIF-1[agr]. *Nature*, *496*(7444), 238–242. http://doi.org/10.1038/nature11986

Titus, R. G., & Ribeiro, J. M. (1988). Salivary gland lysates from the sand fly Lutzomyia longipalpis enhance Leishmania infectivity. *Science (New York, N.Y.)*, *239*(4845), 1306–1308.

Torrentera, F. A., Lambot, M.-A., Laman, J. D., Van Meurs, M., Kiss, R., Noël, J.-C., & Carlier, Y. (2002). Parasitic load and histopathology of cutaneous lesions, lymph node, spleen, and liver from BALB/c and C57BL/6 mice infected with Leishmania mexicana. *The American Journal of Tropical Medicine and Hygiene*, *66*(3), 273–279. http://doi.org/10.4269/ajtmh.2002.66.273

Troutman, T. D., Hu, W., Fulenchek, S., Yamazaki, T., Kurosaki, T., Bazan, J. F., & Pasare, C. (2012). Role for B-cell adapter for PI3K (BCAP) as a signaling adapter linking Toll-like receptors (TLRs) to serine/threonine kinases PI3K/Akt. *Proceedings of the National Academy of Sciences*, *109*(1), 273–278. http://doi.org/10.1073/pnas.1118579109

Van den Bossche, J., Baardman, J., Otto, N. A., van der Velden, S., Neele, A. E., van den Berg, S. M., et al. (2016). Mitochondrial Dysfunction Prevents Repolarization of Inflammatory Macrophages. *Cell Reports*, *17*(3), 684–696. http://doi.org/10.1016/j.celrep.2016.09.008

Van den Bossche, J., O'Neill, L. A., & Menon, D. (2017). Macrophage Immunometabolism: Where Are We (Going)? *Trends in Immunology*. http://doi.org/10.1016/j.it.2017.03.001

Van Dyken, S. J., & Locksley, R. M. (2013). Interleukin-4- and Interleukin-13-Mediated Alternatively Activated Macrophages: Roles in Homeostasis and Disease. *Annual Review of Immunology*, *31*(1), 317–343. http://doi.org/10.1146/annurev-immunol-032712-095906

van Zandbergen, G., Hermann, N., Laufs, H., Solbach, W., & Laskay, T. (2002). Leishmania Promastigotes Release a Granulocyte Chemotactic Factor and Induce Interleukin-8 Release but Inhibit Gamma Interferon-Inducible Protein 10 Production by Neutrophil Granulocytes. *Infection and Immunity*, *70*(8), 4177–4184. http://doi.org/10.1128/IAI.70.8.4177-4184.2002

van Zandbergen, G., Klinger, M., Mueller, A., Dannenberg, S., Gebert, A., Solbach, W., & Laskay, T. (2004). Cutting edge: neutrophil granulocyte serves as a vector for Leishmania entry into macrophages. *The Journal of Immunology*, *173*(11), 6521–6525.

Vander Heiden, M. G., Locasale, J. W., Swanson, K. D., Sharfi, H., Heffron, G. J., Amador-Noguez, D., et al. (2010). Evidence for an alternative glycolytic pathway in rapidly proliferating cells. *Science (New York, N.Y.)*, *329*(5998), 1492–1499. http://doi.org/10.1126/science.1188015

Vats, D., Mukundan, L., Odegaard, J. I., Zhang, L., Smith, K. L., Morel, C. R., et al. (2006). Oxidative metabolism and PGC-1β attenuate macrophage-mediated inflammation. *Cell Metabolism*, *4*(3), 255. http://doi.org/10.1016/j.cmet.2006.08.006

Vázquez-López, R., Argueta-Donohué, J., Wilkins-Rodríguez, A., Escalona-Montaño, A., Aguirre-García, M., & Gutiérrez-Kobeh, L. (2015). Leishmania mexicana amastigotes inhibit p38 and JNK and activate PI3K/AKT: role in the inhibition of apoptosis of dendritic cells. *Parasite Immunology*, *37*(11), 579–589.

http://doi.org/10.1111/pim.12275

Vergadi, E., Ieronymaki, E., Lyroni, K., Vaporidi, K., & Tsatsanis, C. (2017). Akt Signaling Pathway in Macrophage Activation and M1/M2 Polarization. *The Journal of Immunology*, *198*(3), 1006–1014. http://doi.org/10.4049/jimmunol.1601515

Verhasselt, V., Buelens, C., Willems, F., De Groote, D., Haeffner-Cavaillon, N., & Goldman, M. (1997). Bacterial lipopolysaccharide stimulates the production of cytokines and the expression of costimulatory molecules by human peripheral blood dendritic cells: evidence for a soluble CD14-dependent pathway. *The Journal of Immunology*, *158*(6), 2919–2925.

Warburg, O. (1925). Iron, the oxygen-carrier of respiration-ferment. *Science (New York, N.Y.)*, *61*(1588), 575–582. http://doi.org/10.1126/science.61.1588.575

Warburg, O., Wind, F., & Negelein, E. (1927). The metabolism of tumors in the body.*The Journal of General Physiology*, *8*(6), 519–530. http://doi.org/10.1085/jgp.8.6.519

Weichhart, T., & Säemann, M. D. (2009). The multiple facets of mTOR in immunity. *Trends in Immunology*, *30*(5), 218–226. http://doi.org/10.1016/j.it.2009.02.002

Weichhart, T., Costantino, G., Poglitsch, M., Rosner, M., Zeyda, M., Stuhlmeier, K. M., et al. (2008). The TSC-mTOR Signaling Pathway Regulates the Innate Inflammatory Response. *Immunity*, *29*(4), 565–577. http://doi.org/10.1016/j.immuni.2008.08.012

Westrop, G. D., Williams, R. A. M., Wang, L., Zhang, T., Watson, D. G., Silva, A. M., & Coombs, G. H. (2015). Metabolomic Analyses of Leishmania Reveal Multiple Species Differences and Large Differences in Amino Acid Metabolism. *Plos One*, *10*(9), e0136891. http://doi.org/10.1371/journal.pone.0136891

Wiley, M., Sweeney, K. R., Chan, D. A., Brown, K. M., McMurtrey, C., Howard, E. W., et al. (2010). Toxoplasma gondii activates hypoxia-inducible factor (HIF) by stabilizing the HIF-1alpha subunit via type I activin-like receptor kinase receptor signaling. *Journal of Biological Chemistry*, *285*(35), 26852–26860. http://doi.org/10.1074/jbc.M110.147041

Wilkins-Rodríguez, A. A., Escalona-Montaño, A. R., Aguirre-García, M., Becker, I., & Gutiérrez-Kobeh, L. (2010). Regulation of the expression of nitric oxide synthase by Leishmania mexicana amastigotes in murine dendritic cells. *Experimental Parasitology*, *126*(3), 426–434. http://doi.org/10.1016/j.exppara.2010.07.014

Woods, S., Schroeder, J., McGachy, H. A., Plevin, R., Roberts, C. W., & Alexander, J. (2013). MAP kinase phosphatase-2 plays a key role in the control of infection with Toxoplasma gondii by modulating iNOS and arginase-1 activities in mice. *PLoS Pathogens*, *9*(8), e1003535. http://doi.org/10.1371/journal.ppat.1003535

Wu, M., Neilson, A., Swift, A. L., Moran, R., Tamagnine, J., Parslow, D., et al. (2007). Multiparameter metabolic analysis reveals a close link between attenuated mitochondrial bioenergetic function and enhanced glycolysis dependency in human tumor cells. *American Journal of Physiology-Cell Physiology*, *292*(1), C125–C136. http://doi.org/10.1152/ajpcell.00247.2006

Xie, S., Chen, M., Yan, B., He, X., Chen, X., & Li, D. (2014). Identification of a role for the PI3K/AKT/mTOR signaling pathway in innate immune cells. *Plos One*, *9*(4), e94496. http://doi.org/10.1371/journal.pone.0094496

Xu, T., Ping, J., Yu, Y., Yu, F., Yu, Y., Hao, P., & Li, X. (2010). Revealing parasite influence in metabolic pathways in Apicomplexa infected patients. *BMC Bioinformatics*, *11 Suppl 11*(11), S13. http://doi.org/10.1186/1471-2105-11-S11-S13

Yu, T., Wang, Y., Zhang, H., Johnson, C. H., Jiang, Y., Li, X., et al. (2016). Metabolomics reveals mycoplasma contamination interferes with the metabolism of PANC-1 cells. *Analytical and Bioanalytical Chemistry*, *408*(16), 4267–4273. http://doi.org/10.1007/s00216-016-9525-9

Zamai, L., Ahmad, M., Bennett, I. M., Azzoni, L., Alnemri, E. S., & Perussia, B. (1998). Natural Killer (NK) Cell–mediated Cytotoxicity: Differential Use of TRAIL and Fas Ligand by Immature and Mature Primary Human NK Cells. *Journal of Experimental Medicine*, *188*(12), 2375–2380. http://doi.org/10.1084/jem.188.12.2375

Zhao, Yanlin, Marple, A. H., Ferguson, D. J. P., Bzik, D. J., & Yap, G. S. (2014). Avirulent strains of Toxoplasma gondii infect macrophages by active invasion from the phagosome. *Proceedings*

of the National Academy of Sciences of the United States of America, *111*(17), 6437–6442. http://doi.org/10.1073/pnas.1316841111

Zhao, Yanlin, Wilson, D., Matthews, S., & Yap, G. S. (2007). Rapid Elimination of Toxoplasma gondii by Gamma Interferon-Primed Mouse Macrophages Is Independent of CD40 Signaling. *Infection and Immunity*, *75*(10), 4799–4803. http://doi.org/10.1128/IAI.00738-07

Zhou, C.-X., Zhou, D.-H., Elsheikha, H. M., Liu, G.-X., Suo, X., & Zhu, X.-Q. (2015). Global Metabolomic Profiling of Mice Brains following Experimental Infection with the Cyst-Forming Toxoplasma gondii. *Plos One*, *10*(10), e0139635. http://doi.org/10.1371/journal.pone.0139635

Zhou, C.-X., Zhou, D.-H., Elsheikha, H. M., Zhao, Y., Suo, X., & Zhu, X.-Q. (2016). Metabolomic Profiling of Mice Serum during Toxoplasmosis Progression Using Liquid Chromatography-Mass Spectrometry. *Scientific Reports*, *6*, 19557. http://doi.org/10.1038/srep19557

Zhu, L., Zhao, Q., Yang, T., Ding, W., & Zhao, Y. (2015). Cellular Metabolism and Macrophage Functional Polarization. *International Reviews of Immunology*, *34*(1), 82–100. http://doi.org/10.3109/08830185.2014.969421

Zou, C., Wang, Y., & Shen, Z. (2005). 2-NBDG as a fluorescent indicator for direct glucose uptake measurement. *Journal of Biochemical and Biophysical Methods*, *64*(3), 207–215. http://doi.org/10.1016/j.jbbm.2005.08.001

Chapter 8

Appendix

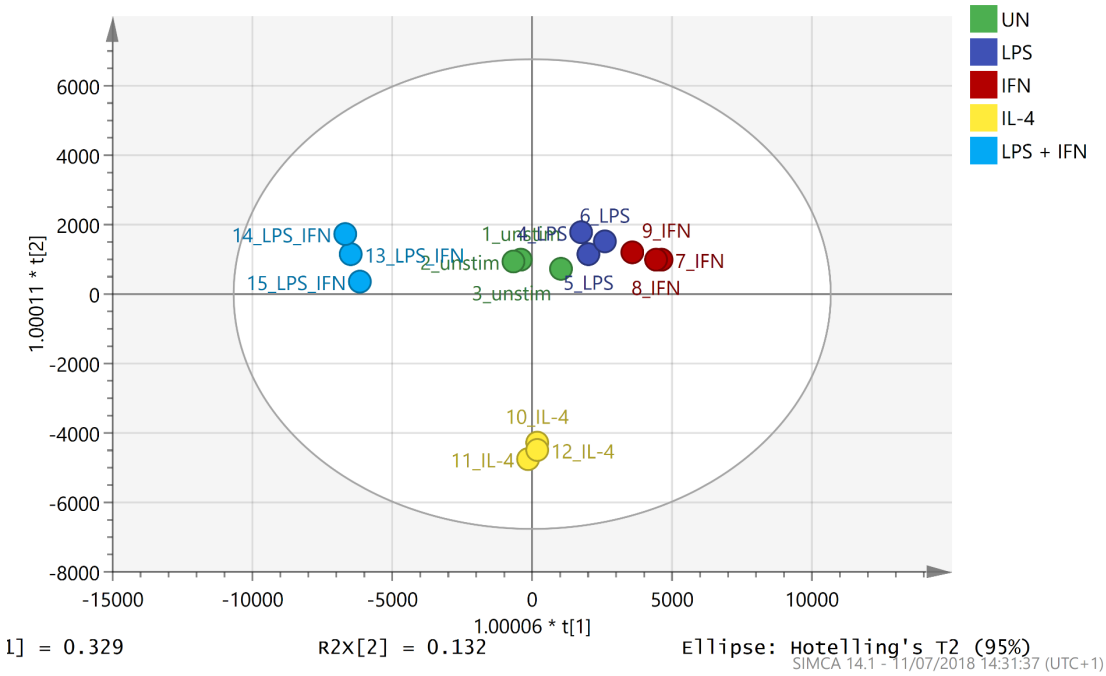

Figure 8.1 Orthogonal Projections to Latent Structures Discriminant Analysis of BMDCs stimulated with LPS, IFN-γ or IL-4. (Biological run 2). Bone marrow derived DCs were stimulated LPS, IFN-γ or IL-4. After this time, the metabolites of the DCs were extracted and run via Liquid chromatography mass spectroscopy (LCMS). The data was then analysed by SIMCA and a Orthogonal Projections to Latent Structures Discriminant Analysis (OPLS-DA) plot was generated. Key: Green, unstimulated; Dark blue, LPS; Red, IFN-γ; Yellow, IL-4 and Light blue, LPS + IFN-γ.

Table 8.1. VIP scores, formula, m/z ratios and retention times of BMDCs activated with LPS, IFN-γ or IL-4.

Metabolite name	Formula	M/z[1]	RT[2]	M1.VIP [4+6+0][3]	2.44693 * M1.VIP [4] cvSE[4]
didesmethyl tocotrienol	C25H36O2	368.27	4.003	10.4661	3.38762
Orthophosphate	H3O4P	97.97	13.35	6.25254	6.12936[6]
Citrate	C6H8O7	192.03	18.3	6.12453	3.76885
Mesaconate	C5H6O4	130.03	15.27	6.0072	1.81045
(R)-Lactate	CH36O3	90.03	9.80	4.71875	1.84347
L-Aspartate	C4H7NO4	15.35	133.04	4.16522	0.422868
Taurine	C2H7NO3S	15.11	125.01	4.01094	1.91337
Phosphonate	H3O3P	13.19	81.98	3.57691	1.52852
(S)-Malate	C4H6O5	16.26	134.02	3.57235	3.00074
O-Acetyl-L-serine	C5H9NO4	15	147.05	3.47418	1.78496
L-1-Pyrroline-3-hydroxy-5-carboxylate	C5H7NO3	10.45	129.04	3.32851	1.23207
Glutathione	C10H17N3O6S	14.66	307.08	3.08722	1.56513
[SP (16:0)] N-(hexadecanoyl)-sphing-4-enine	C34H67NO3	3.981	537.51	2.65325	0.856109
Phosphocreatine	C4H10N3O5P	15.45	211.04	2.27599	0.460029
Theophylline	C7H8N4O2	9.82	90.032	2.10964	2.81174
sn-glycero-3-Phosphoethanolamine	C5H14NO6P	15.91	215.06	2.09417	1.01854
Ethanolamine phosphate	C2H8NO4P	16.25	141.02	2.04952	1.08794
L-Glutamine	C5H10N2O3	15.31	146.07	1.86488	0.797577
N-(L-Arginino) succinate	C10H18N4O6	17.1	290.12	1.77658	0.652732
myo-Inositol	C6H12O6	14.66	180.06	1.74874	0.696057
Sulfate	H2O4S	18.1	97.967	1.66235	0.407945
Succinate	C4H6O4	15.43	118.03	1.59789	0.308169
sn-Glycerol 3-phosphate	C3H9O6P	14.87	172.01	1.57173	0.487452
[FA trihydroxy(4:0)] 2_3_4-trihydroxy-butanoic acid	C4H8O5	12.63	136.04	1.54532	0.833252
ATP	C10H16N5O13P3	16.33	507	1.47544	0.522892
D-Glucosamine	C6H13NO5	11.57	179.08	1.47071	0.441111
[FA (5:1/13:0)] 13-(2-cyclopentenyl)-tridecanoic acid	C18H32O2	3.888	280.24	1.38737	0.634557
L-Gulonate	C6H12O7	13.94	196.06	1.37893	0.745524
2-Oxoglutarate	C5H6O5	15.84	146.02	1.2703	0.326084
3'-Phosphoadenylyl sulfate	C10H15N5O13P2S	16.33	506.99	1.26677	0.979296
Creatine	C4H9N3O2	14.98	131.07	1.2391	0.529488

2-Furoate	C5H4O3	18.29	112.02	1.21503	0.406937
5-Hydroxyisourate	C5H4N4O4	11.52	92.012	1.16044	1.49434
L-Arginine	C6H14N4O2	25.92	174.11	1.15269	0.794265
D-Sorbitol	C6H14O6	14.17	182.08	1.1308	0.356313
[FA hydroxy(6:0)] 6-hydroxy-hexanal	C6H12O2	4.985	116.08	1.11838	0.51621
L-Serine	C3H7NO3	15.76	105.04	1.10113	0.365254
UTP	C9H15N2O15P3	17.66	483.97	1.08881	0.604077
L-Dehydroascorbate	C6H6O6	18.02	174.02	1.08629	0.285279
2-C-Methyl-D-erythritol 4-phosphate	C5H13O7P	14.55	216.04	1.03783	1.57526
[PR] Loroxanthin ester/ Loroxanthin dodecenoate	C52H76O4	4.521	764.58	1.00883	0.517075
UDP-glucose	C15H24N2O17P2	16.61	566.06	0.976127	0.319294
N-Acetyl-L-aspartate	C6H9NO5	14.87	175.05	0.953206	0.545355
[SP (16:0)] N-(hexadecanoyl)-sphinganine	C34H69NO3	3.98	539.53	0.950639	0.662099
L-Citrulline	C6H13N3O3	16.22	175.1	0.940013	0.258818
[PC (15:0)] 1-pentadecanoyl-sn-glycero-3-phosphocholine	C23H48NO7P	4.805	481.32	0.932165	0.562698
6-aza-uridine	C8H11N3O6	15.38	245.06	0.925117	0.443286
L-Leucine	C6H13NO2	11.08	131.09	0.905953	0.737123
[PR] (+)-15-nor-4-thujopsen-3-one	C14H22O	4.155	206.17	0.904191	0.718263
L-Ornithine	C5H12N2O2	22.7	132.09	0.876937	0.1977
allopurinol	C5H4N4O	12.67	136.04	0.871505	0.610457
N-stearoyl glutamine	C23H44N2O4	4.16	206.16	0.870186	0.751156
[PC (15:1)] 1-(1Z-pentadecenyl)-sn-glycero-3-phosphocholine	C23H48NO6P	4.746	465.32	0.867095	0.533002
[FA (20:3)] 8Z_1Z1_14Z-Eicosatrien-5-ynoic acid	C20H30O2	3.971	302.23	0.845798	0.632257
(R)-2-Hydroxyglutarate	C5H8O5	15.43	148.04	0.83493	0.325581
Diacetyl	C4H6O2	7.583	86.037	0.829856	0.861658
[SP (24:0)] N-(15Z-tetracosenoyl)-sphing-4-enine	C42H81NO3	3.942	647.62	0.803521	0.40176
[ST] (22R_25R)-spirosol-5-en-3beta-ol	C27H43NO2	3.97	413.33	0.796073	0.278574
L-Alanine	C3H7NO2	15.04	89.04	0.794513	0.275643
UDP-N-acetyl-D-glucosamine	C17H27N3O17P2	15.4	607.08	0.785286	0.363136

adrenochrome o-semiquinone	C9H10NO3	14.72	180.07	0.781977	0.778221
L-Asparagine	C4H8N2O3	15.6	132.05	0.776196	0.454245
[SP (22:0)] N-(docosanoyl)-sphing-4-enine	C40H79NO3	3.954	621.61	0.769309	0.499132
Pyruvate	C3H4O3	8.275	88.01	0.760384	0.51047
N-Acetyl-L-glutamate	C7H11NO5	9.761	189.06	0.74924	0.377203
[PE (16:1)] 1-(1Z-hexadecenyl)-sn-glycero-3-phosphoethanolamine	C21H44NO6P	4.837	437.29	0.744485	0.598925
Ximaosteroid C	C26H38O3	3.975	398.28	0.735728	0.556407
[PR] bacteriohopane-31_32_33_34-tetrol-35-cyclitol	C41H73NO9	3.968	723.53	0.730611	0.349674
1-Phosphatidyl-1D-myo-inositol3-phosphate	C11H20O16P2	15.89	235.01	0.722662	0.292006
2-Hydroxyethanesulfonate	C2H6O4S	10.89	126	0.712362	0.507633
Kigelinone	C14H10O5	15.26	258.05	0.699282	0.180029
3-phosphoglucarate	C6H11O11P	18.32	290	0.697729	0.178821
[PR] 9_13-di-cis-retinoic acid	C20H28O2	4.041	300.21	0.692376	0.606399
5-Oxoavermectin "2a" aglycone	C34H48O9	4.579	600.33	0.683401	0.570923
Pantothenate	C9H17NO5	8.856	219.11	0.674156	0.377367
7E_9E_11-Dodecatrienyl acetate	C14H22O2	4.019	222.16	0.644897	0.426483
Allantoin	C4H6N4O3	14.03	158.04	0.64189	0.234061
[Fv] Naringenin	C15H12O5	15.03	272.07	0.640858	0.115156
2-Dehydro-3-deoxy-L-rhamnonate	C6H10O5	14.47	162.05	0.640359	0.188112
6-Methylpretetramide	C20H15NO6	11.83	365.09	0.632459	0.536453
D-Glucose 6-phosphate	C6H13O9P	17.09	260.03	0.632139	0.158251
[PS (18:0)] 1-octadecanoyl-sn-glycero-3-phosphoserine	C24H48NO9P	4.493	525.31	0.623219	0.423377
Glycerophosphoglycerol	C6H15O8P	13.06	246.05	0.622984	0.232312
L-Tyrosine	C9H11NO3	13.13	181.07	0.606042	0.238681
Ophiobolin A	C25H36O4	4.036	400.26	0.601909	0.428307
4-Methylene-L-glutamine	C6H10N2O3	13.93	158.07	0.59971	0.296795
L-Glutamate	C5H9NO4	10.95	147.05	0.59164	0.547677
Hydantoin-5-propionate	C6H8N2O4	9.064	172.05	0.588453	0.423188

L-Methionine	C5H11NO2S	11.73	149.05	0.585776	0.252513
1-deoxynojirimycin	C6H13NO4	11.56	163.08	0.577137	0.229225
N-Undecanoylglycine	C13H25NO3	7.47	243.18	0.570744	0.595704
L-Histidine	C6H9N3O2	14.86	155.07	0.570655	0.298001
ethyl propionate	C5H10O2	5.045	102.07	0.565569	0.526147
Cholesterolsulfate	C27H46O4S	3.702	466.31	0.554617	0.533973
1-18:3-2-16:2-monogalactosyldiacylglycerol	C43H70O10	3.661	746.5	0.548609	0.581037
4_5-epoxy-17R-HDHA	C25H34O4	3.681	398.25	0.54561	0.184857
[PG (16:0)] 1-hexadecanoyl-sn-glycero-3-phospho-(1'-sn-glycerol)	C22H45O9P	4.685	484.28	0.545099	0.322113
L-Valine	C5H11NO2	12.77	117.08	0.542589	0.208265
CTP	C9H16N3O14P3	18.14	482.99	0.5416	0.355846
meso-2_6-Diaminoheptanedioate	C7H14N2O4	13.98	190.1	0.5356	0.187259
nonulose 9-phosphate	C9H19O12P	17.14	350.06	0.522813	0.455789
(3R)-hydroxy-N-acetyl-(L)-arginine	C8H16N4O4	13.56	232.12	0.520271	0.209255
5-Hydroxypentanoate	C5H10O3	7.551	118.06	0.514897	0.400311
Hippurate	C9H9NO3	7.815	179.06	0.514027	0.196979
Phenolsulfonphthalein	C19H14O5S	5.126	354.06	0.514	0.364634
[FA hydroxy(26:0)] 2-hydroxy-hexacosanoic acid	C26H52O3	3.709	412.39	0.511841[5]	0.536062

[1] m/z (mass to charge ratio)

[2] RT (retention time)

[3] The value represents the difference between the distinct groups

[4] Value highlights variety between each sample group

[5] The VIP list was limited to 50 metabolites

[6] Glycolysis (green), TCA (blue), OXPHOS (yellow), Arginine metabolism (Orange), undefined (Grey).

Table 8.2. Pairwise analysis between LPS activated and naïve BMDCs

Metabolite	M2.VIP [1+2+0][1]	2.57059 * M2.VIP [1] cvSE[2]
didesmethyl tocotrienol	11.2573	9.17296
Citrate	7.8898	1.22379 [3]
Orthophosphate	7.70323	9.9326
L-Aspartate	5.7159	1.81175
(R)-Lactate	5.4125	2.33317
Taurine	3.87614	2.06259
Phosphonate	3.76085	4.36883
[SP (16:0)] N-(hexadecanoyl)-sphing-4-enine	3.62015	2.12584
(S)-Malate	3.12235	1.34501
3_5_7_11_13_15-heptaoxo-9-hydroxy-heptadecanoyl-[acp]	2.78179	4.57918
Phosphocreatine	2.57015	1.3442
O-Acetyl-L-serine	2.54773	1.89493
Mesaconate	2.26007	2.58438
Glutathione	2.15674	2.74353
sn-glycero-3-Phosphoethanolamine	1.86191	0.989738
N-(L-Arginino)succinate	1.72776	0.409015
L-Gulonate	1.69694	0.965702
L-1-Pyrroline-3-hydroxy-5-carboxylate	1.68518	1.15315
2-Furoate	1.66083	0.224661
[FA trihydroxy(4:0)] 2_3_4-trihydroxy-butanoic acid	1.56081	0.938356
Ethanolamine phosphate	1.51414	1.70635
2-Oxoglutarate	1.49007	0.828047
ATP	1.47893	0.604303
5-Hydroxyisourate	1.22179	2.07419
[SP (16:0)] N-(hexadecanoyl)-sphinganine	1.17249	0.596595
sn-Glycerol 3-phosphate	1.12585	0.446841
Theophylline	1.07619	2.55704
Sulfate	1.05244	0.994453
D-Glucosamine	1.04909	1.22637
[PR] Loroxanthin ester/ Loroxanthin dodecenoate	0.991609	0.641134
[PR] (+)-15-nor-4-thujopsen-3-one	0.986028	0.433718
L-Dehydroascorbate	0.979816	0.563892
Kigelinone	0.967035	0.320848
[SP (24:0)] N-(15Z-tetracosenoyl)-sphing-4-enine	0.957529	0.670057
3-phosphoglucarate	0.949205	0.248219
L-Arginine	0.922966	0.890674
2-Dehydro-3-deoxy-L-rhamnonate	0.921257	0.193519
HEPES	0.897143	0.399644
L-Citrulline	0.888065	0.129228

[PC (15:0)] 1-pentadecanoyl-sn-glycero-3-phosphocholine	0.886362	0.564436
Succinate	0.865566	1.00465
2-C-Methyl-D-erythritol 4-phosphate	0.854602	1.84821
Ximaosteroid C	0.843803	0.70531
D-Glucose 6-phosphate	0.843397	0.141862
[SP (22:0)] N-(docosanoyl)-sphing-4-enine	0.823822	0.74129
Diacetyl	0.821008	1.41025
L-Leucine	0.799156	0.229294
[FA hydroxy(6:0)] 6-hydroxy-hexanal	0.788668	1.06635
L-Glutamine	0.785416[4]	0.40355

Table 8.3 Pairwise analysis between IFN-γ treated and naïve BMDCs

Metabolite	M3.VIP[1+3+0][1]	2.57059 * M3.VIP[1]cvSE[2]
didesmethyl tocotrienol	13.2266	7.01269
Orthophosphate	8.6168	4.07899 [3]
Mesaconate	6.1351	2.49409
Taurine	5.49167	1.89195
Citrate	4.52238	1.73394
Phosphonate	4.25154	5.09851
(R)-Lactate	2.68148	2.71196
sn-glycero-3-Phosphoethanolamine	2.55608	1.1792
[SP (16:0)] N-(hexadecanoyl)-sphing-4-enine	2.52097	3.14641
Glutathione	2.5136	4.05732
L-1-Pyrroline-3-hydroxy-5-carboxylate	2.27502	3.04869
3_5_7_11_13_15-heptaoxo-9-hydroxy-heptadecanoyl-[acp]	2.27237	3.08007
(S)-Malate	2.05085	2.05573
Ethanolamine phosphate	1.89385	1.54004
L-Aspartate	1.86075	1.44174
ATP	1.75011	1.5102
Succinate	1.6923	0.846606
L-Gulonate	1.65588	0.927545
Theophylline	1.48155	2.05856
sn-Glycerol 3-phosphate	1.3758	0.376191
[FA hydroxy(6:0)] 6-hydroxy-hexanal	1.27062	0.947645
L-Dehydroascorbate	1.22003	1.17417
Phosphocreatine	1.15198	2.15132
N-stearoyl glutamine	1.14344	1.07381
O-Acetyl-L-serine	1.14061	1.6848
[PC (15:0)] 1-pentadecanoyl-sn-glycero-3-phosphocholine	1.10249	0.748104
3'-Phosphoadenylyl sulfate	1.08855	0.904675

2-Oxoglutarate	1.08087	0.808404
6-aza-uridine	1.0438	0.482835
L-Glutamine	0.991892	1.23952
[FA trihydroxy(4:0)] 2_3_4-trihydroxy-butanoic acid	0.960037	0.967364
[PR] Loroxanthin ester/ Loroxanthin dodecenoate	0.943123	0.897503
[PR] (+)-15-nor-4-thujopsen-3-one	0.933961	1.33564
2-Furoate	0.933845	0.387619
UDP-glucose	0.917017	0.344494
L-Serine	0.901399	0.698708
L-Arginine	0.900776	0.896859
Diacetyl	0.88792	0.961769
Creatine	0.876355	1.03938
myo-Inositol	0.851577	1.22983
[PR] bacteriohopane-31_32_33_34-tetrol-35-cyclitol	0.850686	0.799023
[SP (16:0)] N-(hexadecanoyl)-sphinganine	0.84421	0.957703
allopurinol	0.822189	0.649971
5-Oxoavermectin "2a" aglycone	0.797462	0.966461
N-(L-Arginino)succinate	0.790501	0.153688
D-Glucose 6-phosphate	0.781176	0.421179
N-Undecanoylglycine	0.78117	0.733915
[PR] 9_13-di-cis-retinoic acid	0.769081	1.36768
2-Dehydro-3-deoxy-L-rhamnonate	0.758535	0.46751
UTP	0.755552 [4]	0.605951

Table 8.4. Pairwise analysis between LPS + IFN-γ stimulated and naïve BMDCs

Metabolite	M4.VIP[1+2+0][1]	2.57059 * M4.VIP[1]cvSE[2]
didesmethyl tocotrienol	13.5924	6.15841
Orthophosphate	6.81431	9.66283 [3]
L-Aspartate	5.1529	0.963876
Citrate	5.14428	3.61211
Mesaconate	4.86252	1.95671
(S)-Malate	4.49033	2.91305
(R)-Lactate	4.45773	1.17245
Taurine	3.69823	1.8217
[SP (16:0)] N-(hexadecanoyl)-sphing-4-enine	3.59273	2.04563
O-Acetyl-L-serine	2.32267	1.28844
N-(L-Arginino)succinate	2.2077	0.698937
[FA trihydroxy(4:0)] 2_3_4-trihydroxy-butanoic acid	2.10423	0.852444

L-1-Pyrroline-3-hydroxy-5-carboxylate	2.10354	1.35859
sn-glycero-3-Phosphoethanolamine	1.94889	0.833824
Theophylline	1.9225	2.72038
3_5_7_11_13_15-heptaoxo-9-hydroxy-heptadecanoyl-[acp]	1.91942	2.28695
Phosphonate	1.88481	3.06225
L-Gulonate	1.84872	1.14797
Glutathione	1.68743	1.78237
Phosphocreatine	1.67785	1.22509
sn-Glycerol 3-phosphate	1.64613	0.64806
2-Furoate	1.42621	0.154988
[FA (5:1/13:0)] 13-(2-cyclopentenyl)-tridecanoic acid	1.33121	0.330513
[SP (16:0)] N-(hexadecanoyl)-sphinganine	1.31421	0.92709
Succinate	1.17618	0.743058
L-Citrulline	1.155	0.235332
2-Oxoglutarate	1.11648	0.510319
[SP (24:0)] N-(15Z-tetracosenoyl)-sphing-4-enine	1.03279	0.575181
L-Glutamine	1.01573	0.704019
[SP (22:0)] N-(docosanoyl)-sphing-4-enine	0.983973	0.741623
D-Glucosamine	0.953822	0.793602
Ethanolamine phosphate	0.942444	0.728396
2-Dehydro-3-deoxy-L-rhamnonate	0.921793	0.360501
[ST] (22R_25R)-spirosol-5-en-3beta-ol	0.919971	0.244427
Sulfate	0.913868	1.21624
D-Glucose 6-phosphate	0.860108	0.082029
ATP	0.851498	0.523532
allopurinol	0.846101	0.940455
3'-Phosphoadenylyl sulfate	0.845095	1.14893
[PR] Loroxanthin ester/ Loroxanthin dodecenoate	0.825227	0.809766
myo-Inositol	0.80123	0.976888
[FA hydroxy(6:0)] 6-hydroxy-hexanal	0.770628	0.837306
Kigelinone	0.767382	0.398831
L-Glutamate	0.762635	0.700496
N-Acetyl-L-aspartate	0.759207	0.673096
3-phosphoglucarate	0.728284	0.191556
L-Leucine	0.714561	0.926042
[PC (15:0)] 1-pentadecanoyl-sn-glycero-3-phosphocholine	0.680159	0.763292
adrenochrome o-semiquinone	0.67796 [4]	0.512882

Table 8.5. Pairwise analysis between IL-4 treated and naïve BMDCs

Metabolite	M5.VIP[1+0+0][1]	2.57059 * M5.VIP[1]cvSE[2]
didesmethyl tocotrienol	14.9058	8.25166
Orthophosphate	6.25671	10.2204 [3]
(R)-Lactate	5.41086	0.399578
L-1-Pyrroline-3-hydroxy-5-carboxylate	4.40195	0.413355
Taurine	4.07987	1.73787
Glutathione	3.74849	1.67365
Mesaconate	3.39725	2.01982
Citrate	3.23208	0.558475
O-Acetyl-L-serine	3.036	2.978
Phosphonate	2.89036	4.3606
L-Aspartate	2.5983	1.23082
(S)-Malate	2.53836	1.22474
L-Glutamine	2.30598	0.67935
myo-Inositol	1.91737	0.356454
Sulfate	1.8015	0.392597
ATP	1.78381	1.19133
Phosphocreatine	1.75675	0.79391
[SP (16:0)] N-(hexadecanoyl)-sphing-4-enine	1.74437	4.09648
L-Arginine	1.53848	0.60248
Succinate	1.51547	0.307003
D-Glucosamine	1.46942	0.517295
sn-glycero-3-Phosphoethanolamine	1.45399	1.07628
L-Dehydroascorbate	1.28701	0.459664
3_5_7_11_13_15-heptaoxo-9-hydroxy-heptadecanoyl-[acp]	1.28523	1.52701
D-Sorbitol	1.27762	0.723095
L-Leucine	1.24655	0.743758
[FA trihydroxy(4:0)] 2_3_4-trihydroxy-butanoic acid	1.21909	0.978151
L-Gulonate	1.15328	0.566682
[PR] (+)-15-nor-4-thujopsen-3-one	1.12549	1.86627
[PR] Loroxanthin ester/ Loroxanthin dodecenoate	1.09821	1.77108
N-Acetyl-L-aspartate	1.07261	0.439362
Creatine	0.992331	0.409113
L-Ornithine	0.964252	0.148201
UTP	0.960244	0.732232
D-Glucose 6-phosphate	0.913657	0.294139
L-Serine	0.912234	0.269402
(R)-2-Hydroxyglutarate	0.870607	0.415733
Glycerophosphoglycerol	0.869458	0.244983
L-Asparagine	0.846526	0.153677

[PR] bacteriohopane-31_32_33_34-tetrol-35-cyclitol	0.844781	0.626609
2-Hydroxyethanesulfonate	0.84386	1.12182
Ximaosteroid C	0.829948	0.519745
L-Alanine	0.817589	0.08889
Ophiobolin A	0.800764	0.616474
Pantothenate	0.796946	0.339871
L-Histidine	0.769978	0.2848
2-Oxoglutarate	0.765379	0.597971
N-Acetyl-L-glutamate	0.750776	0.359194
6-aza-uridine	0.748143 [4]	0.382427

[1] The value represents the difference between the distinct groups

[2] the value highlights variety within each sample group

[3] Metabolites from each metabolite are highlighted in the VIP table where glycolysis is coloured green, TCA cycle; blue, OXPHOS; yellow and arginine metabolism; orange.

[4] VIP score list was limited to 50 metabolites but show that the top metabolites do not differ even if the VIP score does

Table 8.6. VIP score of BMDCs treated with LPS, IFN-γ, LPS+IFN-γ or IL-4 (Biological run 2)

Metabolite	M1.VIP[4+5+0][1]	2.44693 * M1.VIP[4]cvSE[2]
didesmethyl tocotrienol	10.632	2.47086
[FA methyl(17:0)] 15-methyl-heptadecanoic acid	8.98958	5.09148
[SP (16:0)] N-(hexadecanoyl)-sphing-4-enine	5.72937	2.0372
Glycerone	5.07724	3.2673
2_5-Dioxopentanoate	3.51052	1.76449
Citrate	3.44473	1.60767
(S)-Malate	3.02763	1.33553
L-Aspartate	2.92466	0.937892
Glutathione	2.85937	1.28952
L-Glutamate	2.27705	0.601241
Taurine	2.21486	1.17026
[SP (16:0)] N-(hexadecanoyl)-sphinganine	1.93943	1.06856
2-C-Methyl-D-erythritol 4-phosphate	1.89265	2.41382
L-Glutamine	1.78093	1.00282
[PS (18:0/20:4)] 1-octadecanoyl-2-(5Z_8Z_11Z_14Z-eicosatetraenoyl)-sn-glycero-3-phosphoserine	1.7748	0.470942
[PC (15:1)] 1-(1Z-pentadecenyl)-sn-glycero-3-phosphocholine	1.77423	0.768166
3R_5S-Dimethyldodecanoic acid	1.74874	1.09822
N-Acetylneuraminate	1.66094	2.3919
[PC (15:0)] 1-pentadecanoyl-sn-glycero-3-phosphocholine	1.63092	1.16573
[SP (24:0)] N-(15Z-tetracosenoyl)-sphing-4-enine	1.62789	0.707481
[FA methyl(11:0)] 3-methyl-undecanoic acid	1.61635	1.33808
4-Oxoproline	1.56946	1.26006
[SP (22:0)] N-(docosanoyl)-sphing-4-enine	1.55455	0.657635
[FA trihydroxy(4:0)] 2_3_4-trihydroxy-butanoic acid	1.55082	0.509427
Urate	1.47884	0.937552
[SP (24:0)] N-(tetracosanoyl)-sphing-4-enine	1.40271	0.537679
sn-Glycerol 3-phosphate	1.33121	0.86595
Phenolsulfonphthalein	1.22553	1.09186
[PE (16:1)] 1-(1Z-hexadecenyl)-sn-glycero-3-phosphoethanolamine	1.2237	0.70353
Succinate	1.17794	0.239602
[PS (18:0)] 1-octadecanoyl-sn-glycero-3-phosphoserine	1.14269	1.31049
[PI (18:0)] 1-octadecanoyl-sn-glycero-3-phospho-(1'-myo-inositol)	1.11285	0.947557

alpha-Irone	1.10157	0.261384
[PE (18:1/20:4)] 1-(1Z-octadecenyl)-2-(5Z_8Z_11Z_14Z-eicosatetraenoyl)-sn-glycero-3-phosphoethanolamine	1.06336	0.616226
[SP (18:0)] N-(octadecanoyl)-sphing-4-enine	1.05504	0.499518
N-(L-Arginino)succinate	1.04539	0.755514
L-Isoleucine	1.02747	0.825683
Octyl acetate	1.00723	0.986551
2-Furoate	1.00571	0.499686
[PG (18:0/22:6)] 1-octadecanoyl-2-(4Z_7Z_10Z_13Z_16Z_19Z-docosahexaenoyl)-sn-glycero-3-phospho-(1'-sn-glycerol)	1.00084	0.231226
[FA trimethyl(12:0)] 3_7_11-trimethyl-dodecanoic acid	0.997667	0.652788
[PS (16:0/18:1)] 1-hexadecanoyl-2-(9Z-octadecenoyl)-sn-glycero-3-phosphoserine	0.99297	0.249798
[SP (16:0)] N-(hexadecanoyl)-sphing-4-enine-1-phosphate	0.985767	0.96658
(R)-Malate	0.977582	1.17532
Ethanolamine phosphate	0.967677	0.642917
Phytanate	0.959544	0.524008
HEPES	0.95328	0.461932
L-Asparagine	0.946114	0.362086
3-Dehydro-L-threonate	0.937675	1.13156
sn-glycero-3-Phosphoethanolamine	0.935401	0.541365
[PC (15:0/20:4)] 1-pentadecanoyl-2-(5Z_8Z_11Z_14Z-eicosatetraenoyl)-sn-glycero-3-phosphocholine	0.905659	0.552345
[PG (16:0/18:1)] 1-Hexadecanoyl-2-(9Z-octadecenoyl)-sn-glycero-3-phospho-sn-glycerol	0.869891	0.165786
L-Citrulline	0.867927[3]	0.410004

---

[1] The value represents the difference between the distinct groups

[2] the value highlights variety within each sample group

[3] VIP score list was limited to 50 metabolites but show that the top metabolites are similar between biological runs

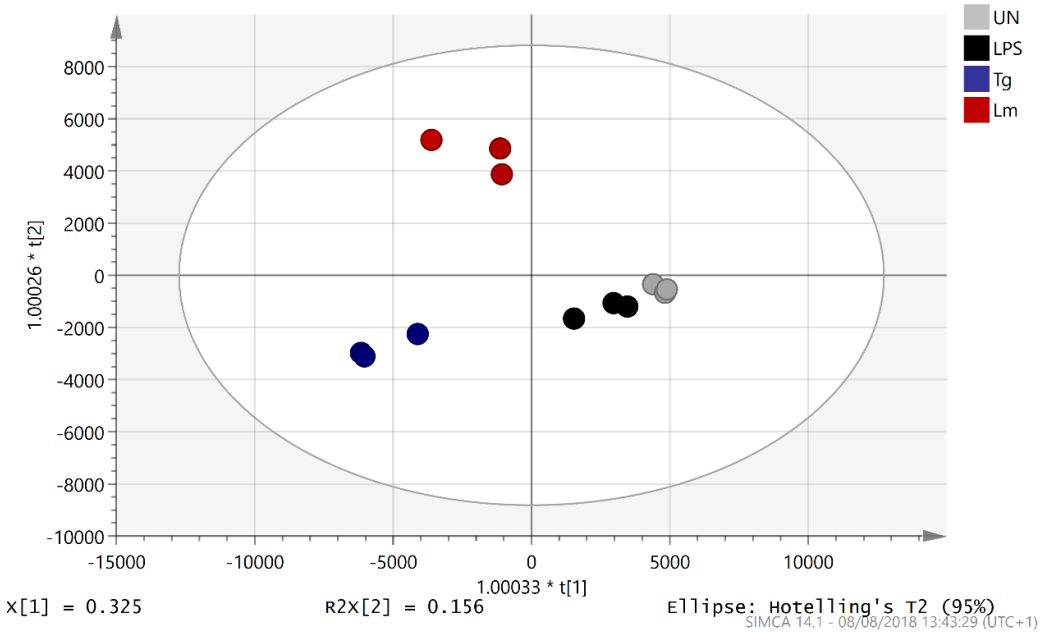
UN
LPS
Tg
Lm
8000
6000
4000
2000
0
-2000
-4000
-6000
-8000
-10000
1.00026 * t[2]
-15000
-10000
-5000
0
5000
10000
1.00033 * t[1]
X[1] = 0.325
R2X[2] = 0.156
Ellipse: Hotelling's T2 (95%)
SIMCA 14.1 - 08/08/2018 13:43:29 (UTC+1)

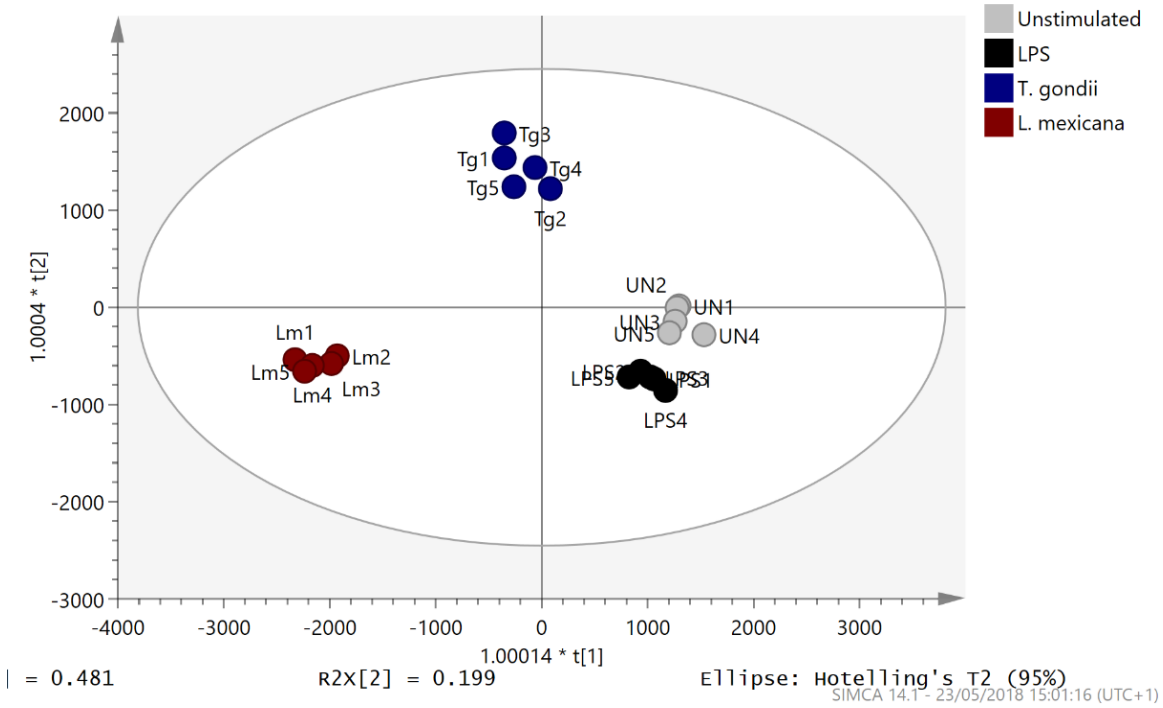
Unstimulated
LPS
T. gondii
L. mexicana
2000
1000
0
-1000
-2000
-3000
1.0004 * t[2]
Tg3
Tg1
Tg4
Tg5
Tg2
UN2
UN1
UN3
UN5
UN4
Lm1
Lm2
Lm5
Lm4
Lm3
LPS4
-4000
-3000
-2000
-1000
0
1000
2000
3000
1.00014 * t[1]
= 0.481
R2X[2] = 0.199
Ellipse: Hotelling's T2 (95%)
SIMCA 14.1 - 23/05/2018 15:01:16 (UTC+1)

Figure 8.2. Orthogonal Projections to Latent Structures Discriminant Analysis of DCs co-cultured with *L. mexicana* or *T. gondii* (Biological run 2 and run 3). Bone marrow derived DCs were stimulated with LPS or co-cultured *with L. mexicana* or *T. gondii* for 24 hours. After this time, the metabolites of the DCs were extracted and run via Liquid chromatography mass spectroscopy (LCMS). The data was then analysed by SIMCA and a Orthogonal Projections to Latent Structures Discriminant Analysis (OPLS-DA) plot was generated. Key: grey, Unstimulated; black, LPS; red, *L. mexicana*; blue, *T. gondii*. The confidence ellipses are based on Hotelling's $T^2 = 95$.

Table 8.7. VIP scores, formula, m/z ratios and retention times of DCs activated with LPS or infected with *L. mexicana* or *T. gondii* (Biological run 1).

Metabolite Name	Formula	M/z[1]	RT[2]	M1.VIP[3+2+0][3]	2.44693 * M1.VIP[3]cvSE[4]
Creatine	C4H9N3O2	131.069498	11.86063334	7.17638	1.91735 [5]
sn-glycero-3-Phosphocholine	C8H20NO6P	257.102618	11.35021386	5.37841	1.12957
Choline phosphate	C5H14NO4P	183.066141	11.5056483	5.21489	1.82639
L-Proline	C5H9NO2	115.063348	10.70280649	3.87489	1.71911
5-Aminopentanoate	C5H11NO2	117.078974	9.649227792	3.22087	2.24294
L-Glutamine	C5H10N2O3	146.069138	12.0099333	2.84404	0.998226
(R)-Lactate	C3H6O3	90.0317493	9.032497265	2.30119	0.843689
4-Aminobutanoate	C4H9NO2	103.063327	12.13145825	2.0425	0.564119
2-C-Methyl-D-erythritol 4-phosphate	C5H13O7P	216.040423	12.26576199	1.8991	1.32314
L-Arginine	C6H14N4O2	174.111751	18.7848886	1.73945	1.24658
L-Leucine	C6H13NO2	131.09467	9.465870327	1.71549	0.897266
Hexadecanoic acid	C16H32O2	256.240375	3.357800943	1.58732	1.25919
Choline	C5H13NO	103.0997	16.60569356	1.55346	0.704989
Creatinine	C4H7N3O	113.058972	8.701228559	1.52422	0.870155
L-Carnitine	C7H15NO3	161.105234	10.78948336	1.50131	1.55855
L-Glutamate 5-semialdehyde	C5H9NO3	131.058381	11.72101932	1.40209	0.626307
L-1-Pyrroline-3-hydroxy-5-carboxylate	C5H7NO3	129.042676	9.29643792	1.39383	0.691196
(S)-Malate	C4H6O5	134.021658	12.72153049	1.37848	0.97326
L-Citrulline	C6H13N3O3	175.095769	12.41556662	1.37413	0.483455
Citrate	C6H8O7	192.027324	13.63994627	1.31064	0.762461
(R)-2-Hydroxyglutarate	C5H8O5	148.037384	12.06612131	1.29479	0.43532
O-Acetylcarnitine	C9H17NO4	203.115907	9.175302802	1.26889	0.50991
4-Trimethylammoniobutanoate	C7H15NO2	145.110327	10.75164258	1.21407	0.595506
L-Ornithine	C5H12N2O2	132.089898	16.3770314	1.18294	0.501147

Ovothiol A	C7H11N3O2S	201.057259	12.30491672	1.16876	0.351902
Orthophosphate	H3O4P	97.9770722	12.256938	1.15714	0.70353
L-Glutamate	C5H9NO4	147.053173	11.79031389	1.13522	0.618048
Itaconate	C5H6O4	130.026729	12.16640371	1.05636	0.552976
L-Methionine	C5H11NO2S	149.051109	9.871672171	0.98744	0.43954
L-Lysine	C6H14N2O2	146.105559	16.560107 37	0.976152	0.294933
4-Imidazolone-5-propanoate	C6H8N2O3	156.053577	9.931910084	0.968625	0.290111
L-Phenylalanine	C9H11NO2	165.079079	8.872741699	0.925302	0.465894
N6_N6_N6-Trimethyl-L-lysine	C9H20N2O2	188.152539	15.821036 05	0.914794	0.260297
Guanidinoacetate	C3H7N3O2	117.053826	12.7453602	0.859735	1.17965
Dimethisterone	C23H32O2	340.240789	3.22511762	0.856961	0.458559
Taurine	C2H7NO3S	125.014725	12.48435579	0.843562	0.753297
2-Acetolactate	C5H8O4	132.042363	11.86290272	0.806231	0.235882
L-Aspartate	C4H7NO4	133.03763	12.02827312	0.804333	0.465368
L-Pipecolate	C6H11NO2	129.079049	10.45308894	0.79522	0.290124
Glutathione	C10H17N3O6S	307.083681	11.47389721	0.738408	0.336809
[FA trihydroxy(4:0)] 2_3_4-trihydroxy-butanoic acid	C4H8O5	136.037315	10.84983984	0.710498	0.319564
Triethanolamine	C6H15NO3	149.105258	8.209045382	0.679535	0.941787
Bis(2-ethylhexyl)phthalate	C24H38O4	390.276888	3.252543513	0.673367	0.292212
Pyridoxine	C8H11NO3	169.073977	7.228682398	0.664359	0.437778
L-Alanine	C3H7NO2	89.0477136	12.13384637	0.660627	0.720882
N2-(D-1-Carboxyethyl)-L-arginine	C9H18N4O4	246.132897	11.2991941	0.656837	0.23401
myo-Inositol	C6H12O6	180.063709	13.44038894	0.64964	0.16835
4-Guanidinobutanoate	C5H11N3O2	145.085158	12.10323978	0.630218	0.112236
N-Acetyl-L-histidine	C8H11N3O3	197.080147	8.168723156	0.592159	0.328684
LL-2_6-Diaminoheptanedioate	C7H14N2O4	190.09543	11.02030006	0.580204 [6]	0.119633

[1] m/z (mass to charge ratio)

[2] RT (retention time)

[3] The value represents the difference between the distinct groups

[4] Value highlights variety between each sample group

[5] Glycolysis (green), TCA (blue), OXPHOS (yellow), Arginine metabolism (Orange), undefined (Grey).

[6] The VIP list was limited to 50 metabolites

Table 8.8. Pairwise analysis between LPS stimulated and naïve BMDCs

Metabolite	M1.VIP[1+2+0][1]	2.57059 * M1.VIP[1]cvSE[2]
Creatine	6.3808	3.18602
sn-glycero-3-Phosphocholine	5.79294	2.09949
L-Proline	4.78237	1.32636 [3]
L-Glutamine	3.6562	1.21007
5-Aminopentanoate	3.62745	4.36732
(R)-Lactate	3.07121	0.552185
Choline phosphate	2.32226	3.92437
Hexadecanoic acid	2.14372	1.9965
L-Arginine	2.04938	1.4134
L-Leucine	2.02796	0.759566
L-Citrulline	1.8282	0.268927
(S)-Malate	1.81556	0.70968
L-1-Pyrroline-3-hydroxy-5-carboxylate	1.79401	1.14217
Citrate	1.70937	0.432366
O-Acetylcarnitine	1.69219	1.17336
L-Ornithine	1.68615	0.649887
4-Trimethylammoniobutanoate	1.65289	1.06466
L-Carnitine	1.63514	2.54921
L-Glutamate	1.32708	1.55263
L-Glutamate 5-semialdehyde	1.32572	0.474043
Creatinine	1.25666	1.07967
Dimethisterone	1.1949	0.926273
L-Methionine	1.14539	0.456413
Itaconate	1.13803	1.32046
Guanidinoacetate	1.09384	1.71369
L-Phenylalanine	1.07525	0.245463
Taurine	1.04082	1.57372
2-C-Methyl-D-erythritol 4-phosphate	1.02918	1.79602
L-Aspartate	1.00358	0.30503
Choline	0.95457	1.16894
Orthophosphate	0.947722	1.40492
N2-(D-1-Carboxyethyl)-L-arginine	0.809032	0.0792187
N6_N6_N6-Trimethyl-L-lysine	0.80748	0.402302
LL-2_6-Diaminoheptanedioate	0.780014	0.261569
Triethanolamine	0.76807	1.95475
L-Alanine	0.763904	0.815921
Imidazole-4-acetate	0.731588	0.120605
N-(omega)-Hydroxyarginine	0.710251	0.154233
L-Threonine	0.708113	0.116189
4-Guanidinobutanoate	0.698755	0.427768
Glutathione	0.688964	1.13186

4-Aminobutanoate	0.663716	0.629633
N-Acetyl-L-histidine	0.613333	0.30308
Pyridoxine	0.596566	0.546327
N(pi)-Methyl-L-histidine	0.588798	0.242497
sn-glycero-3-Phosphoethanolamine	0.578397	0.266971
L-Tyrosine	0.554168	0.148588
5-Guanidino-2-oxopentanoate	0.528328	0.0875291
L-4-Hydroxyglutamate semialdehyde	0.509195 [4]	0.280166

Table 8.9. Pairwise analysis between *T. gondii* infected and naïve BMDC cultures

Metabolite	M2.VIP[1+3+0][1]	2.57059 * M2.VIP[1]cvSE[2]
Choline phosphate	6.76561	1.69423
Creatine	5.8087	1.69916 [3]
L-Proline	5.01163	2.40337
sn-glycero-3-Phosphocholine	4.73618	1.5894
L-Glutamine	3.50525	0.844527
(R)-Lactate	2.50828	0.988988
2-C-Methyl-D-erythritol 4-phosphate	2.38283	1.99676
L-Leucine	2.33065	0.923908
Creatinine	2.12574	0.883704
5-Aminopentanoate	2.02457	1.52706
L-Glutamate 5-semialdehyde	1.93553	0.31568
L-1-Pyrroline-3-hydroxy-5-carboxylate	1.64142	0.764856
Hexadecanoic acid	1.52687	1.25065
Orthophosphate	1.37493	0.806918
4-Aminobutanoate	1.3434	0.127449
L-Methionine	1.32596	0.60832
O-Acetylcarnitine	1.27266	0.436977
L-Phenylalanine	1.24928	0.588447
L-Ornithine	1.19816	1.1703
L-Arginine	1.00167	0.670487
(S)-Malate	0.967498	0.13752
L-Glutamate	0.939875	0.122805
Taurine	0.935706	0.535007
4-Trimethylammoniobutanoate	0.933063	0.509923
Pyridoxine	0.906283	0.421611
Citrate	0.849383	0.472178
L-Carnitine	0.829259	0.613708
N6_N6_N6-Trimethyl-L-lysine	0.812306	0.241484
N-Acetyl-L-histidine	0.809274	0.255653
Glutathione	0.808115	0.223587

L-Threonine	0.757361	0.104131
Choline	0.729203	0.196104
L-Tyrosine	0.698689	0.268397
Itaconate	0.69624	0.626784
LL-2_6-Diaminoheptanedioate	0.638327	0.263085
L-Alanine	0.635326	0.343015
Guanidinoacetate	0.568336	0.850776
N(pi)-Methyl-L-histidine	0.527641	0.285239
Dimethisterone	0.498988	0.515432
L-Aspartate	0.461348	0.0754728
4-Guanidinobutanoate	0.406417	0.265405
Imidazole-4-acetate	0.337415	0.1142
5-Guanidino-2-oxopentanoate	0.317114	0.0671731
sn-glycero-3-Phosphoethanolamine	0.294295	0.301633
L-4-Hydroxyglutamate semialdehyde	0.293947	0.162372
Triethanolamine	0.252115	0.704541
L-Citrulline	0.226159	0.0918497
N2-(D-1-Carboxyethyl)-L-arginine	0.114314 [4]	0.0739838

Table 8.10. Pairwise analysis between *L. mexicana* infected and naïve BMDC cultures

Metabolite	M3.VIP[1+0+0][1]	2.57059 * M3.VIP[1]cvSE[2]
Creatine	9.95592	0.502715
sn-glycero-3-Phosphocholine	5.2806	1.02497
L-Proline	3.54672	1.2187 [3]
4-Aminobutanoate	2.58529	0.17082
L-Glutamine	2.5349	0.883088
5-Aminopentanoate	1.97695	1.27055
(R)-Lactate	1.86841	0.37305
Choline	1.86767	0.573268
Choline phosphate	1.83599	3.3188
(R)-2-Hydroxyglutarate	1.62554	0.304145
Ovothiol A	1.4559	0.212964
L-Leucine	1.43149	1.30569
Hexadecanoic acid	1.43108	1.27057
L-Ornithine	1.29436	0.852413
N6_N6_N6-Trimethyl-L-lysine	1.28762	0.176841
Creatinine	1.28055	0.701864
2-C-Methyl-D-erythritol 4-phosphate	1.26301	1.06044
L-Lysine	1.25202	0.122145
4-Imidazolone-5-propanoate	1.22586	0.195297
L-Methionine	1.12783	0.384809

L-Glutamate 5-semialdehyde	1.06999	0.303993
L-1-Pyrroline-3-hydroxy-5-carboxylate	1.06087	0.397847
L-Carnitine	1.05488	0.601888
L-Citrulline	1.03518	0.193579
2-Acetolactate	1.00153	0.156837
L-Pipecolate	0.988557	0.254893
L-Glutamate	0.965105	0.243124
O-Acetylcarnitine	0.89164	0.345433
4-Trimethylammoniobutanoate	0.889649	0.262873
L-Phenylalanine	0.88948	0.323124
4-Guanidinobutanoate	0.856797	0.0987925
myo-Inositol	0.824477	0.0911691
[FA trihydroxy(4:0)] 2_3_4-trihydroxy-butanoic acid	0.823658	0.0645247
Bis(2-ethylhexyl)phthalate	0.80081	0.187371
LL-2_6-Diaminoheptanedioate	0.747847	0.128202
Orthophosphate	0.737497	0.903205
Itaconate	0.726568	0.697535
(S)-Malate	0.688201	0.701685
2-Butenoate	0.669339	0.0488705
L-Arginine	0.656601	1.40744
1-deoxyxylonojirimycin	0.651469	0.281391
L-Threonine	0.627637	0.153933
Nicotinate	0.626426	0.115551
Citrate	0.624738	0.290151
Trypanothione disulfide	0.613325	0.0706787
L-Tyrosine	0.516373	0.110953
Dimethisterone	0.500745	0.748867
5-Guanidino-2-oxopentanoate	0.457751	0.0396509
1-O-Methyl-myo-inositol	0.442977 [4]	0.290144

[1] The value represents the difference between the distinct groups

[2] The value highlights variety within each sample group

[3] Metabolites from each metabolite are highlighted in the VIP table where glycolysis is coloured green, TCA cycle; blue, OXPHOS; purple, arginine metabolism; orange and parasite specific metabolites; yellow.

[4] VIP score list was limited to 50 metabolites but show that the top metabolites do not differ even if the VIP score does

Table 8.11. VIP scores of DCs activated with LPS or infected with *L. mexicana* or *T. gondii* (Biological run 2).

Metabolite	M1.VIP [3+3+0][1]	2.44693 * M1.VIP [3] cvSE[2]
Octadecanoic acid	6.92035	2.25152
Hexadecanoic acid	6.61347	1.88258
didesmethyl tocotrienol	6.49026	4.76331
2_5-Dioxopentanoate	6.30504	2.03173
Glycerone	6.07233	3.90186
D-Glutamate	3.76015	1.57781
Linoleate	3.60454	0.986675
Citrate	3.58015	1.78089
Glutathione	3.53062	0.978414
Orthophosphate	3.45619	1.7797
4-Oxoproline	3.19143	1.23627
D-Arabinono-1_4-lactone	2.99552	1.05811
HEPES	2.84961	1.2177
L-Glutamine	2.8192	0.664909
[FA (18:1)] 9Z-octadecenoic acid	2.75407	0.530661
Orthophosphate	2.66808	0.992168
(S)-Malate	2.60406	1.28826
Mannitol	2.1677	0.663042
Taurine	2.09352	0.834373
Sulfate	2.0154	0.557808
N-Acetyl-L-aspartate	1.99124	0.670239
D-Fructose	1.98404	0.622456
L-Aspartate	1.95942	1.29243
ATP	1.85521	0.663689
Tetradecanoic acid	1.83193	0.518642
[FA (18:3)] 6Z_9Z_12Z-octadecatrienoic acid	1.8027	0.48268
Ethanolamine phosphate	1.74536	0.431408
Phosphocreatine	1.68047	0.717671
2-Oxoglutarate	1.63819	1.1153
L-Isoleucine	1.60297	0.426868
Ethyl 3-oxobutanoate	1.56306	0.518492
UDP-glucose	1.49893	0.460393
LPA(0:0/16:0)	1.47682	0.533195
LysoPE(0:0/18:2(9Z_12Z))	1.43874	0.376091
[PC (15:0)] 1-pentadecanoyl-sn-glycero-3-phosphocholine	1.41706	0.801356
Urate	1.34724	0.267804
sn-Glycerol 3-phosphate	1.32297	0.385728
L-Serine	1.31339	0.489196
L-Asparagine	1.30433	0.78459

[SP (16:0)] N-(hexadecanoyl)-sphing-4-enine	1.30239	0.724061
2-C-Methyl-D-erythritol 4-phosphate	1.29322	0.560976
[SP (18:0)] N-(octadecanoyl)-sphing-4-enine	1.28824	0.381637
UTP	1.28156	0.317216
[FA trihydroxy(4:0)] 2_3_4-trihydroxy-butanoic acid	1.28046	1.00059
Dodecanoic acid	1.25724	0.269468
[SP (18:0)] N-(octadecanoyl)-sphinganine	1.25586	0.366687
sn-glycero-3-Phosphoethanolamine	1.24949	0.414871
L-Threonine	1.22131	0.405044
D-Galactose	1.21994	0.632942
[PC (15:1)] 1-(1Z-pentadecenyl)-sn-glycero-3-phosphocholine	1.176 [3]	0.636123

Table 8.12. VIP scores of DCs activated with LPS or infected with *L. mexicana* or *T. gondii* (Biological run 3)

Var ID	M1.VIP [3+2+0][1]	2.44693 * M1.VIP [3] cvSE[2]
Choline phosphate	4.90878	1.04655
L-Valine	3.50132	0.40348
L-Proline	3.2409	0.284127
L-Citrulline	2.95048	0.315447
Choline	2.4873	0.926349
L-Arginine	2.04119	0.488245
L-Carnitine	1.72954	0.149016
4-Trimethylammoniobutanoate	1.5515	0.145616
4-Imidazolone-5-propanoate	1.52933	0.223431
Phosphocreatine	1.46064	0.209694
Creatinine	1.38858	0.531813
4-Methylene-L-glutamine	1.28769	0.418835
L-Ornithine	1.22754	0.161079
L-Leucine	1.22271	0.864424
2_3_4_5-Tetrahydropyridine-2-carboxylate	1.10053	0.238037
O-Acetylcarnitine	1.09439	0.342906
Taurine	1.05141	0.368192
sn-glycero-3-Phosphoethanolamine	1.01081	0.279511
indole-S-cysteine-adduct	0.988308	0.4398
L-Methionine	0.903048	0.267558
N2-(D-1-Carboxyethyl)-L-arginine	0.875201	0.237353
L-Aspartate	0.842277	0.345361
L-Pipecolate	0.828659	0.158212
N6_N6_N6-Trimethyl-L-lysine	0.825762	0.223673
Nicotinamide	0.824552	0.47308
L-Histidine	0.791136	0.205535

O-Propanoylcarnitine	0.775208	0.249612
L-Lysine	0.766086	0.093712
L-Phenylalanine	0.749492	0.249439
L-Tyrosine	0.697062	0.369391
Pyridoxine	0.688664	0.377434
2-C-Methyl-D-erythritol 4-phosphate	0.648488	0.246108
L-Asparagine	0.643486	0.157768
4_6-Dihydroxyquinoline	0.637886	0.524084
4-Guanidinobutanoate	0.634643	0.053119
Guanidinoacetate	0.597359	0.375514
S-Formylglutathione	0.596729	0.071281
5_6-Dihydrothymine	0.584771	0.126572
Gyromitrin	0.578872	0.147595
Imidazole-4-acetaldehyde	0.575289	0.094932
N-Acetyl-L-histidine	0.512064	0.163472
UDP-glucose	0.483749	0.106483
Ethanolamine phosphate	0.479309	0.247696
gamma-Glutamyl-beta-aminopropiononitrile	0.47381	0.18577
sn-glycero-3-Phospho-1-inositol	0.460605	0.103393
ATP	0.453728	0.092172
3'_5'-Cyclic IMP	0.452901	0.123633
NG_NG-Dimethyl-L-arginine	0.452629	0.114077
sn-glycero-3-Phosphocholine	0.451836[3]	0.056863

[1] The value represents the difference between the distinct groups

[2] the value highlights variety within each sample group

[3] VIP score list was limited to 50 metabolites but show that the top metabolites are similar between biological runs

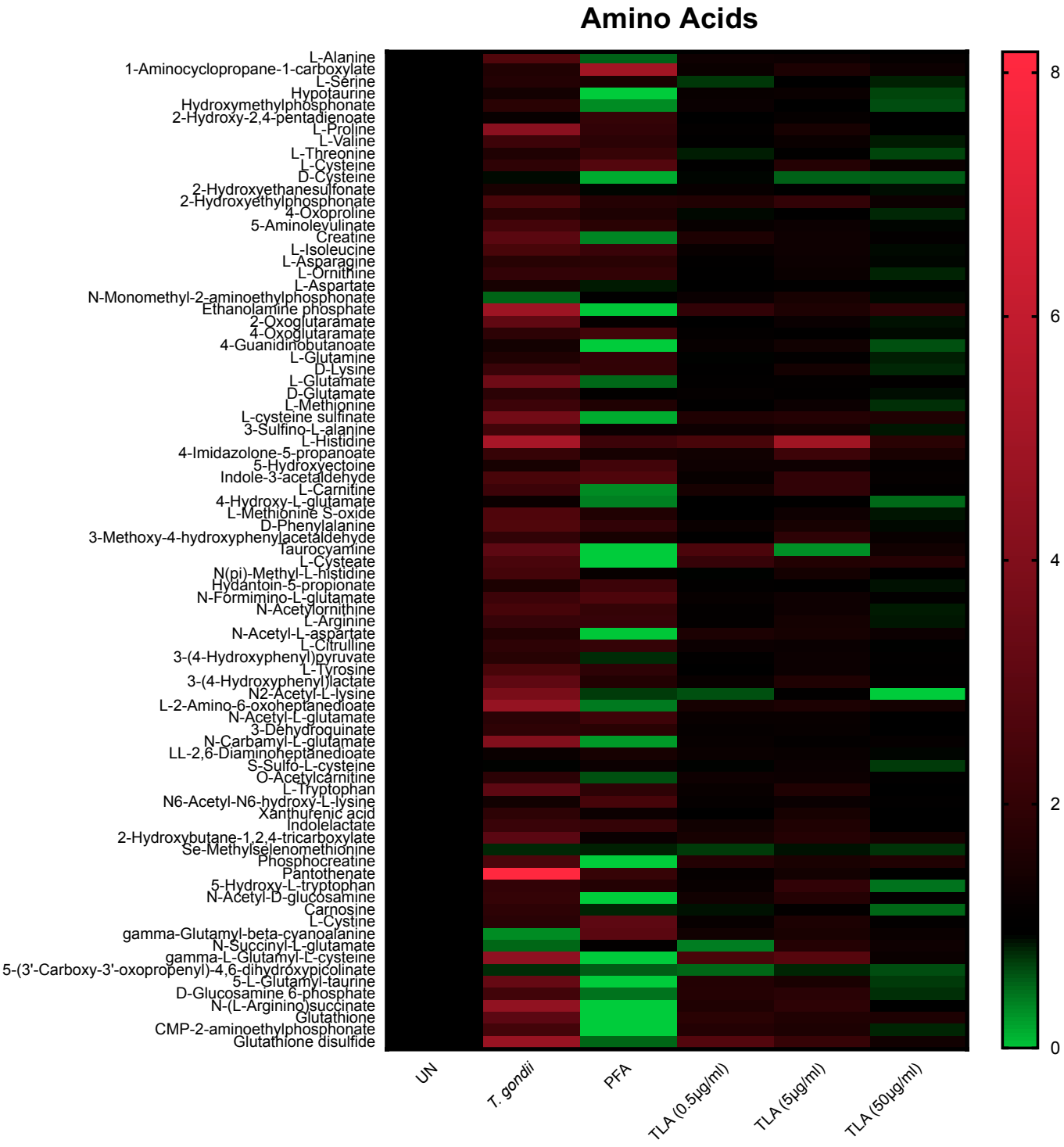
Amino Acids
L-Alanine
1-Aminocyclopropane-1-carboxylate
L-Serine
Hypotaurine
Hydroxymethylphosphonate
2-Hydroxy-2,4-pentadienoate
L-Proline
L-Valine
L-Threonine
L-Cysteine
D-Cysteine
2-Hydroxyethanesulfonate
2-Hydroxyethylphosphonate
4-Oxoproline
5-Aminolevulinate
Creatine
L-Isoleucine
L-Asparagine
L-Ornithine
L-Aspartate
N-Monomethyl-2-aminoethylphosphonate
Ethanolamine phosphate
2-Oxoglutaramate
4-Oxoglutaramate
4-Guanidinobutanoate
L-Glutamine
D-Lysine
L-Glutamate
D-Glutamate
L-Methionine
L-cysteine sulfinate
3-Sulfino-L-alanine
L-Histidine
4-Imidazolone-5-propanoate
5-Hydroxyectoine
Indole-3-acetaldehyde
L-Carnitine
4-Hydroxy-L-glutamate
L-Methionine S-oxide
D-Phenylalanine
3-Methoxy-4-hydroxyphenylacetaldehyde
Taurocyamine
L-Cysteate
N(pi)-Methyl-L-histidine
Hydantoin-5-propionate
N-Formimino-L-glutamate
N-Acetylornithine
L-Arginine
N-Acetyl-L-aspartate
L-Citrulline
3-(4-Hydroxyphenyl)pyruvate
L-Tyrosine
3-(4-Hydroxyphenyl)lactate
N2-Acetyl-L-lysine
L-2-Amino-6-oxoheptanedioate
N-Acetyl-L-glutamate
3-Dehydroquinate
N-Carbamyl-L-glutamate
LL-2,6-Diaminoheptanedioate
S-Sulfo-L-cysteine
O-Acetylcarnitine
L-Tryptophan
N6-Acetyl-N6-hydroxy-L-lysine
Xanthurenic acid
Indolelactate
2-Hydroxybutane-1,2,4-tricarboxylate
Se-Methylselenomethionine
Phosphocreatine
Pantothenate
5-Hydroxy-L-tryptophan
N-Acetyl-D-glucosamine
Carnosine
L-Cystine
gamma-Glutamyl-beta-cyanoalanine
N-Succinyl-L-glutamate
gamma-L-Glutamyl-L-cysteine
5-(3'-Carboxy-3'-oxopropenyl)-4,6-dihydroxypicolinate
5-L-Glutamyl-taurine
D-Glucosamine 6-phosphate
N-(L-Arginino)succinate
Glutathione
CMP-2-aminoethylphosphonate
Glutathione disulfide
UN
T. gondii
PFA
TLA (0.5µg/ml)
TLA (5µg/ml)
TLA (50µg/ml)
8
6
4
2
0

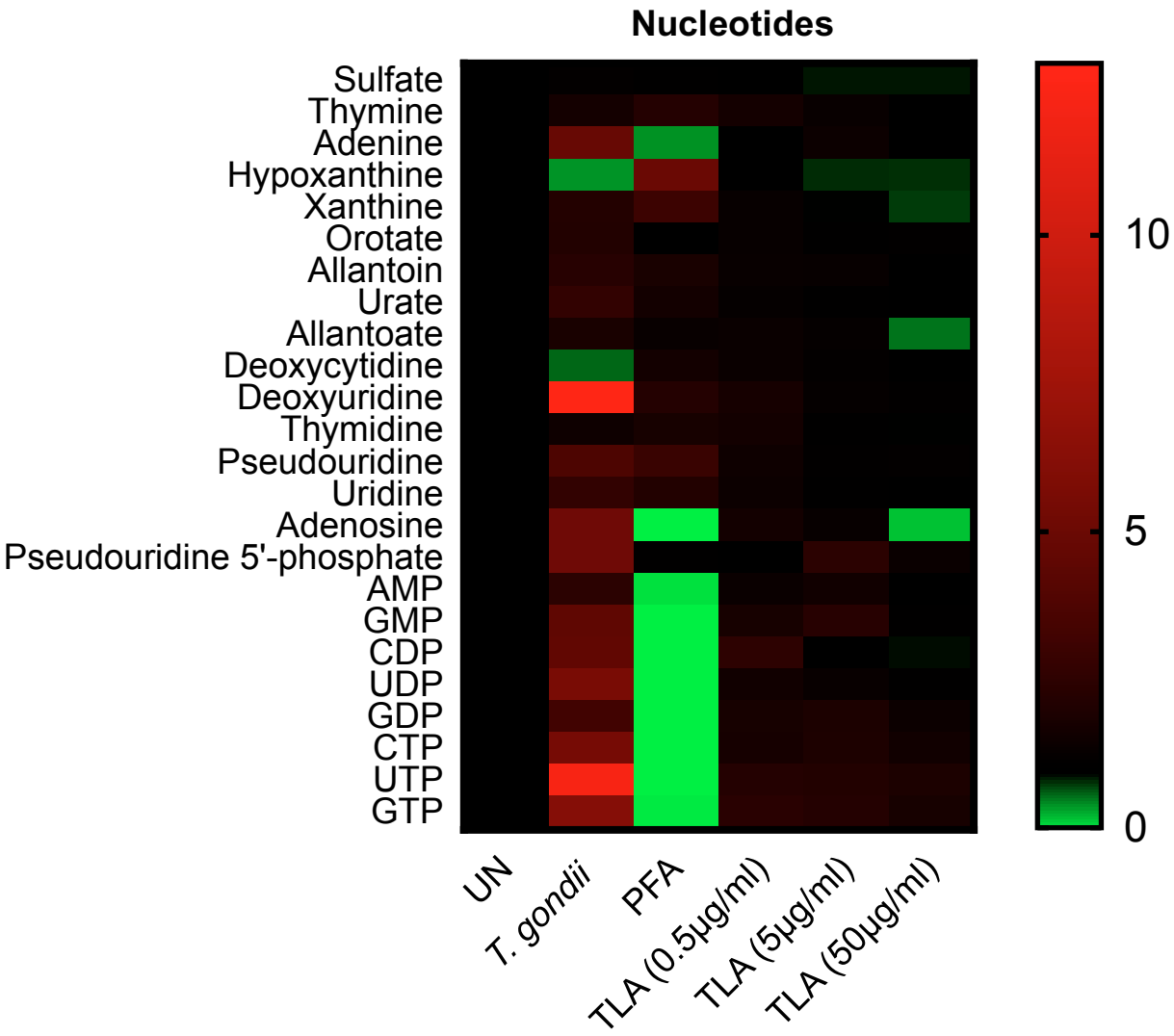
Nucleotides
Sulfate
Thymine
Adenine
Hypoxanthine
Xanthine
Orotate
Allantoin
Urate
Allantoate
Deoxycytidine
Deoxyuridine
Thymidine
Pseudouridine
Uridine
Adenosine
Pseudouridine 5'-phosphate
AMP
GMP
CDP
UDP
GDP
CTP
UTP
GTP
10
5
0
UN
T. gondii
PFA
TLA (0.5µg/ml)
TLA (5µg/ml)
TLA (50µg/ml)

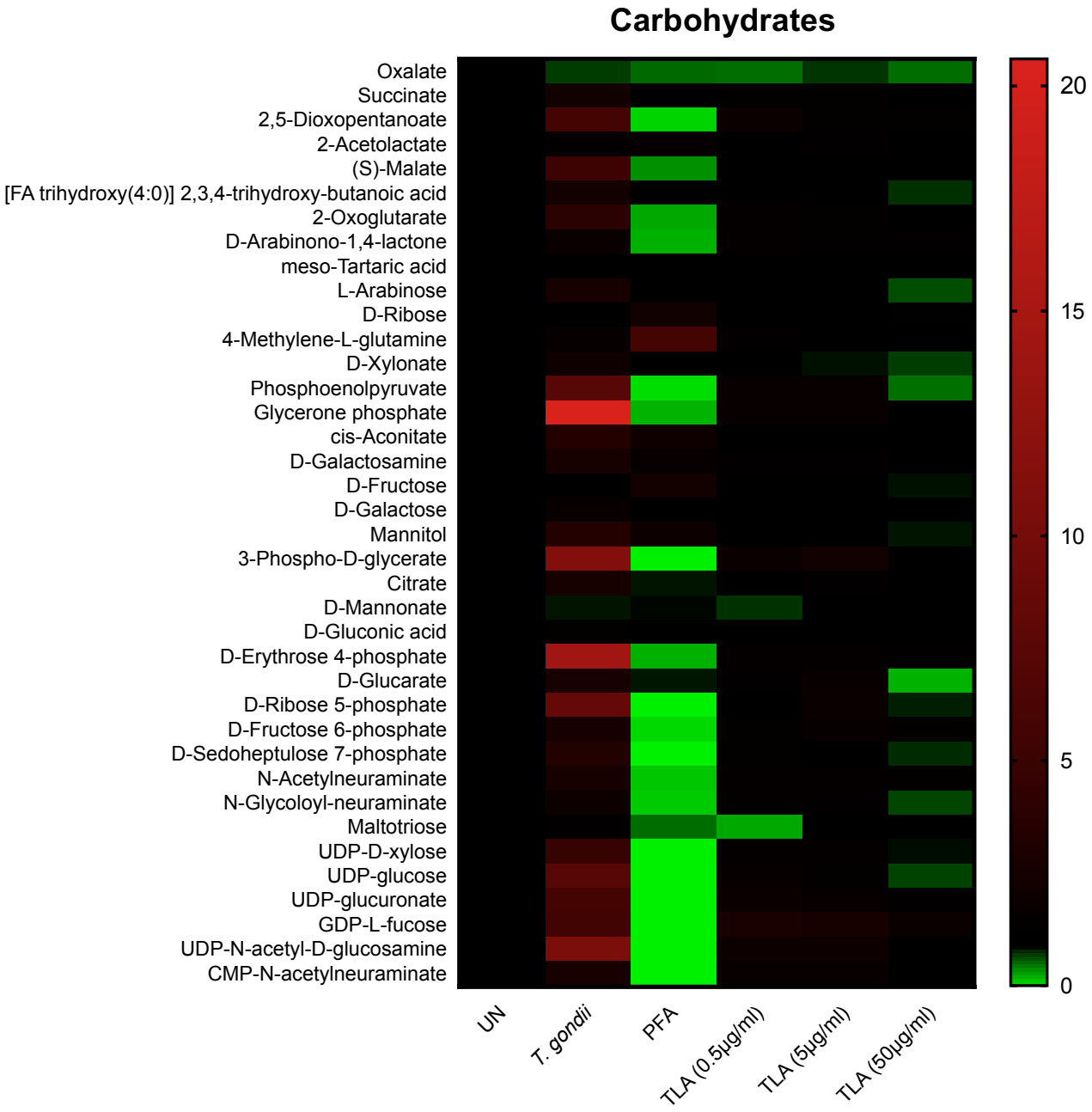
Carbohydrates
Oxalate
Succinate
2,5-Dioxopentanoate
2-Acetolactate
(S)-Malate
[FA trihydroxy(4:0)] 2,3,4-trihydroxy-butanoic acid
2-Oxoglutarate
D-Arabinono-1,4-lactone
meso-Tartaric acid
L-Arabinose
D-Ribose
4-Methylene-L-glutamine
D-Xylonate
Phosphoenolpyruvate
Glycerone phosphate
cis-Aconitate
D-Galactosamine
D-Fructose
D-Galactose
Mannitol
3-Phospho-D-glycerate
Citrate
D-Mannonate
D-Gluconic acid
D-Erythrose 4-phosphate
D-Glucarate
D-Ribose 5-phosphate
D-Fructose 6-phosphate
D-Sedoheptulose 7-phosphate
N-Acetylneuraminate
N-Glycoloyl-neuraminate
Maltotriose
UDP-D-xylose
UDP-glucose
UDP-glucuronate
GDP-L-fucose
UDP-N-acetyl-D-glucosamine
CMP-N-acetylneuraminate
UN
T.gondii
PFA
TLA (0.5µg/ml)
TLA (5µg/ml)
TLA (50µg/ml)
20
15
10
5
0

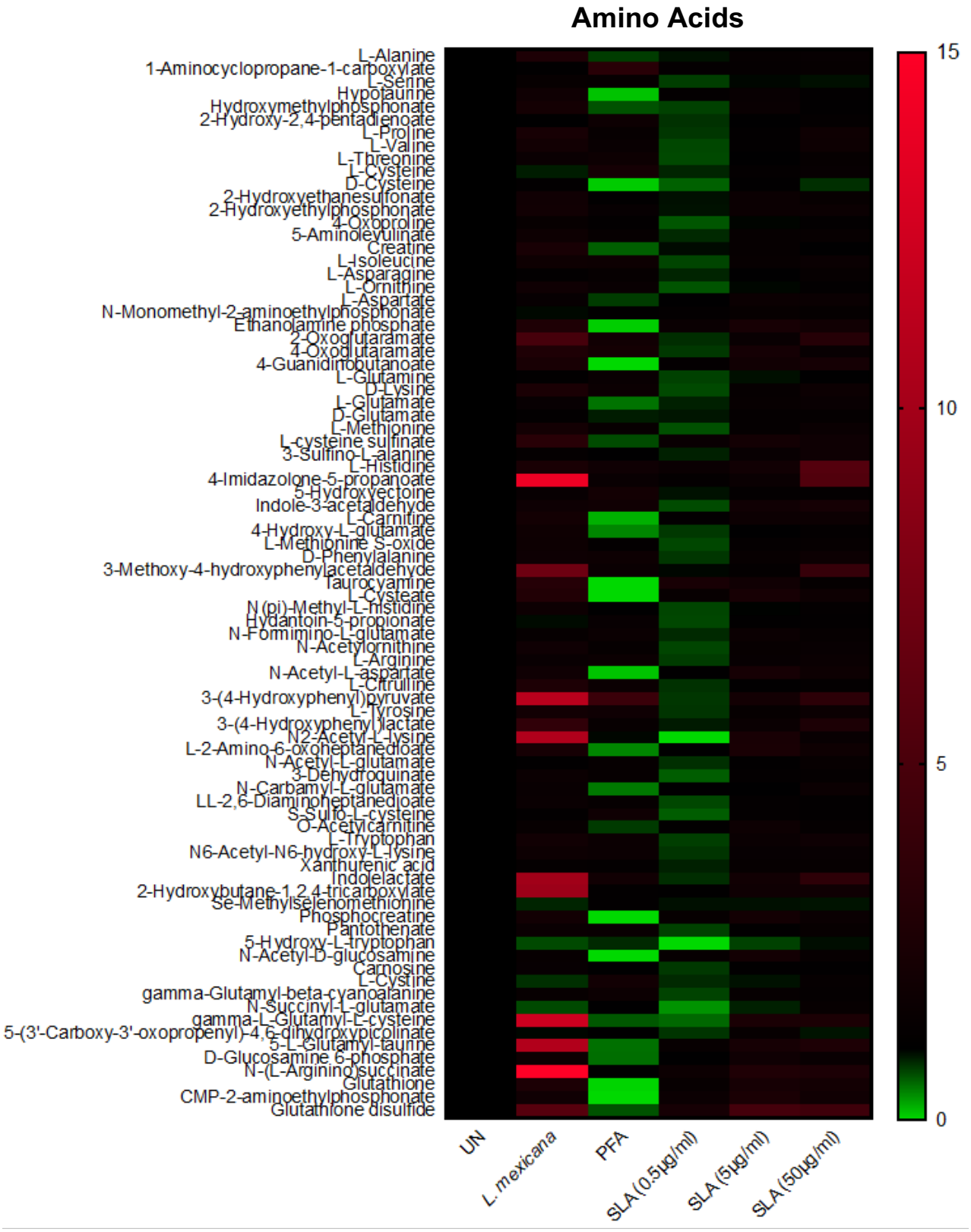
Amino Acids
L-Alanine
1-Aminocyclopropane-1-carboxylate
L-Serine
Hypotaurine
Hydroxymethylphosphonate
2-Hydroxy-2,4-pentadienoate
L-Proline
L-Valine
L-Threonine
L-Cysteine
D-Cysteine
2-Hydroxyethanesulfonate
2-Hydroxyethylphosphonate
4-Oxoproline
5-Aminolevulinate
Creatine
L-Isoleucine
L-Asparagine
L-Ornithine
L-Aspartate
N-Monomethyl-2-aminoethylphosphonate
Ethanolamine phosphate
2-Oxoglutaramate
4-Oxoglutaramate
4-Guanidinobutanoate
L-Glutamine
D-Lysine
L-Glutamate
D-Glutamate
L-Methionine
L-cysteine sulfinate
3-Sulfino-L-alanine
L-Histidine
4-Imidazolone-5-propanoate
5-Hydroxyectoine
Indole-3-acetaldehyde
L-Carnitine
4-Hydroxy-L-glutamate
L-Methionine S-oxide
D-Phenylalanine
3-Methoxy-4-hydroxyphenylacetaldehyde
Taurocyamine
L-Cysteate
N(pi)-Methyl-L-histidine
Hydantoin-5-propionate
N-Formimino-L-glutamate
N-Acetylornithine
L-Arginine
N-Acetyl-L-aspartate
L-Citrulline
3-(4-Hydroxyphenyl)pyruvate
L-Tyrosine
3-(4-Hydroxyphenyl)lactate
N2-Acetyl-L-lysine
L-2-Amino-6-oxoheptanedioate
N-Acetyl-L-glutamate
3-Dehydroquinate
N-Carbamyl-L-glutamate
LL-2,6-Diaminoheptanedioate
S-Sulfo-L-cysteine
O-Acetylcarnitine
L-Tryptophan
N6-Acetyl-N6-hydroxy-L-lysine
Xanthurenic acid
Indolelactate
2-Hydroxybutane-1,2,4-tricarboxylate
Se-Methylselenomethionine
Phosphocreatine
Pantothenate
5-Hydroxy-L-tryptophan
N-Acetyl-D-glucosamine
Carnosine
L-Cystine
gamma-Glutamyl-beta-cyanoalanine
N-Succinyl-L-glutamate
gamma-L-Glutamyl-L-cysteine
5-(3'-Carboxy-3'-oxopropenyl)-4,6-dihydroxypicolinate
5-L-Glutamyl-taurine
D-Glucosamine 6-phosphate
N-(L-Arginino)succinate
Glutathione
CMP-2-aminoethylphosphonate
Glutathione disulfide
15
10
5
0
UN
L. mexicana
PFA
SLA (0.5µg/ml)
SLA (5µg/ml)
SLA (50µg/ml)

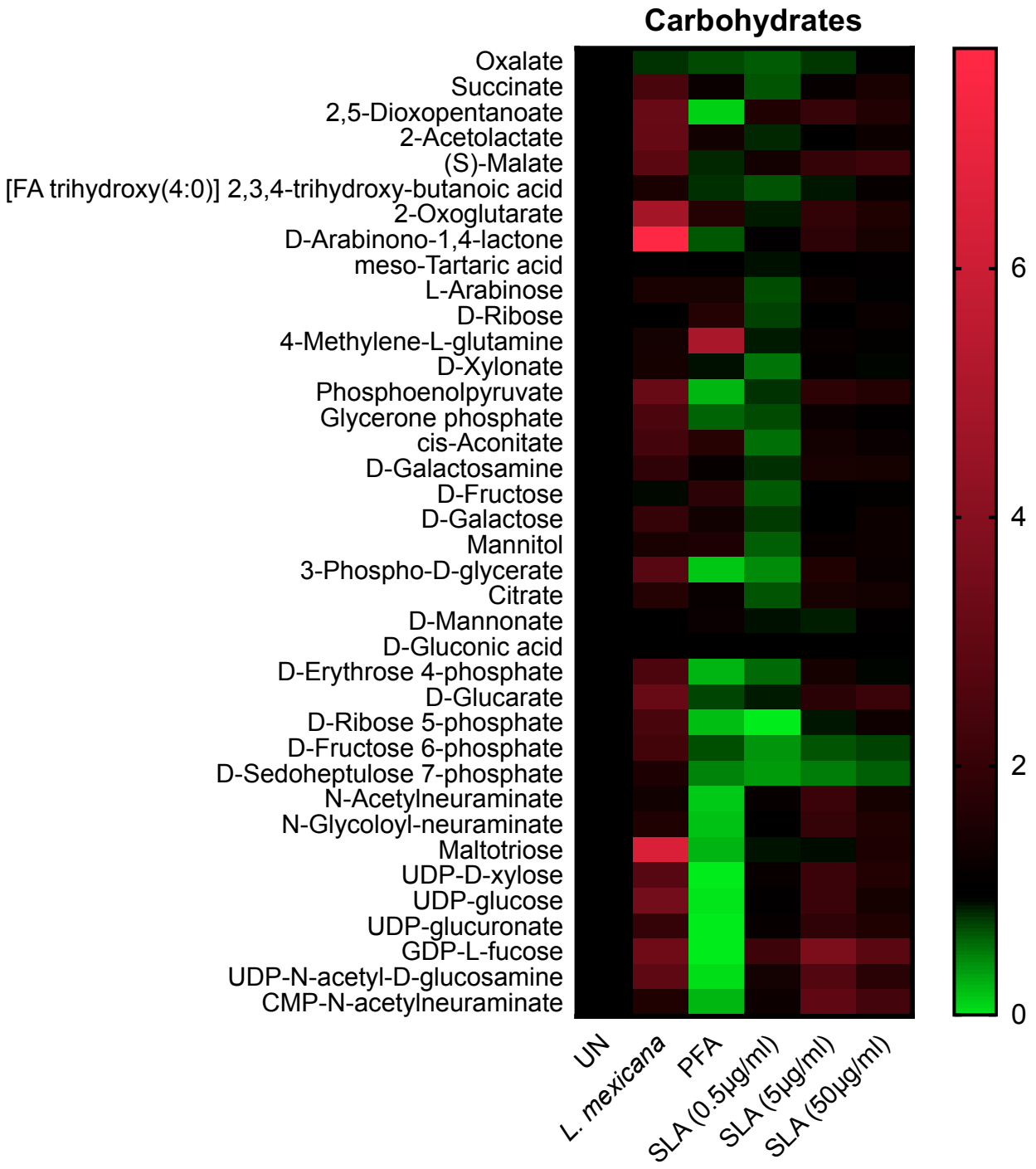
Carbohydrates
Oxalate
Succinate
2,5-Dioxopentanoate
2-Acetolactate
(S)-Malate
[FA trihydroxy(4:0)] 2,3,4-trihydroxy-butanoic acid
2-Oxoglutarate
D-Arabinono-1,4-lactone
meso-Tartaric acid
L-Arabinose
D-Ribose
4-Methylene-L-glutamine
D-Xylonate
Phosphoenolpyruvate
Glycerone phosphate
cis-Aconitate
D-Galactosamine
D-Fructose
D-Galactose
Mannitol
3-Phospho-D-glycerate
Citrate
D-Mannonate
D-Gluconic acid
D-Erythrose 4-phosphate
D-Glucarate
D-Ribose 5-phosphate
D-Fructose 6-phosphate
D-Sedoheptulose 7-phosphate
N-Acetylneuraminate
N-Glycoloyl-neuraminate
Maltotriose
UDP-D-xylose
UDP-glucose
UDP-glucuronate
GDP-L-fucose
UDP-N-acetyl-D-glucosamine
CMP-N-acetylneuraminate
6
4
2
0
UN
L. mexicana
PFA
SLA (0.5µg/ml)
SLA (5µg/ml)
SLA (50µg/ml)

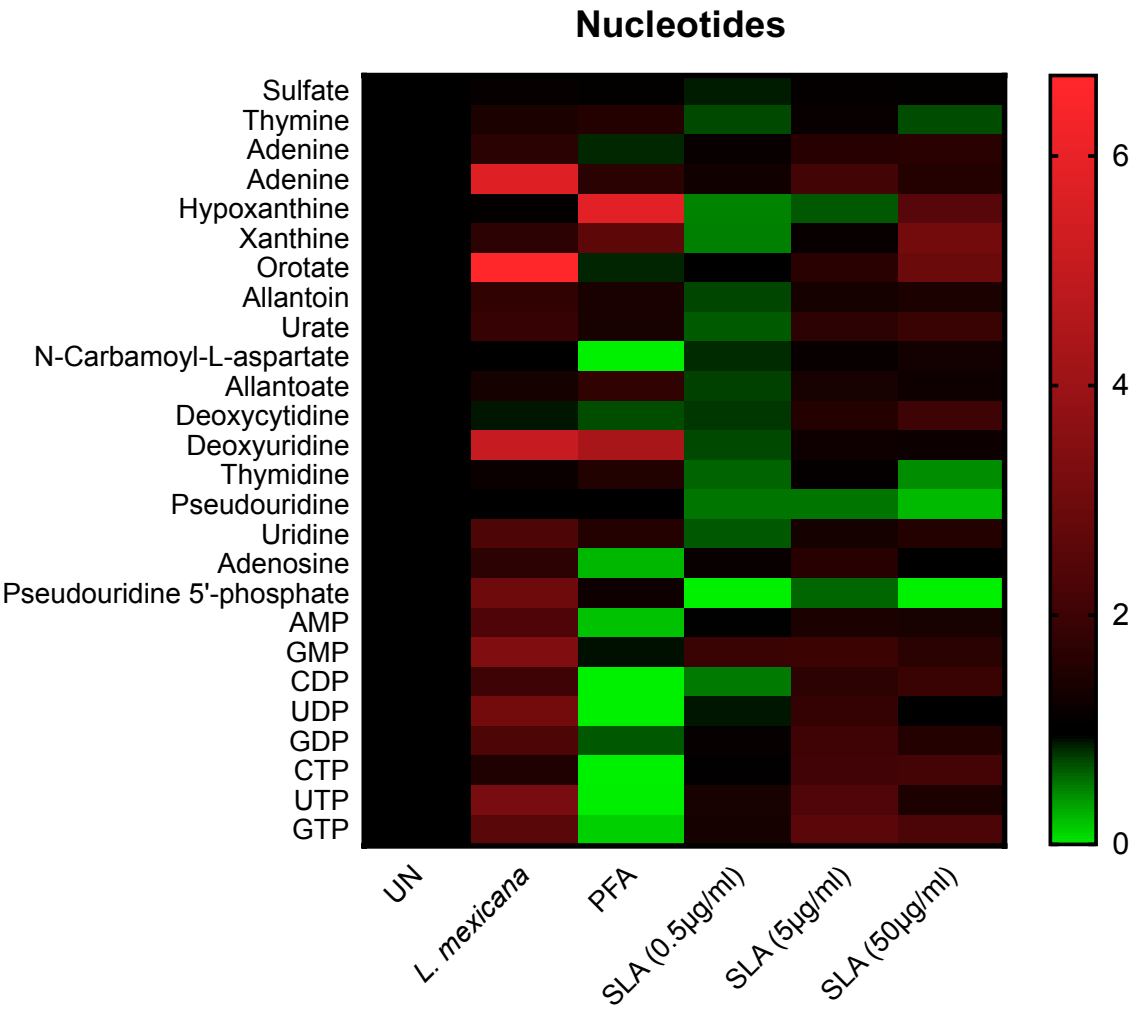

Figure 8.3. Global metabolic activity of DCs treated with TLA, SLA or co-cultured with PFA fixed *L. mexicana* or *T. gondii*. Bone marrow derived DCs were treated with TLA, SLA or co-cultured *with* PFA fixed *L. mexicana* or *T. gondii* for 24 hours. After this time, the metabolites of the DCs were extracted and measured via Liquid chromatography mass spectroscopy (LCMS). A heat map was constructed from the analysed data on IDEOM and Prism7 and shows the fold change increase (Red) or the decrease (Green) of each metabolite compared to its representative unstimulated control (Black).

Table 8.13. Pairwise analysis of transcripts between LPS stimulated and naïve BMDCs

Transcript abbreviation	M5.VIP[1+2+0][1]	2.57059 * M5.VIP[1]cvSE[2]
Mctp2	22.0702	4.80413
Gm7665	21.7438	11.6129
Gm7204	20.3053	13.1787
Il1rapl1	16.0886	6.48698 [3]
Mir6236	15.3491	7.46573
Rps28	13.5543	7.66528
Gm7897	13.0526	1.9577
Lyz2	12.9911	1.85868
Mir6240	12.8504	20.4726
Pde1c	12.7338	16.52
Ptprb	12.4172	2.37236
Bbx	12.3005	16.8467
Il1b	11.8522	1.49574
Gm23374	11.2611	5.78903
Gm8909	11.065	9.40863
Txlnb	10.9932	2.65231
Saa3	10.0443	2.32692
Gm15487	9.67846	4.90614
Bach2	9.59113	2.67182
Gm14303	9.52444	3.3843
Slc8a3	9.46479	6.41463
Ftl1	9.06359	3.66487
Ccl3	8.77091	0.671771
Fam19a3	8.4366	6.8673
Fth1	8.16427	9.03162
Il1a	8.14683	1.00103
Ccl5	7.89059	1.83975
Negr1	7.85983	6.07063
Gm26745	7.84256	3.80377
Tpt1-ps3	7.74534	8.87472
Lhx9	7.73474	2.62715
Rsad2	7.66712	1.28333
Gm26615	7.64091	3.44969
Cacna2d4	7.55598	3.124
Hormad2	7.48156	11.855
Cxcl3	7.48058	0.939714
RP23-166L22.1	7.30342	4.77406
Ctcf	7.21433	6.12382
Marcksl1	7.14277	0.68757

Cntnap2	7.01352	4.95127
Ccl22	6.96612	0.68272
Ctsd	6.80572	4.25124
Gm26825	6.75372	2.37898
Gm19963	6.73385	1.93428
Timp4	6.64684	3.29144
Il1rn	6.50856	1.91968
Gm16505	6.50137	2.50128
Gm10425	6.40629	1.34229
Eif1ax	6.39948	5.59206
Gm8984	6.37843	5.15289
Gm7846	6.37261	3.9862
Gm43841	6.34765	9.63577
Batf2	6.17821	1.83577
Gm16418	6.17146	5.46803
Gm32444	6.07836	4.63169
Gm11560	6.01328	8.28045
Gm18957	5.96585	4.59768
Vmn2r-ps54	5.88722	2.52573
Gm12111	5.81265	5.06548
Lgals3	5.8012	3.68418
Rpl3-ps1	5.69433	2.58102
Gm24951	5.61477	3.12648
Gm17638	5.58299	3.37085
Zfp36l1-ps	5.57901	5.50155
Usp32	5.56623	2.41646
Pou2f3	5.43142	2.98944
Gm8529	5.42166	4.24297
Sh3gl3	5.38371	5.26674
Gm7676	5.36873	4.37514
Uqcrh-ps2	5.3558	4.41975
Acod1	5.34843	0.497866
Cd74	5.30519	1.44851
Rit2	5.26721	4.30553
Mir703	5.2332	2.28982
Cxcl2	5.17602	0.587109
Clec4n	5.16185	2.24777
Cdk8	5.15566	2.93539
4930552N02Rik	5.09	3.41931
Serpina3n	5.07299	0.870231
Gm7332	5.07283	2.66959
Ccl4	5.07052	0.642739
Isg15	5.05694	1.21715
Il12b	5.02507	0.249562

Gm35106	5.01144	4.96362
Anks1b	5.00236	3.40691
Eif4a-ps4	4.99003	4.98352
9330179D12Rik	4.98448	6.674
Hp	4.97575	1.11623
Ctss	4.93679	2.98342
Rnf24	4.91556	2.71245
Gm8814	4.8721	0.921598
Rn18s-rs5	4.86515	8.85417
Gpx1	4.81536	1.54816
Cmpk2	4.80964	0.754949
Gm5870	4.73405	3.71078
Gm45211	4.72901	1.23173
AA467197	4.71926	1.25108
H3f3a-ps2	4.68161	4.98012
Gm10180	4.61995	3.5864
Gm15925	4.616	1.69804
Lcn2	4.61336	0.224425
Fscn1	4.5963	1.02945
Gm7634	4.55951	3.62055
Eef1a1	4.52435	1.14882
Macrod2	4.50138	5.12147
Clec4e	4.48615	1.14011
Cxcl10	4.46435	0.457183
Tcea1	4.45069	6.15291
Aldoart1	4.42872	5.00991
Mmp12	4.41911	4.31692
Sepw1	4.41133	7.88075
Gm609	4.3991	3.16189
Gm13392	4.38426	9.18607
Gm6863	4.36515	4.25726
Ptgs2	4.3636	0.235512
Gm12158	4.35452	4.75412
Usp37	4.35308	3.34348
Actg1	4.31708	0.796986
H2-Q3	4.3103	2.0023
Gm16589	4.30603	3.37432
4833427G06Rik	4.26012	1.8037
Prdx5	4.25794	2.96928
Gm6394	4.2084	4.36168
Gm26981	4.18815	1.96592
Gm9824	4.17474	3.74528
Cep72	4.17273	0.628737
Gm13736	4.17054	1.73419

6030443J06Rik	4.12441	5.03333
Il6	4.11913	0.797053
Gm5548	4.09999	2.13572
Mt2	4.0952	0.7988
RP23-183A4.1	4.07256	3.39732
Serpina3g	4.03763	0.586658
Mmp13	4.02591	0.815249
Tyrobp	4.01295	1.98474
Gbp2	4.00843	0.462921
Cd40	3.99453	0.777081
H2-Bl	3.98634	4.50697
G6pd2	3.97624	3.13266
AW112010	3.9681	0.575498
RP23-74O12.6	3.95426	2.00043
Il31ra	3.93047	4.67513
Gbp2b	3.92764	0.57648
Gm6913	3.91291	4.10817
Gm6682	3.90886	4.98436
Crocc	3.9011	4.27762
Cpa6	3.88717	1.83706
Eef2	3.8773	0.727642
Pcsk5	3.87437	4.41553
Rplp1	3.87324	2.05142
Gm12892	3.86935	5.17795
Gm42989	3.86429	3.75413
Tmem232	3.85915	2.88169
Oasl1	3.85645	0.386414
Camk1d	3.84676	6.3562
Gm29610	3.84557	0.896652
Cotl1	3.83888	1.59583
Gm4585	3.83561	2.85326
Gm5578	3.82587	3.39583
Cntnap5b	3.79971	3.56663
Gm5607	3.78758	1.1937
Mvp	3.77658	4.44171
B830042I05Rik	3.76287	1.84582
Oaz1-ps	3.75452	6.04302
Tmcc1	3.72408	2.03723
Spp1	3.70178	3.87178
Nckap5	3.68878	2.39833
Ccl9	3.67012	3.47673
Gm9089	3.66666	1.7213
Sema3a	3.66173	5.28868
Gm9025	3.66104	4.67956

Gm15173	3.6468	3.4604
Gm28539	3.62501	2.97957
Gm37103	3.61535	1.7364
Lrrc20	3.61457	5.47451
Plek	3.60782	0.847415
Rps18	3.59692	1.62441
Clic4	3.59041	0.445724
Sepp1	3.58529	0.57123
Gm28196	3.56717	4.07747
Gm20470	3.55425	0.692599
Gm7816	3.54085	2.52019
S100a16	3.53959	3.0332
Csf1r	3.5183	0.256595
Gm5560	3.50735	3.37848
Gm11970	3.50514	2.87821
Socs3	3.50237	0.189562
2410017I17Rik	3.49657	2.94009
Cxcl1	3.49553	0.29737
Plxdc1	3.49071	5.66769
Serpine1	3.48596	0.425144
Vim	3.48157	0.961071
Dmd	3.47511	4.58991
Gm11258	3.46996	5.22512
Gm44090	3.46531	2.75824
Coro1a	3.46343	0.36377
Gm19587	3.45462	3.09517
Pnp	3.45329	1.33662
Rps14	3.44457	2.18043
Rpl32	3.44113	1.65154
Gm5244	3.44083	2.42039
Slk	3.43613	2.6815
Txn1	3.43104	1.25686
Cd36	3.42787	2.7859
Irf7	3.42754	0.778798
Fxyd5	3.4196	1.35697
Gm44737	3.41591	1.39366
Pkm	3.41064	1.41173
Scp2-ps2	3.40902	2.76861
Ccl6	3.3998	2.4682
Rps5	3.37858	1.51743
Crb1	3.37623	2.50465
Lamp1	3.37295	0.452457
Rps19-ps10	3.36333	1.81186
Txnrd1	3.3553	1.48357

Erbb4	3.3546	4.32679
Slc15a3	3.35025	0.767382
H3f3b	3.33796	0.530627
Ebf1	3.33697	2.16784
Ms4a6d	3.33401	0.671548
H2-Aa	3.31398	1.70986
Gm12428	3.31296	0.867835
Gm26852	3.30875	2.78979
Zfp839	3.30065	3.30031
Rpl8	3.29756	1.16527
Slc2a6	3.28998	0.551542
Tpt1	3.28235	1.87407
Zfp956	3.27602	0.50509
Zfyve28	3.274	3.70641
Apoe	3.2724	1.00506
Gm5940	3.26968	4.79248
Rps9	3.26634	1.36666
Upp1	3.25719	0.971944
Cebpb	3.25572	0.600858
Lpl	3.23954	3.14418
Gm8304	3.2378	4.08211
Laptm5	3.23656	0.263358
Gm7293	3.2296	4.58769
Pnp	3.22292	0.653491
Gm13502	3.21379	2.57604
Atp5e	3.21215	2.36349
Fry	3.20557	1.29696
Cd14	3.18475	1.35672
Oca2	3.1808	4.47946
Gm3145	3.1704	4.29608
Gm2670	3.16996	1.96766
Ifit2	3.1668	0.327351
Gm13450	3.14405	2.58875
Tnfaip2	3.13978	0.201345
Acsl1	3.13667	0.167353
Gm36551	3.10755	3.10526
Fn1	3.10634	2.73731
Gm6180	3.09951	5.37202
Gbp3	3.09634	0.424083
Gm6987	3.08896	5.50969
Psme2	3.08493	0.902506
Gm4852	3.08398	4.89768
Rps17	3.08019	1.38832
Fam227b	3.07984	0.54735

F10	3.07888	0.524093
Prdx1	3.07878	1.53504
Pfn1	3.06827	1.77966
S100a9	3.0671	2.70094
Lipa	3.06607	1.51157
BC048502	3.06524	1.02872
Ehd1	3.06382	0.357829
Gm20589	3.05286	3.30845
Retnla	3.04887	1.63601
Asap2	3.04572	2.7473
Gm8979	3.04171	2.98705
Gm12497	3.0356	3.70043
Ifi47,Olfr56	3.0346	0.86441
Gm43083	3.03139	0.903122
Gm12060	3.0304	3.70268
Gm28343	3.02311	3.94269
Mmp8	3.02011	0.98913
Rack1	3.01022	1.31122
Rps11	3.00586	1.05231
Slc7a2	3.00532	0.396886
Slfn2	3.00334	0.864154
Rps26	3.00306	0.913244
Gm5615	2.99031	1.42287
Ctsb	2.9896	3.13614
Rps16	2.98846	1.24276
Gm42418	2.9881	5.27854
Tagln2	2.97706	1.51111
Gm5997	2.97247	3.9031
Antxr1	2.97173	3.25881
Rpl18a	2.96856	0.885574
Tnfrsf1b	2.96115	0.0882285
Nos2	2.95144	6.20242
Kcp	2.93074	2.72255
Lcp1	2.91477	0.967603
Usp18	2.91456	0.506088
Nfkbia	2.90698	0.427773
Tnf	2.90177	0.413997
Rps19	2.90033	1.27147
Pla2g7	2.89866	0.767175
Gm4374	2.89407	1.68355
Wfdc21	2.8924	0.984978
Sdc4	2.89191	0.446792
Id2	2.88865	0.688839
Lgals1	2.87891	2.46663

Itm2b	2.87481	1.01916
Rps12	2.87446	1.25276
Mapkapk2	2.86619	0.391048
Fshr	2.86205	1.24873
Tpt1-ps6	2.8615	2.11084
Hck	2.85841	0.581284
Rps15	2.85702	1.35275
Grm8	2.84842	2.14474
Gm10221	2.84661	1.1567
Gm20511	2.84038	2.61819
Cks1brt	2.83433	2.02921
H2-Eb1	2.83311	1.2399
Gm15703	2.82352	1.27497
Rps4x	2.81904	0.665833
Anxa2	2.81896	1.38346
Rps21	2.81356	2.16656
Cdkn1a	2.80542	0.384012
Tapbp,Zbtb22	2.80264	0.453199
Gm7335	2.79979	1.2279
Rnft2	2.79898	1.8003
Gm44978	2.79193	2.99615
Mmp14	2.78056	0.296787
Ifi44	2.77857	0.739124
4930509G22Rik	2.77678	4.83223
Lgals9	2.77629	0.688719
Slc39a1-ps	2.76883	4.01684
Srgn	2.76279	1.31715
Spock3	2.75844	1.40919
Rpl9	2.73605	1.15298
P4hb	2.73523	1.15321
Gm26659	2.729	2.32897
Itfg1	2.72013	3.71283
H2-Ea-ps	2.71277	1.95307
Rpl18	2.70007	1.13272
Tspo	2.67385	0.904701
Gapdh	2.67103	0.692244
Tpt1-ps4	2.67043	4.70627
Gm37945	2.66347	2.48272
Gm17275	2.65444	1.84493
Gnaq	2.6535	2.25354
Tcp1	2.65159	2.23636
Rpl13	2.64703	0.752309
Gpx4	2.64421	0.876561
Sod2	2.64357	0.314076

Emp3	2.64141	0.861668
Gm43972	2.639	4.53148
Slc28a1	2.63233	3.341
Rps10	2.62613	1.46986
Ifi204	2.62555	0.431153
Gdi2	2.61952	0.544517
Cfp	2.6148	0.715343
Rps3	2.61098	1.26913
Gm44850	2.61042	0.701345
Rap1b	2.60522	0.918325
Cox4i1	2.60522	1.42919
Bst2	2.60205	0.515908
Gm16755	2.59684	2.48249
Cst3	2.59549	2.7613
Gm42522	2.59113	1.23485
Irf8	2.58919	0.549127
Gbp5	2.58656	0.141689
Sh3bgrl3	2.58642	1.09609
Senp7	2.58351	1.52057
Fau	2.58335	1.39592
Hs6st3	2.58196	4.79081
Ifit1	2.5734	0.375328
Gm38005	2.57266	1.66458
B2m	2.56687	1.79722
Fpr2	2.56224	0.840314
Trim30e-ps1	2.56058	0.817301
Ccnd2	2.56034	0.136942
Clec7a	2.56033	1.64592
Gm16505	2.55775	1.68433
Rpsa	2.54608	0.570002
Grn	2.54448	1.62052
Samhd1	2.54305	0.199419
Gm12352	2.54184	1.85558
Aida	2.53679	1.05258
Gm13132	2.53551	1.5354
Ldha	2.53008	1.55545
Rpl4	2.52956	0.350129
Gpi1	2.515	0.197864
RP24-83E15.3	2.50301	0.749867
Ifi30	2.48837	0.21331
EU599041	2.48169	2.3413
Gm42641,Trex1	2.47941	0.340109
Gm6421	2.47571	2.20461
Phf11b	2.47325	0.608203

Hexa	2.47121	0.839812
Angel1	2.4624	5.2115
Gm26809	2.46191	0.15887
Adam8	2.4607	0.607344
Alox5ap	2.46007	0.168594
Ccl17	2.45546	0.688799
S100a11	2.45276	0.861777
Tmsb4x	2.45021	1.97058
Gm38283	2.44685	1.28839
Ucp2	2.44673	0.443519
Myo9a	2.43789	4.98087
Gm2199	2.43525	1.80538
Ctsa	2.43354	1.38124
Mx1	2.42968	0.112757
Ass1	2.42666	0.646067
Kctd12	2.42582	0.301817
Ccr7	2.41951	2.2189
Eno1	2.41747	0.726509
Idh1	2.41565	0.245657
Nfkb2	2.41393	0.18259
RP24-229E19.1	2.4131	0.609477
Gm16069	2.40894	0.446364
Gm9575	2.40879	2.14355
Psmb8	2.40849	1.12383
Gm5809	2.40549	1.89847
Gm44209	2.39827	1.96457
Socs1	2.38805	0.193652
Tpi1	2.38787	0.878939
Rpl26	2.38429	1.0076
Msn	2.38396	0.341381
Slc1a1	2.37644	3.23901
Gm8545	2.37615	5.30664
Garnl3	2.37528	1.31759
Acyp2	2.3737	2.06903
RP24-285L8.3	2.37015	1.3115
Taldo1	2.35546	0.591207
1700021J08Rik	2.35246	0.642729
Chpt1	2.35053	1.99007
Slc25a5-ps	2.3409	3.45887
Rpl34	2.33746	1.65785
Gm4076	2.33421	1.69411
Ch25h	2.33063	0.245146
Mmp9	2.32871	1.0011
Chchd7	2.32804	2.08771

Rnf19b	2.3277	0.206804
Fgl2	2.32547	0.531586
Zfp36	2.32444	0.51626
Gm42413	2.32206	0.66737
H2-D1	2.31938	0.768421
Gm2824	2.31127	2.69659
Gm10698	2.30509	3.51958
Nme1	2.29865	0.849249
Rab7	2.29324	1.48912
Csrp1	2.29303	0.568482
Psma6	2.2843	0.927582
Six2	2.26833	1.0947
Ifitm3	2.26648	1.89849
Gpr84	2.26395	0.236583
Txnrd1	2.26186	1.39451
Rpl7	2.25899	0.761295
Arg1	2.25499	0.249424
Ryr3	2.25486	2.63722
Cyba	2.25285	1.62561
Ighv1-64	2.24522	1.45937
H2-Q2	2.24498	0.834971
Sepw1	2.24399	1.3067
Gm17711	2.24238	1.58204
Gm42959	2.23968	0.508458
Cxcl14	2.2391	1.42987
Mtpn	2.23851	0.735174
RP24-560O24.2	2.23637	0.325582
Rpl3	2.22722	0.459069
Rpl14	2.22271	0.529895
Hspe1-ps6	2.22145	1.39595
Inhba	2.2199	0.214875
Rnh1	2.21841	1.09841
Gm15482	2.20991	1.75792
Capg	2.19887	2.22132
Psap	2.19847	2.76726
Grid1	2.1969	1.24882
Gm8801	2.18709	2.36182
Irgm1	2.18336	0.457369
Gm11867	2.17643	2.18132
Gm20412	2.17279	0.188788
Nt5c3	2.17174	0.58084
Pgd	2.16202	0.776179
Gbx1	2.1533	2.23084
Ybx1	2.1532	1.03657

Sqstm1	2.15198	0.418388
Wfdc17	2.15123	3.25141
Gm21961	2.15052	2.6749
Fam26f	2.14915	0.547939
Psmb10	2.14777	0.632228
Prex2	2.13984	1.93291
Rpl23a	2.13221	0.88459
Snx22	2.1305	1.10669
Gm8221	2.1299	0.226555
Tnfaip3	2.12924	0.1418
Dusp1	2.12651	0.198317
Gm30292	2.12619	1.59556
Gm15932	2.12601	0.628304
Zfp280c	2.12208	4.36897
Calr	2.12167	2.01946
Gm16407	2.11595	2.93881
Gm43842	2.11536	0.20969
Gm13453	2.11058	3.82685
Cd69	2.11003	0.365441
Gm29585	2.10914	0.951327
Gm16234	2.10219	1.01388
Slc25a5	2.10136	1.01487
Gm44364	2.09728	1.26053
Sh3bgrl	2.09397	0.391375
Cntnap2	2.08982	1.25241
Calm2	2.08863	0.48895
Rpl36a-ps1	2.08493	4.00681
Calm1	2.0788	1.33098
Cd63	2.07776	1.66504
Itgb2	2.06671	1.54708
Cfhr1	2.06652	0.910512
Ctsh	2.06629	0.657358
Tgfbi	2.06593	0.603445
Gm6265	2.06386	2.85354
Pcbp2	2.05896	0.533139
Sepn1	2.05407	0.504427
Gm26762	2.05016	0.543848
Rpl17	2.04702	0.91954
Gm8410	2.04313	1.50342
Gm6788	2.03824	1.09526
Gm43963	2.03564	0.337152
Rpl7a	2.03382	0.602058
RP23-96L20.1	2.03109	3.38757
Rps7	2.03052	0.852045

RP23-457I3.2	2.03002	1.91737
Pou3f4	2.02927	2.49551
Ifitm1	2.02917	1.73622
Ms4a4c	2.02748	0.550882
Rpl31	2.02461	0.896818
Gadd45b	2.02412	0.344203
Gm18733	2.02229	0.338088
Kxd1	2.02076	3.11027
Tap1	2.01722	0.260297
Rps29	2.01712	3.06822
Eif5a	2.01627	1.76561
5830462I19Rik	2.01327	0.326901
Snx5	2.00808	0.24989
Chmp4b	2.00709	0.348776
Gm18367	2.00613	2.78277
Rps13	2.00467	1.01123
Gm26561	2.00016 [4]	1.52978

Table 8.14. Pairwise analysis of transcripts between *T. gondii* infected and naïve BMDC cultures.

Transcript abbreviation *T. gondii* compared to UN	M4.VIP[1+3+0] [1]	2.57059 * M4.VIP[1]cvSE [2]
Pde1c	29.7705	23.2439
Gm7665	28.7759	19.2809
Gm7204	26.5943	23.1214
Il1rapl1	26.3048	21.7306 [3]
Mir6236	24.518	20.1035
Bbx	18.925	12.5943
Lyz2	18.752	19.3814
Mir6240	17.297	16.1975
Gm23374	16.1579	3.90884
Tpt1-ps3	14.1425	8.14689
Cntnap2	13.014	11.6975
Ctcf	10.6099	7.63508
Gm8984	9.92352	5.78935
Uqcrh-ps2	9.15427	5.72923
Gm37361	8.68752	4.30196
Rps28	8.63668	9.30479
Gm26981	8.60619	2.50468
Rpl27a-ps2	8.55443	6.42522
Rnf24	8.4904	3.15227
Hormad2	8.43401	5.27322

Gm14303	8.25401	10.1217
Fth1	8.20817	11.0134
Gm5870	8.18754	4.45409
Tcea1	8.06605	6.9676
Pcsk5	7.94417	4.11131
Cd74	7.84299	3.80337
Gm43841	7.53214	11.6668
Grm8	7.33362	2.25636
Oaz1-ps	7.16246	2.25568
Gm11560	7.14158	7.66582
Negr1	7.11428	4.10265
Gm7846	7.04815	6.73632
Cdk8	7.03808	6.73842
Gm10180	7.029	6.3423
Gm16418	6.99669	8.061
Gm8909	6.97261	8.41092
Gm12864	6.95786	6.18829
Gm6394	6.92172	6.94704
Gm13450	6.8032	6.15994
G6pd2	6.65068	5.31818
Macrod2	6.43796	5.34899
Gm12111	6.4306	6.47916
Bach2	6.332	5.25935
9330179D12Rik	6.28371	8.66867
Gm6682	6.24743	9.16653
Mvp	6.20346	6.42487
Rpl3-ps1	6.19751	4.98168
Tmcc1	6.10234	5.60922
Cntnap5b	6.0119	5.54144
Gm15487	6.00558	9.20558
S100a16	5.98421	3.53761
Hs6st3	5.90294	7.5743
Gm11822	5.8708	2.40601
Cacna2d4	5.82441	5.30595
Mmp12	5.82363	4.12476
Gm12497	5.79329	4.86386
Antxr1	5.76625	9.19581
Gm12892	5.71355	7.31651
Gm26745	5.66327	5.56723
Gm24951	5.65057	5.84737
Ldha	5.64679	2.93692
Gm7984	5.6226	5.32374
Gm5809	5.60578	7.64309
Rpl10l	5.50105	1.72889

Gm6987	5.46291	5.20976
Vmn2r-ps54	5.46176	2.8816
Gm15925	5.46	1.94196
Zfp839	5.44477	6.92873
Gm9575	5.33539	1.8852
Anks1b	5.24789	7.44367
Gm2522	5.21617	3.13893
Gm38187	5.19813	3.00196
Gm16372	5.1112	3.57602
H3f3a-ps2	5.0413	5.27278
Gm6180	5.01923	5.42147
Eif4a-ps4	5.01865	7.56183
Gm43972	5.00667	5.65328
Gm14130	4.98418	5.00535
Actg1	4.95565	2.39176
Gm7332	4.90504	3.54579
Gm15173	4.89639	6.01423
Txnrd1	4.77871	2.95159
Zfp36l1-ps	4.76386	1.20818
Gm44090	4.76187	4.77858
Ftl1	4.76101	3.59679
Mir703	4.72025	4.25601
Gm2824	4.71066	3.24511
Camk1d	4.7083	5.11768
H2-Eb1	4.68394	1.80401
Gm15482	4.65823	5.26864
Gm12906	4.59467	2.99649
Gm19087	4.55338	6.23466
RP23-96L20.1	4.54006	6.54513
Gm13453	4.53788	5.14045
H2-Aa	4.53547	3.1295
Fam19a3	4.53028	3.95316
Il31ra	4.51987	3.82526
Gm11970	4.51889	5.67451
RP23-166L22.1	4.51419	5.20508
Itfg1	4.4906	6.54473
Gm13736	4.45762	5.57017
Gm14877	4.43218	3.0881
Lrrc20	4.41766	5.30971
Rn18s-rs5	4.40228	2.36714
Plxdc1	4.39943	3.43812
Oca2	4.38513	6.58284
Hp	4.37617	1.42688
Gm9025	4.3421	5.27872

Cntnap2	4.34151	3.95479
Ctsd	4.3234	3.49933
Trim30e-ps1	4.30239	2.1315
Gm3145	4.29543	5.10707
Gm10698	4.26661	4.00935
Lrp1b	4.25801	7.4716
Sh2d2a	4.22432	4.54484
Gm8048	4.21024	2.5951
Tpt1-ps6	4.18195	3.26607
Scp2-ps2	4.1585	6.23664
Mup-ps16	4.14291	4.93893
Tmem232	4.13982	4.39107
Angel1	4.13494	6.91054
Slc39a1-ps	4.12768	5.41029
Gm7634	4.12577	4.54922
Gm8304	4.11228	5.30512
Prdx1	4.10223	1.80965
Lgals3	4.09547	1.88656
Gm4852	4.05341	4.23926
Rnft2	4.05179	5.10186
Ccl22	4.04173	1.66659
Gm44978	4.01591	2.77378
Gm10221	4.0134	3.47887
Gm8529	4.00488	5.44795
Spp1	3.98866	1.32201
Gm29610	3.98571	3.92216
Coro1a	3.97979	0.700581
Rpl36a-ps1	3.97777	5.96198
Ralgps2	3.96167	2.71459
Gm44737	3.95973	3.44625
Gpx1	3.95636	2.65059
Clec4n	3.95573	5.77471
Myo9a	3.95026	3.59838
Gm15529	3.92407	2.17757
Gm35106	3.91488	3.14183
Usp32	3.90663	5.7439
Gm7676	3.88365	2.40948
2410017I17Rik	3.86103	4.96845
Lpl	3.85776	3.01992
Eef1a1	3.84943	2.5738
Chd2	3.84328	2.82575
Tmsb4x	3.84058	4.35322
Gm6863	3.82726	3.00587
Sepw1	3.78945	3.9936

Gm16755	3.77349	4.53077
Rpl9-ps8	3.77246	2.2026
Mt1	3.76974	1.35457
Rit2	3.76368	4.87941
Crocc	3.75711	2.80243
Ctss	3.74291	2.51818
Gm42989	3.73269	6.14086
Gm11258	3.73191	5.32677
Gm5560	3.70122	6.75786
4833427G06Rik	3.67907	2.52195
Nckap5	3.67728	3.06549
Gm16111	3.6763	4.8957
Gm16407	3.67372	5.22696
Trim28	3.6581	3.35552
Frem1	3.62962	2.33604
Gm11951	3.61937	2.66448
Eif1ax	3.60366	3.68303
H2-Ab1	3.59643	1.39966
Gm5548	3.58819	6.18967
Gm7293	3.58123	1.13832
Rps14	3.57689	3.14828
Tcp1	3.57533	3.35064
Gm7964	3.56283	4.73159
H2-Ea-ps	3.55803	3.32547
Gm2199	3.53226	4.48624
Gm609	3.51457	3.6672
Gm37945	3.51039	2.47147
Slc25a5-ps	3.48172	5.1535
mt-Nd6	3.47737	4.26539
Gm6913	3.47064	5.28359
Gm26825	3.45706	2.61038
Gm26659	3.45699	3.79212
Mmp9	3.44703	0.754628
Gm42418	3.44556	2.35034
Lrba	3.44167	3.95871
Gm9840	3.42667	1.07144
Gm38305	3.42039	3.73919
mt-Cytb	3.40916	3.93789
Batf2	3.40843	4.4449
Cotl1	3.39753	2.39081
Slc28a1	3.36566	4.70904
Gm42522	3.36538	2.54249
4930552N02Rik	3.36231	6.17561
Rps5	3.36002	2.48686

Ccdc7b	3.35309	1.6141
Gm44209	3.35282	2.85952
Gm20589	3.31998	3.28937
Gm9824	3.31583	6.60793
Gm13132	3.29796	2.55142
Gm28343	3.29792	6.35634
Gm18848	3.28422	1.1003
Gm12428	3.2793	3.07351
Ifitm1	3.27594	2.09789
Gnaq	3.27537	3.93779
Gm10814	3.26834	3.41308
Gm9159	3.26605	2.22355
Syngr2	3.26125	0.883411
Prdx5	3.25833	2.98722
Gm4374	3.25167	3.47938
Gm7335	3.24404	3.02952
Tcf12	3.23635	3.64253
Magee2	3.22996	5.21722
Gm5244	3.2264	4.41611
Eef2	3.22635	2.17653
RP23-457I3.2	3.22534	4.97695
Acyp2	3.2238	3.66693
Fcrla	3.21823	2.03935
Usp37	3.20715	0.977969
Gm20412	3.20043	0.707146
Gm17638	3.20017	0.763761
Rplp1	3.19469	3.27905
Zfyve28	3.17322	1.64631
RP23-183A4.1	3.17225	6.71829
Gm6265	3.16873	3.17535
Gm5940	3.16044	4.30964
Rps9	3.15775	2.43598
Gm15703	3.1503	4.00203
Sepp1	3.14895	1.23889
Gm36551	3.14232	4.14277
Gm26530	3.13706	0.788046
Rps18	3.13281	2.37131
Tubb5	3.11681	1.28341
Rps29	3.11244	3.53373
Ryr3	3.10459	4.34159
Mt2	3.10096	0.566107
Gm15645	3.09509	3.75885
Gm6788	3.09125	4.5796
Sirpb1b	3.07948	3.28369

Gm38015	3.05446	2.80662
Tpt1	3.03868	2.78492
RP23-297C11.2	3.02961	2.71333
Gm8814	3.02691	2.83466
Prex2	3.01209	3.47267
Sh3gl3	3.00789	1.844
Ebf1	3.00191	4.11093
Hhat	2.99936	2.33029
Gm19587	2.99349	4.30423
Gm5615	2.99103	2.12047
Rack1	2.97926	2.07832
Pou2f3	2.97254	4.36922
Gm43495	2.9704	2.74603
Csf1r	2.96061	0.765463
Gm16589	2.94774	2.18388
Saa3	2.93209	3.00792
Gm20511	2.92113	4.14412
Capg	2.91775	2.07158
Ccni	2.90955	1.08531
Sh3bgrl	2.90034	0.843186
Ctsb	2.89716	0.936777
6030443J06Rik	2.89444	3.0006
4930506C21Rik	2.88868	1.22332
Gpnmb	2.88479	0.790067
Gm43083	2.88189	1.37842
Gm12017	2.8091	1.51908
Gm12125	2.78314	1.6283
Rps10	2.777	2.29398
Gm13392	2.76123	5.04857
Spock3	2.74958	1.47045
Gm5578	2.74881	4.57025
Gm36938	2.74568	2.66601
Aldoart1	2.745	2.50499
mt-Nd5	2.73599	3.68155
Ptma	2.7327	2.07598
B830042I05Rik	2.73223	2.71576
Gm5997	2.72379	5.43495
Gm5315	2.71067	3.05149
Tyrobp	2.71048	1.89888
Cd36	2.70668	0.915411
Gm22553	2.70144	2.97563
Gm18957	2.69651	3.66086
RP23-74O12.6	2.67539	2.79426
Atp5e	2.66807	0.786915

Txlnb	2.66169	2.74303
Rps19	2.66123	2.27991
Lgals1	2.65136	0.598193
Gm5124	2.6419	2.18558
Gm5871	2.63452	1.03473
Agtpbp1	2.62464	4.02059
Txnrd1	2.62018	2.69631
Gm14204	2.6183	1.9697
Ccl6	2.61685	0.723318
Zyx	2.61578	0.692749
Tgm2	2.59514	0.463243
Gm26873	2.57344	3.53754
Gm26561	2.56825	2.12063
4930509G22Rik	2.55814	4.97498
Zbtb20	2.54878	2.96127
Cks1brt	2.54724	3.00336
Gm42535	2.54165	2.90771
Gm19587	2.54141	1.45803
Lhx9	2.53884	1.50163
Erbb4	2.53552	3.30369
Asap2	2.53238	4.41624
Gm17087	2.52596	1.43899
Itm2b	2.51577	1.51591
Gm8801	2.51532	0.661912
Laptm5	2.51344	1.14121
Ighv1-64	2.5043	2.94832
Anxa1	2.50381	1.91332
Pla2g7	2.50066	1.18629
Trim2	2.49666	3.22072
Rhbdd3	2.48524	1.54749
Gm19963	2.47428	2.84547
Fn1	2.46758	3.31568
Slk	2.44651	2.48834
Gm4076	2.44593	1.36253
Gm28196	2.44473	2.52581
H2-Bl	2.42743	1.74633
Gm1840	2.41336	2.91487
Arg1	2.40537	1.0499
Gm17909	2.40506	1.03824
Loxl3	2.40437	0.642673
Txnrd1	2.40084	2.38725
RP24-426B21.1	2.39807	3.2292
Ccl9	2.38185	0.926765
Pou3f4	2.37735	3.5034

Txnrd1	2.37461	1.33565
Gm26852	2.37444	1.55096
Cybb	2.37179	0.517222
Cox4i1	2.36546	2.16626
Tpi1	2.34359	2.4009
Gm16575	2.32971	1.36631
Gm7291	2.32527	3.10158
Rpl18a	2.32418	2.00522
Rpl26	2.31261	1.29894
Anxa3	2.30792	0.800649
Gm26586	2.3001	1.59325
Tmsb10	2.29201	3.56717
Hspe1-ps6	2.29022	2.89707
Rps17	2.28837	2.26792
Mei4	2.28722	2.76123
Tmem123	2.28181	2.27334
Gm9825	2.28176	3.49502
Gpc5	2.26249	3.59243
Slc8a3	2.24725	3.09118
Tmprss11b	2.2471	2.50304
Gm18367	2.23843	1.5239
Cep72	2.23698	2.17489
Cyba	2.23367	1.83855
Ptprb	2.23364	1.15693
Gm37103	2.23274	1.83368
Clec7a	2.23079	3.46261
Gm13502	2.22676	0.967478
Ly6e	2.22657	1.08732
Gm43942	2.21284	1.14906
Fpr2	2.21106	1.05546
Myl6	2.20932	1.7448
Hmox1	2.20001	3.12712
Gm7935	2.1964	1.94073
Gm15932	2.19472	1.67094
Sema3a	2.19388	2.34419
Txnip	2.18916	1.29229
Rps12	2.18554	2.46301
Lars2	2.18554	1.85184
Gm13709	2.1756	0.431107
Gsn	2.16595	2.49548
Mmp8	2.16047	1.48866
Gm10390	2.15856	1.66479
Gm15603	2.15682	1.8342
Gm6166	2.15462	0.940891

Glipr1	2.15329	0.737688
Gm38033	2.15169	3.44981
Unc93b1	2.14626	0.961251
Emp3	2.14024	1.57349
Sfi1	2.13677	1.76918
Fam227b	2.13535	2.21682
Lipa	2.12784	1.57197
Gm8425	2.12748	0.959372
Gm12352	2.11994	3.19424
Gm14849	2.10247	3.15522
Pfn1	2.10188	1.44442
Gm27747	2.10147	2.89165
Calr	2.09312	1.1859
Rps21	2.09295	1.20812
Gm42801	2.08739	2.27046
Cfb	2.08659	0.531291
P4hb	2.08584	3.19934
H2afj	2.08115	0.592108
Gm26819	2.07907	1.46975
Slc3a2	2.07798	2.13197
Kifc5c-ps	2.07531	2.44581
Pcbp2	2.07512	1.28986
Cfp	2.07394	1.62126
Fau	2.07386	2.24204
Rps19-ps10	2.07298	3.52639
Ccdc7a	2.0727	1.88345
Ctsh	2.06902	1.55617
Wfdc17	2.06753	1.25129
Pkm	2.06153	3.26901
Actr3	2.05916	0.71206
Fxyd5	2.05645	3.36338
Tacr3	2.04815	1.37777
Crb1	2.0417	2.03847
Cd9	2.03685	0.448327
Gm13361	2.03412	2.2152
Gm14912	2.03344	2.51531
Ctsz	2.02721	0.432684
Gm13365	2.02545	1.24368
Srgn	2.02506	2.20766
Gm7816	2.02118	1.36828
Rpl8	2.01887	2.3688
Il1rn	2.01829	2.65501
Txnrd1	2.01797	2.95835
Atp6v1b2	2.01399	1.36923

Gm17275	2.01061	2.45762
Gm13082	2.0062	4.33137
Vapb	2.00349	0.531742
Rpl32	2.00223 [4]	1.5237

Table 8.15. Pairwise analysis of transcripts between *L. mexicana* infected and naïve BMDC cultures.

Transcript abbreviation	M1. VIP [3+3+0] [1]	2.44693*M1. VIP [3] cvSE [2]
Gm7204	54.9959	58.0403
Bbx	39.1715	26.8812
Rps28	24.3982	11.6334
Il1rapl1	19.5771	15.9935 [3]
Mir6236	18.514	14.7757
Lyz2	18.0515	9.71269
Pde1c	17.6503	18.4056
Gm7665	17.0419	19.3498
Fth1	11.3148	11.174
Ftl1	11.1947	8.76513
Mir6240	11.0565	10.3449
Hmox1	10.628	5.0406
Gm15487	10.1255	5.99136
Chd2	9.80622	3.90995
Cntnap2	9.18694	7.10892
Gm23374	9.15115	8.71589
Gm14303	8.99388	3.53608
Mt1	8.48164	4.25841
Vmn2r-ps54	8.20384	7.01512
Gm26825	8.0859	2.02368
Hormad2	8.05831	10.5466
Gm6682	7.40341	10.2709
Mt2	7.16579	2.59978
Gm43841	7.15952	11.68
Tpt1-ps3	7.1134	11.2032
Prdx1	6.88896	5.98739
Ldha	6.88124	4.03976
Negr1	6.71742	7.34693
Bach2	6.58462	4.70819
Cacna2d4	6.52316	4.49688
9330179D12Rik	6.44637	6.34672
Gm10180	6.40444	5.2769
Gm7676	6.36271	5.61152
Txnrd1	6.33144	1.6275

Ctsd	6.28903	7.14716
RP23-183A4.1	6.08657	6.02035
Gm9575	6.04555	1.35781
Lgals3	5.97606	6.53411
Gm8304	5.96675	4.95175
Gm8529	5.78548	7.79248
Cntnap5b	5.77215	4.37726
Gm609	5.67719	7.46412
Gm15173	5.65125	5.91628
Ctcf	5.64854	6.72636
Gm12111	5.61035	4.27738
Gm7897	5.55753	5.09036
Gm9840	5.51966	3.07698
Cdk8	5.51375	4.21969
Gm19587	5.43626	5.06909
Gm8984	5.37678	3.4631
Gm8909	5.30033	3.31601
Rnf24	5.23282	6.81389
Gm14130	5.17885	5.61682
Gm24951	5.17631	4.12396
4930445B16Rik	5.11141	7.72856
Gm6394	5.06903	4.6059
Gm16418	4.97512	7.1547
Adgrl3	4.92381	6.6619
Gm1840	4.92035	2.27949
Ryr3	4.90351	7.51812
Gm26745	4.87391	5.97988
Uqcrh-ps2	4.81494	4.90118
Txlnb	4.81408	1.20201
Tmcc1	4.75925	6.59937
Eif4a-ps4	4.75302	5.14029
Il31ra	4.67711	3.62136
Pkm	4.67476	2.87631
Gm16505	4.66532	3.60052
Vim	4.55831	2.68052
Tmsb4x	4.54493	2.85505
S100a9	4.53575	2.87242
4930552N02Rik	4.51602	3.09074
Hs6st3	4.5081	2.80875
Gm16407	4.49739	2.44869
Tpi1	4.48552	2.75914
Batf2	4.45563	3.7037
Gm2199	4.4483	6.00227
Cd74	4.44407	2.01624

Gm11560	4.42098	2.9636
Pcsk5	4.41672	6.48897
Gm17638	4.37351	3.67761
Tcea1	4.19394	7.61021
Gm13453	4.16498	3.49783
Rn18s-rs5	4.16312	4.47844
Rpl3-ps1	4.15191	2.87773
Actg1	4.10781	1.45297
Sh2d2a	4.08608	3.85926
Zfp36l1-ps	4.08199	5.98077
Plxdc1	4.08077	0.731245
Gm42989	4.05445	4.80749
Pou2f3	4.04425	5.27205
Gm11258	4.00979	3.42365
Macrod2	4.00782	3.32395
G6pd2	3.98079	4.87031
Mir703	3.95637	2.63542
Mmp12	3.94684	5.03985
H3f3a-ps2	3.94165	4.62805
Clec4n	3.93532	4.49624
Gm7816	3.91079	2.21319
Slc39a1-ps	3.89711	3.17895
Spp1	3.8756	6.74588
Fn1	3.86049	3.31667
Nckap5	3.82342	4.59355
Cstb	3.81292	3.13292
Txnrd1	3.8109	1.93577
Ctsb	3.77451	5.06699
B830042I05Rik	3.77137	2.46142
Gm5578	3.7524	4.70497
Gm12428	3.74193	5.12739
Trim2	3.7314	2.31616
Eef1a1	3.7171	2.19074
Lrrc20	3.70252	5.68213
Scp2-ps2	3.66067	2.98357
Zfp280c	3.65558	3.01842
Crocc	3.62792	5.27049
Aldoart1	3.62662	5.66176
Txnrd1	3.61116	1.82947
P4hb	3.60975	2.44943
Gm5548	3.60331	4.67728
Txnrd1	3.59081	0.786663
Fcrla	3.58754	3.84295
Gm6180	3.57865	1.84235

Gm13082	3.56335	4.31535
Gm6913	3.55693	3.43265
Mup-ps16	3.54965	3.00736
Gapdh	3.53663	2.37604
Usp37	3.51084	3.87449
Gm43972	3.48719	2.94336
Gm5870	3.48303	5.0249
S100a16	3.4705	4.53383
Cd9	3.46798	3.40274
Gm11951	3.45766	3.37564
Gm44090	3.44261	3.8431
Gm16111	3.42401	4.3323
Gm9025	3.40188	6.01796
Gm8979	3.39213	1.68691
Sepp1	3.38781	1.29537
Gm16372	3.38217	2.33853
Eif1ax	3.37668	3.5863
Oaz1-ps	3.3661	1.2285
Sqstm1	3.35613	1.77782
Acyp2	3.29792	2.32431
Gm26852	3.29039	4.23707
4930509G22Rik	3.29014	4.23072
Gm7846	3.2899	3.41074
Gm5940	3.26744	4.82916
2410017I17Rik	3.26376	2.84618
Rps5	3.26316	1.91296
Slc25a5-ps	3.25642	3.08778
Gm9824	3.25504	5.37789
Ebf1	3.21071	2.60593
Rnft2	3.20741	3.20105
Lipa	3.20132	2.78061
Esd	3.19752	2.40441
Gm4852	3.19752	4.28253
Gnaq	3.18515	3.43236
Gm6863	3.17971	2.36076
Gm5809	3.17795	3.01615
Gm7335	3.14615	3.40189
Il1rn	3.1415	3.05779
Anxa2	3.12931	1.90243
Frem1	3.11946	2.89301
Slk	3.11381	3.79683
Gm44209	3.10709	1.71749
RP23-74O12.6	3.09766	3.95973
Ifitm1	3.09191	1.91373

Gm42418	3.06811	3.27125
Cxcl3	3.05537	1.65282
Gm6421	3.04092	4.701
RP23-297C11.2	3.02904	0.950426
Ctss	3.02646	2.53186
Eef2	3.01886	1.32285
Tmem232	2.99554	3.07721
Hp	2.96947	1.69167
Pgam1	2.96815	1.9112
Zfp839	2.96342	2.61834
Rplp1	2.9587	2.33366
Eno1	2.94948	1.9917
Lhx9	2.94628	4.20157
Txnrd1	2.93737	0.7339
Gm43083	2.9217	1.59988
RP24-285L8.3	2.91617	2.59759
Ifitm3	2.90279	1.59453
Myo9a	2.90195	4.00893
Coro1a	2.88998	1.15885
Txnrd1	2.87635	1.05141
Sepw1	2.87189	3.06801
Antxr1	2.86331	2.21488
Gm7964	2.84848	2.8171
Gm26981	2.84617	4.26855
Cst3	2.84525	2.13063
Oca2	2.84197	4.69796
Gm5615	2.84033	1.38196
Gm13132	2.83777	1.99877
Basp1	2.83309	1.72566
Cks1brt	2.8238	3.73764
Gm29610	2.80806	2.39349
Gm35106	2.80503	4.58817
Saa3	2.80193	2.738
RP23-96L20.1	2.8004	2.01881
Gm26561	2.79414	2.16993
Id2	2.79013	1.64571
Camk1d	2.78182	3.71281
Rps18	2.78053	2.25487
Rpl36a-ps1	2.77476	4.11659
Gm6987	2.77331	3.09091
Lpl	2.77236	2.87149
Rit2	2.76967	3.46383
Sema3a	2.76935	3.62978
Lrp1b	2.768	2.54185

Vat1	2.76356	2.32366
Gm26659	2.74755	2.74513
Cebpb	2.74502	2.20068
Gm7332	2.74395	2.90994
Zbtb20	2.7413	2.08635
Rnh1	2.71771	2.20282
Gm36551	2.71707	3.25401
Fry	2.70946	1.78316
Wdr54	2.70516	4.66618
Mmp9	2.69707	1.47164
Ctsz	2.69688	3.51214
Cacng4	2.69195	1.59268
Erbb4	2.6872	2.17157
Gm16907	2.66167	2.59049
Ndrg1	2.65878	1.70235
Gm7984	2.64616	3.31612
Ccl22	2.62662	2.05552
Rps14	2.61699	2.17211
Gm37315	2.60836	1.90499
Tpt1	2.60758	2.19003
Ptgr1	2.60746	1.46248
Slc28a1	2.6038	2.8658
Agtpbp1	2.60281	3.61832
Gm16505	2.60206	2.25267
Gpatch4	2.59383	1.08777
Rps9	2.59003	1.89348
Gm38015	2.58613	3.62571
Tcf12	2.58084	2.18517
Gm7935	2.57823	3.3428
Rpl32	2.558	2.09338
Gpx1	2.541	2.25847
Pgk1	2.53406	1.59855
Gm3145	2.53097	4.7475
Clec4e	2.53044	1.50285
Gm20589	2.52893	3.56714
Thbs1	2.52408	1.71606
Fam19a3	2.51498	4.97359
Angel1	2.50281	5.0376
Ero1l	2.49167	1.33015
Ctnnb1	2.4853	1.26599
Ccl6	2.4828	2.29263
Ass1	2.48116	1.52386
Sirpb1b	2.47994	1.58147
Gm43495	2.4791	1.80945

Fshr	2.46641	1.95807
S100a8	2.46287	1.19385
Cd68	2.45776	1.77973
Rps19-ps10	2.45364	2.02237
Prex2	2.44344	2.45234
Csf1r	2.44205	0.968247
Gm13736	2.43681	2.92217
Cotl1	2.43649	2.31503
Txnrd1	2.42875	1.74478
F10	2.42394	1.22742
Rps17	2.42143	2.00475
Gm15703	2.41793	1.88566
Tmem123	2.41348	4.20946
Gm10221	2.40084	2.63038
Mmp8	2.39244	1.72473
Gm8545	2.39115	2.89795
Itfg1	2.383	1.97009
Rack1	2.36728	1.79457
Gm37945	2.36634	3.12792
Cd36	2.36559	4.20896
EU599041	2.36202	2.94308
Srxn1	2.36188	1.26396
Txn1	2.35771	2.22255
Gm15989	2.34127	2.48027
Gm8801	2.33774	1.98958
Cybb	2.3354	1.00821
Ighv1-64	2.3301	2.01819
Gm15925	2.31834	2.05826
Gm7634	2.31825	2.38983
Gm4076	2.31673	4.8081
Gm2824	2.31198	2.30414
Gm4374	2.31074	3.79144
Ccl9	2.30763	2.08453
Rpl27a-ps2	2.30028	3.52593
Lrba	2.28733	5.2504
Sat1	2.28648	1.11182
Tacr3	2.28638	2.26896
Ninj1	2.28524	1.84635
Itm2b	2.27711	1.62325
Kctd12	2.27352	0.991081
Asap2	2.26155	1.72253
Rpl18a	2.25343	1.33603
Tpt1-ps6	2.2512	1.58199
Gm5997	2.25046	5.43155

Acod1	2.2452	1.0301
Mif	2.24344	1.43312
Gm37401	2.24002	1.56795
Atp5e	2.2398	1.39304
Gm17035	2.23379	1.34875
Trim28	2.23018	2.29621
Gpi1	2.2249	1.05322
Gm44737	2.22243	1.79176
Gm19963	2.21092	2.47862
Bsg	2.19692	1.77648
Sh3gl3	2.19417	2.03224
Lgals1	2.19339	2.69097
Tyrobp	2.18785	1.85853
Atp6v1a	2.16886	1.71118
Cd63	2.16205	2.81228
Anxa5	2.15936	1.88761
Plin2	2.15796	1.64132
Rps16	2.15324	1.73101
Anks1b	2.1527	1.67713
Fpr2	2.14773	1.01693
Ly6e	2.14578	1.1727
Gm13392	2.13885	1.11922
Mctp2	2.13755	2.69925
Txnrd1	2.12178	3.09046
Gm20412	2.11894	1.19859
Hvcn1	2.11749	1.28716
Cndp2	2.10737	2.01112
Gm11970	2.10613	2.33021
Rps12	2.10463	1.80812
Rps4x	2.1036	1.00375
Rps21	2.10338	1.59333
Gm7293	2.10246	2.65795
Rps26	2.10064	1.33233
Gm12158	2.10061	0.517501
Gm15518	2.09417	2.21953
Pla2g7	2.09206	1.60214
Gm8814	2.08653	2.4471
Rpl34	2.08598	1.93448
Kcp	2.08576	2.04273
Rps11	2.0856	1.96481
Txnrd1	2.08324	1.15617
Gm11867	2.08174	1.3493
Gm10814	2.07669	2.41481
Sdcbp	2.07447	2.49576

H2-Bl	2.07311	0.804599
Rpl26	2.07283	1.10941
Creg1	2.07004	1.67475
Psmd8	2.06603	1.36971
Prdx6	2.06165	1.37482
Capg	2.05641	3.44781
Gm13502	2.05428	2.41129
Hsp90ab1	2.05308	0.828356
Il1b	2.0393	2.11749
Fam162a	2.03915	1.10776
Gm38305	2.03507	3.76216
Rps15	2.0334	1.59383
Pfn1	2.03337	1.81745
Cntnap2	2.03336	0.340805
Rps29	2.03121	1.18003
Gm12060	2.02551	2.80046
Slc16a3	2.01631	1.18089
Mei4	2.00952	1.6438
Ppbp	2.00507	2.02498
Pcbp2	2.00141 [4]	1.00213

[1] The value represents the difference between the distinct groups

[2] The value highlights variety within each sample group

[3] mRNA transcripts indicating immune function are shaded in blue, metabolism shaded in green and regulation shaded in orange and show that the top metabolites do not differ even if the VIP score does

[4] The VIP list was limited to a VIP score ≥ 2.00